Role of Kinetic Lability on the Recognition of Achiral and Chiral Amines on the Scaffold of Co(III)/Fe(III) Complexes Through Non-Covalent Interactions

A
Thesis Submitted
In Partial Fulfilment of the Requirement
For the degree of

DOCTOR OF PHILOSOPHY

By

Somnath Paik

Department of Chemistry
Indian Institute of Technology Guwahati
Guwahati- 781039

October 2024

Dedicated to my parents

..... Somnath

INDIAN INSTITUTE OF TECHNOLOGY GUWAHATI

Department of Chemistry

STATEMENT

I hereby declare that the matter embodied in this thesis is the result of investigations carried out by me in the Department of Chemistry, Indian Institute of Technology Guwahati, India, under the supervision of Prof. Manabendra Ray, Professor, Department of Chemistry, Indian Institute of Technology Guwahati, India.

In keeping with the general practice of reporting observations, due acknowledgments have been made wherever the work described is based on the findings of other investigations.

October, 2024

I. I. T. Guwahati Somnath Paik

Prof. Manabendra Ray
Professor
Indian Institute of Technology Guwahati
Department of Chemistry
Tel. 91 361 258 2310
Fax.91 361 258 2349

CERTIFICATE

This is to certify that Mr. Somnath Paik has been working under my supervision since December 2018. I am forwarding his thesis, entitled, " **Role of Kinetic Lability on the Recognition of Achiral and Chiral Amines on the Scaffold of Co(III)/Fe(III) Complexes Through Non-Covalent Interactions "** being submitted for the degree of Doctorate of Philosophy of this Institute. I certify that he has fulfilled all the requirements according to the rules of this Institute and that the investigations embodied in this thesis have not been submitted elsewhere for a degree.

October, 2024

I. I. T. Guwahati

Prof. Manabendra Ray
Supervisor

Acknowledgment

At the very outset, I take the opportunity to express my deep sense of gratitude to my Ph.D. supervisor, Prof. Manabendra Ray, Department of Chemistry, IIT Guwahati, for his excellent guidance, tireless efforts, constant encouragement, and moral support at each and every step of my research work, which enable me to complete my thesis work. I am fortunate enough to have had his teachings about how to cultivate scientific thoughts.

I would like to acknowledge my sincere gratitude to the chairman of my doctoral committee, Prof. Gopal Das, and the members of the Doctoral Committee, Prof. Chandan. K. Jana and Prof. Animesh. Das, Prof. Samir Kumar Sarkar, for their insightful advice and valuable suggestions.

I also express my sincere thanks to all faculty members of the Department of Chemistry, IIT Guwahati, for their help and encouragement.

I am thankful to the Institute, Indian Institute of Technology Guwahati for providing me with the state of the art infrastructure and facilities for advanced research.

I am grateful to all non-teaching staff of the Department of Chemistry, IIT Guwahati, for their technical support.

I would like to thank DST under the FIST program for providing single crystal XRD instrument Facility.
I acknowledge the Ministry of Education (MoE) India for the research scholarship.

I would like to thank my former group members Dr. Sounak Bhattacharya, Dr. Tanmoy Dutta, Dr. Jinat Aktar, and Dr. Chanreingam.L for their timely help, support and for the wonderful time we shared during this period.

I extend my sincerest special thanks to my dear friends Sourav Mandal, Supriyo Halder, Sribash Das, Suvendu Halder, Indraneel Debnath, Samir Roy, and Subhamoy Biswas for their enthusiastic company and all the wonderful time we spent together.

Last but not least, I want to express my sincere thanks to my parents and elder brother for their constant encouragement and moral support during my research work. They are the main soul and inspiration for each and every step that I achieve in my life.

Somnath Paik

Synopsis

Metal-ligand coordination bonds can undergo dissociation and recombination under suitable conditions, and this dynamic nature of the coordination bonds can be tuned, controlling the lability and inertness of the central metal ion. To date, utilizing this feature of coordination bond, various kinds of dynamic metal-ligand coordination structures, e.g., metal-organic cages (MOCs)[1–5], metallopeptides[6,7], metal-helicates[7,8], and other metal complex hosts, have been developed which offer dynamic conversion of their molecular shapes in response to external stimuli like light[9], heat, redox reaction[10], pH change[11], binding of organic or inorganic substrates[12–15], etc.

In this thesis, we investigated guest (achiral, chiral ammonium ions, and secondary metal cations) induced structural changes of chiral octahedral metal complexes of L-tryptophan derived ligand. We synthesized a kinetically inert anionic chiral Co(III) complex having multiple H-bond capable sites and used it to bind a series of achiral and chiral ammonium cations. The anionic Co(III) complex adopts different shapes to recognize different achiral and chiral ammonium ions. The change in shape, at least in one case, involves the reorganization of coordination bonds despite the inert nature of the complex. Structural reorganization of the complexes could be monitored in solution using 1D and 2D NMR spectroscopy. Recognition of enantiomer was also observed when racemic amino alcohols were used. To understand the role of kinetic inertness in these recognitions and transformations, we synthesized a labile but structurally analogous Fe(III) complex and repeated some of the transformations. In some cases, the Fe(III) complex adopts a very different shape where ligand coronation on the Fe(III) center has changed completely. The thesis contains detailed investigations and our conclusions.

The thesis has been divided into six chapters. A chapter-wise summary of the work is given below.

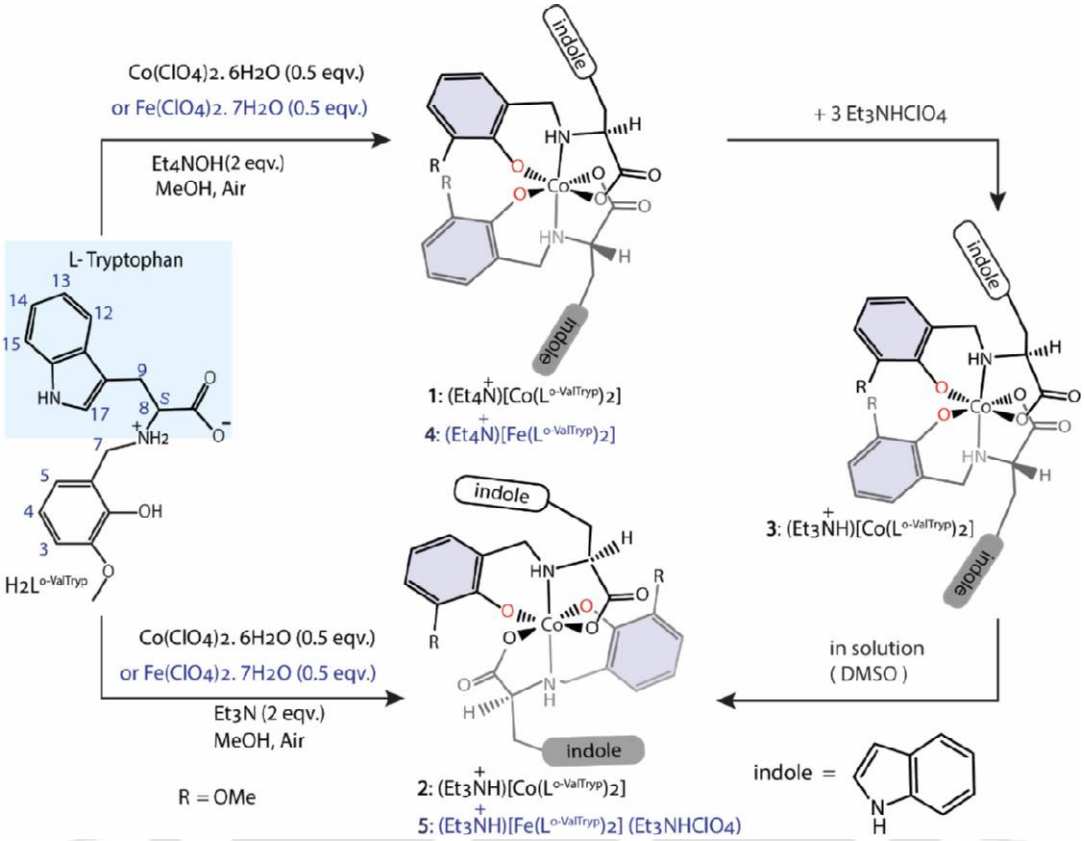

Scheme 1. Synthesis and conversions of the Co(III) complexes (**1** & **2**) and their Fe(III) analogs (**4** & **5**). The drawings reflect the organization of the complexes as in crystal structure.

Chapter 1. This chapter summarizes the literature on the various types of dynamic metal-coordination structures like metal-organic cages, metal helicates or metallo foldamers, and other metal-complex hosts, which showed conformational or structural changes due to the presence of different external stimuli (e.g., temperature, neutral substrates, cations, anions, chiral additives, pH). A literature review on chiral recognition using rigid metal-complex hosts has also been performed in this chapter. Based on this, the objectives of the thesis have been defined.

Chapter 2. In this chapter, we have synthesized two Co(III) complexes, $(Et_4N)[Co(L^{O\text{-}ValTryp})_2]$ (**1**) and $(Et_3NH)[Co(L^{O\text{-}ValTryp})_2]$ (**2**), by the reaction of L-tryptophan derived tridentate ligand ($H_2L^{O\text{-}ValTryp}$) with $Co(ClO_4)_2.6H_2O$ in the presence of either Et_4NOH or Et_3N as a base.

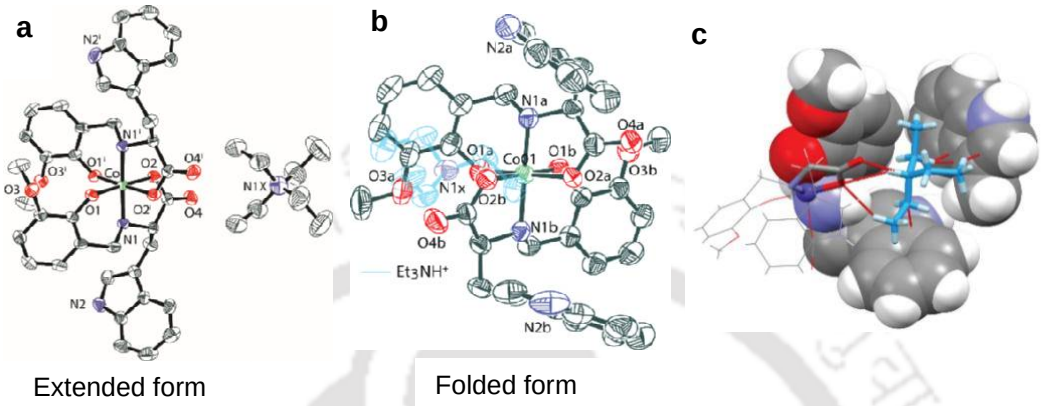

Figure 1. ORTEP views of complex **1** (a) and **2** (b) with 40% ellipsoid probability; triethylammonium ion inside the molecular cleft in **2** (c).

The only difference between the two ammonium ions is the presence of one H-bond capable N-H group in Et_3NH^+, substituting one of the ethyl arms in the Et_4N^+ ion. X-ray single crystal analysis of the Co(III) complexes revealed that the anionic Co(III) complex adapts two distinct structural arrangements depending on the cation (Scheme 1 and Fig. 1). In **1**, the anionic complex $[Co(L^{O\text{-}ValTryp})_2]^-$ has two indole arms that are further apart, and the Et_4N^+ ions interact with anions through inter-molecular weak CH…π interactions and CH…O interactions. In **2**, the complex reorganized around the Et_3NH^+ binding the cation on one side of a molecular cleft (Figure 1). The indole arms folded, and one of the ligands reversed its coordination compared to the other (Scheme 1). The Et_3NH^+ is bound through a stronger intramolecular H-bond between the NH group and the carboxylate oxygen. The number of weaker intermolecular interactions was reduced.

^{1}H NMR spectra of the complexes showed that their structural differences remained intact in the solution due to their inert nature. We investigated if the structural conversion of these two inert Co(III) complexes (**1** & **2**) is possible because structural conversion among these two complexes required metal-ligand bond breaking and recombination differently and also C-C bond rotations.

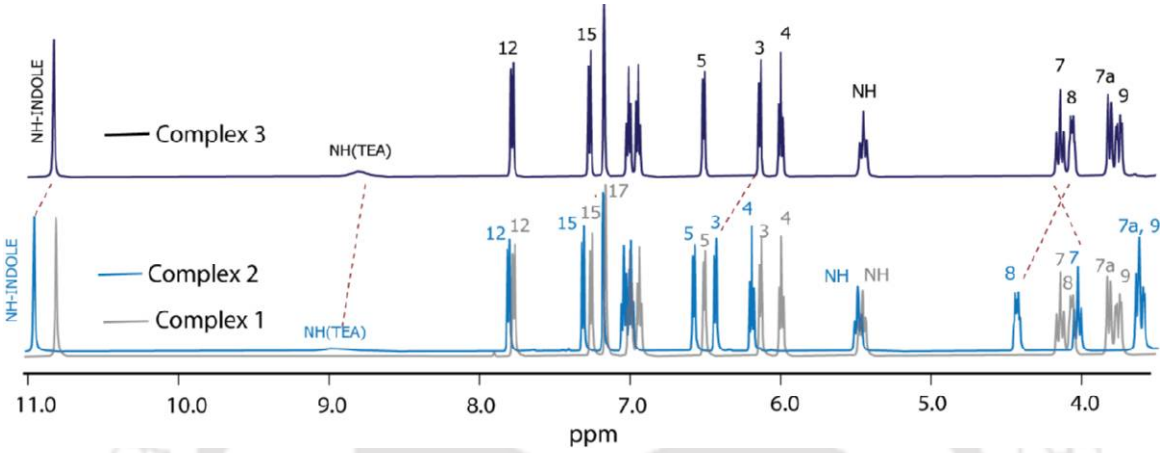

Figure 2. Partial ^{1}H NMR spectra (500 MHz, d_6-DMSO) of the complexes.

For this, when complex **1** was treated with three equivalents of Et_3NHClO_4 salt, it produced complex **3** having formula $(Et_3NH)[Co(L^{O\text{-}ValTryp})_2]$. Though **2** and **3** have the same counterion, triethylammonium ion (Et_3NH^+), they gave very different ^{1}H NMR signals, which refer to their distinct identities. (Fig. 2) Except for the counterion parts, complex **3** showed identical NMR signals to complex **1**. The NMR spectra of **3** changed over time, showing >90% conversion to **2** after 23 days (Fig. 3).

The conversion of **3** to **2** is faster at 60˚C, and it took only 8 hr for >90% conversion. The UV-visible and circular dichroism (CD) spectroscopy showed that the Co(III) complexes behave differently in the solution (Fig. 3). The change in CD spectra also supports the **3** to **2** structural transformation in the solution. From these observations, it is clear that when **1** was treated with Et_3NHClO_4 salt (3 equivalents), it formed an intermediate compound (**3**), which slowly converted

to **2** in the solution, i.e., structural transformation of **1** to **2** is possible, and the transformation proceeded through the formation of a stable intermediate.

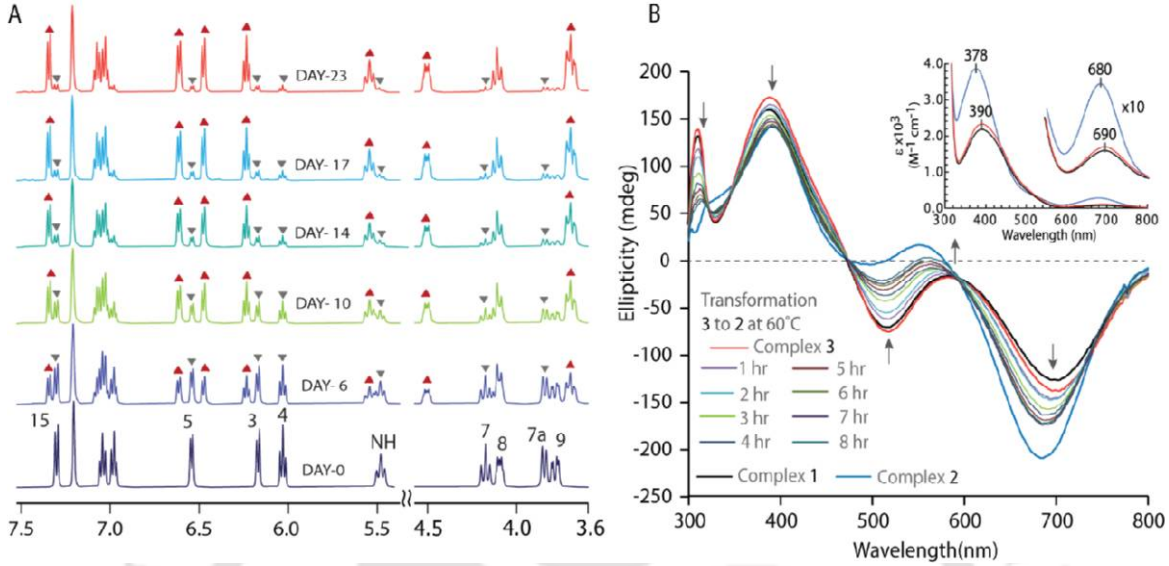

Figure 3. (A) structural transformation of **3** to **2** in solution at room temperature, (B) the time-dependent CD spectroscopic changes of **3** heating its DMF solution at 60˚ compared to complexes **1** and **2**; the inset showing the UV-visible spectra of all three complexes.

Also, we have synthesized the kinetically labile Fe(III) analogs i.e., $(NEt_4)[Fe(L^{O\text{-}ValTryp})_2]$(**4**) and $(HNEt_3)[Fe(L^{O\text{-}ValTryp})_2]\cdot Et_3NHClO_4$(**5**) has almost identical structural arrangements with their Co(III) partners to investigate whether the metal center lability could affect the structural transformation process. Here, we observed by changing the metal center from inert Co(III) to labile Fe(III), the transformation from the unfolded to folded structural arrangement process became faster.

The cyclic voltammograms of the Fe(III) complexes are quite different. Complex **4** showed a quasi-reversible wave having $E_{½}$ = -1.51 V (ΔE_p = 330 mV) attributed to the $Fe^{III/II}$ redox couple, whereas complex **5** showed a completely irreversible wave at $E_{½}$ = -1.06 V (ΔE_p = 810 mV) corresponding to $Fe^{III/II}$ redox couple. Upon adding Et_3NHClO_4 salt (3 equivalents) to the DMF solution of **4**, the quasi-reversible cyclic voltammogram of the complex became completely irreversible, like the cyclic voltammogram of **5**.

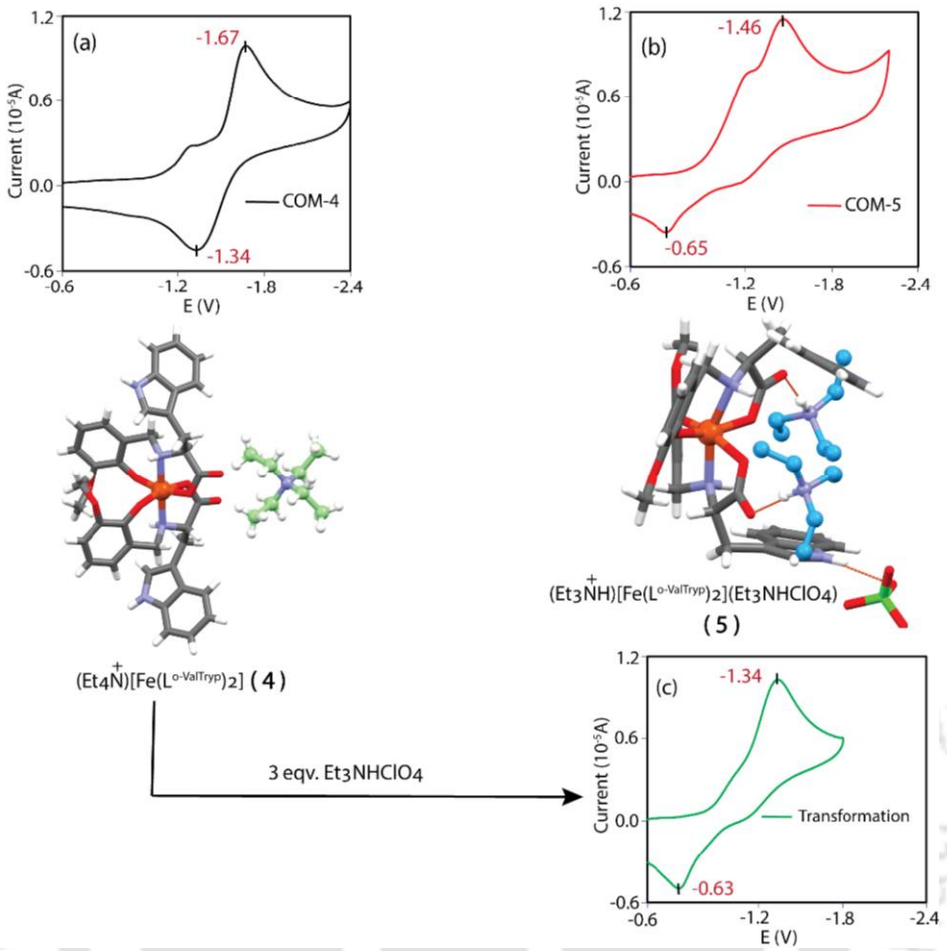

Figure 4. Cyclic voltammetry diagrams of the Fe(III) complexes.

Thus, in this chapter, we proved that one single H-bond between a kinetically inert anionic Co(III) host complex and an Et_3NH^+ ion could trigger its structural transformation from its extended form to the folded conformation, involving inert metal-ligand coordination bond breaking and reformation in a new arrangement.

Chapter 3. In this chapter, we tried to find out what would happen if we employed the anionic host complex to recognize secondary metal cations instead of the ammonium ions, showed in the previous chapter. For this, we used a coordinatively saturated labile Fe(III) complex as a host for the binding of alkali and alkaline earth metal ions of different charges and sizes. When

$(NEt_4)[Fe(L^{O\text{-}ValTryp})_2]$ (**1**) was treated with the salts of alkali or alkaline earth metal cations, the anionic Fe(III) complex, $[Fe(L^{O\text{-}ValTryp})_2]^-$, showed a drastic structural change.

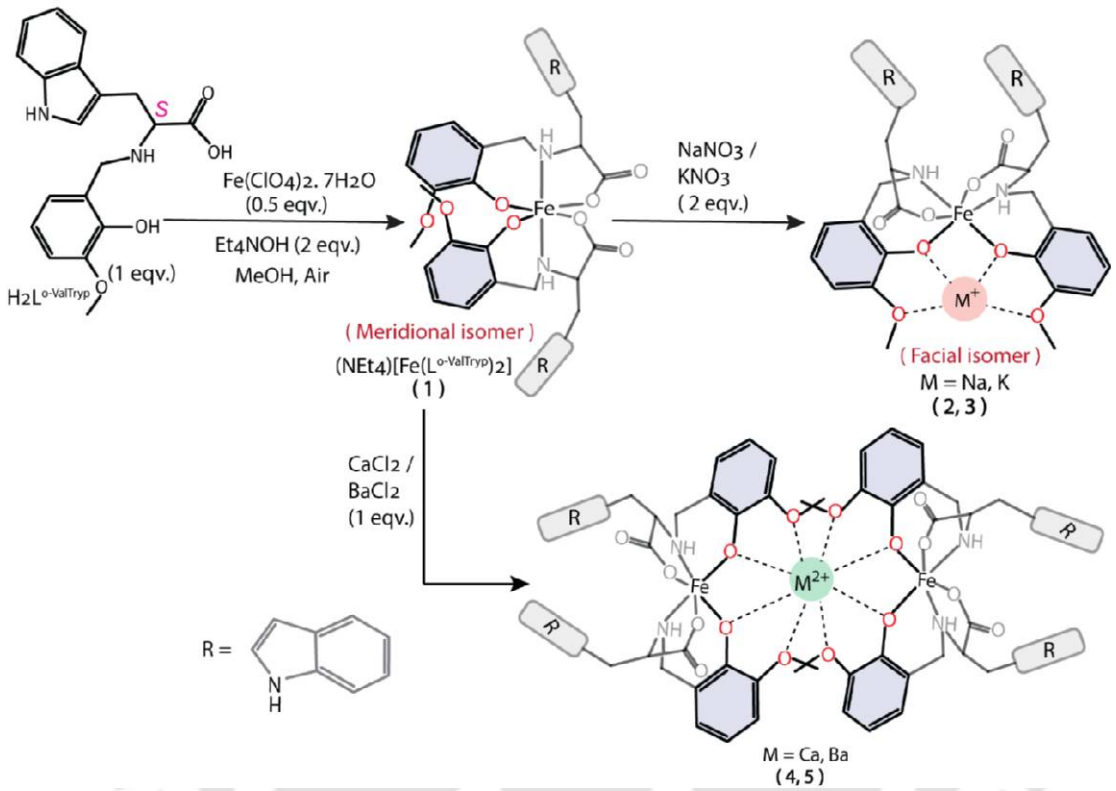

Scheme 2. Syntheses of the complexes (**1**, **2**, **3**, **4**, **5**)

The addition of alkali metal nitrate salt ($NaNO_3$ or KNO_3) to the methanolic solution of **1**, the meridional $[Fe(L^{O\text{-}ValTryp})_2]^-$ complex transformed into its facial isomer where a hemicircular O4 polar pocket has formed and inside the pocked alkali metal ions bound. Though Na^+ and K^+ both have the same charge due to the larger size of the K^+ favored 1D coordination polymer formation in **3**, which is absent in **2.** In the presence of Ca^{2+} or $Ba^{2+,}$ the $[Fe(L^{O\text{-}ValTryp})_2]^-$ complex anion also showed meridional to facial transformation, and in that case, two anionic facial units bound one alkaline earth metal ion to neutralize its +2 charge. In **4**, the Ca^{2+} ion, due to its smaller size,

is more strongly bound inside the circularly arranged O8 oxo-door environment than the larger Ba^{2+} in **4**.

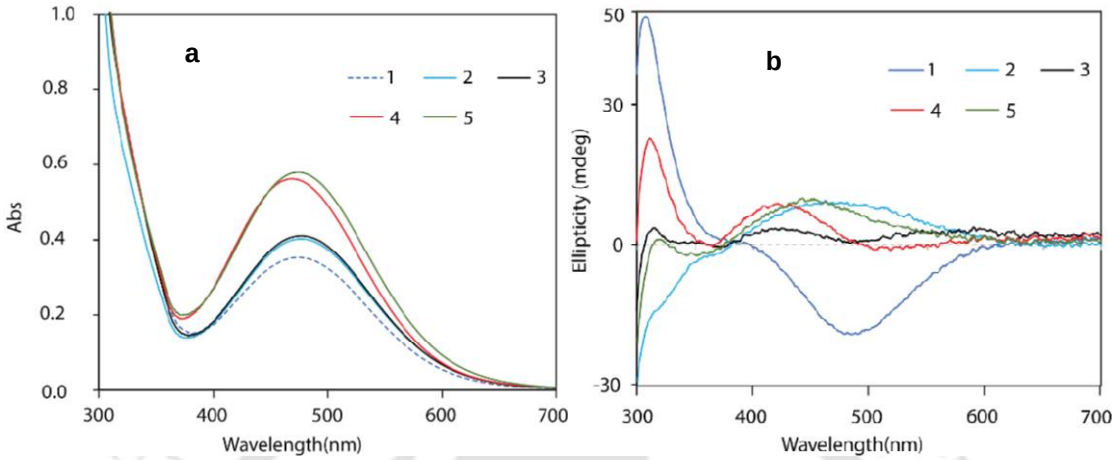

Figure 5. (a) UV-visible and (b) CD spectra of Fe(III) complexes.

Among all four secondary metal ions used, $Ca^{2+,}$ having the highest charge/radius value, is strongly bound with the anionic host complex, and for that reason, visible spectra of 4 showed a ~7 nm blue shift in the LMCT transition region compared to **1**. All five Fe(III) complexes not only showed structural differences in the solid state but also behaved differently in solution, which is evident from their circular dichroism spectra. (Fig. 5)

Chapter 4. Chapter **2** showed that only one H-bond capable N-H group present in Et_3NH^+ ion triggered the structural transformation of $[Co(L^{O\text{-ValTryp}})_2]^-$ complex anion from its extended form to the folded conformation. In this chapter, we intended to find out what would be the structural organization of the $[Co(L^{O\text{-ValTryp}})_2]^-$ complex anion towards recognition of the primary ammonium ion ($R\text{-}NH_3^+$) having three N-H bonds potential for H-bonding. For this, we have structurally characterized three Co(III) complexes (**1**, **2**, and **3**) that bind three different ammonium ions varying from less hindered to more hindered.

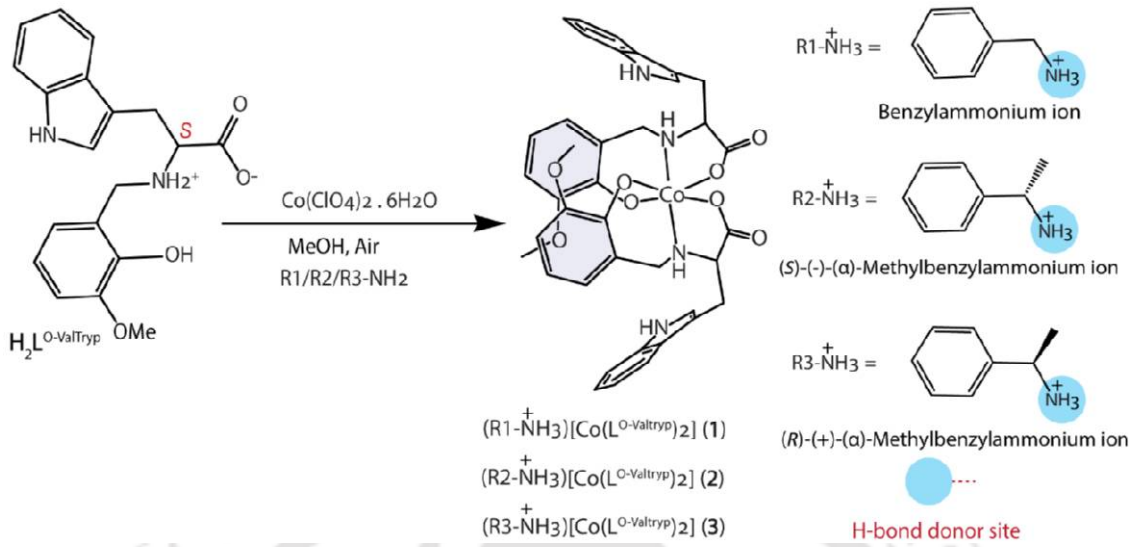

Scheme 3. Syntheses of the Co(III) complexes with primary ammonium cations.

Results showed that the anionic Co(III) complex adapts a new shape, which is different from the other two Co(III)-complexes reported in Chapter **2**. Here, the $[Co(L^{O\text{-}ValTryp})_2]^-$ complex anion folded itself backward, exposing the polar carboxylate oxygens used in H-bonding with the $-NH_3^+$ group of the cationic guest molecules.

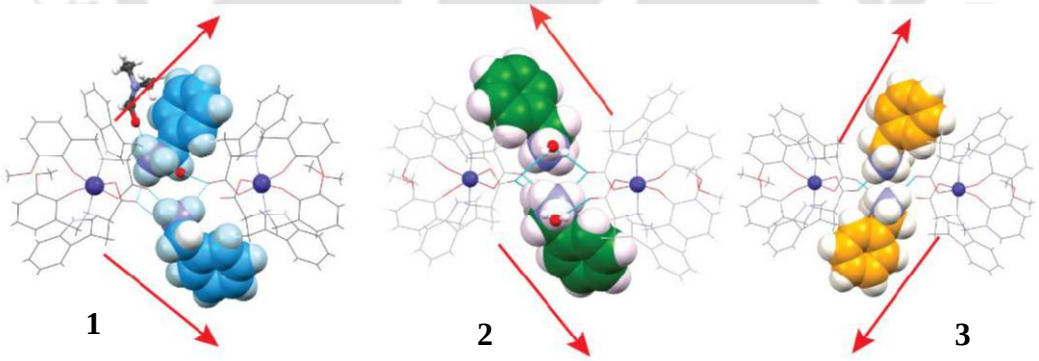

Figure 6. Different orientations of the three different ammonium ions in complexes **1**, **2**, and **3**.

This structural motif is common for all three Co(III) complexes; however, the guest ammonium ions themselves are slightly reoriented in different directions in their respective host-guest complexes to be accommodated in a similar type lattice arrangement. (Fig. 6) Here, the anionic Co(III)-host complex did not show any diastereomeric selectivity toward the recognition of (α)-

methylbenzyl ammonium ions, which might be due to the minimum host-guest interaction (interaction through -NH_3^+ group of chiral ammonium ion).

Chapter 5. In this chapter, we employed ammonium ions of the chiral amino alcohols as guests, varying the position of the chiral center with respect to the -NH_3^+ ion and changing the smaller aliphatic to the larger aromatic sidearm. Expect that the presence of the alcoholic -OH group and the -NH_3^+ group might assist the better host-guest interactions, which favor the selective recognition of one of the diastereomers from the racemic mixture of the respective chiral amino alcohols.

We have divided this chapter into two parts- part **A** and part **B**.

Part A

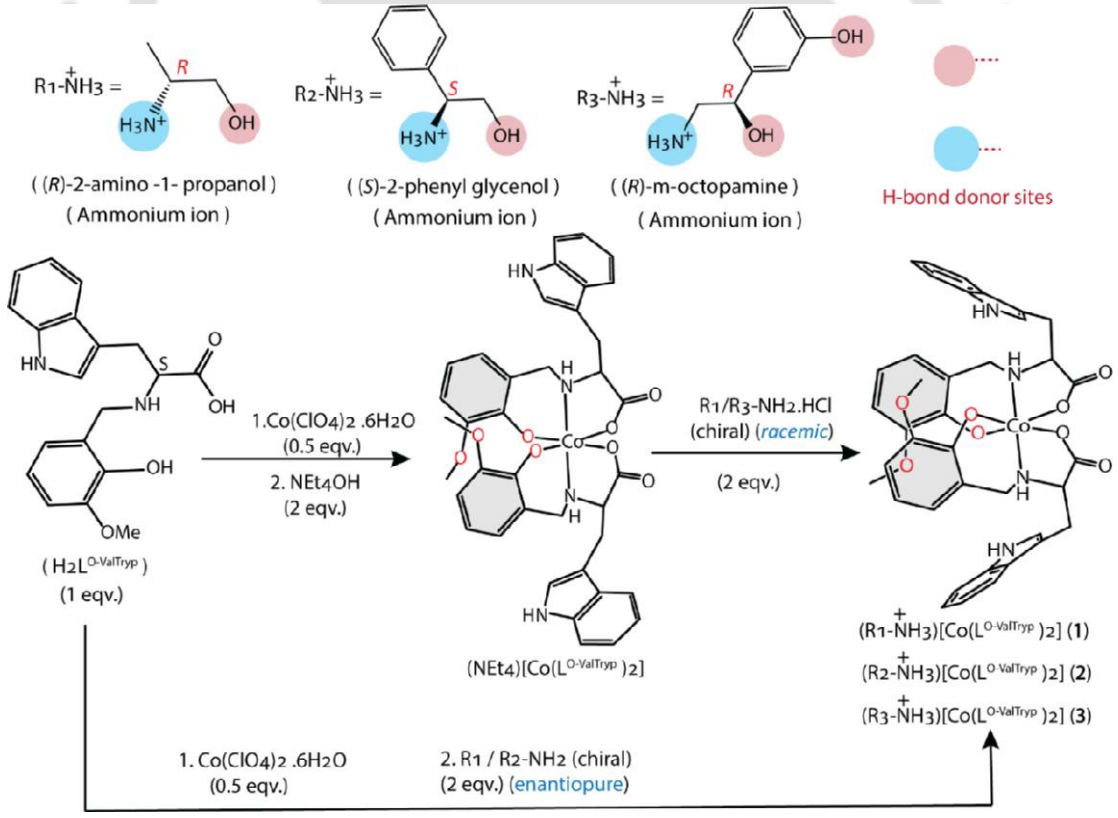

Scheme 4. Syntheses of the Co(III) complexes with ammonium ion of chiral amino alcohols.

Here, we have employed three different biogenic amino alcohols (Scheme 4) as a guest because of their structural similarity to adrenaline and nor-adrenaline, a hormone and neurotransmitter, respectively. We have structurally characterized three Co(III) complexes with ammonium ions of different chiral amino alcohols. Selective recognition of one isomer of respective amino alcohol from its racemic analog is also observed from the crystal structures. In all three complexes, the $[Co(L^{O\text{-}ValTryp})_2]^-$ complex anion imparted a common structural motif as described in Chapter **4**.

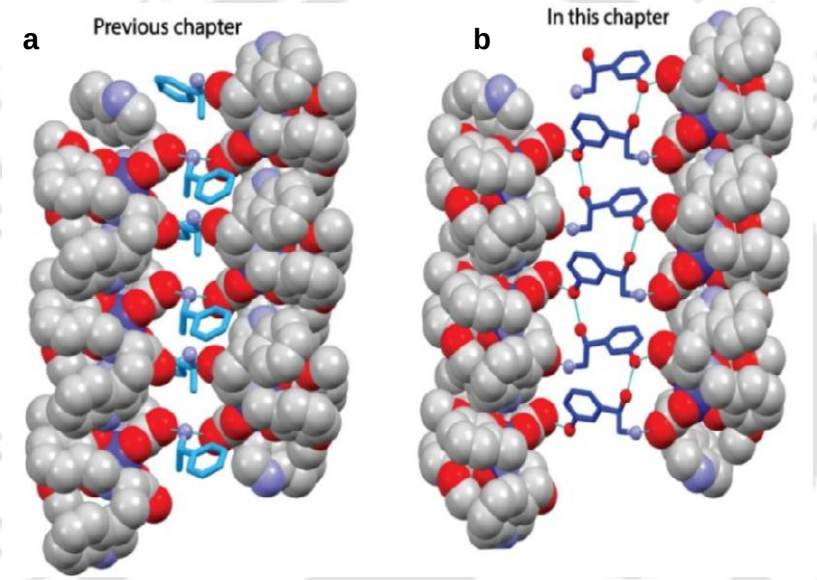

Figure 7. (a) Narrow channel with smaller size chiral amine (in chapter 4), (b) wider channel with amino alcohol bridging (in this chapter).

The complexes' X-ray single crystal structure analyses showed the guest cations using their -OH and $-NH_3^+$ functional groups acting as a bridge between two adjacent anionic Co(III)-complex units (Fig. 7). The single crystal structure analyses of **1** and **3** also revealed that the Co(III) complex anion recognized one of the enantiomers from their respective racemic analog. It is not surprising because previously, our group reported the chiral recognition of amino alcohol from its racemic mixture using the metal complex of a similar type of amino acid-derived ligand.

The solution-state behavior of the Co(III)-complexes (**1**-**3**) was monitored using NMR spectroscopy. The ^{1}H NMR spectra of all the complexes showed sharp and well-resolved resolve signals, confirming the 1:1 host-guest binding. In solution, complexes showed structural reorganization, which is evident from the NMR spectral change when their NMR solution in d_6-DMSO was heated.

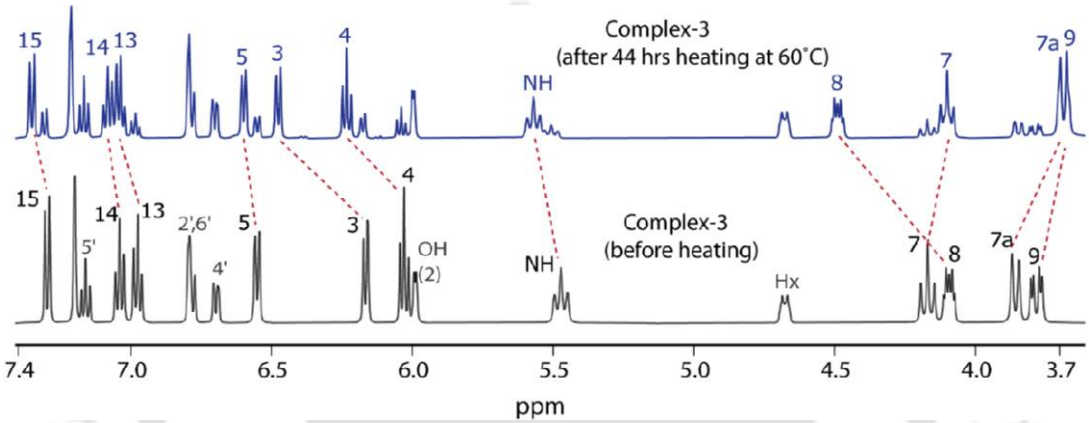

Figure 8. Combined partial NMR spectra (500 MHz, d_6-DMSO) of the **3** collected before and after heating.

Part B

Here**,** we employed the $[Co(L^{O\text{-}ValTryp})_2]^-$ complex anion to recognize the ammonium ion of adrenaline as that anionic Co(III) host complex showed recognition of ammonium ions of different chiral amino alcohols having structural similarities to adrenaline and nor-adrenaline, discussed in part **A**. The catechol -OH groups in protonated adrenaline have lower pK_a values and are prone to oxidize in their semi-quinone form in aerobic conditions. So, recognition of adrenaline using metal complex hosts is challenging.

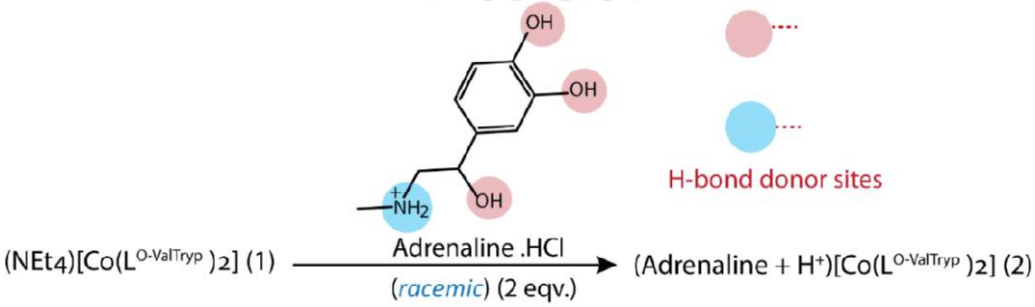

Scheme 5. Synthesis of the Co(III) complex with adrenaline ammonium ion.

The addition of hydrochloride salt of racemic adrenaline to the solution of $(Et_4N)[Co(L^{O\text{-}ValTryp})_2]$ in acetonitrile-methanol (3:1) mixed solvent gave a yellow-colored solid complex.

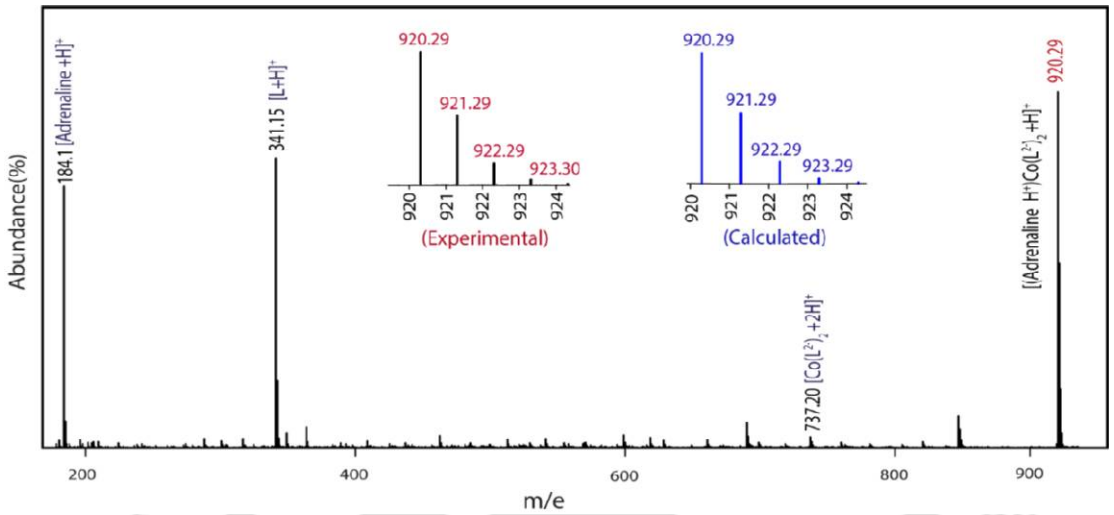

Figure 9. ESI(+) mass spectrum of **2** shows that the adrenaline ammonium ion remains associated with the anionic Co(III) complex in solution.

The prominent peak at m/z = 920.29 corresponds to $\{(Adrenaline.H^+)\ [Co(L^{o\text{-}ValTryp})_2] + H\}^+$ observed in the ESI-Mass (+ve) spectrum of **2** suggests the existence of host-guest binding in the solution.

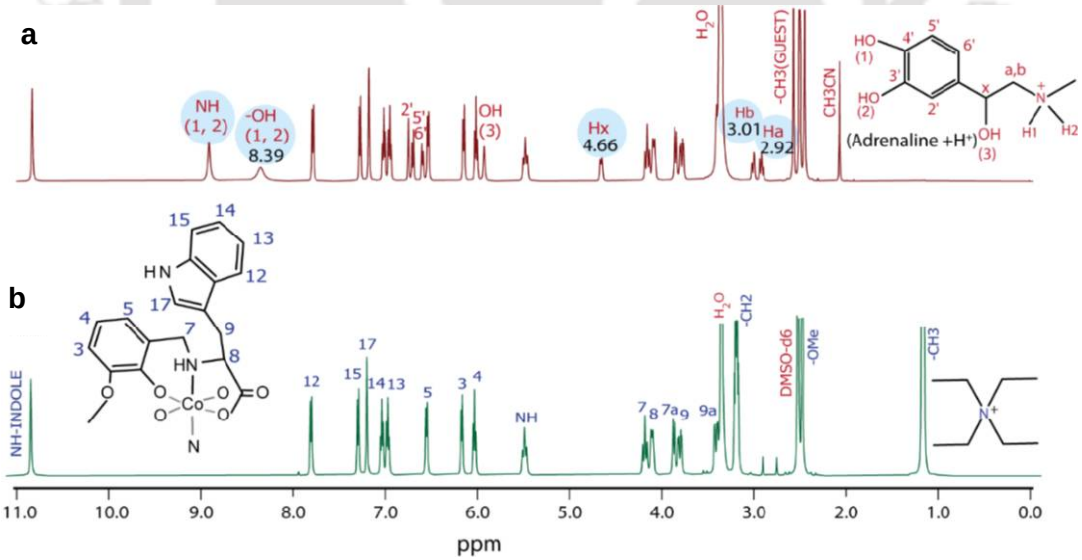

Figure 10. ^1H NMR spectra (500 MHz, DMSO-d_6) of $(Et_4N)[Co(L^{O\text{-}ValTryp})_2]$(a) and adrenaline ammonium ion bound Co(III) complex (b).

The ^{1}H NMR spectrum of **2** showed sharp and well-resolved signals. The intensity ratio also confirmed that the $[Co(L^{O\text{-ValTryp}})_2]^-$ complex anion and the adrenaline ammonium ion exist as a 1:1 host-guest adduct in solution. Complex **2** also showed a similar type of ^{1}H NMR spectroscopic change as the other Co(III) complexes reported in part **A** revealed its structural reorganization in the solution. As the crystals of the complex could not be formed, we could not determine which isomer of adrenaline ammonium ion (*R* or *S*) has bound in **2**. However, other solution state characterizations showed that our Co(III)-complex anion has bound the adrenaline ammonium ion.

Chapter 6. In Chapter **2**, we observed that $(Et_4N)[Co(L^{O\text{-ValTryp}})_2]$ and $(Et_3NH)[Co(L^{O\text{-ValTryp}})_2]$ are isostructural to their labile Fe(III) analogs. In this chapter, we wanted to see whether labile Fe(III) analogs of the Co(III)-complexes recognizing different amino alcohols (in chapter **5)** exert isostructural arrangements or not, as the ammonium ion of chiral amino alcohol has multiple H-bond donor groups potential for H-bonding with the anionic host complex.

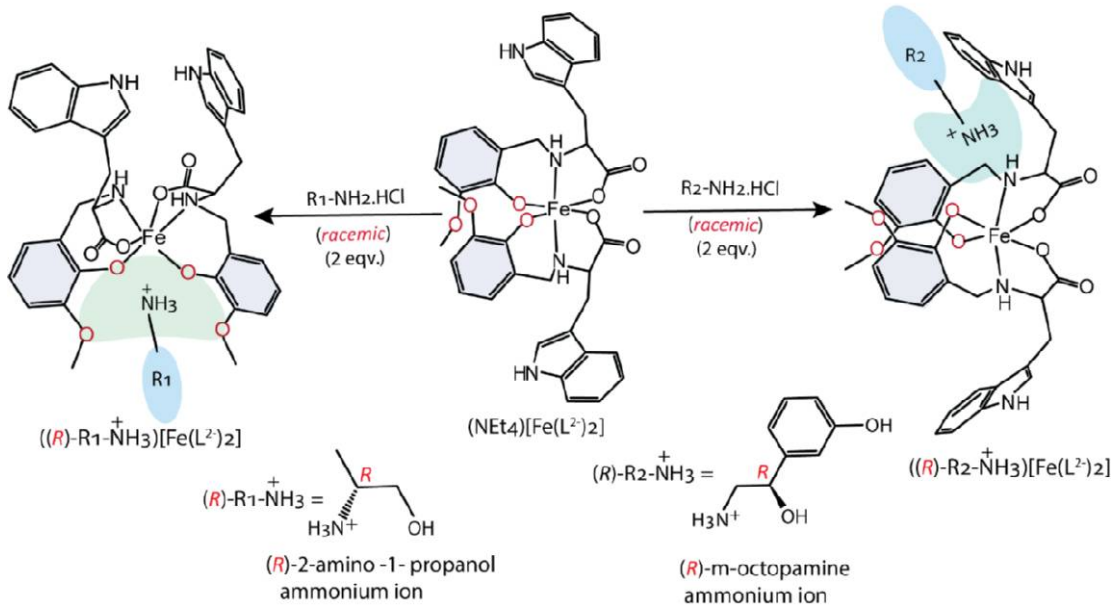

Scheme 6. Syntheses of the Fe(III) complexes with ammonium ion of chiral amino alcohols.

To investigate this, we have synthesized their kinetically labile Fe(III) analogs (Scheme 6). It exerts new structural arrangements to recognize different chiral guests. The solid-state structural analyses of the Fe(III) complexes showed that the $[Fe(L^{O\text{-}ValTryp})_2]^-$ complex anion changed its shape from a meridional to a facial arrangement to recognize the (*R)*-2-amino-1-propanol ammonium ion from its racemic analog. A similar structural change also occurred for recognizing (*S)*-2-phenyleglycinol ammonium ion. Whereas, to recognize *(R)*-norphenylephrine (or *m*-octopamine) from its racemic mixture, the Fe(III) host complex adapted a new shape where one of the indole units and phenolate ring folded to form a chiral cleft inside the molecule.

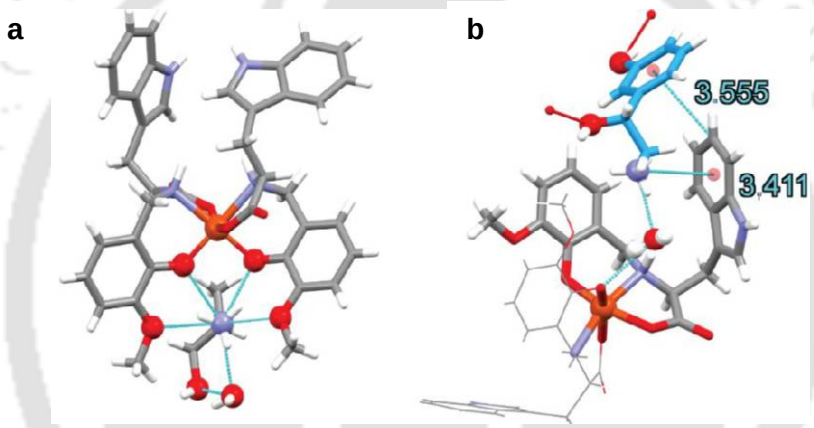

Figure 11. (a) (*R)*-2-amino-1-propanol ammonium ion bound inside the O4 polar pocket in **1**, (b) m-octopamine ammonium ion bound inside the cleft in **2** through non-covalent interactions.

The dynamic nature of the metal-ligand coordination bonds in labile Fe(III) complexes speeds up the structural reorganization process, and the non-covalent interactions between the Fe(III)-anionic host and the chiral guest ammonium ions triggered the drastic structural changes of the metal-complex host.

Conclusions

In conclusion, we used a coordinatively saturated chiral Co(III)-host complex to recognize two different achiral ammonium ions (Et_4N^+ and Et_3NH^+). The only difference between the Et_4N^+ ion and the Et_3NH^+ ion is that instead of four ethyl arms (in the Et_4N^+ ion), the triethyl ammonium ion contains three ethyl arms and one N-H group, which can act as an H-bond donor. That one single H-bond between a kinetically inert anionic Co(III) host complex and an Et_3NH^+ ion could trigger its structural transformation from its extended form to the folded conformation, involving inert metal-ligand coordination bond breaking and reformation in a new arrangement. The structural transformation process is slow due to the kinetic inertness of the Co(III)-complex. Changing the metal center from inert Co(III) to the labile Fe(III) gave isostructural complexes, which showed faster structural transformation due to the more dynamic nature of the metal-ligand coordination bonds in the labile complex. The labile Fe(III)-complex anion also showed drastic structural transformation in the presence of secondary metal cations and bound the secondary cations in a crown ether-like arrangement. The anionic Co(III) complex (exerts a new shape for the recognition of ammonium ions of different amino alcohols, and it) can also recognize one of the enantiomers of different chiral amino alcohols from their respective racemic mixtures. These chiral ammonium ion-containing Co(III) complexes showed structural reorganization in the solution when their solutions were heated. The kinetically labile Fe(III) analogs showed very different structural arrangements to recognize the chiral guest cations through non-covalent interactions. Thus, we showed that for kinetically labile Fe(III) complex, non-covalent interactions are sufficient to modify the structure of the anionic host to recognize different guest cations but insufficient to do the same for an inert Co(III) complex without extra energy.

Contents

V. Chapter 5. Recognition of biogenic chiral amino alcohols using anionic Co(III)-host

Chapter 1

1.1 Introduction

In biology, receptor molecules play a crucial role in the functioning of living organisms by recognizing and responding to specific chemical signals or molecules in their environment by changing the shape, size, and conformation of their binding sites. This ability of receptors to adapt their shape, size, and conformation to bind specific ligands is essential for various physiological processes, including neurotransmission, hormone signaling, immune responses, and many others, ultimately sustaining life.[1,2] In many of these biological recognition processes, the configurational changes of the receptor molecules are triggered by several non-covalent interactions between substrate molecules and receptor binding sites.[3–5] For example, the highly polar adrenaline molecule is efficiently bound to the natural G-protein coupled receptors through various non-covalent interactions, which trigger structural change in the transmembrane helices of the receptor.[6]

Designing stimuli-responsive synthetic molecular systems is challenging but important for understanding these sophisticated biological functions. In the past two decades, several synthetic organic receptor molecules, polymers, and assemblies have been reported that can switch from one structural arrangement to another in response to different external stimuli.[7–13] In most cases, structural change or rearrangement occurs by introducing responsive groups into the host structure through chemical or covalent bond formation. For example, photo-responsive synthetic receptors are obtained by functionalizing it with groups such as azo (N=N), imine (C=N), vinyl (C=C), anthracene, and hydrazones as these groups are capable of photochemical reaction.[14] Metal-ligand coordination bond, weaker than the C-C bond, can reversibly and dynamically form and dissociate. This important feature of metal complexes can be useful in constructing different shape adaptive molecular systems, like metal-organic cages (MOCs)[41-45], metallopeptides[47,48],

and metal-helicates[46,50,51], which offer dynamic conversion of their molecular shapes in response to external stimuli.

In the following, we compiled the literature on the host-guest complexes. We focused on hosts that (i) incorporate metal ions as a structural element, (ii) undergo structural changes upon guest binding, and (iii) recognize small chiral or achiral guest molecules. Some of these hosts are large cages formed out of small organic molecules coordinated to metal ion(s). These are capable of trapping molecules inside the cage. These metal ions are coordinatively saturated and do not participate in guest binding. Others have relatively open structures with available binding sites on the metal. We choose the examples where the host complexes showed structural changes either as a result of guest binding or in the presence of other external stimuli.

1.2 Literature Survey

1.2.1 Metal-organic cages where metals do not have a vacant site

Three-dimensional (3D) metal-organic cages, obtained from the spontaneous organization of metal ions and organic ligands, having well-defined shapes and cavities found used in molecular recognition[15–22], chemical sensing[23–26], gas storage[27–31], molecular separation[32,33], catalysis[34–37], and drug delivery[38–40]. Due to the reversibility of ligand→metal dative connection in MOCs, they can exert dynamic structural transformation in response to different external stimuli- like light, heat, pH, and neutral/charged guest molecules. In 1999, Raymond and co-workers published one of the first observations of guest-induced structural transformation of a triple helicate to a tetrahedral cage complex.[41] They have shown that the reaction of three equivalents of a bis-catecholamine derivative with two equivalents of $[M(acac)_n]$ (M = TiO, Ga; n = 2, 3) in the presence of KOH produced the triple helicate of the respective metal-ligand assembly. Using

Me_4NOH instead of KOH while synthesizing, they afforded the tetrahedral cages. Again, the Ga(III)-triple helicate solution in D_2O, upon treatment with an excess amount of Me_4NCl, transformed into the same tetrahedral cage complex. (Fig. 1.1A). The author concluded that the strong host-guest interactions between the anionic cage and cationic Me_4N^+ drive the transformation of anionic triple helicates into entropically unfavoured tetrahedrons. In another example, Fujita *et al.* have shown that the reaction of $[(en)Pd(NO_3)_2]$ with 1,3,5-tris(3,5-pyrimidyl)pyridine ligand formed a trigonal bipyramidal MOC having a composition of $Pd^{II}_{18}L_6$ which showed structural transformation to encapsulate the guest molecules acenapthylene and calix[4]arene.[42] To bind acenapthylene, the parent MOC increased its component composition and showed expansion of its inner cavity. Acenapthylene bound newly formed host-guest

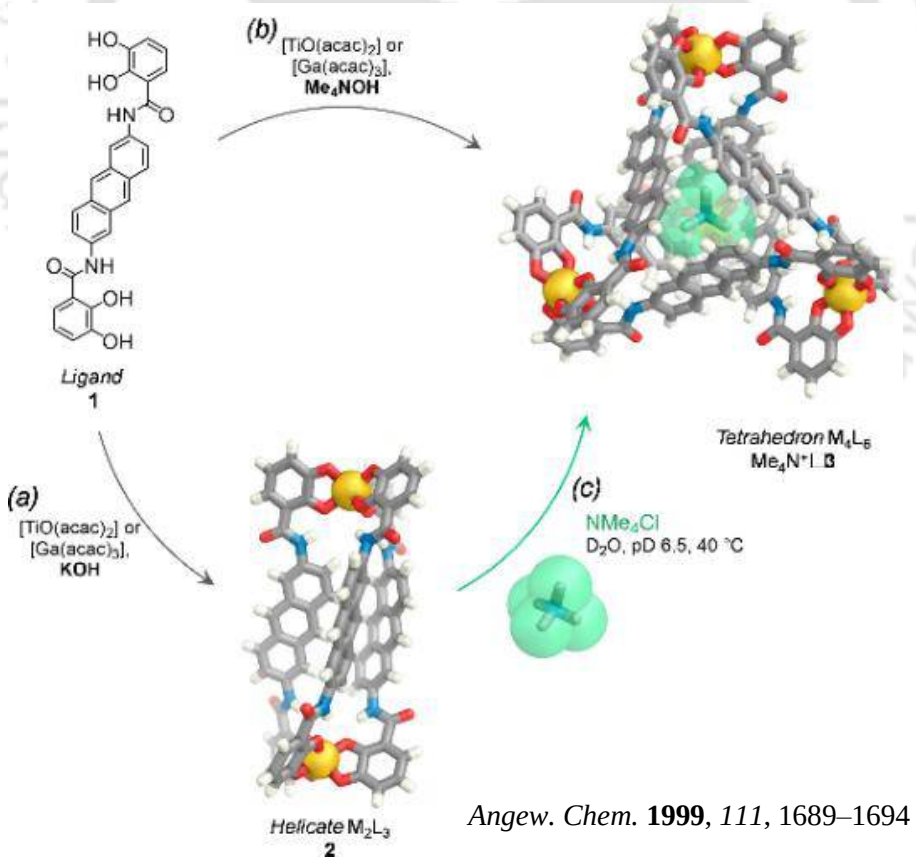

Angew. Chem. **1999**, *111*, 1689–1694

Figure 1.1 Cationic neutral guest-driven structural transformation of anionic MOCs.

complex upon heating at 60˚C, release the guest and reconvert to the parent cage. (Fig. 1.1B) In that case, the dynamic structural conversion of the MOC was triggered by the strong π…π interaction between the electron-rich aromatic regions of the guest and the electron-deficient planes of the MOC.

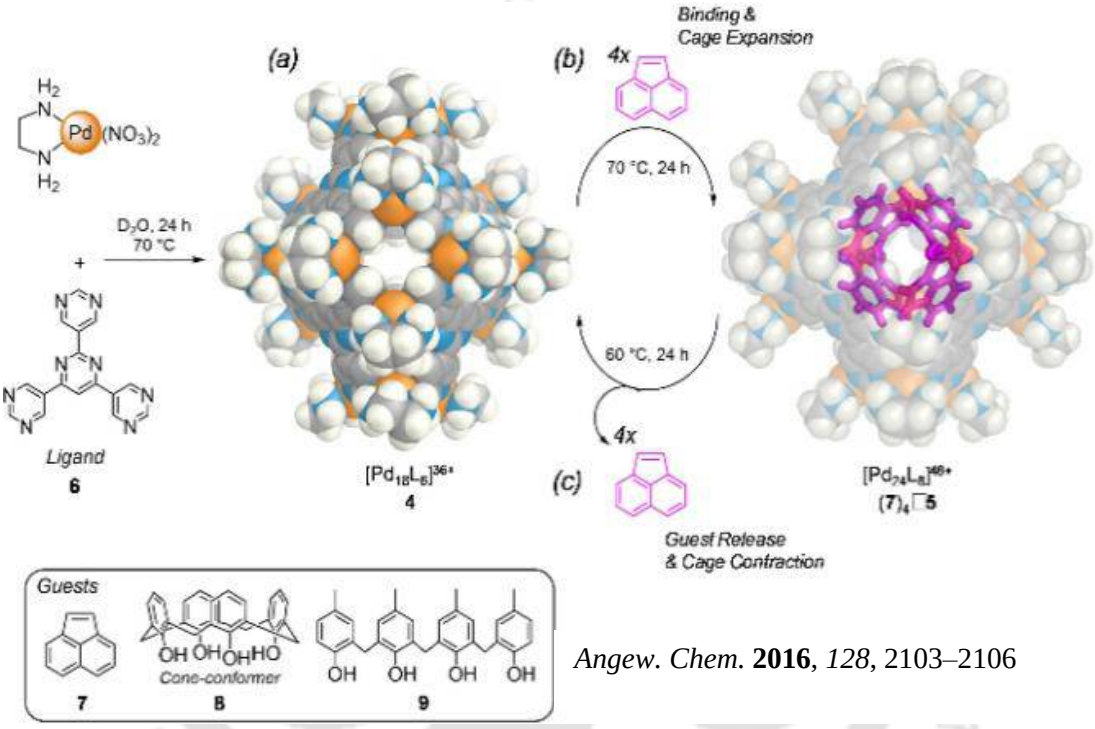

Angew. Chem. **2016**, *128*, 2103–2106

Figure 1.2 The host-guest interactions between $Pd^{II}_{18}L_6$ (host MOC) and neural aromatic guests cause structural transformation of the cage.

Kuroda *et al.* reported an anion-responsive structural transformation of MOC. They have shown that a monomeric $Pd^{II}_4L_6$ capsule synthesized from the self-assembly reaction of $Pd(NO_3)_2$ and 4,4'-(3-pyridinemethoxy)benzophenone transformed into NO_3^- ions encapsulated $Pd^{II}_4L_6$ double cage over the time or heating at 80˚C.[43] When the NO_3^- in the dimeric cage was replaced with another anion like napthalenesulfonate, PF_6^-, and BF_4^- ions, the dimeric MOC transformed into the monomeric cage. The reason for this NO_3^- induced monomeric to dimeric MOC

transformation is that the pockets of the dimeric cage perfectly fit the smaller NO_3^- ions, whereas the other comparatively larger-sized anions like PF_6^- and napthalenesulfonate preferred the monomeric cage as they fit well inside it. (Fig. 1.3)

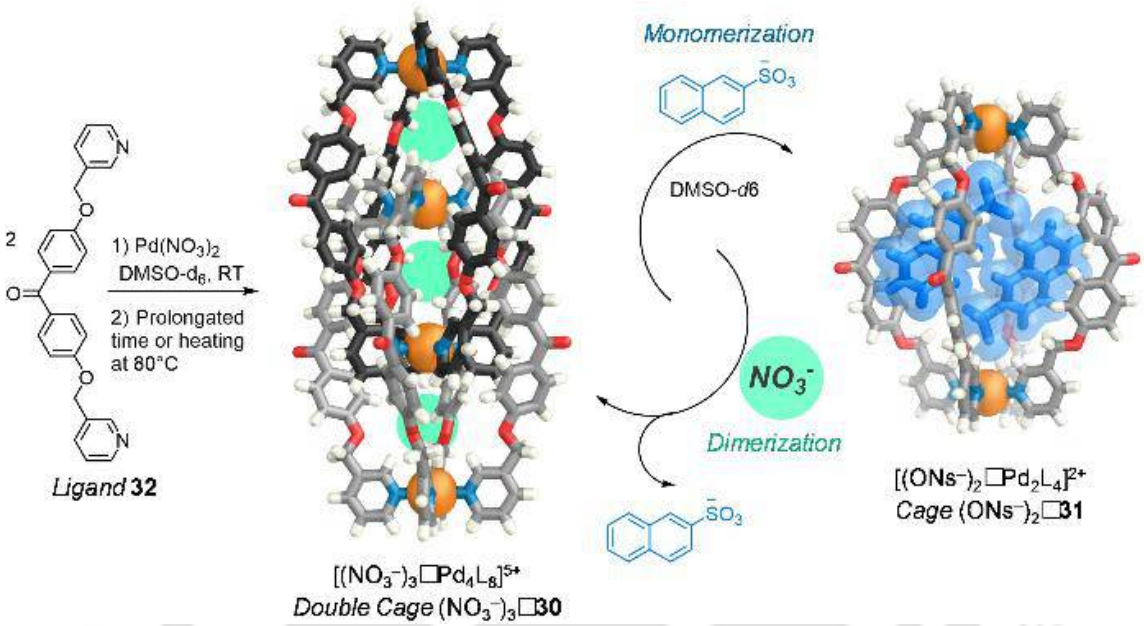

J. Am. Chem. Soc. **2012**, *134*, 10987–10997

Figure 1.3 Anionic guest-induced structural transformations of MOCs.

Shionoya and co-workers have described the multi-stimuli responsive structural transformation of MOCs derived from the assembly of Zn^{II} ions and porphyrin-based ligands.[44] The interconversion between the bowl-shaped $[Zn^{II}_4L_3X_6]$ complex and the tetrahedral capsule-shaped cage $[Zn^{II}_4L_4]$ can be triggered by different external stimuli like Bronstead acid/base, exogenous ligands, solvents, and guest molecules. They have shown that when excess adamantane was added to the solution of the bowl-shaped cage, $[Zn^{II}_4L_3X_6]$, it transformed into the tetrahedral cage ($[Zn^{II}_4L_4]$) due to strong donor-acceptor stacking interactions between the host-guest. The addition of bulky sulfonamide (guest) to the solution of the adamantane-

encapsulated cage, the reverse cage transformation, i.e., from the tetrahedral cage ($[Zn^{II}_4L_4]$) to the bowl-shaped cage transformation ($[Zn^{II}_4L_3X_6]$) occurred. (Fig. 1.3)

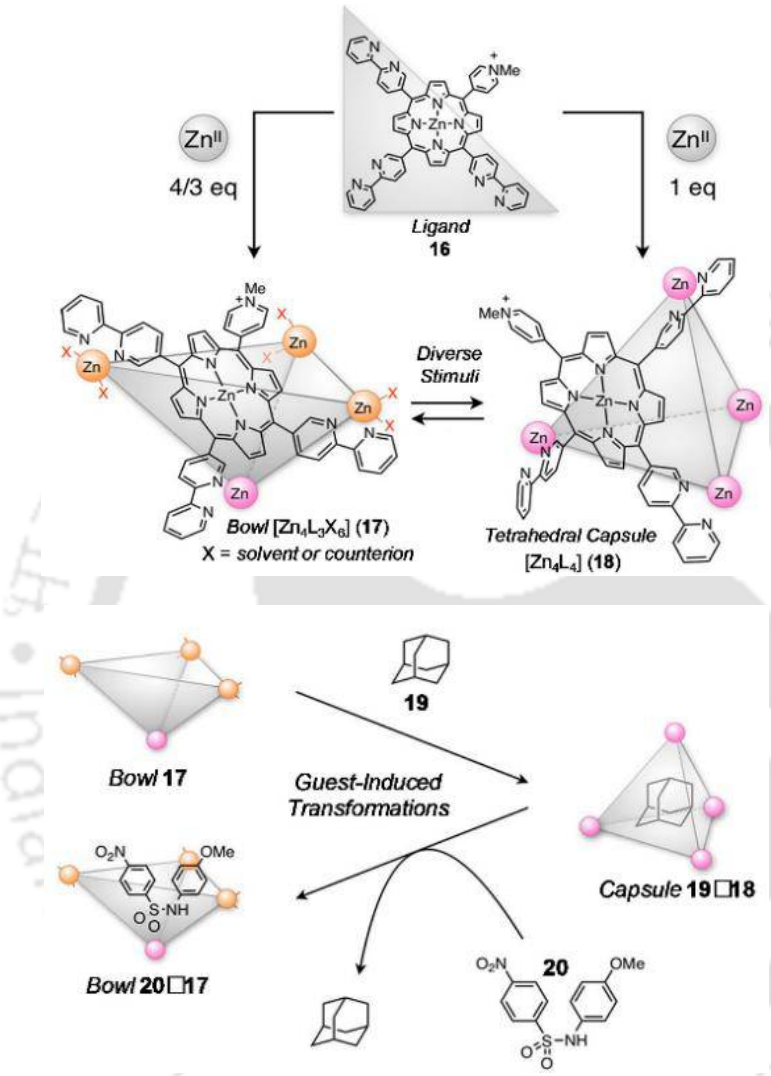

J. Am. Chem. Soc. **2020**, *142*, 407–416

Figure 1.4 Neutral guest-induced structural transformations of MOCs.

Recently, Sun group has reported chiral and achiral guest-driven structural changes in lanthanide-organic cages.[45] They've demonstrated that tetrahedral hosts of the Ln_4L_4 type (where Ln = Eu^{III} or Tb^{III} and L = tris-tridentate ligands) undergo a structural transformation to adjust the size of

their inner cavity in response to guest molecules. This adaptation is achieved by leveraging the flexibility in coordination geometry exhibited by f-elements.

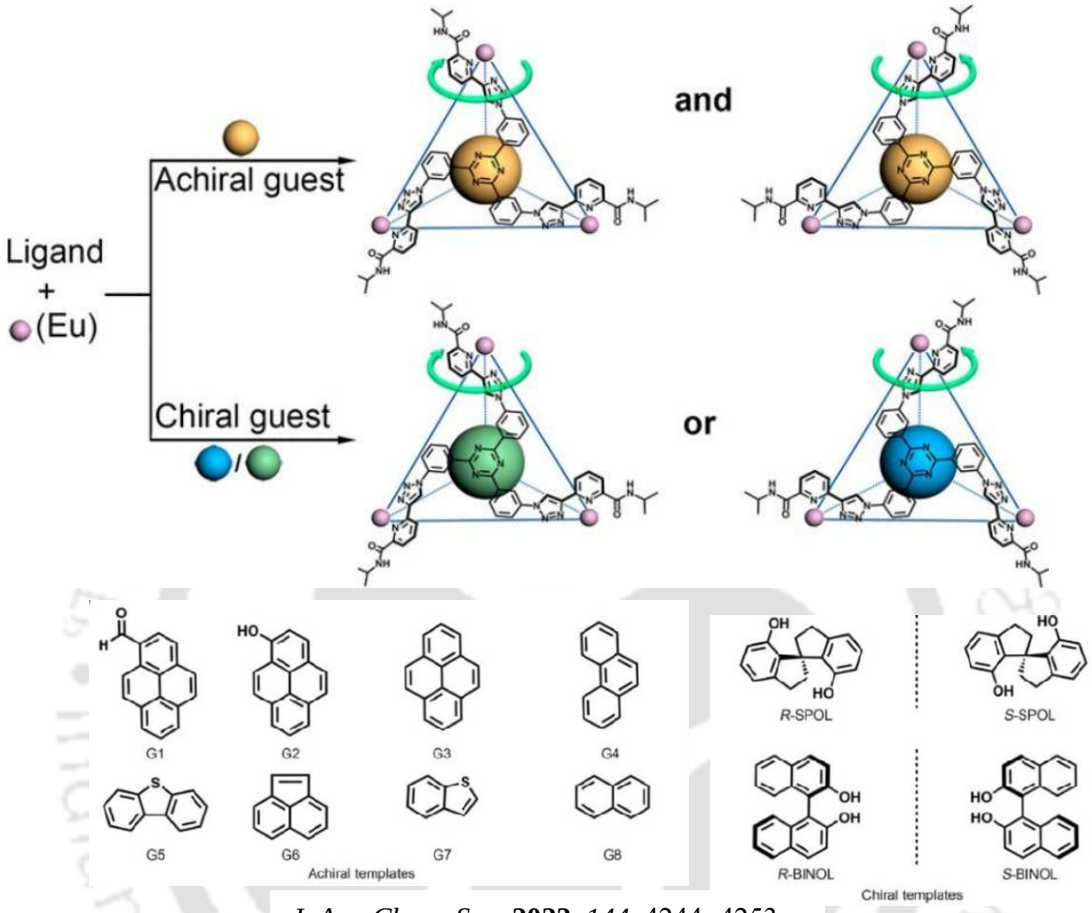

J. Am. Chem. Soc. **2022**, *144*, 4244−4253

Figure 1.5 Achiral and chiral guest-driven structural transformation of lanthanide organic cages.

1.2.2 Hosts having a binding site on the metal

Coordination bonds formed between a metal ion and ligands exhibit dynamic attachment and detachment properties that can be used in constructing molecular machines. These molecular machines can perform various functions by undergoing controlled structural changes in response to external stimuli such as pH, temperature, or the presence of specific molecules.

Canary and Zahn have reported redox-triggered structural dynamics for the copper complexes. Using the oxidation state-dependent coordination preferences of copper ions, i.e., the binding

affinity of Cu(II) ion to the hard donor like oxygen, whereas Cu(I) prefers to bind soft sulfur donor, they have synthesized Cu(II) and Cu(I) complexes of quinoline-attached (S)-methionine ligand having opposite helicity.[46] In the Cu(I) complex, the metal center is coordinated with the sulfur atom of the methionine side arm, whereas in the Cu(II) complex, carboxylate oxygen is coordinated to the Cu(II)-center. Under electrochemical conditions, these two copper complexes switched from one structural arrangement to another.

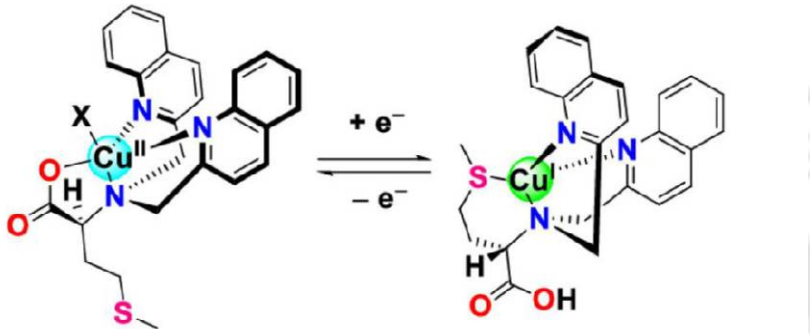

Science **2000,** *288,* 1404-1407

Figure 1.6 Redox-triggered helicity inversion of copper complexes.

Miyake *et al.* reported the helicity inversion of a helical labile Co(II)-complex with a chiral tetradentate ligand containing amide linkage triggered by nitrate anion (NO_3^-).[47] The reaction of the chiral ligand and $Co(ClO_4)_2 \cdot 6H_2O$ gave *Λ* -isomer of the Co(II)-complex, which rapidly converted into *Δ*-isomer of the complex in the presence of excess nitrate anion. The single crystal structure of the *Δ*- isomer revealed that this *Λ*→ *Δ* conversion is driven by the nitrate coordination with the Co(II) center as well as the formation of hydrogen bonding between another nitrate anion and amide NH groups of the ligand. However, in polar solutions like methanol or aqueous solution, dissociation of the nitrate ion from the *Δ*-form of the complex occurred due to less favorable nitrate binding and weaker hydrogen bonding between the NH groups and the nitrate anion and the complex only exist in *Λ* -form. Later, they reported multi-stimuli responsive multiple structural conversions of Co(II) complexes with a bis alanine ligand having

dimethoxyphenyl groups.[48] The extended *Λ*-form of the Co(II)-complex (ext- *Λ*-Co(II) complex) showed nitrate anion-induced chirality inversion and form extended *Δ*-Co(II)-complex (ext- *Δ*-Co(II)-complex. NO_3^-). Deprotonation of the amide NH groups present in extended *Λ*-Co(II)-complex using triethyl amine or proton sponge gave folded *Λ*-Co(II)-complex (fold-*Λ*-Co(II)-complex) where two deprotonated secondary amide groups and two terminal methoxy groups coordinated to the Co(II)-center of the complex. The fold- *Λ*-Co(II)- complex transformed into ext-*Λ*-Co(II)- complex by its protonation using trifluoromethanesulfonic acid. The fold-*Λ*-Co(II)-complex can also converted to ext-*Δ*-Co(II)-complex. NO_3^- when acid and nitrate anion were added. One electron oxidation of fold-*Λ*-Co(II)- complex gave fold- *Λ*-Co(III)- complex, which did not respond to external stimuli as Co(III)-center is kinetically inert. That inert fold-*Λ*-Co(III)-complex again allowed structural transformation in response to acid or NO_3^- only when the Co(III) center was reduced to Co(II).

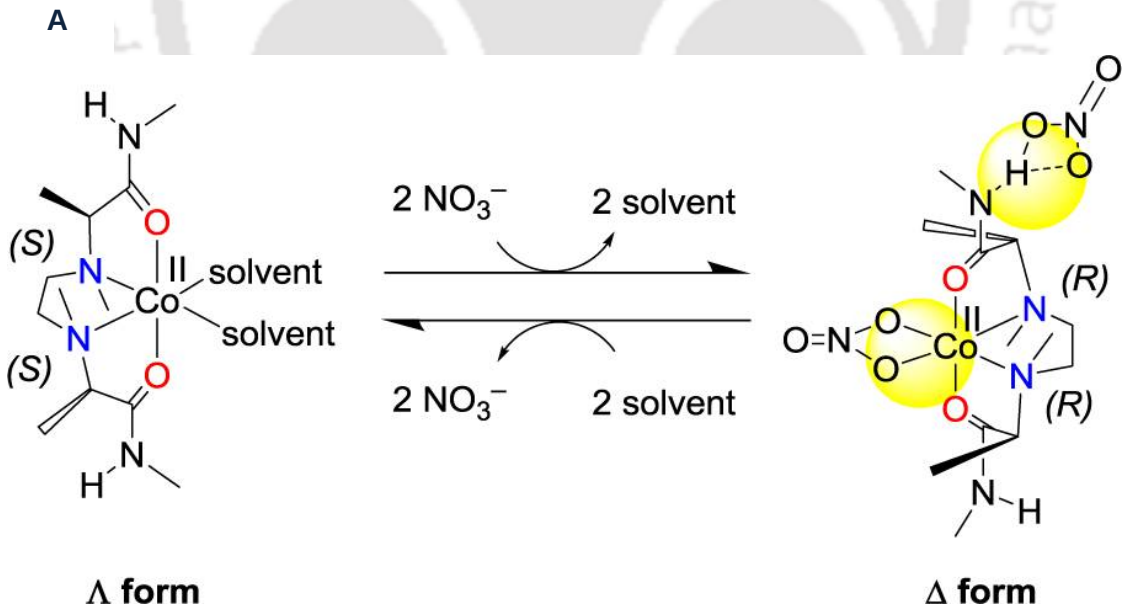

J. Am. Chem. Soc **2008**, *130*, 792–793

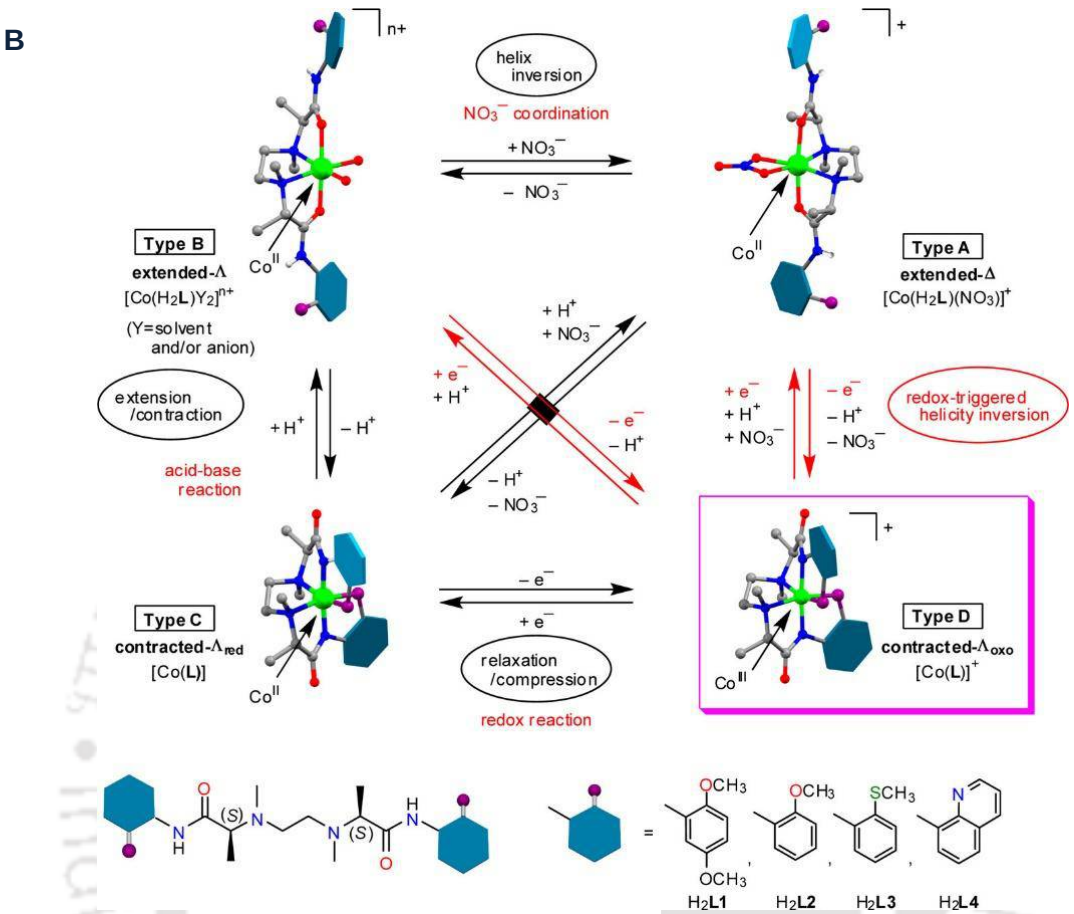

Inorg. Chem. **2016**, *55*, 633−643

Figure 1.7 Nitrate anion (A), Acid/base, and redox (B) triggered the multistate structural transformation of the cobalt complexes.

Akine and Nabeshima have investigated the helicity inversion of Zn_3La complexes with a ligand system that contains a chiral ethylenediamine unit attached to two benzocrown rings.[49] They have used these metal-ligand complexes to recognize diammonium guests with varying chain lengths. $Zn^{II}_3La^{III}$ complex system recognizes shorter diammonium guests H_3N^+-$(CH_2)_n$-NH_3^+ (n = 4, 5 or 6) in *P*-helical structural arrangement while for the recognition of diammonium ion with longer aliphatic chain it adopts *M*-helical structure. In another report, the Nabeshima group has also described the multi-sequential helicity inversion of the trinuclear Zn(II) complex of chiral hexaoxime ligand through the exchange of secondary metal ions.[50] The right-handed helical

structure of the trinuclear Zn(II) complex inverted to left-handed in the presence of two more equivalents, Zn(II)-ion. The helical direction of the structure was inverted further in a stepwise manner, first transitioning from left-handed (*M*) to right-handed (*P*) structures through the addition of Ba(II) cation and then reversing this transition back to left-handed structures by introducing La(III) cation

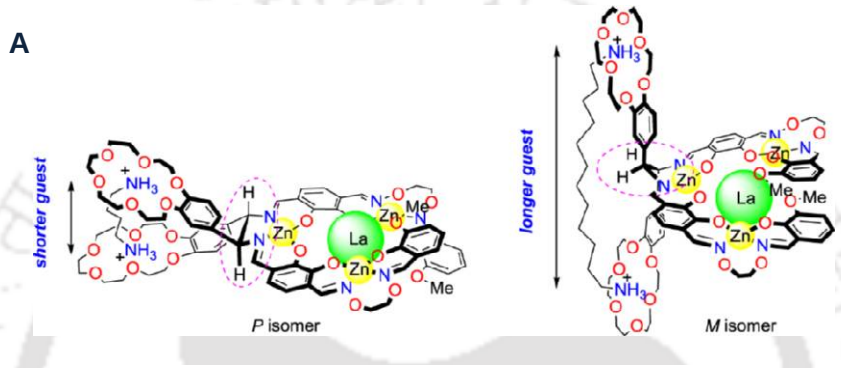

J. Am. Chem. Soc **2011**, *133*, 13868–13871

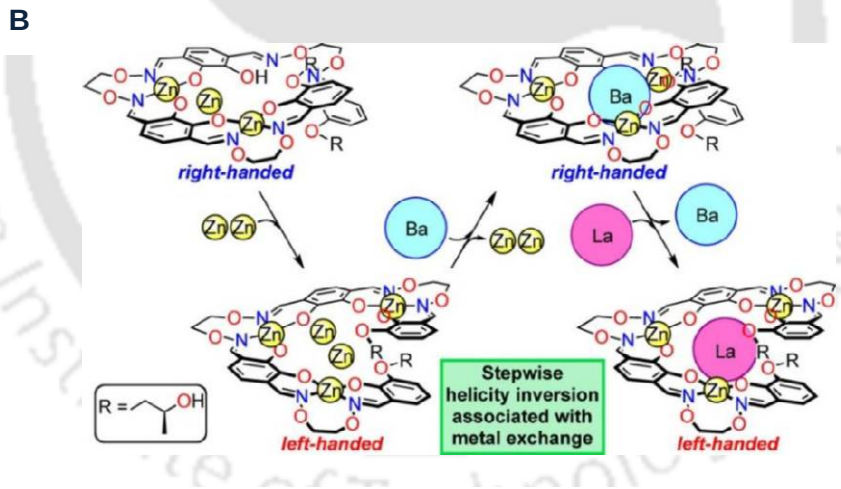

J. Am. Chem. Soc **2013**, *135*, 12948–12951

Figure 1.8 (A) Guest-induced helicity inversion of Zn_3La complex**; (**B) Stepwise multi-sequential helicity inversions of a hexaoxime–metal helicate having chiral salen units.

In another notable example, Akeine and coworkers synthesized triple-helical Co(III) metallocryptand where each of the Co(III) centers has two guest-accessible axial coordination sites.[51] When these axial coordination sites are occupied by achiral guest amines like dimethyl

amine or piperidine, the Co(III)-metallohelicate could exist in a mixture of left-handed and right-handed amine-bound metal helicates. But by replacing these achiral amines with suitable chiral amines, the Co(III)-helicate exists either in pure left-hand or pure right-handed helicate form (*P*), depending upon the chirality of the guest amines. When "*S*" amines coordinate to the axial positions of the Co(III) centers, the metal-helicate preferably exists in right-handed form. Replacing "*S*" amines with "*R"* isomers, the structure of the metal helicate transformed into its left-handed (*M*)form.

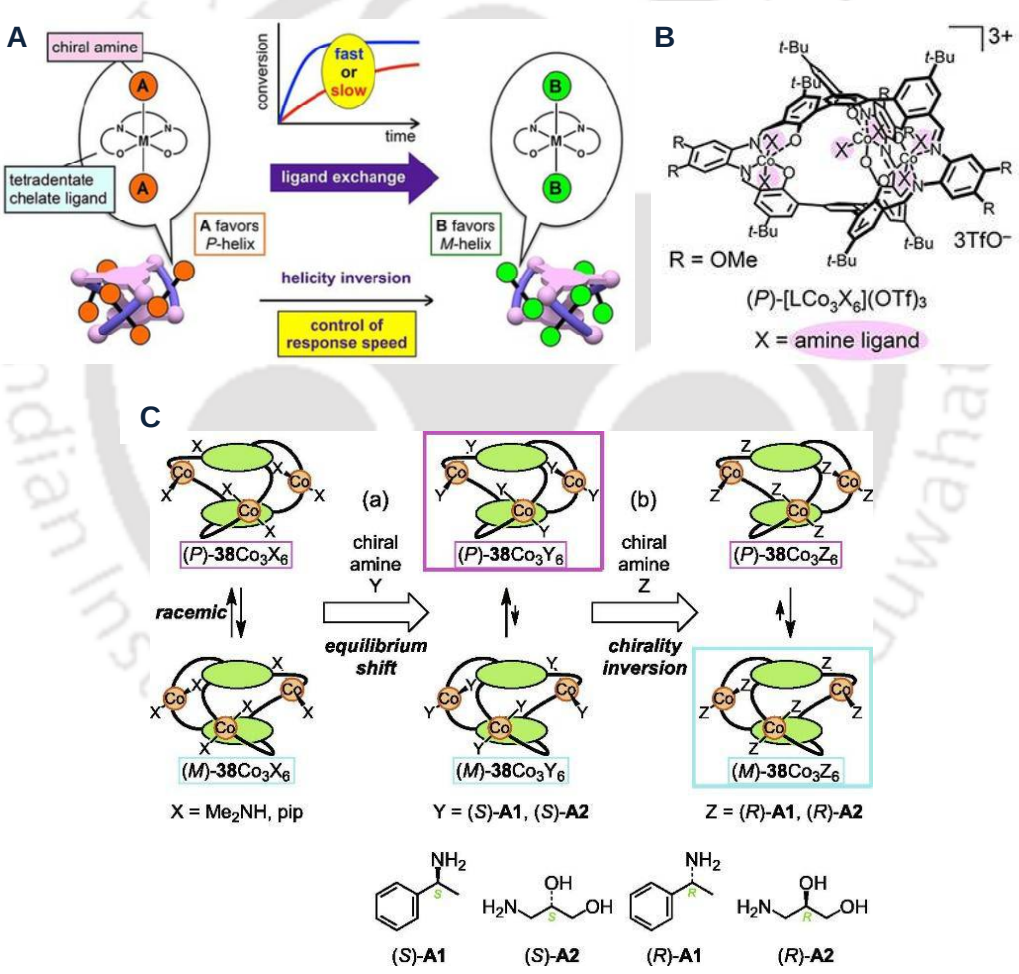

*Chem. Eur. J.***2019**, *25*, 2962 –2966

Figure 1.9 (A) Concept of ligand exchange indued helicity change**; (**B) amine bound Co(III)-metallocryptand and (C) helicity transformation of the metallocryptand by amine exchange at Co(III) centers.

1.2.3 Rigid metal-complex host for chiral guest recognition

Several examples in the previous two sections used chiral guests, including chiral amines. Chiral amines and amino alcohols play important roles in biology.[52] Especially many of the chiral amino alcohols, such as octopamine or adrenaline, function as neurotransmitters.[53] In these chiral systems, only one enantiomer functions as an active agent, while the other does not.[54] In biology, the recognition of these chiral molecules functions through non-covalent interactions. Researchers have approached the recognition and separation of enantiomers by employing various synthesized hosts like large organic receptors, metal-organic frameworks, etc.[55,56] In most cases, the molecular-level understanding of these recognition processes is limited to molecular modeling due to the difficulty in the structural characterization of the receptor molecules. For example, Kubo and co-workers demonstrated that the chirality of an amino alcohol resulted in distinct color changes upon its interaction with a large chiral host.[57] Although the receptor's characterization relied on NMR techniques, the recognition mechanism was proposed based on molecular modeling.

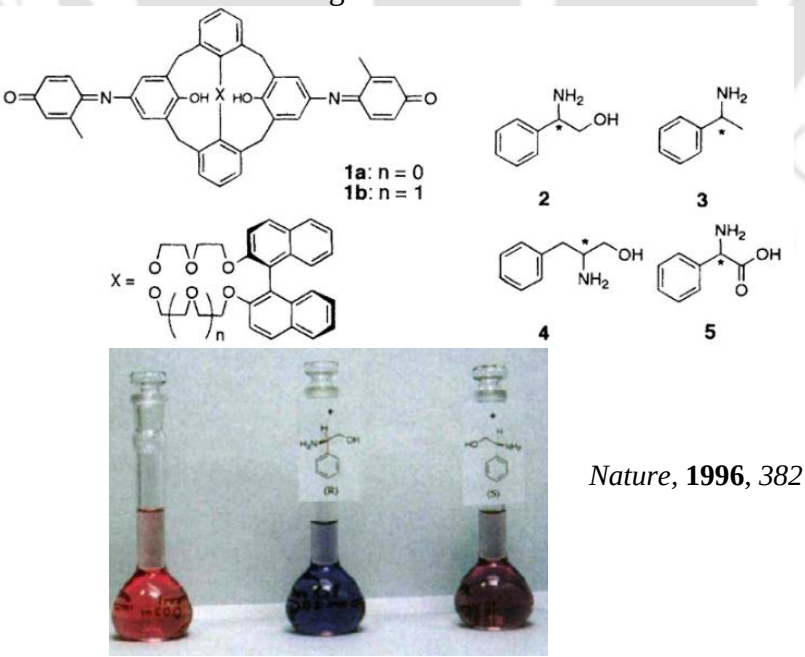

Nature, **1996**, *382*

Figure 1.10 Visible difference between enantiomers after binding with the chiral host.

The low-molecular-weight rigid host would, in principle, facilitate structural characterization, but it is challenging to accommodate three different recognition sites within a small host. For the first time, Kim and Co-workers recognized isomers of alanine using a chiral Co(III) complex, showing that it was possible to study molecular recognition mechanisms in a structurally characterized host-guest adduct owing to the rigidity.[58] But in the isolated crystals of Co(III) complex with the tetradentate ligand, both D- and L-alanine were in a ratio of 70:30.

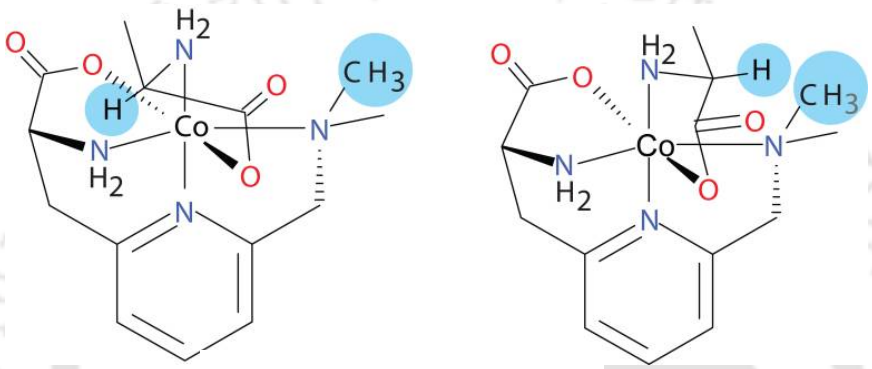

Nature, **1996**, *401*, 254.

Figure 1.11 Different interactions in Co(III)-complex bound D and L-alanine.

Earlier, our group reported that L-histidine derived ligand-based anionic binuclear Ni(II) metal complex host recognized chiral amines and amino alcohols as guests. The guest molecules are bound to the host complex through several noncovalent bonding interactions.[59,60]

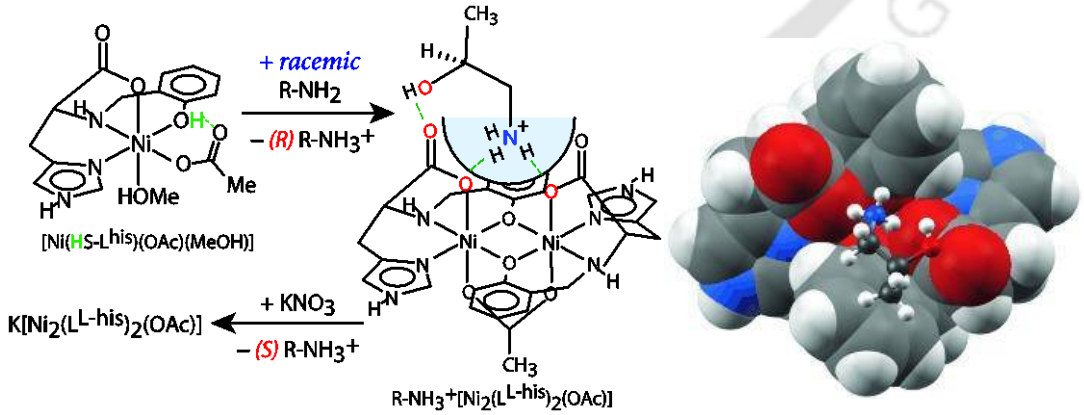

Chem. Eur. J. **2010**, *16*, 5004 – 5007

Figure 1.11 Binuclear Ni(II)-host complex recognizing chiral amino alcohol through noncovalent interactions.

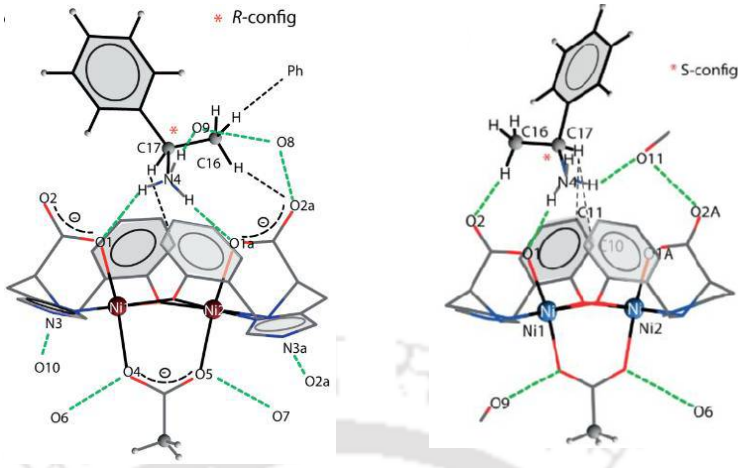

Cryst. Growth Des. **2014**, *14*, 3958−3966

Figure 1.12 Binuclear Ni(II)-host complex recognizing chiral amines through noncovalent interactions.

Our group also synthesized another anionic binuclear Ni(II) host complex using a methionine-derived tetradentate ligand and employed it to recognize 1-phenylethylamine isomers.[61]

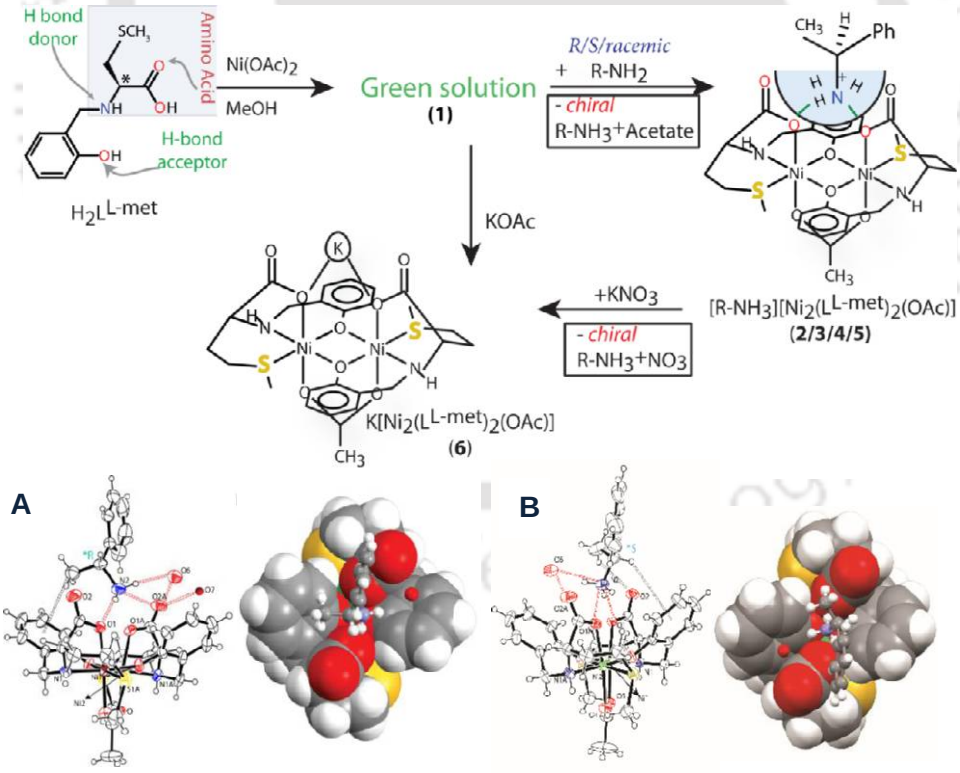

Inorganica Chim. Acta, **2019**, *486*, 367–376

Figure 1.13 Recognition of (*R*)- 1-phenylethylamine (A) and (*S*)- 1-phenylethylamine using metal complex host.

Replacing the stronger imidazole…carboxylate intermolecular H-bond, present in the above-mentioned host-guest system, increases the weak C-H…π interactions between the guest amines and the binuclear Ni(II)-complex of methionine derived ligand.

1.3 Conclusions from the literature survey

From the literature survey, we made some observations:

(i) The large cages (Section 1.2.1) showed structural changes for suitable guest recognition without altering the metal coordination environment. They mostly have relatively inert M-L coordination bonds, stabilizing their cage-like architectures. One exception is the use of a labile Zn(II)-based cage by Shionoya and co-workers (Fig. 1.4).[44] All these cages function as hosts by trapping guest molecules through π-π and other non-covalent interactions. Hardly any example where the relatively stronger H-bonded interactions were used to hold the trapped molecule.

(ii) Many metallo-hosts having vacant sites (Section 1.2.2) showed structural change upon guest binding.[47,50,51] In others, structural change occurred in the presence of different external stimuli (redox, heat, pH, acid-base).[46,48,49] No such system is reported where non-covalent host-guest interaction could trigger a drastic structural change of the kinetically inert host complex.

(iii) The rigid metal complex hosts in Section 1.2.3 can bind chiral guest molecules; these metallo-hosts are relatively simple to construct, and it is easier to modulate their functions by modifying functional groups/steric groups in the ligand backbone.

(iv) Both kinetically inert and labile metal ions have been used in the hosts but never both in the same design to check how the inertness/lability affects the recognition.

Lacuna in the literature:

The literature overview showed some of the cage complexes, and metallo-hellicates showed structural changes while binding to chiral guest molecules. The literature revealed that effective

chiral recognition does not require a large cage; even a low molecular weight complex can do it, but the ligand in the complex should contain at least one chiral center. However, the chiral cages containing achiral ligand frameworks (Section 1.2.1) or the achiral metal-helicates (Section 1.2.2) can bind one enantiomer of the chiral guest but did not resolve from the racemic mixture. None of the above examples, other than from our group,[56] showed chiral resolution using a meta-complex host.

1.4 Objectives of this thesis

As the non-covalent interactions play a crucial role in biological substrate recognition, triggering the structural reorganization or conformational changes of the bio-receptors to fit the target substrate, our group is interested in the synthesis and structural characterization of small molecular weight chiral host-guest complexes for a better understanding of the guest recognition mechanism through various non-covalent interactions. Earlier, we demonstrated the recognition of chiral amine and amino alcohols (in the ammonium form) through multiple non-covalent interactions inside the cleft of the rigid binuclear Ni(II) host complex of amino acid derivatives. Though the structural characterization of those host-guest complexes unraveled the contribution of individual factors responsible for the chiral recognition within the host, the paramagnetic nature of the chiral host-guest complex restricted us from unveiling their identity in the solution. In this thesis,

(i) We redesigned the chiral ligand framework using L-tryptophan and o-vanillin. This combination was not used before. The first one introduced an H-bond capable indole, and the other one added an additional -OMe. We used Co(III) metal ion to use NMR as a probe in solution. The use of trivalent metal ions would make the complex anionic. This has not been

done previously. The flexible arms of L-tryptophan and having multiple hydrogen-bonding (H-bond) sites can be utilized to bind a series of achiral and chiral ammonium cations.

(ii) By studying the structure of these host-guest complexes, we aim to deepen our understanding of how various H-bond donor sites in guest molecules influence substrate recognition mechanisms.

(iii) The research will focus on synthesizing kinetically inert Co(III) complexes to facilitate the use of NMR spectroscopy in probing host-guest interactions in solution.

(iv) Additionally, chiral Fe(III) analogs will be synthesized to investigate the impact of metal center lability on host-guest recognition processes (see Section 1.3 (iv)).

References

(1) Boehr, D. D.; Nussinov, R.; Wright, P. E. *Nat Chem Biol* **2009**, *5* (11), 789–796.

(2) Fatima, S.; Boggs, D. G.; Ali, N.; Thompson, P. J.; Thielges, M. C.; Bridwell-Rabb, J.; Olshansky, L. *J. Am. Chem. Soc.* **2022**, *144* (47), 21606–21616.

(3) Phillips, R. *The Molecular Switch: Signaling and Allostery*; Princeton University Press, 2020.

(4) Pearcy, A. C.; Crowley, J. D. *Chemistry A European J* **2023**, *29* (21), e202203752.

(5) Liu, Q.; He, X.; Tao, J.; Tang, H.; Liu, Z. *ChemNanoMat* **2021**, *7* (1), 1–1.

(6) Ring, A. M.; Manglik, A.; Kruse, A. C.; Enos, M. D.; Weis, W. I.; Garcia, K. C.; Kobilka, B. K. *Nature* **2013**, *502* (7472), 575–579.

(7) Pedrini, A.; Marchetti, D.; Pinalli, R.; Massera, C. *ChemPlusChem* **2023**, *88* (12), e202300383.

(8) Wu, W.; Chen, K.; Wang, T.; Wang, N.; Huang, X.; Zhou, L.; Wang, Z.; Hao, H. *J. Mater. Chem. C* **2023**, *11* (6), 2026–2052.

(9) Nakahata, M.; Takashima, Y.; Yamaguchi, H.; Harada, A. *Nat Commun* **2011**, *2* (1), 511.

(10) Zhao, J.; Zhang, Y.; Sun, H.; Chang, X.; Liu, Y. *Chemistry A European J* **2014**, *20* (46), 15108–15115.

(11) Song, S.; Wang, L.; Su, J.; Xu, Z.; Hsu, C.-H.; Hua, C.; Lyu, P.; Li, J.; Peng, X.; Kojima, T.; Nobusue, S.; Telychko, M.; Zheng, Y.; Chuang, F.-C.; Sakaguchi, H.; Wong, M. W.; Lu, J. *Chem. Sci.* **2021**, *12* (35), 11659–11667.

(12) Morozov, B. S.; Gargiulo, F.; Ghule, S.; Lee, D. J.; Hampel, F.; Kim, H. M.; Kataev, E. A. *J. Am. Chem. Soc.* **2024**, *146* (10), 7105–7115.

(13) Fang, L.; Hmadeh, M.; Wu, J.; Olson, M. A.; Spruell, J. M.; Trabolsi, A.; Yang, Y.-W.; Elhabiri, M.; Albrecht-Gary, A.-M.; Stoddart, J. F. *J. Am. Chem. Soc.* **2009**, *131* (20), 7126–7134.

(14) Yagai, S.; Kitamura, A. *Chem. Soc. Rev.* **2008**, *37* (8), 1520.

(15) Saha, R.; Devaraj, A.; Bhattacharyya, S.; Das, S.; Zangrando, E.; Mukherjee, P. S. *J. Am. Chem. Soc.* **2019**, *141* (21), 8638–8645.

(16) Kim, T. Y.; Vasdev, R. A. S.; Preston, D.; Crowley, J. D. *Chemistry A European J* **2018**, *24* (56), 14878–14890.

(17) Galan, A.; Ballester, P. *Chem. Soc. Rev.* **2016**, *45* (6), 1720–1737.

(18) Whitehead, M.; Turega, S.; Stephenson, A.; Hunter, C. A.; Ward, M. D. *Chem. Sci.* **2013**, *4* (7), 2744.

(19) Percástegui, E. G.; Ronson, T. K.; Nitschke, J. R. *Chem. Rev.* **2020**, *120* (24), 13480–13544.

(20) Ward, M. D.; Hunter, C. A.; Williams, N. H. *Acc. Chem. Res.* **2018**, *51* (9), 2073–2082.

(21) Amouri, H.; Desmarets, C.; Moussa, J. *Chem. Rev.* **2012**, *112* (4), 2015–2041.

(22) Percástegui, E. G.; Mosquera, J.; Nitschke, J. R. *Angewandte Chemie* **2017**, *129* (31), 9264–9268.

(23) Brzechwa-Chodzyńska, A.; Drożdż, W.; Harrowfield, J.; Stefankiewicz, A. R. *Coordination Chemistry Reviews* **2021**, *434*, 213820.

(24) Yao, Y.; Zhou, Y.; Zhu, T.; Gao, T.; Li, H.; Yan, P. *ACS Appl. Mater. Interfaces* **2020**, *12* (13), 15338–15347.

(25) Dey, N.; Haynes, C. J. E. *ChemPlusChem* **2021**, *86* (3), 418–433.

(26) Plajer, A. J.; Percástegui, E. G.; Santella, M.; Rizzuto, F. J.; Gan, Q.; Laursen, B. W.; Nitschke, J. R. *Angewandte Chemie* **2019**, *131* (13), 4244–4248.

(27) Park, J.; Perry, Z.; Chen, Y.-P.; Bae, J.; Zhou, H.-C. *ACS Appl. Mater. Interfaces* **2017**, *9* (33), 28064–28068.

(28) Gosselin, A. J.; Rowland, C. A.; Bloch, E. D. *Chem. Rev.* **2020**, *120* (16), 8987–9014.

(29) Valencia-Loza, S. D. J.; López-Olvera, A.; Martínez-Ahumada, E.; Martínez-Otero, D.; Ibarra, I. A.; Jancik, V.; Percástegui, E. G. *ACS Appl. Mater. Interfaces* **2021**, *13* (16), 18658–18665.

(30) Lee, S.; Lee, J. H.; Kim, J. C.; Lee, S.; Kwak, S. K.; Choe, W. *ACS Appl. Mater. Interfaces* **2018**, *10* (10), 8685–8691.

(31) Zhang, X.; Dong, X.; Lu, W.; Luo, D.; Zhu, X.-W.; Li, X.; Zhou, X.-P.; Li, D. *J. Am. Chem. Soc.* **2019**, *141* (29), 11621–11627.

(32) Wu, K.; Li, K.; Hou, Y.-J.; Pan, M.; Zhang, L.-Y.; Chen, L.; Su, C.-Y. *Nat Commun* **2016**, *7* (1), 10487.

(33) García-Simón, C.; Garcia-Borràs, M.; Gómez, L.; Parella, T.; Osuna, S.; Juanhuix, J.; Imaz, I.; Maspoch, D.; Costas, M.; Ribas, X. *Nat Commun* **2014**, *5* (1), 5557. h

(34) Bogie, P. M.; Holloway, L. R.; Ngai, C.; Miller, T. F.; Grewal, D. K.; Hooley, R. J. A *Chemistry A European J* **2019**, *25* (43), 10232–10238.

(35) Martí-Centelles, V.; Spicer, R. L.; Lusby, P. J. *Chem. Sci.* **2020**, *11* (12), 3236–3240.

(36) Hong, C. M.; Bergman, R. G.; Raymond, K. N.; Toste, F. D. *Acc. Chem. Res.* **2018**, *51* (10), 2447–2455.

(37) Morimoto, M.; Bierschenk, S. M.; Xia, K. T.; Bergman, R. G.; Raymond, K. N.; Toste, F. D. *Nat Catal* **2020**, *3* (12), 969–984.

(38) Therrien, B. *Chemistry A European J* **2013**, *19* (26), 8378–8386.

(39) Zheng, Y.-R.; Suntharalingam, K.; Johnstone, T. C.; Lippard, S. J. *Chem. Sci.* **2015**, *6* (2), 1189–1193.

(40) Fang, Y.; Lian, X.; Huang, Y.; Fu, G.; Xiao, Z.; Wang, Q.; Nan, B.; Pellois, J.; Zhou, H. *Small* **2018**, *14* (47), 1802709.

(41) Scherer, M.; Caulder, D. L.; Johnson, D. W.; Raymond, K. N. *Angew. Chem. Int. Ed.* **1999**, *38* (11), 1587–1592.

(42) Wang, S.; Sawada, T.; Ohara, K.; Yamaguchi, K.; Fujita, M. *Angewandte Chemie* **2016**, *128* (6), 2103–2106.

(43) Sekiya, R.; Fukuda, M.; Kuroda, R. *J. Am. Chem. Soc.* **2012**, *134* (26), 10987–10997.

(44) Endo, K.; Ube, H.; Shionoya, M. *J. Am. Chem. Soc.* **2020**, *142* (1), 407–416.

(45) Hu, S.-J.; Guo, X.-Q.; Zhou, L.-P.; Yan, D.-N.; Cheng, P.-M.; Cai, L.-X.; Li, X.-Z.; Sun, Q.-F. *J. Am. Chem. Soc.* **2022**, *144* (9), 4244–4253.

(46) Zahn, S.; Canary, J. W. *Science* **2000**, *288* (5470), 1404–1407.

(47) Miyake, H.; Kamon, H.; Miyahara, I.; Sugimoto, H.; Tsukube, H. *J. Am. Chem. Soc.* **2008**, *130* (3), 792–793.

(48) Sigel, H.; Martin, R. B. *Chem. Rev.* **1982**, *82* (4), 385–426.

(49) Akine, S.; Hotate, S.; Nabeshima, T. *J. Am. Chem. Soc.* **2011**, *133* (35), 13868–13871.

(50) Akine, S.; Sairenji, S.; Taniguchi, T.; Nabeshima, T. *J. Am. Chem. Soc.* **2013**, *135* (35), 12948–12951.

(51) Sakata, Y.; Chiba, S.; Miyashita, M.; Nabeshima, T.; Akine, S. *Chemistry A European J* **2019**, *25* (12), 2962–2966.

(52) (a) Idzko, M.; Sala, A. L.; Ferrari, D.; Panther, E.; Herouy, Y.; Dichmann, S.; Mockenhaupt, M.; Virgilio, F. D.; Girolomoni, G.; Norgauer, J. *Journal of Allergy and Clinical Immunology* **2002**, *109* (5), 839–846. (b) Wolfbeis, O. S.; Li, H. *Biosensors and Bioelectronics* **1993**, *8* (3–4), 161–166. (c) Yanai, K.; Tashiro, M. T *Pharmacology & Therapeutics* **2007**, *113* (1), 1–15.

(53) Rüdiger, M.; Haupts, U.; Moore, K. J.; Pope, A. J. *SLAS Discovery* **2001**, *6* (1), 29–37. (36) Korać, J.; Todorović, N.; Zakrzewska, J.; Žižić, M.; Spasojević, I. *Struct Chem* **2018**, *29* (5), 1533–1541.

(54) Sugawara, Y.; Hara, C.; Aoki, T.; Sugimoto, N.; Masujima, T. *Chem. Senses* **2000**, *25*, 77.

(55) Späth, A.; König, B. *Beilstein J. Org. Chem.* **2010**, *6*.

(56) Chai, H.; Chen, Z.; Wang, S.-H.; Quan, M.; Yang, L.-P.; Ke, H.; Jiang, W. *CCS Chem* **2020**, *2* (6), 440–452.

(57) Kubo, Y.; Maeda, S.; Tokita, S.; Kubo, M. *Nature* **1996**, *382* (6591), 522–524.

(58) Chin, J.; Lee, S. S.; Lee, K. J.; Park, S.; Kim, D. H. *Nature* **1999**, *401* (6750), 254–257.

(59) Sahoo, S. C.; Ray, M. *Chemistry A European J* **2010**, *16* (17), 5004–5007.

(60) Das, C. R.; Sahoo, S. C.; Ray, M. *Crystal Growth & Design* **2014**, *14* (8), 3958–3966.

(61) Das, C. R.; Dutta, T.; Ray, M. *Inorganica Chimica Acta* **2019**, *486*, 367–376.

Chapter 2

H-bond triggered structural transformation of the anionic metal-complex host

2.1 Introduction

Non-covalent interactions like H-bond, CH-π interactions, salt-bridge interactions, etc., play crucial roles in biological substrate recognition processes. These weak interactions trigger the structural reorganization or conformational changes of the bio-receptors to fit the target substrate.[1,2] For example, non-covalent interactions between different stimuli and protein domains often show stimuli-responsive structural transformations[3,4]; acetylcholine binding to the receptor through non-covalent interaction triggers the opening of sodium channels[5]. Getting structural information or bond parameters on these interactions is difficult as many biological systems are not amenable to structural characterization. We use small metal complexes as chiral hosts and study the interactions with chiral guest ammonium ions.[6–8] The role of metal ions is to rigidify the host, avoiding the synthesis of large organic hosts, which are less amenable to structural characterization. Another advantage of using the metal complex-based host-guest system is the metal-ligand coordination bonds are relatively rigid yet dynamic in nature, this dynamic attachment and detachment features of coordination bonds have been applied to synthesize several kinds of metal-ligand assemblies, which showed structural transformation in response to various external stimuli like pH change, charged (anion) or neutral guest molecule recognition, redox reaction at the metal center.[9–15] However, non-covalent interaction induced significant structural adaptation or rearrangement of the synthetic host-guest systems is limited.[16–18]

In this chapter, we have synthesized a chiral, coordinatively saturated anionic bis-Co(III) complex with an L-tryptophan-derived tridentate reduced Schiff base ligand and employed it for the recognition of two structurally similar ammonium ions, Et_4N^+ and Et_3NH^+ respectively, and explored the non-covalent interaction-induced structural transformation of kinetically inert

Co(III)-complex which is specific for the recognition of Et_3NH^+ ion. Also, we have synthesized kinetically labile analogs of these complexes, i.e., Fe(III)-complexes, to investigate how the lability of the metal-ligand coordination bonds affects this structural transformation.

Primary and secondary ammonium ion recognition is extensively explored using neutral crown ethers, cryptands, and related aza macrocycles.[19] Structural information on the recognition of alkylammonium ions is relatively rare.[20–22] In synthetic systems, specific recognition of one between two structurally similar guests through the drastic structural change of the receptor molecule is challenging.

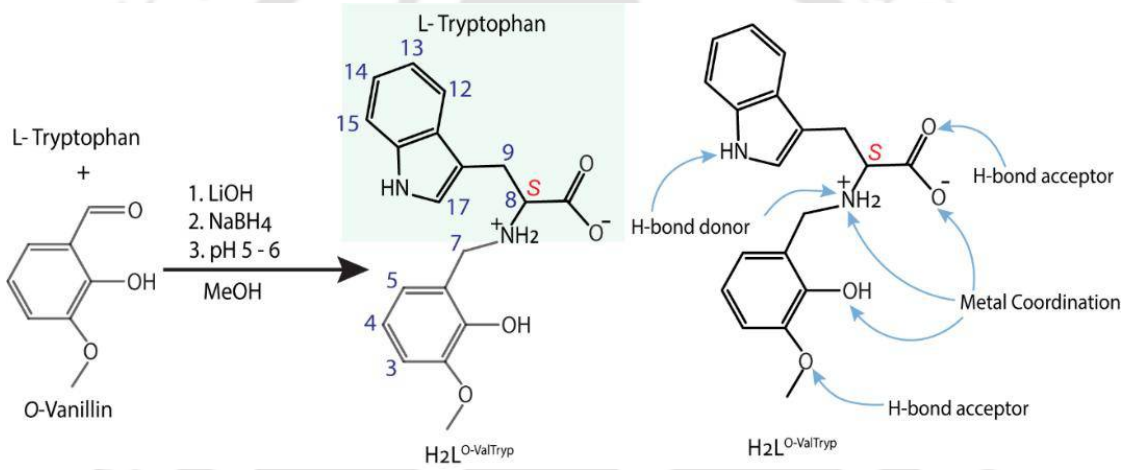

Scheme 2.1 Synthesis of the ligand.

2.2 Experimental Section

2.2.1 Materials and Methods

Solvents and reagents were obtained from commercial sources and used without further purifications unless otherwise asserted. ortho-Vanillin, $Co(ClO_4)_2 \cdot 6H_2O$, $Fe(ClO_4)_2 \cdot 7H_2O$, anhydrous grade *N*, *N*-dimethylformamide, tetraethylammonium hydroxide solution (20 wt. % in H_2O), and tetraethylammonium chloride were purchased from Aldrich Chemical Co., L-tryptophan was purchased from Sisco Research Laboratories Pvt. Ltd, triethylamine was purchased from Finer chemicals Co. The IR spectra were recorded on a Nicolet FT-IR

spectrophotometer with KBr discs in the 4000-400 cm-1 range. UV-visible spectra of the samples were measured with a PerkinElmer Lambda 365^{+} UV/vis spectrometer. NMR spectra were recorded on Bruker 500 MHz. ESI-mass spectra were recorded with a high-resolution mass spectrometer (Agilent 6546 LC/Q-TOF). Circular Dichroism measurements were performed using JASCO-J-1500 CD spectrometer, and CD spectra were analyzed using JASCO spectra manager version 2.0. All the CD spectra were recorded under an inert N_2 atmosphere using HPLC grade DMF as a solvent and a high-precision cell made of quartz SUPRASIL cuvette with a path length of 1 mm.

2.3 Syntheses

2.3.1 Synthesis of the ligand ($H_2L^{O\text{-}ValTryp}$)

At room temperature, L-Tryptophan (3.0 g, 14.7 mmol) and $LiOH{\cdot}H_2O$ (0.616 g, 14.7 mmol) were dissolved in 30 mL of methanol and stirred for 10 min, giving a colorless solution. The methanolic o-vanillin (2.24 g, 14.7 mmol) was added to this solution, and it immediately became yellow-colored. The solution was stirred for 45 min, and then solid $NaBH_4$ (0.667 g, 17.6 mmol) was slowly added to the solution with constant stirring. The yellow-colored solution became colorless within a few minutes, and the reaction mixture was stirred for another 30 min. Then, the solvent was removed using a rotary evaporator, which gave a sticky mass. That sticky solid was dissolved in 10 mL water and acidified by diluting HCl to pH 6-5. A white-colored solid precipitated out and was filtered, washed with water and cold ethanol, and dried under a vacuum desiccator. Yield: 92 %. ^{1}H NMR (CD_3OD, 500 MHz) δ 7.55 (d, 1H, *J* = 8 Hz, H^{12}), δ 7.38 (d, 1H, *J* = 8 Hz, H^{15}), δ 7.19 (s, 1H, H^{17}), δ 7.14 (t, 1H, *J* = 7.5 Hz, H^{14}), δ 6.99 (t, 1H, *J* = 8 Hz, H^{13}), δ 6.85 (d, 1H, *J* = 8 Hz, H^{3}), δ 6.68 (t, 1H, *J* = 8 Hz, H^{4}), δ 6.48 (d, 1H, *J* = 8 Hz, H^{5}), δ 4.04 (d, 1H, *J* = 13 Hz, H^{7}), δ 3.88 (d, 1H, *J* = 13 Hz, H^{7a}), δ 3.86 (dd, 1H, *J* = 4.5, 8 Hz, H^{8}), δ 3.77 (s, 3H, $H^{\text{-}OCH3}$), δ 3.56 (dd, *J* =

4.5/8, 14.5 Hz 1H, H^{9}), δ 3.14 (dd, 1H, *J* = 4.5/8,14.5 Hz, H^{9a}); ^{1}H-^{1}H-COSY was also performed. IR (KBr, cm^{-1}): υ$(COO^{-})_{asym}$ 1607; υ$(COO^{-})_{sym}$ 1400; υ(C-O) 1243; υ(C-H)o/p-ring H 750. m/z (ESI-MS) $\{M+H\}^{+}$, $\{(H_2L^{O\text{-ValTryp}})+H\}^{+}$; calcd: 341.15, found: 341.15.

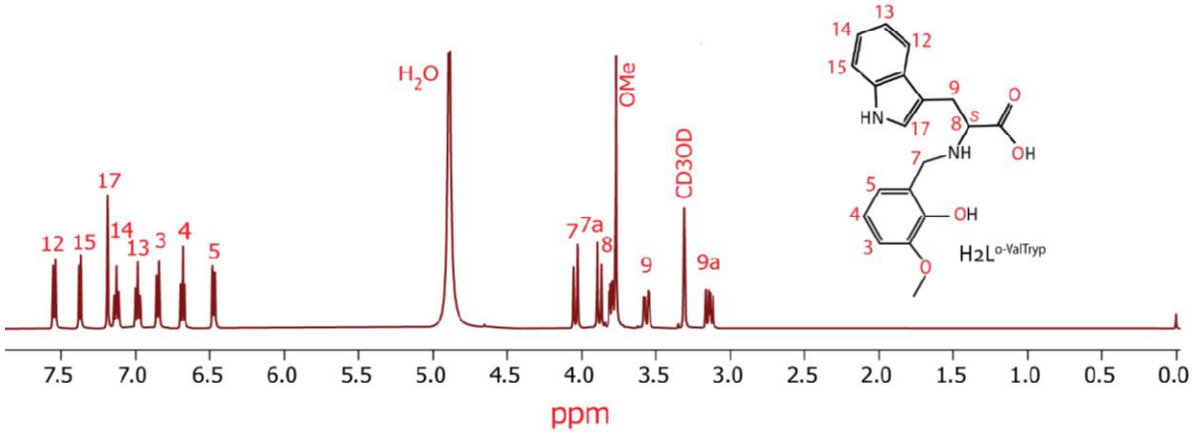

Figure 2.1 ^{1}H NMR spectra of the ligandin (CD_3OD, 500 MHz).

2.3.2 $(NEt_4)[Co(L^{O\text{-ValTryp}})_2]$ (1)

Solid $Co(ClO_4)_2{\cdot}6H_2O$ (0.269 g, 0.735 mmol) was added to the methanolic solution (10 mL) of $H_2L^{O\text{-ValTryp}}$ (0.500 g, 1.47 mmol) and the reaction mixture was stirred for 15 min. The colour of the reaction mixture became pink. After 15 min., tetraethyl ammonium hydroxide solution (2.16 g, 14.7 mmol, 20 wt% in water) was slowly added to the reaction mixture, and the colour of the reaction mixture gradually changed from pink to reddish brown. The reaction mixture was stirred again for six hours at room temperature. Then, the solvent was evaporated using a rotary evaporator to reduce the reaction mixture's volume. DMF was added to it in a proportion of 3:1 (methanol: DMF) and kept in a 50 mL beaker. Diamond-shaped reddish-brown coloured crystals were obtained after 8-10 days of slow evaporation. Crystals were washed with ethyl acetate and diethyl ether and dried under a vacuum. Yield: 72%.

^{1}H NMR (*d*6-DMSO, 500 MHz) δ 10.87 (s, 2H, $H^{NH\ indole}$), δ 7.82 (d, 2H, *J* = 8 Hz, H^{12}), δ 7.30 (d, 2H, *J* = 8 Hz, H^{15}), δ 7.20 (s, 2H, H^{17}), δ 7.04 (t, 2H, *J* = 7 Hz, H^{14}), δ 6.98 (t, 2H, *J* = 8 Hz, H^{13}), δ 6.55 (d, 2H,

J = 7.5 Hz, H^5), δ 6.17 (d, 2H, *J* = 7.5 Hz, H^3), δ 6.03 (t, 2H, *J* = 7.5 Hz, H^4), δ 5.48 (t, 2H, *J* =11 Hz, $H^{NH\ LIGAND}$), δ 4.10 (dd, 2H, *J* = 4.5, 5.5 Hz, H^8), δ 4.17 (t, 2H, *J* = 12 Hz, H^7), δ 3.86 (d, 2H, *J* = 10.5 Hz, H^{7a}), δ 3.79 (dd, *J* = 4.5/5.5, 16 Hz 2H, H^9), δ 3.40 (dd, 2H, *J* = 4.5/5.5,16 Hz, H^{9a}), δ 3.18 (q, 8H, *J* = 7 Hz, H^{CH2}), δ 2.45 (s, 6H, H^{-OCH3}), δ 1.13 (t, 12H, *J* = 7 Hz, H^{CH3}); ^1H-^1H-COSY was also performed. Anal. Calcd for $(NEt_4)[Co(L^{O\text{-}ValTryp})_2]$: C, 63.80; H, 6.52; N, 8.09. Found: C, 63.887; H, 6.83; N, 8.122. IR (KBr, cm^{-1}): $\upsilon(COO^-)_{asym}$ 1646; $\upsilon(COO^-)_{sym}$ 1450; υ(C-O) 1284; υ(C-H)o/p-ring H 757; υ(M-O) 527; υ(M-N) 426. m/z (ESI-MS) $\{M+H\}^+$, $\{[(NEt_4)[Co(L^{O\text{-}ValTryp})_2]+H\}^+$; calcd: 866.35, found: 866.35.

2.3.3 $(HNEt_3)[Co(L^{O\text{-}ValTryp})_2]$ (2)

Solid $Co(ClO_4)_2{\cdot}6H_2O$ (0.269 g, 0.735 mmol) was added to the methanolic solution (10 mL) of $H_2L^{O\text{-}ValTryp}$ (0.500 g, 1.47 mmol) and the reaction mixture was stirred for 15 min. The colour of the reaction mixture became pink. After 15 min., methanolic solution (10 mL) of triethyl amine (0.298 g, 2.95 mmol) was slowly added to the reaction mixture, and the colour of the reaction mixture gradually changed from pink to light purple to reddish brown. The reaction mixture was stirred for 6 hours at room temperature and evaporated using a rotary evaporator to reduce the volume. Acetonitrile was added to it in a proportion of 1:3 (methanol: acetonitrile). Block-shaped dark brown coloured crystals were obtained after 3-4 days of slow evaporation. Crystals were washed with ethyl acetate and diethyl ether and dried under a vacuum.

^1H NMR (d_6-DMSO, 500 MHz) δ 10.93 (s, 2H, $H^{NH\ indole}$), δ 8.95 (s, 1H, $H^{NH\ TEA}$), δ 7.83 (d, 2H, *J* = 7.5 Hz, H^{12}), δ 7.34 (d, 2H, *J* = 8 Hz, H^{15}), δ 7.21 (s, 2H, H^{17}), δ 7.08 (t, 2H, *J* = 7.5 Hz, H^{14}), δ 7.03 (t, 2H, *J* = 7.5 Hz, H^{13}), δ 6.62 (d, 2H, *J* = 7.5 Hz, H^5), δ 6.48 (d, 2H, *J* = 7 Hz, H^3), δ 6.24 (t, 2H, *J* = 8 Hz, H^4), δ 5.55 (t, 2H, *J* =11.5 Hz, $H^{NH\ LIGAND}$), δ 4.50 (dd, 2H, *J* = 4.5, 5.5 Hz, H^8), δ 4.11 (t, 2H, *J* = 11.5 Hz, H^7), δ 3.75-3.65 (m, 4H, $H^{7a,9}$), δ 3.54 (s, 6H, H^{-OCH3}), δ 3.39 (dd, 2H, *J* = 4.5/5.5,16 Hz, H^{9a}), δ 2.93 (q, 6H, *J*

= 7 Hz, H^{CH2}), δ 1.06 (t, 9H, *J* = 7 Hz, H^{CH3}); ^{1}H-^{1}H-COSY was also performed. Anal. Calcd for $(Et_3NH)[Co(L^{O\text{-}ValTryp})_2]$: C, 63.07; H, 6.25; N, 8.36. Found: C, 62.708; H, 6.143; N, 8.034. IR (KBr, cm^{-1}): $\upsilon(COO^-)_{asym}$ 1615,1596; $\upsilon(COO^-)_{sym}$ 1458; υ(C-O) 1281; υ(C-H)o/p-ring H 744; υ(M-O) 532; υ(M-N) 431. m/z (ESI-MS) $\{M+H\}^+$, $\{[(Et_3NH)[Co(L^{O\text{-}ValTryp})_2]+H\}^+$; calcd: 838.32, found: 838.32.

2.3.4 $(HNEt_3)[Co(L^{O\text{-}ValTryp})_2]$ (3)

Complex **1** (0.100 g, 0.115 mmol) was dissolved in 8 mL methanol and methanolic solution (2 mL) of triethylammonium perchlorate (0.070 g, 0.374 mmol) was added to it and kept for stirring. After 10 min stirring, some solid precipitation appeared. Then filtered, filtrate was collected in a 25 mL beaker and kept for slow solvent evaporation at room temperature. Orange-red colored crystalline solids were obtained after three days. The crystals were filtered, washed with acetonitrile and diethyl ether, and dried in a vacuum. Yield: 0.084 g.

^{1}H NMR (d_6-DMSO, 500 MHz) δ 10.86 (s, 2H, $H^{NH\ indole}$), δ 8.83 (s, 1H, $H^{NH\ TEA}$), δ 7.82 (d, 2H, *J* = 8 Hz, H^{12}), δ 7.30 (d, 2H, *J* = 8 Hz, H^{15}), δ 7.20 (s, 2H, H^{17}), δ 7.04 (t, 2H, *J* = 7 Hz, H^{14}), δ 6.98 (t, 2H, *J* = 8 Hz, H^{13}), δ 6.54 (d, 2H, *J* = 7.5 Hz, H^{5}), δ 6.17 (d, 2H, *J* = 7.5 Hz, H^{3}), δ 6.03 (t, 2H, *J* = 7.5 Hz, H^{4}), δ 5.48 (t, 2H, *J* =11 Hz, $H^{NH\ LIGAND}$), δ 4.10 (dd, , *J* = 4.5,5.5 Hz, 2H, H^{8}), δ 4.18 (t, 2H, *J* = 12 Hz, H^{7}), δ 3.85 (d, 2H, *J* = 11 Hz, H^{7a}), δ 3.79 (dd, *J* = 4.5/5.5, 16 Hz 2H, H^{9}), δ 3.40 (dd, 2H, *J* = 4.5/5.5,16 Hz, H^{9a}), δ 3.08 (q, 6H, *J* = 7 Hz, H^{CH2}), δ 2.46 (s, 6H, H^{-OCH3}), δ 1.16 (t, 9H, *J* = 7 Hz, H^{CH3}); ^{1}H-^{1}H-COSY was also performed. Anal. Calcd for $(Et_3NH)[Co(L^{O\text{-}ValTryp})_2]$: C, 63.07; H, 6.25; N, 8.36. Found: C, 62.276; H, 6.203; N, 8.299. IR (KBr, cm^{-1}): $\upsilon(COO^-)_{asym}$ 1657; $\upsilon(COO^-)_{sym}$ 1456; υ(C-O) 1282; υ(C-H)o/p-ring H 754; υ(M-O) 540; υ(M-N) 430. m/z (ESI-MS) $\{M+H\}^+$, $\{(Et_3NH)[Co(L^{O\text{-}ValTryp})_2]+H\}^+$; calcd: 838.32, found: 838.32.

2.3.5 $(NEt_4)[Fe(L^{O\text{-}ValTryp})_2]$ (4)

Solid $Fe(ClO_4)_2 \cdot 7H_2O$ (0.269 g, 0.735 mmol) was added to the methanolic solution (10 mL) $H_2L^{O\text{-}ValTryp}$ (0.500 g, 1.47 mmol) and the reaction mixture was stirred for 15 min. The colour of the reaction mixture became bluish-purple. After 15 min., tetraethyl ammonium hydroxide solution (0.298 g, 2.94 mmol, 20 wt% in water) was slowly added to the reaction mixture, and the colour of the reaction mixture gradually changed from bluish-purple to red. The reaction mixture was stirred again for 3 h. at room temperature. Then, the solvent was evaporated using a rotary evaporator to reduce the volume of the reaction mixture, and acetonitrile was added to it in a proportion of 3:1 (methanol: acetonitrile) and was kept in a 50 mL beaker. Diamond-shaped dark red coloured crystals were obtained after 8-9 days of slow evaporation. Crystals were washed with ethyl acetate and diethyl ether and dried under a vacuum. Yield: 65%.

Anal. Calcd for $(NEt_4)[Fe(L^{O\text{-}ValTryp})_2]$: C, 64.03; H, 6.54; N, 8.12. Found: C, 63.803; H, 7.183; N, 8.159. IR (KBr, cm^{-1}): $\upsilon(COO^-)_{asym}$ 1639; $\upsilon(COO^-)_{sym}$ 1453; υ(C-O) 1283; υ(C-H)o/p-ring H 757; υ(M-O) 579; υ(M-N) 426. μ_{eff} (solid, 292K); 5.75 μB/Fe. m/z (ESI-MS) $\{M+2H\}^+$, $\{[Fe(L^{O\text{-}ValTryp}]^- +2H\}^+$; calcd: 734.21, found: 734.20.

2.3.6 $(Et_3NH)[Fe(L^{O\text{-}ValTryp})_2].(Et_3NHClO_4)$ (5)

The ligand $H_2L^{O\text{-}ValTryp}$ (0.500 g, 1.47 mmol) was dissolved in 10 mL MeOH in a 100 mL round bottom flask, and solid $Fe(ClO_4)_2 \cdot 7H_2O$ (0.270 g, 0.735 mmol) was added into it. The colour of the solution became blue-violet and the reaction mixture was stirred for 15 min. Then, a methanolic solution (10 mL) of triethyl amine (0.446 g, 4.41 mmol) was slowly added to the reaction mixture, and the colour of the reaction mixture gradually changed from blue-violet to red-violet. The resulting red-violet solution was stirred for another 3 h. at room temperature.

Solid crystalline red-violet coloured solid appeared, filtered off, and washed with ethyl acetate and diethyl ether. The solid was dried in a vacuum desiccator. The solid was redissolved in methanol along with a few drops of DMF, and it was kept in a 25 mL beaker for slow evaporation of the solvent. Block-shaped red-violet coloured crystals were obtained after 3 days. Yield: 74%. Anal. Calcd for $(Et_3NH)[Fe(L^{O\text{-}ValTryp})_2]\cdot Et_3NHClO_4$: C, 57.94; H, 6.61; N, 8.11. Found: C, 57.804; H, 6.581; N, 8.088. IR (KBr, cm^{-1}): $\upsilon(COO^-)_{asym}$ 1600; $\upsilon(COO^-)_{sym}$ 1458; υ(C-O) 1276; υ(C-H)o/p-ring H 740; υ(M-O) 583; υ(M-N) 417. μ_{eff} (solid, 292K); 5.8 μB/Fe. m/z (ESI-MS) $\{M+H\}^+$, $\{(HNEt_3)[Fe(L^{O\text{-}ValTryp})_2]+H\}^+$; calcd: 835.33, found: 835.27.

2.4 X-ray Crystallography

The crystal of the complexes obtained during synthesis was used for X-ray analysis. The crystals were mounted on glass fibre. All geometric and intensity data for the crystals were collected at room temperature using a Bruker SMART APEX CCD diffractometer equipped with a fine focus 1.75 kW sealed tube Mo-Kα (λ= 0.71073 Å) X-ray source, with increasing ω (width of 0.3º per frame) at a scan speed of either 3 or 4 s/frame. The SMART software was used for data acquisition, and the SAINT software for data extraction. Absorption corrections were done using a multi-scan. After the initial solution and refinement with SHELXL, the final refinement was performed on the WinGX environment using the SHELXL97 programs.[23] All non-hydrogen atoms were refined anisotropically. In **2,** methanol molecules in the crystals were refined isotropically to avoid alert level A in checkcif. The hydrogen atoms were located from the Fourier maps and refined isotropically wherever possible. Thus, some C-H bonds will not be ideal and may vary. In some places, the hydrogen atoms attached to the solvent molecules could not be located or fixed, so the molecular weight may not match. ORTEP obtained selected crystallographic data of Co(III) & Fe(III) complexes summarized in Tables **2.1A** and **2.1B**.

Table 2.1A Crystallographic data and refinement parameters of **1** and **2**.

Complexes	**1**	**2**
Empirical Formula	$C_{46}H_{60}CoN_5O_{10}$	$C_{47}H_{55}CoN_6O_{10}$
Formula Weight	901.92	922.90
Wavelength (Å)	0.71073	0.71073
Crystal system	tetragonal	orthorhombic
Space group	$P4_32_12$	$P2_1\ 2_1\ 2_1$
a, Å	12.1822(4)	37.955(11)
b, Å	12.1822(4)	9.606(3)
c, Å	30.3583(16)	13.538(4)
α, deg	90	90
β, deg	90	90
γ, deg	90	90
Volume, Å^3	4505.4(4)	4936(2)
Z/ρ	4/1.330	4/1.242
μ	0.444	0.407
Coll reflns	4427	8693
Indep refln	3911	5916
FLACK para.	0.010(5)	0.099(6)
GOF	1.121	1.179
R1[a]	0.0340	0.0565
wR2[a]	0.0876	0.1358
R1[b]	0.0434	0.1076
wR2[b]	0.0969	0.1763

[a] $I > 2\sigma$. [b] All data

Table 2.1B Crystallographic data and refinement parameters of **4** and **5**.

Complexes	4	**5**
Empirical Formula	$C_{46}H_{56}FeN_5O_{10}$	C_{50} H_{65} Cl Fe N_6 O_{12}
Formula Weight	894.80	1033.38
Wavelength (Å)	0.71073	0.71073
Crystal system	tetragonal	monoclinic
Space group	$P4_32_12$	$P2_1$
a, Å	12.1909(7)	9.7580(10)
b, Å	12.1909(7)	19.6919(19)
c, Å	30.773(3)	27.323(3)
α, deg	90	90
β, deg	90	93.402(3)
γ, deg	90	90
Volume, Å^3	4573.4(6)	5240.9(9)
Z/ρ	4/ 1.300	4/ 1.310
μ	0.392	0.404
Coll reflns	4039	18351
Indep refln	3516	11787
FLACK para.	0.009(6)	0.124(7)
GOF	1.147	1.176
R1[a]	0.0450	0.0904
wR2[a]	0.1176	0.1350
R1[b]	0.0570	0.1530
wR2[b]	0.1353	0.1585

[a] $I > 2\sigma$. [b] All data

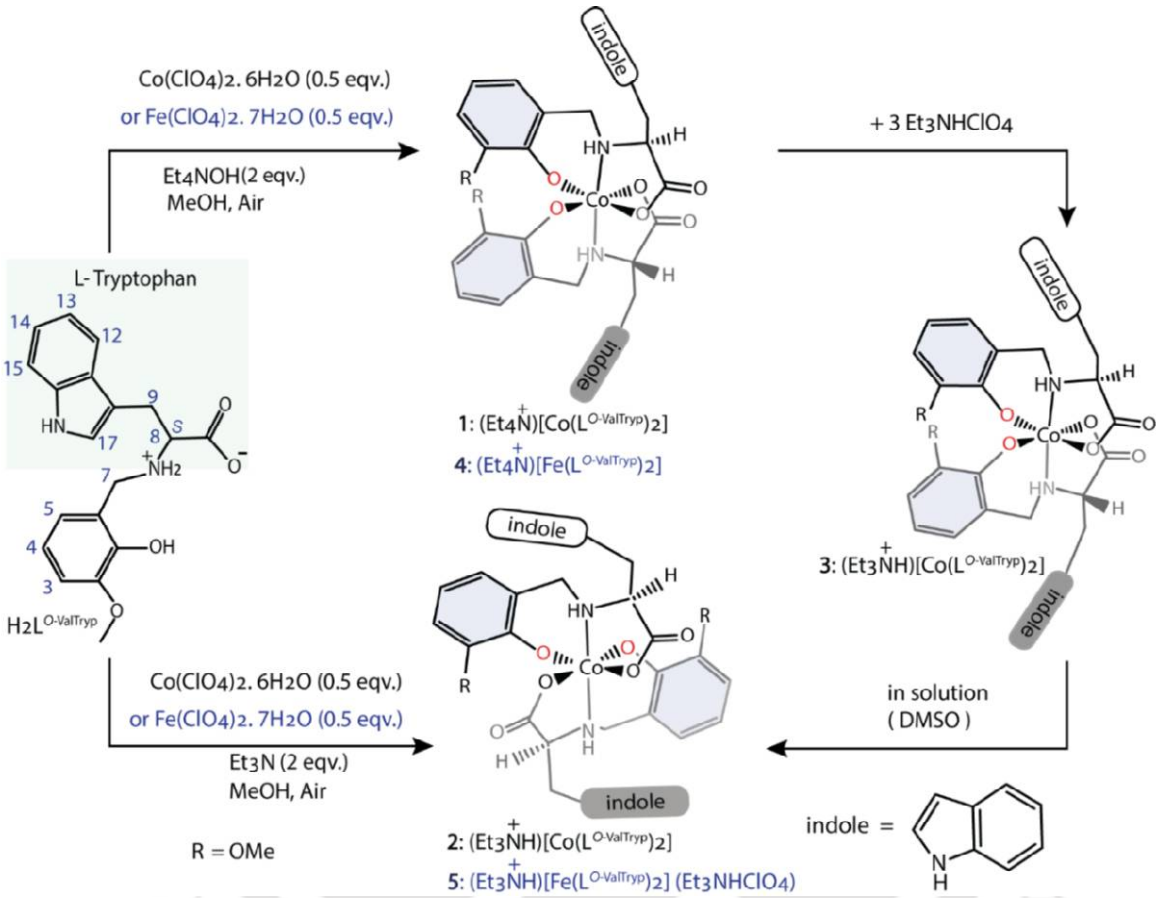

Scheme 2.2 Synthesis of the complexes.

2.5 Result and Discussion

2.5.1 Syntheses and selected properties

The ligand $H_2L^{O\text{-}ValTryp}$ synthesis process is similar to the other amino acid-based ligands reported earlier.[24–26] Here, the Schiff base condensation reaction of L-tryptophan and o-vanillin in methanol, followed by the reduction with $NaBH_4$, gave a sticky solid, which, on acidification with dilute HCl, gave the white-colored solid ligand $H_2L^{o\text{-}ValTryp}$. The ligand was characterized by ^1H NMR spectroscopy (Fig. 2.1), ESI (+ve) mass spectrometry, and IR spectroscopy. The ESI

mass analysis of the ligand showed a prominent molecular ion peak at *m/z* = 341.15, corresponding to $\{[H_2L^{O\text{-Val Tryp}}] + H\}^+$.

When one equivalent of the ligand was reacted with 0.5 equivalent of $Co(ClO_4)_2 \cdot 6H_2O$, it gave a pink-colored solution, which, upon treatment with two equivalents of base, turned into dark-brown colored. Thus, for the synthesis of complex-**1**, we have used triethyl amine as a base, and for the synthesis of complex-**2**, tetraethyl ammonium hydroxide (20 wt.% in H_2O) was used as a base. Complex-**3** was obtained by the salt metathesis reaction where **1** was treated with three equivalents of triethylammonium perchlorate salt and isolated as a yellow-colored crystalline solid. Complex **2** & **3** have the same counter ion, i.e., Et_3NH^+ ion, but behave differently in the solution. Also, we have synthesized labile Fe(III) analogs. All the complexes were characterized by IR, NMR, UV-visible, CD spectroscopy, ESI mass spectrometry, and elemental analysis. The elemental analyses (C, H, and N) of the complexes are consistent with their chemical compositions. The ESI (+) mass analysis of **1** showed a prominent peak at *m/z* = 866.35 for the formation of $\{(NEt_4)[Co(L^{O\text{-Val Tryp}})_2]+H\}^+$, whereas **2** & **3** both showed prominent peak at *m/z* = 838.32 for $\{(HNEt_3)[Co(L^{O\text{-Val Tryp}})_2]+H\}^+$ and the position and isotopic distributions of the observed mass spectra showed good agreement with the simulated spectra of the respective complexes. The ESI (+) mass analysis of both Fe(III)-complexes showed a prominent peak at m/z = 734.20 for $\{Fe(L^{O\text{-Val Tryp}})_2+2H\}^+$ indicating the formation of the anionic bis-iron(III) exists in the solution. IR spectra of the complexes showed broad stretches near 3400 cm^{-1} due to OH (water or H-bonded OH) and N-H stretching. Only the IR spectrum of **5** showed a sharp band at 1081 cm^{-1} due to perchlorate counterion.

ESI-mass (+) spectra

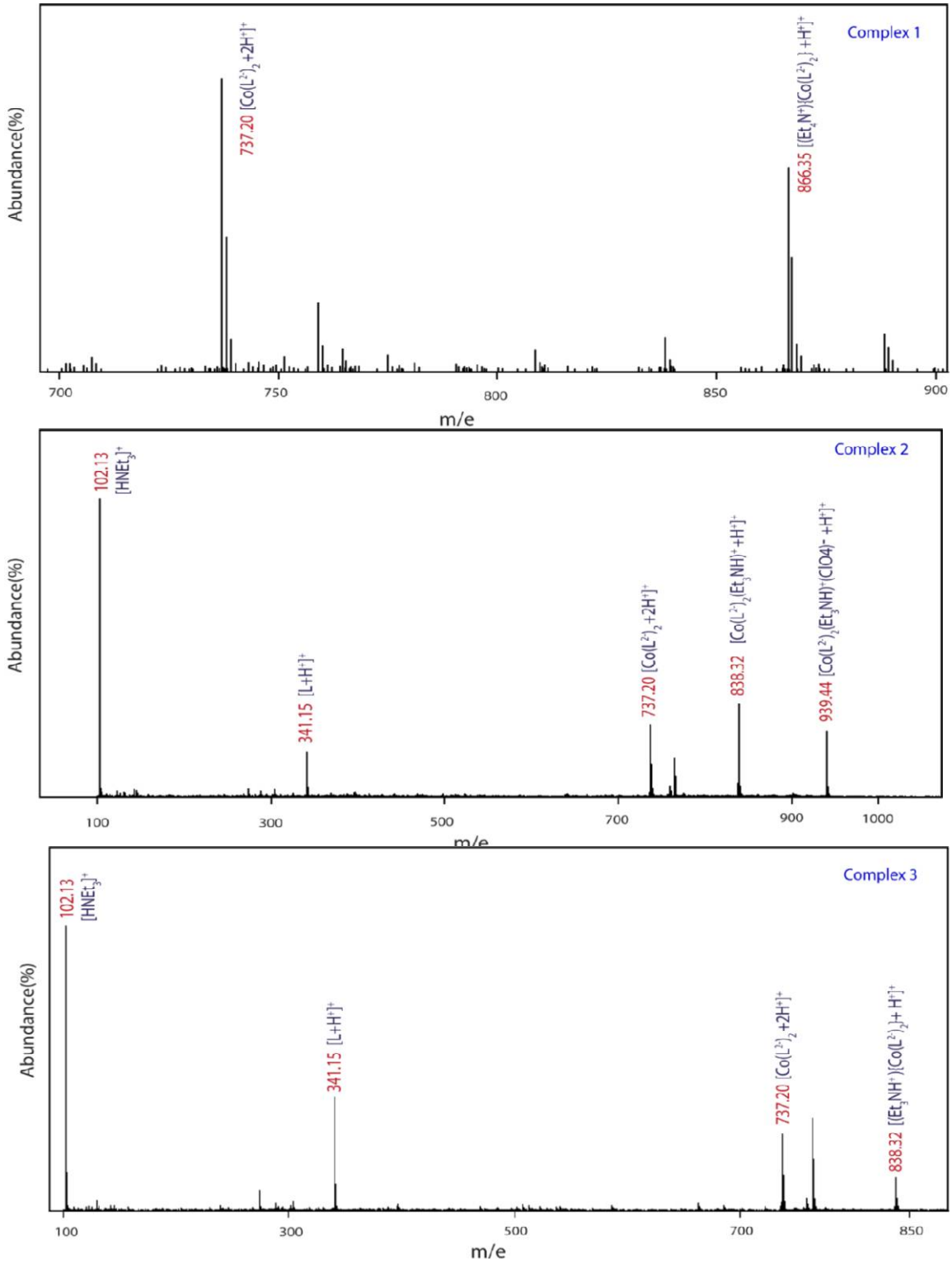

Figure 2.1 ESI-mass (+) spectra of complexes **1**, **2** and **3**.

2.5.2 Crystal structures

Complex **1** has crystallized in the chiral tetragonal space group $P4_32_12$. The asymmetric unit contains half of the anionic $[Co(L^{O\text{-}ValTryp})_2]^-$ unit, half a molecule of tetraethyl ammonium ion, and a water molecule. The crystal structure analysis revealed that the Co(III) ion in **1** is meridionally coordinated by two deprotonated ligands where metal-coordinated carboxylates and phenolates are cis to each other, whereas the two anime nitrogen atoms (N1 & N1′) coordinated to the metal ion are trans to each other. (Figure 2.2a)

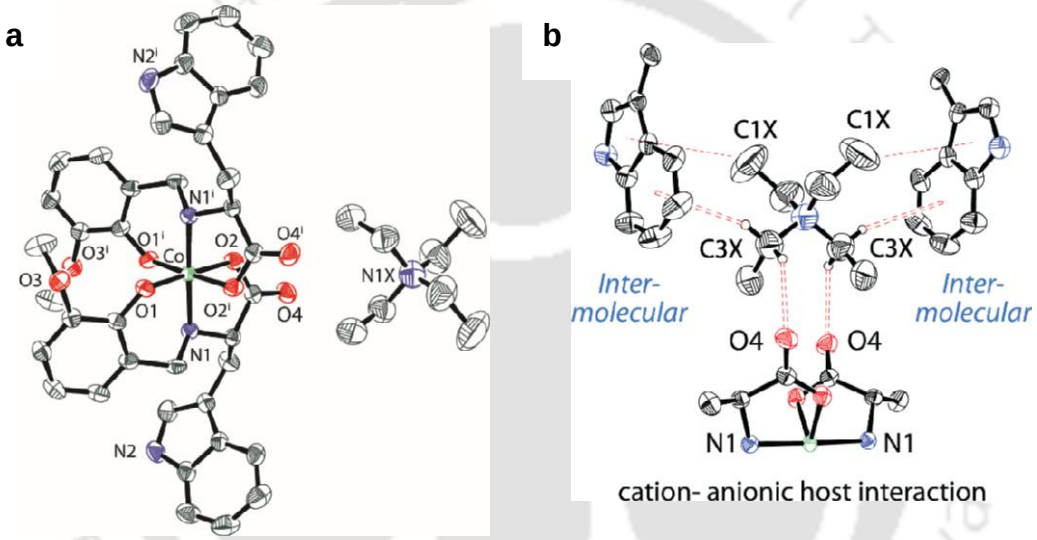

Figure 2.2 (a) The ORTEP figure of complex **1** with 40% ellipsoid probability, (b) non-covalent interactions in **1**.

The geometry around the Co(III) center is slightly distorted from the perfect octahedron as evident from the deviation of angles from ideal 90˚ and 180˚ (Table 2.2). The chiral carbons present in the complexes, C8A & C8B, have "*S*" conformation, originating from the use of L-tryptophan used for ligand synthesis, and Co(III)- coordinated amine N atoms, N1A & N1B, have "*R*" conformation. This opposite conformation preference at chiral carbon and amine N has been observed in all previously reported complexes with analogous amino acid-derived reduced Schiff base ligands.[27–29] The coordination bond distances in **1**, Co^{III} -O(phenolate) = 1.909 Å, Co^{III} -

N(amine) = 1.940 Å, Co^{III} -O(carboxylate) = 1.910 Å, are similar to the other reported Co^{III} complexes.[30,31]

In **l**, two indole units faced outward like open arms, and the Et_4N^+ ion is situated between two indole units of two adjacent complex molecules and the tetraethyl ammonium ions are involved in CH…π interactions with the indole units through terminal metal groups. The solvent water molecule formed an intermolecular H-bonding with the -OMe group of one anionic complex unit and another intermolecular H-bonding to the non-coordinated carbonyl oxygen atom of the metal-coordinated carboxylate of the adjacent complex unit. Thus, it bridges the two adjacent anionic bis-Co^{III} complex units and reinforces the single-strand helical type chain formation along the c-axis.

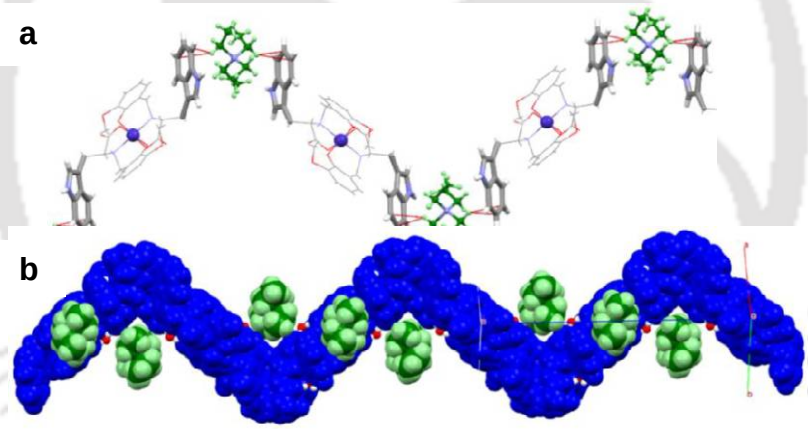

Figure 2.3 (a) Tetraethylammonium ion (in the ball-stick model) situated in-between two indole units of adjacent anionic complex molecules and connected to them through intermolecular CH-π interactions, (b) single strand helical type arrangement of complex molecules (in the space-filled model) along the c-axis.

Complex **2** has crystallized in the chiral orthorhombic space group $P2_12_12_1$, where the asymmetric unit contains one bis-complex, one Et_3NH^+, one disordered methanol where oxygen is in two positions with 50% occupancy, and an isotropic oxygen presumably from water. H-atoms on methanol and water could not be located or fixed. In **2**, the Co(III) ion is meridionally coordinated by two deprotonated ligands that keep the two metal-bound phenolates away from

each other. Two amine nitrogen atoms (N1A, N1B) occupy the axial positions, and the corners of the equatorial plane are occupied by two phenolate oxygen atoms (O1A, O1B) and two carboxylate oxygen atoms (O2A, O2B).

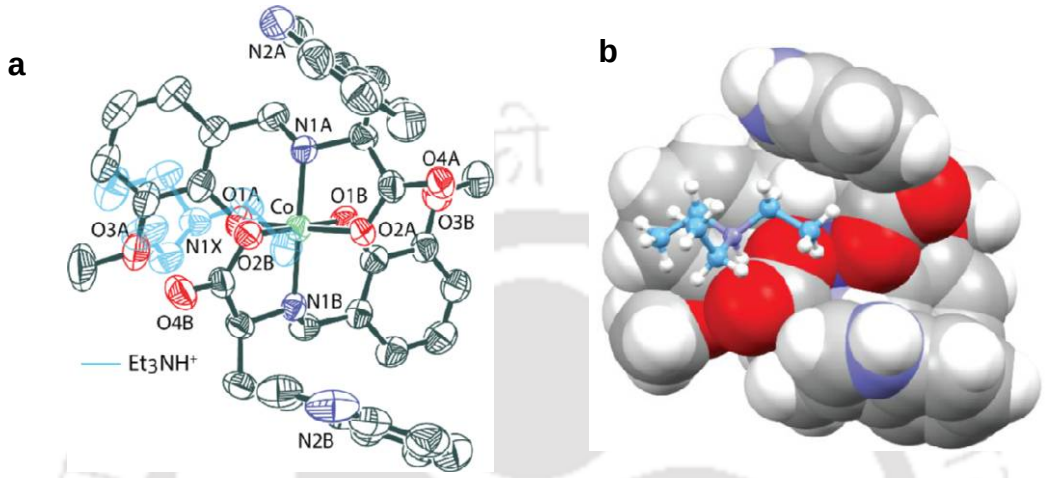

Figure 2.4 (a) The ORTEP figure of complex **2** with 40% ellipsoid probability, (b) space-filling model of **2** where triethylammonium ion is situated inside the chiral cleft (in the ball-stick model).

Table 2.2 Selected bond length (Å) and angles (°) in **1** and **2**

	Co-O_p	**Co-O_c**	**Co-N_a**	**O_p-Co-O_p**	**O_c-Co-O_c**	**O_p-Co-O_c**	**N_a-Co-N_a**
1	1.9088(19)	1.910(2)	1.940(3)	96.18(9)	87.06(9)	88.38(9)	178.58(10)
	1.9088(19)	1.910(2)	1.940(3				
2	1.908(5)	1.905(5)	1.930(5)	87.7(2)	91.9(2)	90.62(19)	171.7(2)
	1.879(4)	1.902(4)	1.926(5)				

Subscripts ***p*** and ***c*** on the oxygen atom and ***a*** on the nitrogen atom denote phenolate, carboxylate, and amine, respectively

The chiral carbons (C8A & C8B) in the complex have the "*S*" conformation, and the Co(III) coordinated amine nitrogens atoms have the "*R*" conformation. The coordination bond lengths around the cobalt(III) ion are Co-O1A$_{(phenolate)}$ 1.908(5), Co-O1B$_{(phenolate)}$ 1.879(4), Co-

$O2A_{(carboxylate)}$ 1.905(5), Co-$O2B_{(carboxylate)}$ 1.902(4), Co-$N1A_{(amine)}$ 1.930(5), Co-$N1B_{(amine)}$ 1.926(5) which are in the typical range for low-spin Co(III) -complexes.

In **2**, two indole rings are organized so that a somewhat deep cleft is formed, and the two carboxylate groups, which are cis to each other, are situated on the inner side of it. The cleft-forming indole units are hydrogen bonded to the other units of the complex but not identically, and because of their different way of organization, the C2 symmetry is broken. One triethyl ammonium ion is bound inside this cleft through H-bonding and other non-covalent interactions. One of the indole units of the adjacent anionic complex unit acts as an aromatic wall to form a bowl-shaped cavity for triethyl ammonium ion recognition (Fig. 2.5a). The back side of the cleft has an interesting linear alignment of four oxygen from methoxy and phenolate, forming a hydrophilic patch within a hydrophobic aromatic environment.

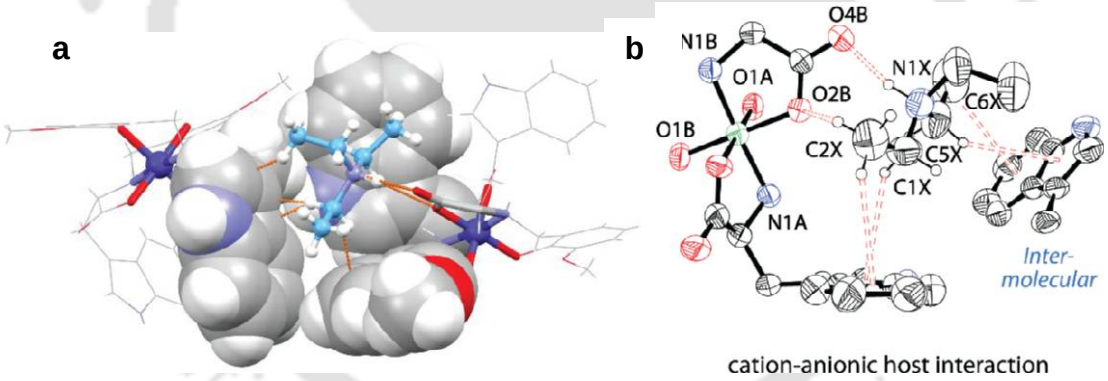

Figure 2.5 (a)Triethylammonium ion (in the ball-stick model, sky-coloured) resided inside the bowl-shaped cavity (in the space-filled model) in **2,** (b) non-covalent interactions in **2**.

So, the single crystal X-ray structures revealed that both **1** and **2** have cobalt(III) octahedrally coordinated by the two tridentate ligands in a meridional fashion (Fig. 2.2a & Fig. 2.4a). However, the ligands are organized quite differently (Scheme 2.2). In **1**, the methoxy groups on the phenolate aromatic rings are closer (O3…O3, 4.934 Å), while in **2**, the rings are away from each other with much higher methoxy oxygen distance (O3a…O3b, 7.785 Å). The other significant change is the way indole rings are further way in **1** (N2…N2′, 12.675 Å) but rotated

to much closure (N2A…N2B, 8.742 Å), forming a pocket surrounding the triethyl ammonium ion (Fig. 2.4a). The NEt_4^+ in **1** shows weaker intra-molecular two CH…π and two CH…O interactions with the indole and carboxylate oxygen of the Co(III) complex and two intermolecular CH…π interactions with a neighboring indole (Fig. 2.2b). Contrary to that, the $HNEt_3^+$ in **2** sits inside a pocket having one relatively stronger H-bond, two CH…π, and one CH…O interaction intramolecularly, along with two intermolecular CH…π interactions (Fig. 2.5b). Overall, the difference is a loss of one CH…O in **1** by a stronger NH…O in **2**.

Table 2.3 Non-covalent interactions in Complex **1**

Atoms	D-H (Å)	H…A (Å)	D…A(Å)	DHA(˚)
O1X-H1XD…O4	0.85	2.07	2.897(5)	163
N2-H2…O1	0.86	2.38	3.198(4)	160
N2-H2…O2	0.86	2.52	3.113(4)	127
O1X-H1HE…O1	0.85	2.57	3.233(6)	136
O1X-H1XE…O3	0.85	2.16	2.926(6)	151
N1-H1…O1	0.77(4)	2.28(4)	2.616(3)	107
C13-H13…O3	0.93	2.37	3.303(5)	176
C19-H19B…O4	0.96	2.59	3.475(5)	154

Table 2.5. Non-covalent interactions in Complex **2**

Atoms	D-H (Å)	H…A (Å)	D…A(Å)	DHA(˚)
N1X-H1X…O2B	0.98	2.51	3.266(8)	133
N1X-H1X…O4B	0.98	1.76	2.720(9)	167
N2A-H2A…O4A	0.86	2.07	2.885(9)	158
N2B-H2B…O1A	0.86	2.24	3.074(10)	163
C8A-H8A…O1B	0.98	2.51	2.870(8)	102
C2X-H2XC…O2B	0.96	2.60	3.328(12)	133
C12A-H12A…O4A	0.93	2.52	3.307(10)	142

2.5.3 NMR spectroscopy

The ^{1}H NMR spectra of complexes **1** and **2** were measured in d_6-DMSO and showed sharp, well-resolved signals. All the ^{1}H NMR signals were assigned based on the ^{1}H-^{1}H COSY and ^{1}H-^{13}C HSQC techniques.

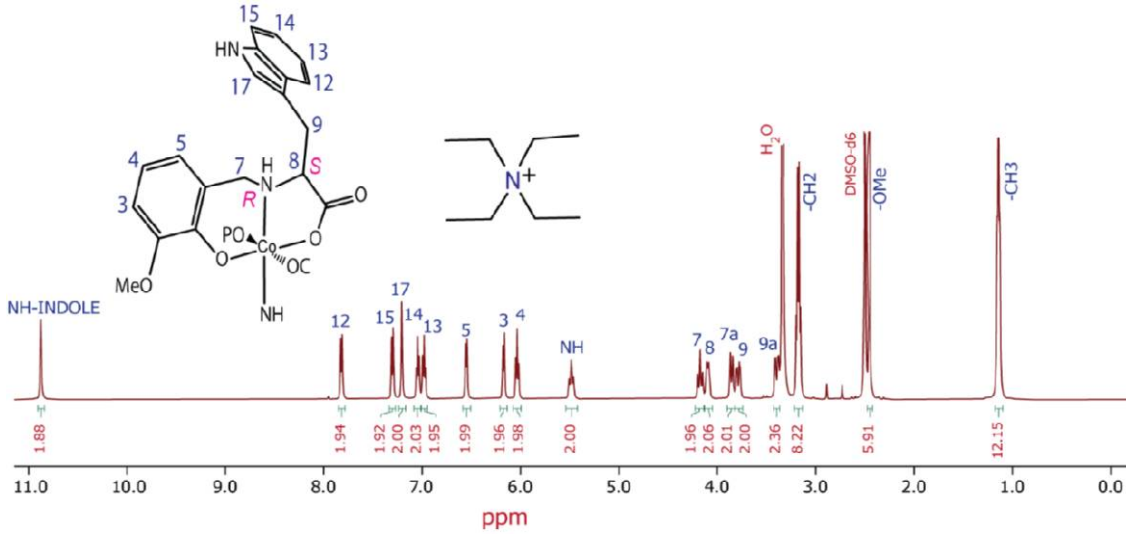

Figure 2.6 ^{1}H NMR spectrum (500 MHz, d_6-DMSO) of **1** with the labeling of hydrogen atoms of the ligand used.

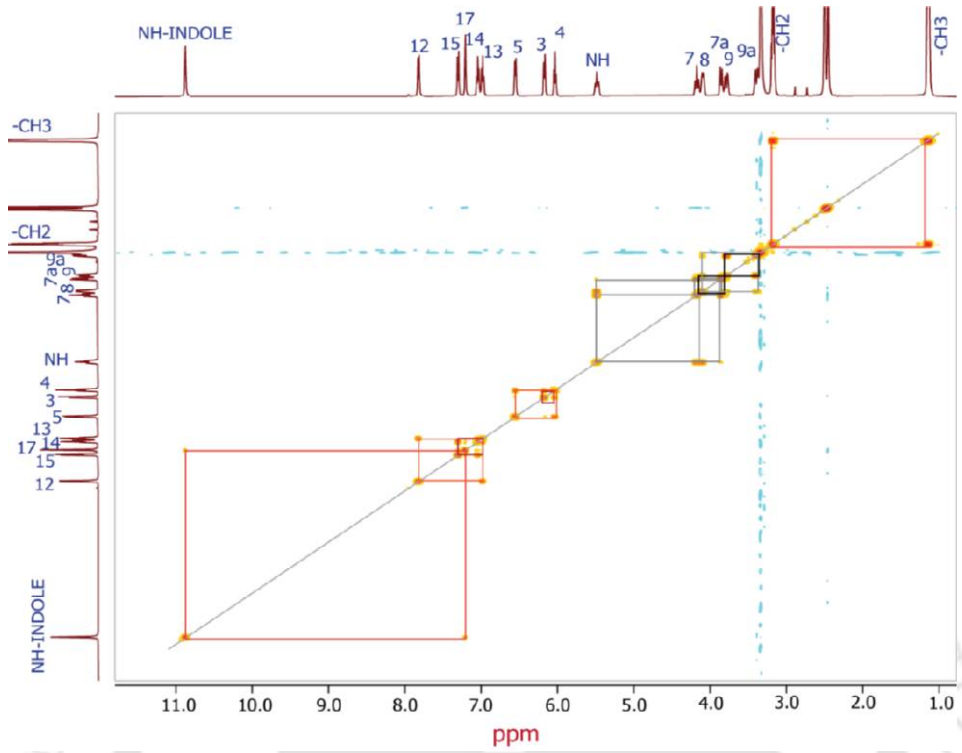

Figure 2.7 ^{1}H-^{1}H COSY spectrum (500 MHz, d_6-DMSO) of **1**.

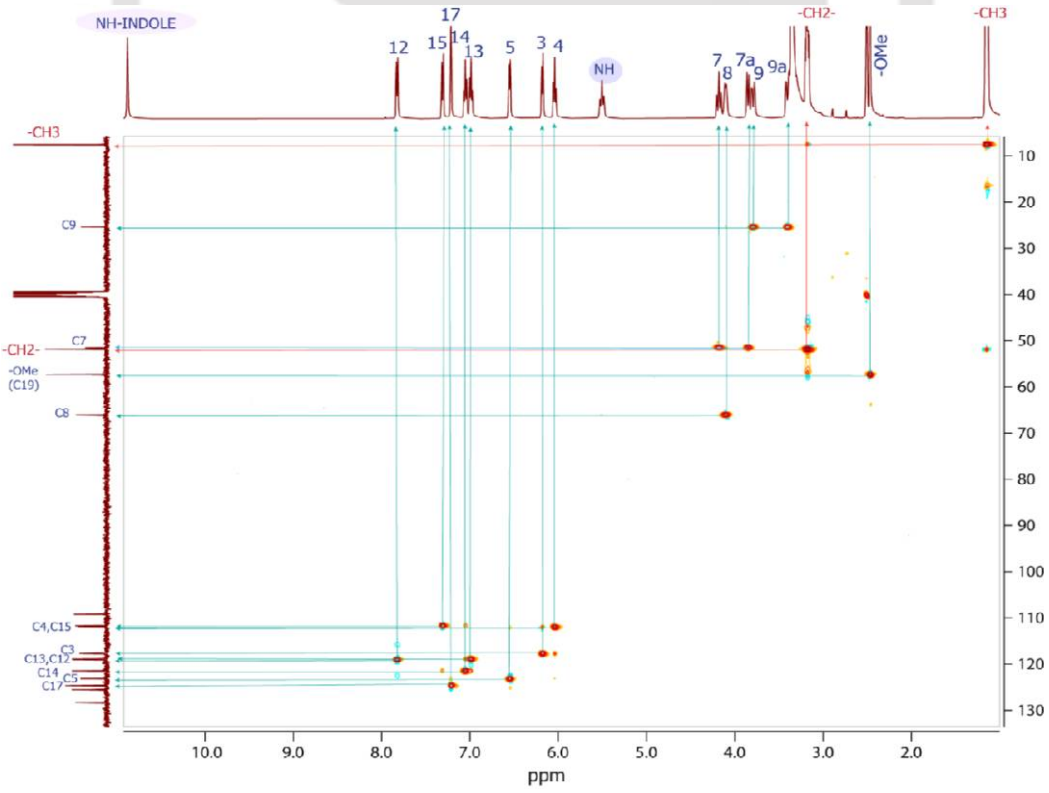

Figure 2.8 ^{1}H-^{13}C HSQC spectrum (500 MHz, d_6-DMSO) of **1**.

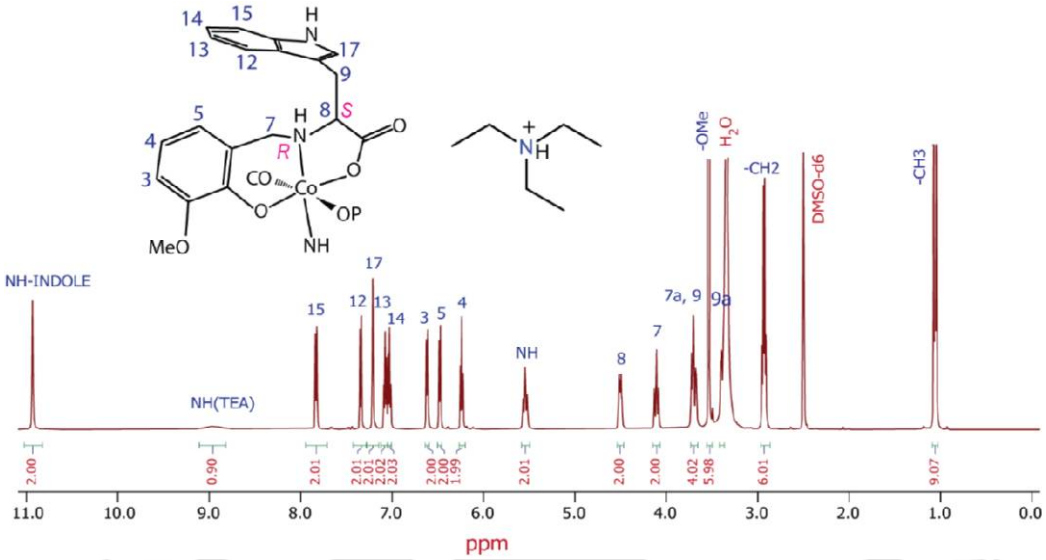

Figure 2.9 ^{1}H NMR spectrum (500 MHz, d_6-DMSO) of **2**.

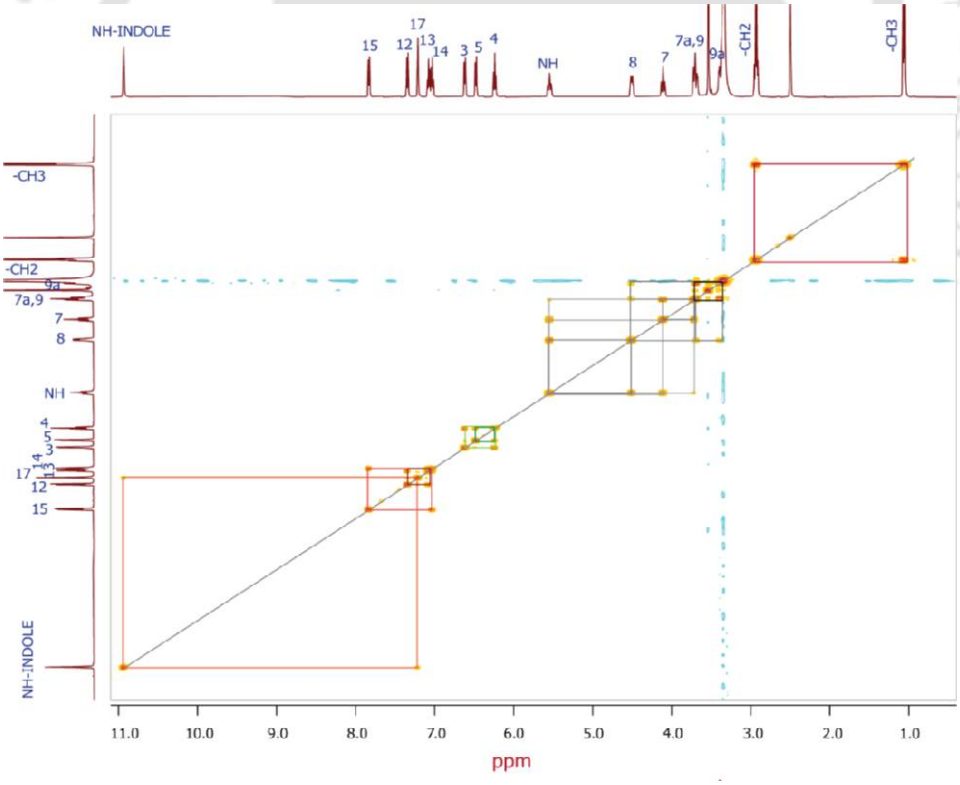

Figure 2.10 ^{1}H-^{1}H COSY spectrum (500 MHz, d_6-DMSO) of **2**.

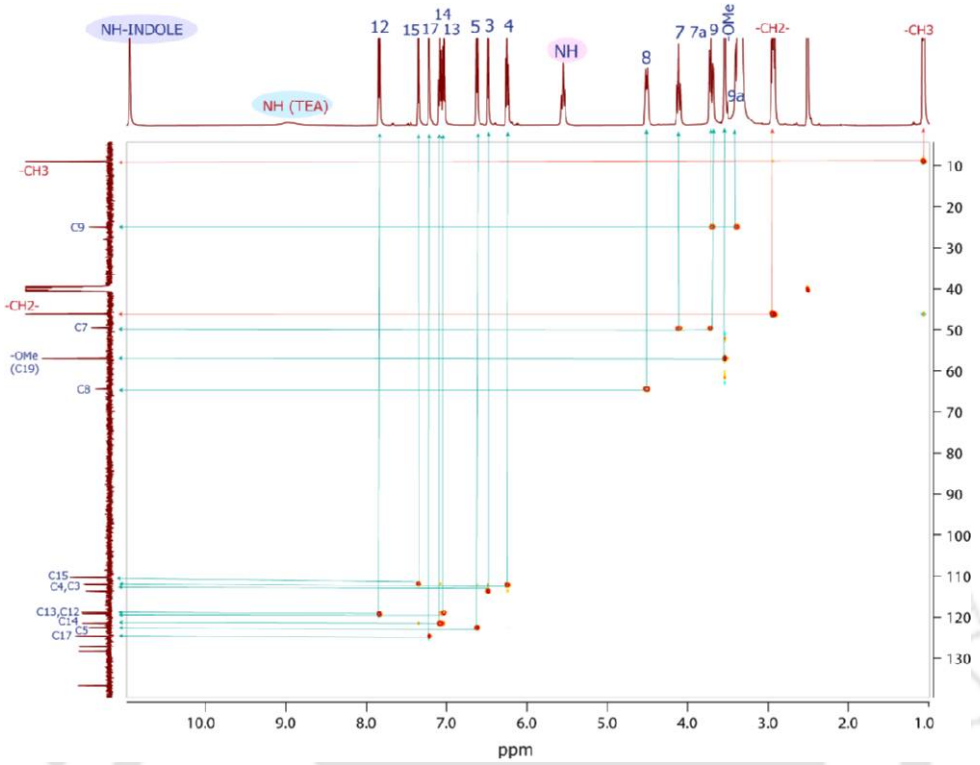

Figure 2.11 ^{1}H-^{13}C HSQC spectrum (500 MHz, d_6-DMSO) of **2**.

The NMR characterization showed that not only in the solid state, these two complexes also behave differently in the solution. The methoxy H's in **1** at 2.45 ppm shifted downfield at 3.45 ppm in **2** (Table 2.6). The H^3 & H^4 of the phenolate ring shifts downfield by a modest 0.31 and 0.21 ppm, respectively (Fig. 2). The aliphatic region shows upfield and downfield shifts ranging from +0.15 (H^{7a}) to -0.40 (H^8) ppm. The negative sign indicates a downfield shift. The regions showing shifts are significant. The highest shift of methoxy protons commensurate with the loss of intra-molecular CH…π (C19…π, 3.482 A) was seen in **1** to none in **2** as phenolate rings shifted apart. Correspondingly, the phenolate H's H^3 to H^5 shows a decreasing shift as the distance from the methoxy increases. The flipping of the aromatic ring along the -CH_2- arm is reflected in the change of H^{7a} position. The structure shows a rotation around the aliphatic H^9 to bring the indole ring closer in **2,** causing shifts around the neighboring H's (Scheme 2.2).

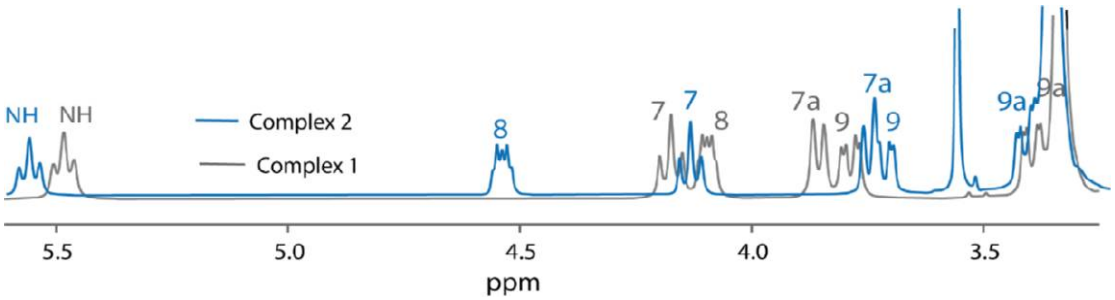

Figure 2.12 Partial combined ^{1}H NMR spectra of **1** & **2**, showing their different solution-state nature.

Table 2.6. The ^{1}H NMR shifts of the Co(III) complexes.

Indole ring	NH	H^{12}	H^{15}	H^{17}	H^{14}	H^{13}			
1	10.87	7.82	7.30	7.20	7.04	6.98			
2	10.93	7.83	7.34	7.21	7.08	7.03			
Phenolate Ring									
	H^{5}	H^{3}	H^{4}	-OMe					
1	6.55	6.17	6.03	2.45					
2	6.62	6.48	6.24	3.54					
Aliphatic protons									
	NH	H^{8}	H^{7}	H^{7a}	H^{9}	H^{9a}	$-CH_2-$	$-CH_3$	NH(TEA)
1	5.48	4.10	4.17	3.86	3.79	3.40	3.18	1.13	-
2	5.55	4.50	4.11	3.71	3.69	3.39	2.93	1.06	8.95

The numbering scheme is given in the ligand synthesis Scheme (Scheme 2.1)

2.5.4 Structural transformation of 1 to 2

Seeing all these results discussed above, then we have investigated whether structural transformation between these two complexes (**1** and **2**) is possible or not. When the methanolic solution of complex **1** was treated with three equivalents of triethyl ammonium perchlorate salt, we obtained complex **3**. The low solubility of complex **3** allowed us to collect it as a solid product. After several attempts, we could only isolate it as a crystalline solid, not the X-ray-suitable single

crystals. As we could not determine the solid-state structure of **3**, we characterized it with ^{1}H NMR spectroscopy, which revealed that the Et_4N^+ ion present in **1** has been replaced by the Et_3NH^+ ion in **3**. and showed different types of ^{1}H NMR signals compared to the proton NMR signals of **2,** which also contains Et_3NH^+ as a counter ion, i.e., despite having identical formulations, the **3** is not **2** (Fig. 2.13). Except for the counter ion, the **3** has the identical NMR signature of **1** (Fig. 2.15). This means the structure did not change upon metathesis.

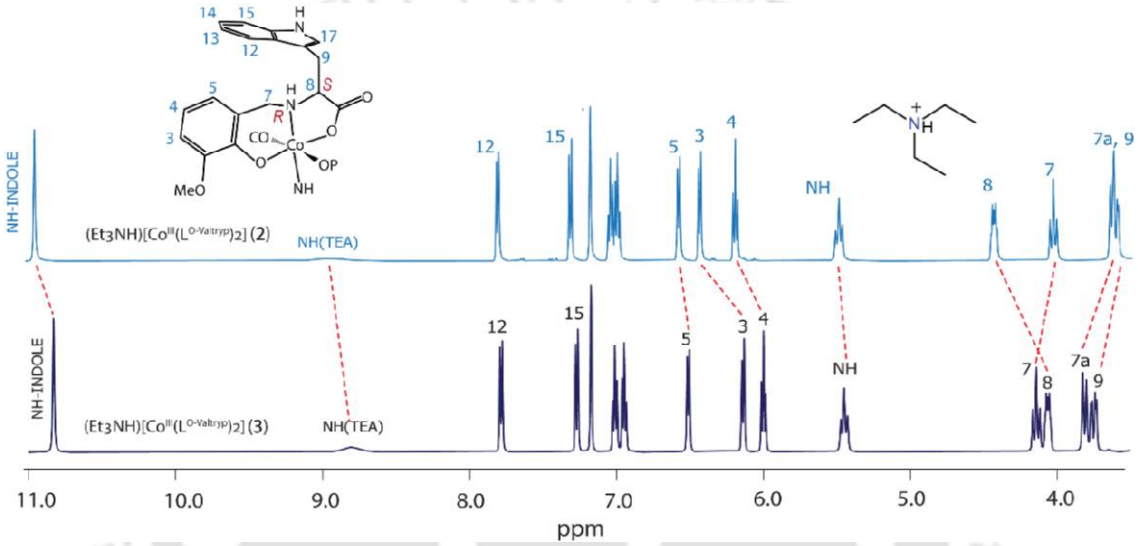

Figure 2.13 ^{1}H NMR spectra (500 MHz, d_6-DMSO) of **2** and **3** have the same counter ion, Et_3NH^+ ion, but show differences in solution.

Table 2.7 Chemical shift differences of similar types of protons in **2** and **3**, respectively.

Protons	NH (Indole)	NH (TEA)	H13	H5	H3	H4	NH (com)	H7	H7a	H8	OMe
δ of 3 (ppm)	10.86	8.83	6.98	6.55	6.17	6.03	5.48	4.18	3.85	4.10	2.46
δ of 2 (ppm)	10.93	8.95	7.03	6.62	6.48	6.24	5.55	4.11	3.71	4.50	3.54
Δδ (ppm)	+0.07	+0.12	+0.05	+0.07	+0.31	+0.21	+0.07	-0.07	-0.14	+0.40	+1.08

Interestingly, when the NMR spectrum of the same solution of **3** was recorded after three days, it showed the appearance of a new set of signals with very low intensity, and then the ^{1}H NMR spectra collection was continued for up to one month. The systematic arrangement and analysis of all the collected ^{1}H NMR spectra of **3** showed the initial positions of the proton NMR signals have shifted to the new positions, and as the days proceeded, the intensities of the old signals decreased, and the newly appeared signals increased, which is shown in Fig. 2.14.

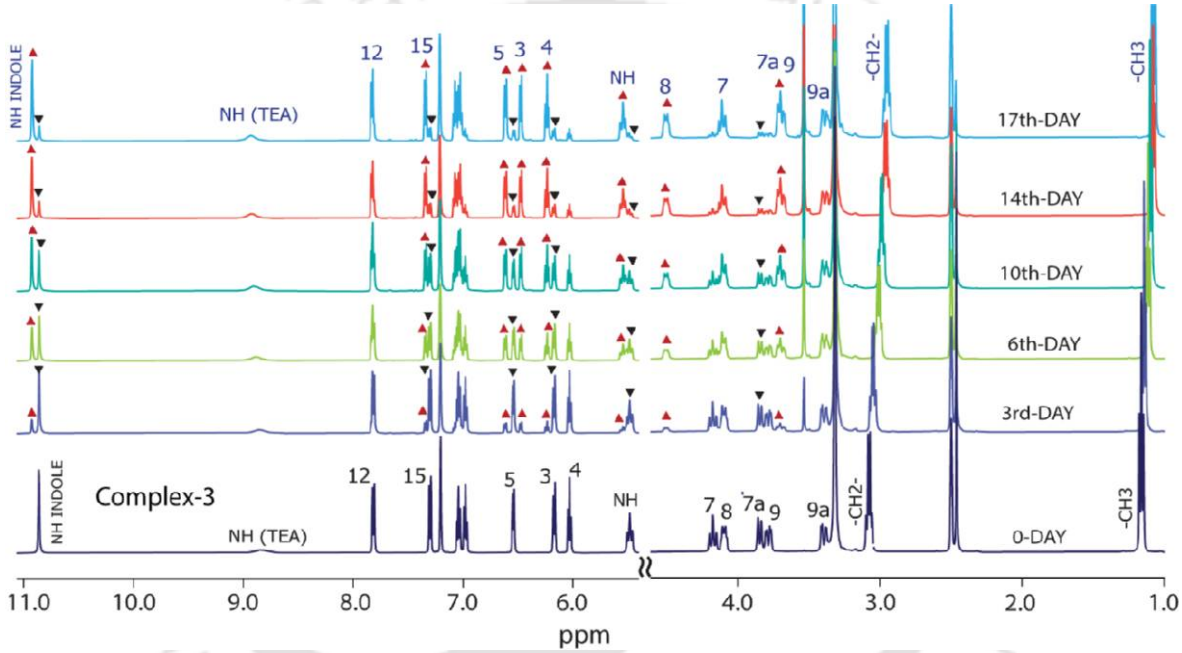

Figure 2.14 Partial combined ^{1}H NMR spectra (500 MHz, d_6-DMSO) of **3** showing gradual change at room temperature.

The -OMe group ^{1}H NMR signal showed the highest down-field shifting with Δδ value of 1.08 ppm. Among the other aliphatic proton signals, H^{7}, H^{7a}, and H^{9} led upfield shifting. In contrast, the ^{1}H NMR signals of the chiral proton H^{8}, NH, and all aromatic proton NMR signals present in the NMR spectrum of **3** also showed downfield shifting. From the ^{1}H NMR spectra, we also observed that the set of signals from Et_3NH^+ in **3** shifted to the high field. Both the positions and

the pattern of the newly appeared signals matched the ^{1}H NMR spectrum of **2**, shown in Fig. 2.15.

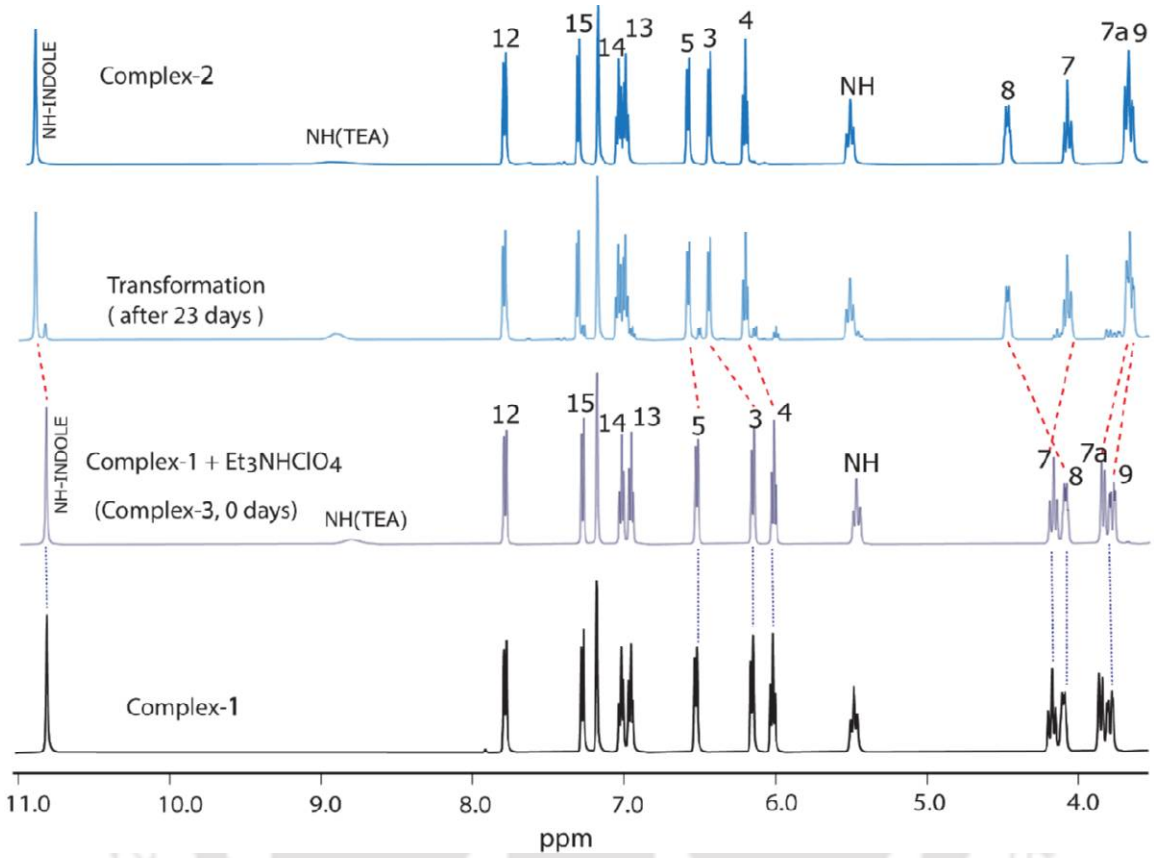

Figure 2.15 Combined partial ^{1}H NMR spectra showing the transformation from **1** to **2** in the presence of Et_3NHClO_4 through the formation of an intermediate product **3.**

When gradual intensity change ratio values of the initial and newly appeared ^{1}H NMR signal for the indole NH proton were plotted, it clearly showed that as the days proceeded, complex-**3** slowly transformed to **2**, having a different structural arrangement in the solution (Fig. 2.16). From the single crystal structure analysis of the complexes (**1** & **2**), we observed that the structural transformation of **1** to **2** required two significant changes: the breaking of metal-ligand bonds and recombination in a new way and the C-C bond rotations. As Co(III) complexes are inert, the metal-ligand coordination bonds are stable. Because of that, the structural

transformation of **3** to **2** is slow in solution at room temperature, it takes 23 days for ~90% conversion.

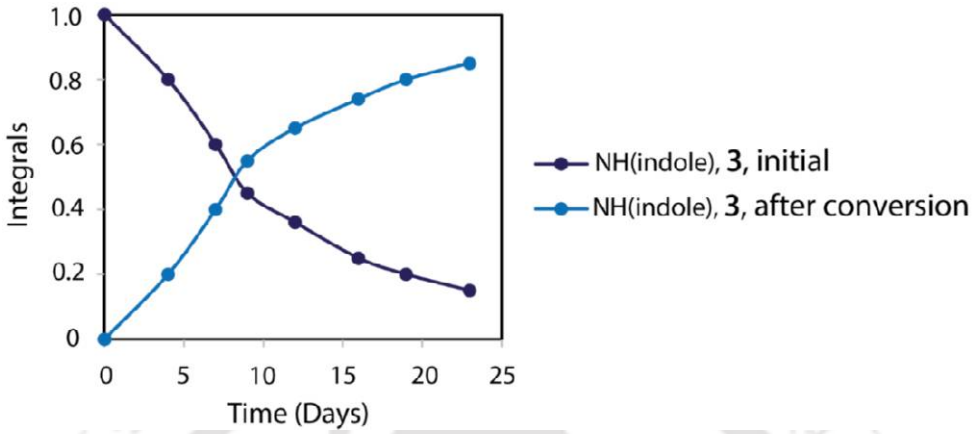

Figure 2.16 NH (indole) signal intensity change during the structural transformation of **3** to **2** in solution.

Increasing the temperature to 60°C, the conversion was essentially complete within 8 hours (Fig. 2.17), i.e., with increasing the temperature, the structural transformation process became faster.

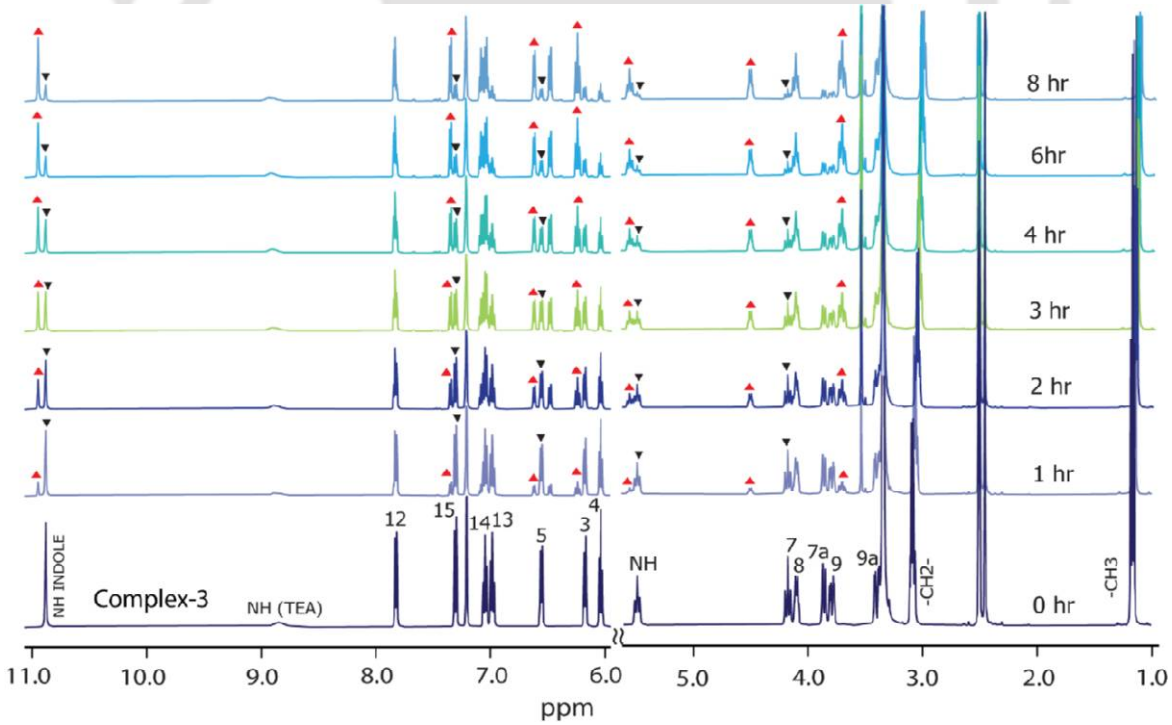

Figure 2.17 Combined partial ^{1}H NMR spectra showing the transformation of **3** to **2** at 60˚C.

2.5.5 UV-visible and CD spectra

The UV-visible spectra of Co(III) complexes were recorded using their 0.1mM solution in DMF. Complex **1** showed the presence of three distinct bands. As Co(III) centre is octahedrally coordinated in **1**, the higher energy intense band appeared at 390 nm because of phenolate (O^-)pπ→Co(III)dσ* charge transfer transition. The other two bands - one at around 518 nm are because of the $^1A_{1g}\rightarrow{}^1T_{2g}$ charge transfer transition, and the other occurred at 690 nm, corresponding to the $^1A_{1g}\rightarrow{}^1T_{1g}$. Complex **2** also showed three distinct absorption bands in the UV-visible spectrum, but blue shifting occurred in the band positions. The phenolate (O^-)pπ→Co(III)dσ* charge transfer transition band occurred at 378 nm, and the intensity of this LMCT band is higher than complex **1**. The two d-d transition bands of complex **2** appeared at 525 nm and around 680 nm. The UV-visible spectrum of **3** is identical to **1**.

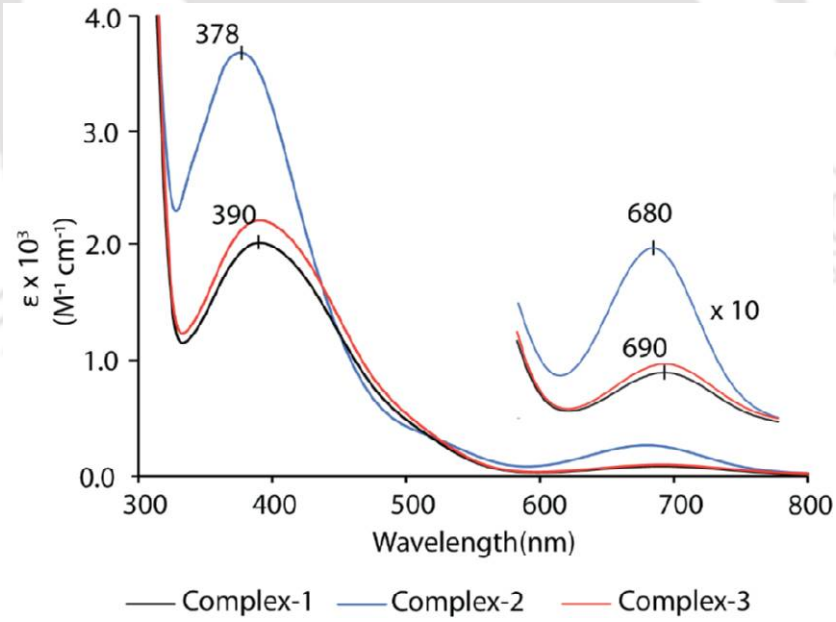

Figure 2.18 UV-visible spectra of Co(III)-complexes (**1**, **2,** and **3**) in DMF.

The LMCT and d-d transition of **2** showed blue shifting of the transition bands and also showed higher molar absorption coefficient values than the other two complexes (**1** & **3**).

Table 2.8 Electronic spectroscopic data for complex **1-3** (In DMF).

Complexes	**λ_{max}/nm (ε/$M^{-1}cm^{-1}$)**
1	690(96), 518(377) (sh), 390(2205)
2	680(280), 525(323) (sh), 378(3860)
3	690(103), 518(389) (sh), 390(2310)

The CD spectra of these two Co(III) complexes (1 & 2) were recorded using their DMF solutions.

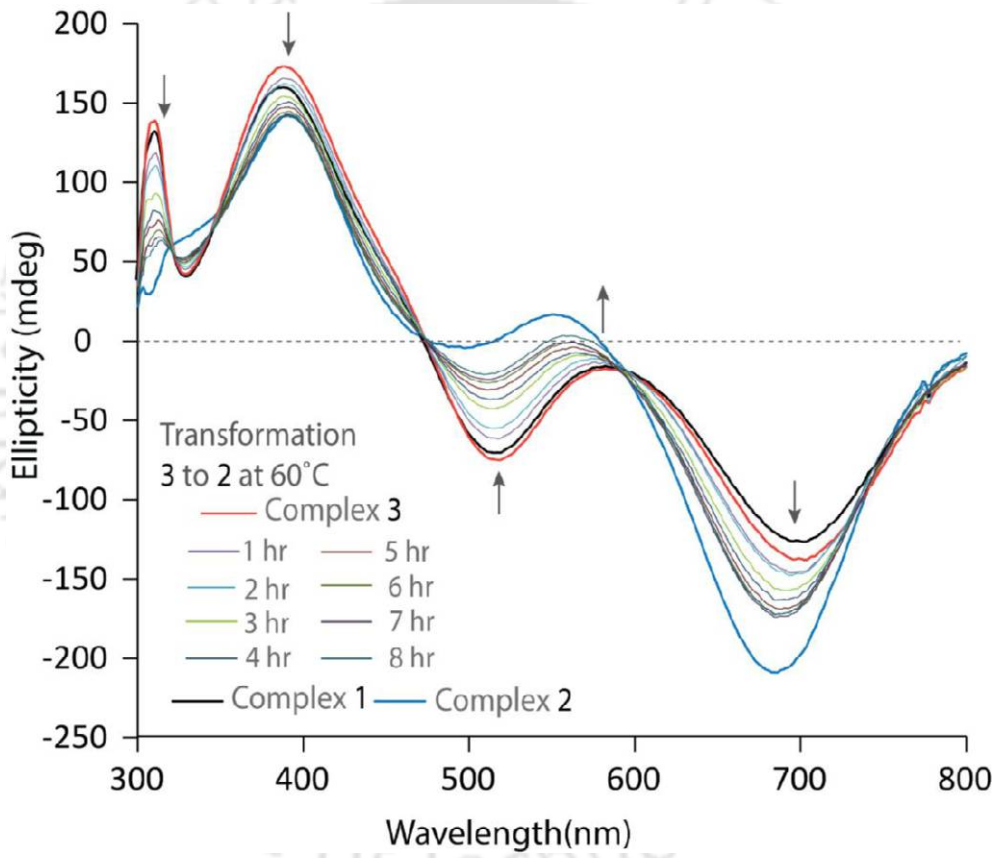

Figure 2.19 The time-dependent changes in CD spectra of **3** heating at 60°C in DMF compared to complexes **1** and **2**.

Complex **1** showed two positive CD signals- one is at 312 nm and the other at 385 nm. It also showed two negative CD signals at 511 nm and 684 nm, respectively. The CD spectrum of **2** also showed two positive CD signals at 321 nm and 392 nm and two negative CD signals, one at 497nm and the other at 679 nm. The CD signals (both positive and negative) that appeared in the

CD spectrum of **2** have shifted to the lower wavelength (blue shift) compared to **1**. In **2**, the negative CD signal appeared at 679 nm and had a much higher intensity than the negative CD signal of **1**, which occurred at 684nm. Whereas the CD spectrum of **3** is identical to to **1**. The structural transformation of **3** → **2** also can be monitored using CD spectroscopy. When the CD experiment was carried out at 60°C, the spectrum of **3** started changing, and after 8 hrs, it looked similar to **2**, i.e., in solution **3** transformed to **2**. (Fig. 2.19)

All these above results suggest that complexes **1** and **2** can hold their structural rigidity in the solid state and the solution. The Et_3NH^+ ion has one N-H bond, which forms a strong intramolecular H-bonding with the anionic $[Co(L^{O\text{-}ValTryp})_2]^-$ unit in **2,** but this is absent in **1** as Et_4N^+ has no H-bond capable N-H functionality. Complex **1** can transformed into **2** through the formation of an intermediate **3** in the presence of excess Et_3NHClO_4 salt, and this structural transformation is triggered by the single N-H in Et_3NH^+ ion. At room temperature, the structural transformation process is slow due to the kinetic inertness of the Co(III) complex.

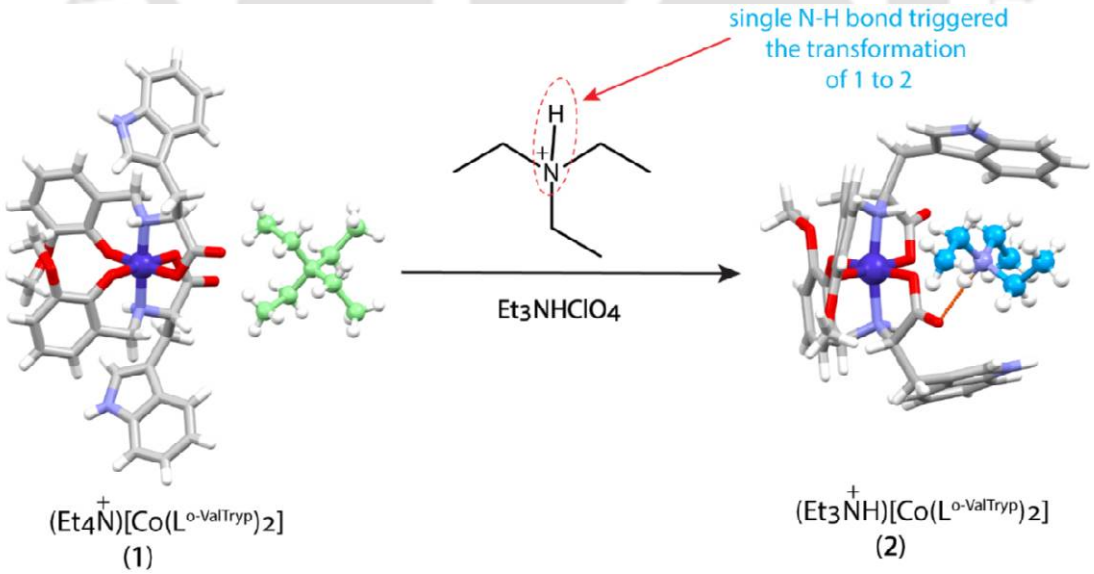

Figure 2.20 Structural transformation of **1** to **2** triggered by a single N-H in Et_3NH^+ ion.

2.5.6 The effect of kinetic lability in the structural transformation process

The role of kinetic lability in the structural transformation process described above was tested by synthesizing the labile Fe(III) analogs, $(Et_4N)[Fe(L^{O\text{-ValTryp}})_2]$(**4**) and $(Et_3NH)[Fe(L^{O\text{-ValTryp}})_2]\cdot(Et_3NHClO_4)$ (**5**). The synthetic procedures of the Fe(III) complexes are shown in Scheme 1. The **4** crystallized in the chiral tetragonal space group $P4_32_12$, the same as **1** (Table 2.1B). The structure of **4** is nearly identical to **1**, with minor changes in bond lengths and angles (Table 2.9). The coordination bond lengths in **4**, Fe-O_p = 1.943(3)Å, Fe-N_a = 2.160(4)Å, Fe-O_c = 2.020(4) Å, are similar to that found in other reported Fe^{III} complexes of similar types of ligand coordination.[32–34] In **4**, due to the high-spin nature of the Fe(III) complex, the coordination bond lengths have higher values than **1**, the Co(III) analog. Complex **5**, the labile Fe(III) analog of **2**, crystallized in the monoclinic space group $P2_1$ (Table 2.1B). The structure of $[Fe(L^{O\text{-ValTryp}})_2]^-$ in **5** is identical to that of $[Co(L^{O\text{-ValTryp}})_2]^-$ in 2 with one exception. In **2**, one Et_3NH^+ ion is bound inside the pocket, whereas the 5 has two Et_3NH^+ ions in the pocket, and it is not surprising, given that the *C2* symmetry of the molecule, two identical positions in the molecular cleft are available. Again, due to the high-spin nature of **5**, the coordination bond lengths and angles have higher values than its Co(III) analog (complex **2**) (Table 2.9).

Table 2.9 Selected bond length (Å) and angles (°) of complexes **4** and **5**.

	Fe-O_p	Fe-O_c	Fe-N_a	O_p-Fe-O_p	O_c-Fe-O_c	O_p-Fe-O_c	N_a-Fe-N_a
4	1.943(3)	2.020(4)	2.160(4)	100.55(15)	85.99(14)	165.08(15)	179.32(14)
	1.943(3)	2.020(4)	2.160(4)				
5	1.902(6)	2.048(7)	2.170(8)	91.4(3)	90.2(3)	165.7(3)	158.6(3)
	1.937(7)	2.054(7)	2.157(8)				

Subscripts *p* and *c* on the oxygen atom and *a* on the nitrogen atom denote phenolate, carboxylate and amine, respectively

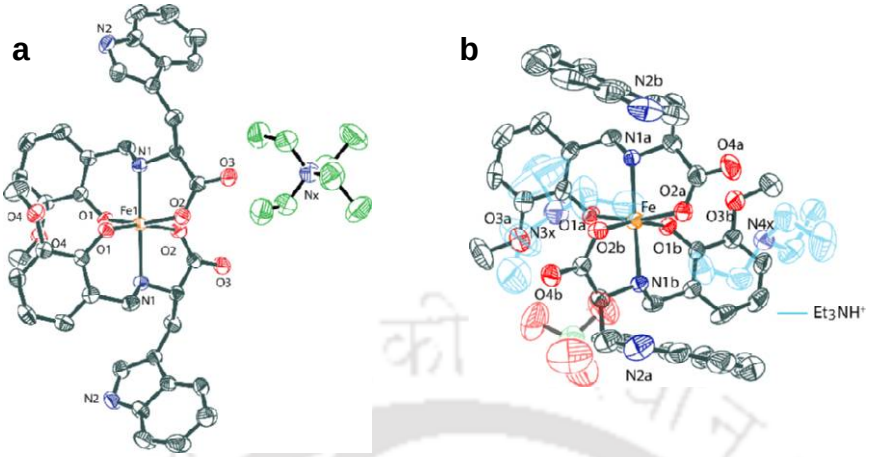

Figure 2.21 The ORTEP figures of **4**(a) and **5**(b) with 40% ellipsoid probability.

Table 2.10 Non-covalent interactions in Complex **4**

Atoms	D-H (Å)	H…A (Å)	D…A(Å)	DHA(˚)
N2-H2…O1	0.91(5)	2.10(5)	2.998(6)	167(4)
C1-H1B…O3	0.96	2.58	3.449(7)	150
C17-H17…O4	0.93	2.37	3.294(7)	171

Table 2.11 Non-covalent interactions in Complex **5**

Atoms	D-H (Å)	H…A (Å)	D…A(Å)	DHA(˚)
N1X-H1X…O4F	0.98	1.71	2.687(12)	172
N2A-H2A…O1B	0.86	2.26	3.113(15)	173
N2B-H2B…O6X	0.86	2.21	3.057(15)	167
N2E-H2E…O1X	0.86	2.19	2.989(19)	155
N2F-H2F…O1E	0.86	2.25	3.078(13)	161
N2X-H2X…O4E	0.98	1.69	2.672(14)	175
N3X-H3X…O4B	0.98	1.75	2.724(13)	171
N4X-H4X…O4A	0.98	1.63	2.602(14)	169

The crystal structure analyses of these two complexes (**4** & **5**) showed that they differ in the solid state. Then, the solution behavior of these two iron(III) complexes was investigated using UV-visible and CD spectroscopy. The UV-visible spectra of **4** and **5** are almost identical; each exhibits a shoulder near 330 nm and a band near 475 nm. The broadband that appeared near 475 nm can be assigned to a transition from the phenolate oxygen pπ orbital to the half-filled dπ* orbitals of the ferric ion, and such transitions are intense and can be attributed to the LMCT transitions. The shoulder appeared near 330 nm due to the charge transfer transition from the phenolate pπ orbital to the dσ* orbital of the Fe(III) ion. The DMF solution of each Fe(III) complex exhibited one positive CD signal near 300 nm and one negative CD signal near 480 nm. The CD spectra of complexes **4** and **5** are almost identical.

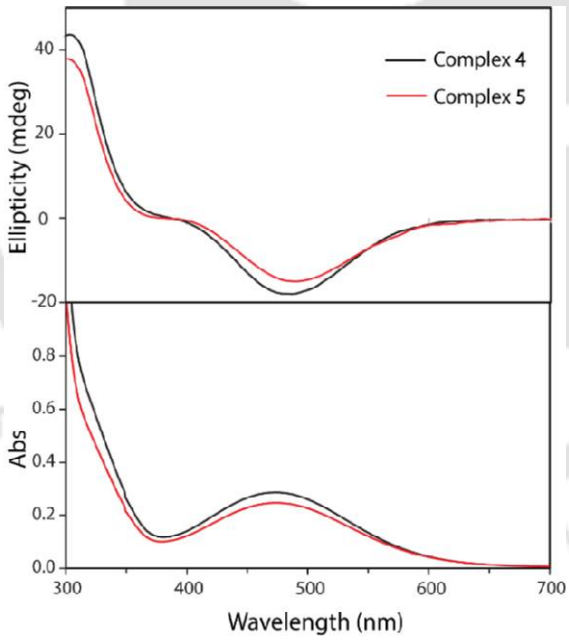

Figure 2.22 Combined UV-visible and CD spectra of **4** & **5**.

Table 2.12 UV-visible spectroscopic data of **4** & **5**

Complexes	λ_{max}/nm (ε/$M^{-1}cm^{-1}$)
4	472(3110), 328(5397)
5	475(3095), 332(4718)

The solution state characterizations (UV-visible spectra & CD spectra) of the complexes (**4** & **5**) showed that they behave similarly in solution. CDs are connected to the electronic transitions. The Co(III) and Fe(III) complexes exhibit different types and different numbers of visible transitions between 300-800 nm. In Co(III), there are three transitions: a ligand field (d-d) at l_{max} 690 nm (e, ~100 M^{-1} cm^{-1}), a shoulder at 520 nm (possibly ligand field transition) and a charge transfer at 400 nm (e, 2000-4000 M^{-1} cm^{-1}). The ligand field transition is known to be sensitive to a particular geometric isomer. The CD of the charge transfer at ~400 nm only differed in intensity, not position (Fig.). Fe(III) has only one LMCT at ~470 nm. Thus, the changes in CD of **4** and **5** are minimal.

Structural transformation of 4 to 5

When the methanolic solution of **4** was treated with 3 equivalents of triethyl ammonium perchlorate salt, it initially formed a red-coloured solution, which, upon slow evaporation at room temperature, gave block-shaped crystals after four days, and the single crystal structure analysis showed that **5** formed, i.e., in the presence of Et_3NHClO_4 salt there occurred structural transformation of **4** to **5**.

Due to the kinetic lability of **4**, the Fe(III)-ligand coordination bonds breaking and the recombination essential for this structural transformation became easier than the transformation process among their Co(III) analogs. As the metal-ligand coordination bonds in Co(III)-complex are inert; in the presence of Et_3NHClO_4, the structural transformation of **1** to **2** is slow, and it requires 23 days for >90% conversion in the solution state, while for Fe(III) complexes, due to their labile nature, the transformation of **4** to **5** becomes faster.

2.6 Cyclic voltammetry of Fe(III) complexes

The redox properties of the Fe(III) complexes (both **4** & **5**) have been discussed by using cyclic voltammetry (CV) experiments performed in a dry DMF solution containing 0.15M tetrabutylammonium perchlorate (TBAP) as a supporting electrolyte. $[Fe(bpy)_3](ClO_4)_2$ (ΔE_p= 59 mV) used as a calibrator of potential and ΔE_p check (. Though UV-visible and CD spectra of complexes **4** & **5** are almost identical, under electrochemical conditions, they behave differently.

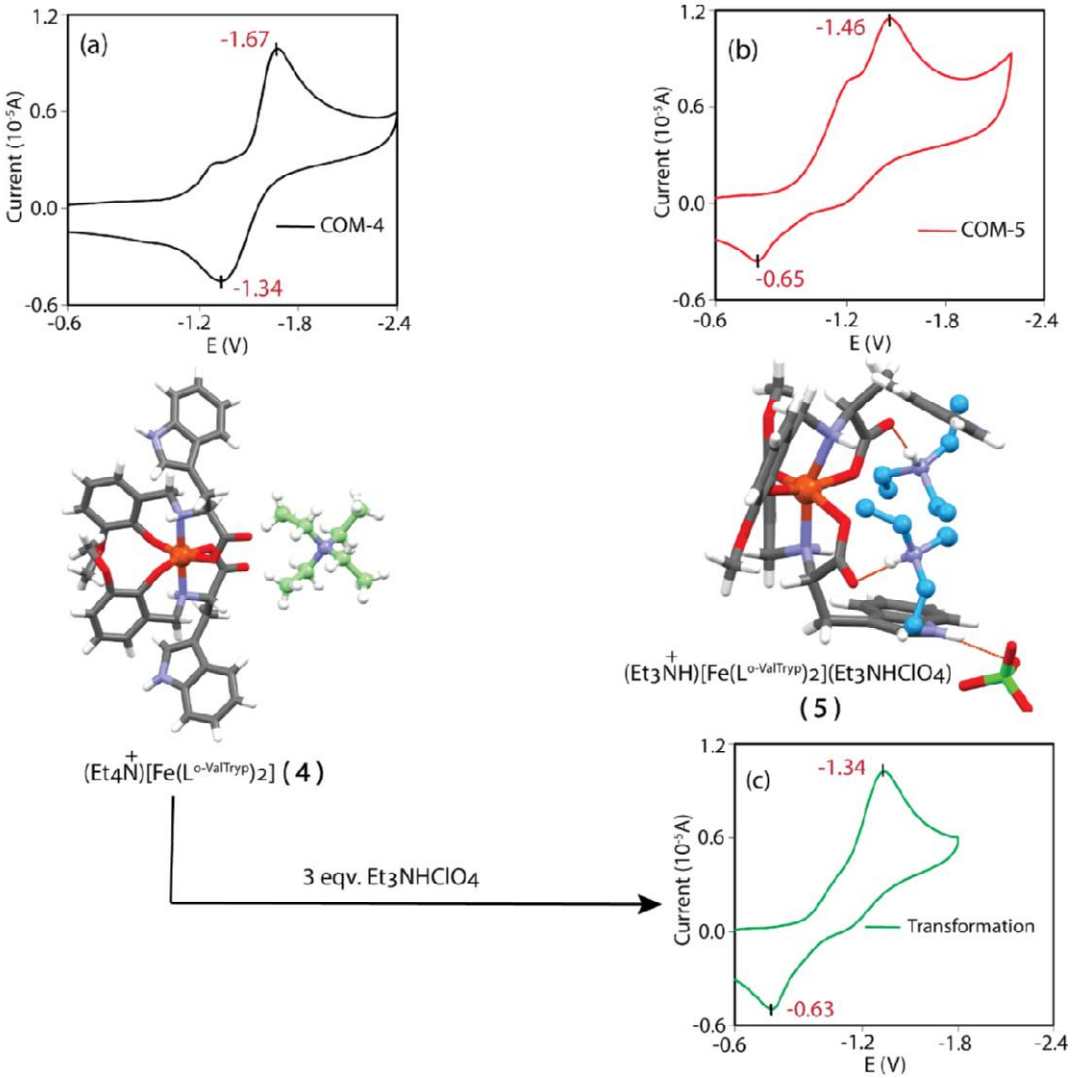

Figure 2.23 Cyclic voltammograms of Complexes **4** (a) & **5** (b) and the change in the cyclic voltammogram of **4** with the addition of Et_3NHClO_4 (c).

The redox potential of the complexes ($E_{½}$ = 0.5x(E_{pa} +E_{pc}), where E_{pa} is anodic, and E_{pc} are

cathodic peak potential, respectively) and peak-to-peak separation (ΔE_p, separation between E_{pa} and E_{pc}) values of these complexes showed drastic differences.

The cyclic voltammogram of **4** showed the reduction peak at E_{pc} = -1.67 V and oxidation peak at -1.34 V. Thus, the anodic scan of complex **4** showed a quasi-reversible wave having $E_{½}$ = -1.51 V (ΔE_p = 330 mV) attributed to the $Fe^{III/II}$ redox couple. The cyclic voltammogram of **5** showed the reduction peak at E_{pc} = -1.46 V with a strongly shifted reoxidation peak at – 0.65 V, i.e., the anodic scan of complex **5** showed a completely irreversible wave at $E_{½}$ = -1.06 V (ΔE_p = 810 mV) corresponding to $Fe^{III/II}$ redox couple. Thus, Complex 5, having an Et_3NH^+ counter ion, shifted the redox potential towards the more positive values than the redox potential value **4**, having an Et_4N^+ counter ion. Also, in the solid-state structural analyses of the complexes, we observed that the Et_3NH^+ ion present in complex **5**, having intermolecular H-bonding capable N-H functionality, caused folding conformation of the anionic complex unit, $[Fe(L^{O\text{-ValTryp}})_2]^-$ rather than unfolded conformation of $(NEt_4)[Fe(L^{O\text{-ValTryp}})_2]$ (**4**). Here, in the case of cyclic voltammetry of the complexes, the Et_3NH^+ ion might be playing a crucial role in the less negative redox potential values of complex **5,** which is confirmed when three equivalents of the Et_3NHClO_4 salt was added to the DMF solution of complex **4,** the quasi-reversible wave of the complex immediately changed to an irreversible wave (like complex **5**) and redox potential values strongly shifted to the more positive region. The above observation suggested that the drastic change in the cyclic voltammogram of complex **4** upon adding Et_3NHClO_4 salt occurred. It could be because of the metal-ligand coordination change or significant structural rearrangement of the Fe(III) complex.

2.7 Conclusion

In conclusion, we have synthesized a coordinatively saturated, chiral anionic Co(III)-host complex with an L-tryptophan-derived reduced Schiff base ligand, which binds Et_4N^+ and Et_3NH^+ ions through non-covalent interactions. The Co(III)-host anion recognizes the Et_4N^+ ion in an extended form, whereas, for the recognition of the Et_3NH^+ ion, the host anion adopts a folded conformation. The only difference between the Et_4N^+ ion and the Et_3NH^+ ion is that instead of four ethyl arms (in the Et_4N^+ ion), the triethyl ammonium ion contains three ethyl arms and one N-H group, which can act as an H-bond donor. This single N-H in Et_3NH^+ ion could trigger the structural transformation of the anionic Co(III)-host from its extended form to the folded conformation, involving inert metal-ligand coordination bond breaking and reformation in a new arrangement, and this structural transformation process is slow at room temperature due to the inert nature of the Co(III)-complex, i.e., the reorganization is specific to triethylammonium ion. The role of kinetic inertness in the structural transformation process was tested by synthesizing the kinetically labile Fe(III)-analogs. At room temperature, in the presence of Et_3NH^+ ion, the isostructural labile Fe(III)-complex showed much faster transformation from its extended form to the folded conformation due to the more dynamic nature of the metal-ligand coordination bonds in it, i.e., the process of structural reorganization can be tuned by changing the lability of central metal ion.

References

(1) Boehr, D. D.; Nussinov, R.; Wright, P. E. *Nat Chem Biol* **2009**, *5* (11), 789–796.

(2) Schrader, T. *J. Org. Chem.* **1998**, *63* (2), 264–272.

(3) Amoli, V.; Kim, J. S.; Jee, E.; Chung, Y. S.; Kim, S. Y.; Koo, J.; Choi, H.; Kim, Y.; Kim, D. H. *Nat Commun* **2019**, *10* (1), 4019.

(4) Zeng, F.; Zimmerman, S. C. *Chem. Rev.* **1997**, *97* (5), 1681–1712.

(5) Haga, K.; Kruse, A. C.; Asada, H.; Yurugi-Kobayashi, T.; Shiroishi, M.; Zhang, C.; Weis, W. I.; Okada, T.; Kobilka, B. K.; Haga, T.; Kobayashi, T. *Nature* **2012**, *482* (7386), 547–551.

(6) Sahoo, S. C.; Ray, M. *Chemistry A European J* **2010**, *16* (17), 5004–5007. h

(7) Das, C. R.; Dutta, T.; Ray, M. *Inorganica Chimica Acta* **2019**, *486*, 367–376. h

(8) Das, C. R.; Sahoo, S. C.; Ray, M. *Crystal Growth & Design* **2014**, *14* (8), 3958–3966.

(9) Miyake, H.; Sugimoto, H.; Tamiaki, H.; Tsukube, H. *Chem. Commun.* **2005**, No. 34, 4291. https://doi.org/10.1039/b506130j.

(10) Cai, L.-X.; Yan, D.-N.; Cheng, P.-M.; Xuan, J.-J.; Li, S.-C.; Zhou, L.-P.; Tian, C.-B.; Sun, Q.-F. *J. Am. Chem. Soc.* **2021**, *143* (4), 2016–2024.

(11) Goodwin, T. J.; Williams, P. A.; Vagg, R. S. Chiral Metal Complexes. Part 16. *Inorganica Chimica Acta* **1984**, *86* (3), L73–L75.

(12) Zahn, S.; Canary, J. W. *Science* **2000**, *288* (5470), 1404–1407.

(13) Sakata, Y.; Chiba, S.; Miyashita, M.; Nabeshima, T.; Akine, S. *Chemistry A European J* **2019**, *25* (12), 2962–2966.

(14) Zahn, S.; Das, D.; Canary, J. W. *Inorg. Chem.* **2006**, *45* (15), 6056–6063.

(15) Gregoliński, J.; Hikita, M.; Sakamoto, T.; Sugimoto, H.; Tsukube, H.; Miyake, H. *Inorg. Chem.* **2016**, *55* (2), 633–643.

(16) Wang, S.; Sawada, T.; Ohara, K.; Yamaguchi, K.; Fujita, M. *Angew Chem Int Ed* **2016**, *55* (6), 2063–2066.

(17) He, Z.; Ye, G.; Jiang, W. *Chemistry A European J* **2015**, *21* (7), 3005–3012.

(18) Scherer, M.; Caulder, D. L.; Johnson, D. W.; Raymond, K. N. *Angew. Chem. Int. Ed.* **1999**, *38* (11), 1587–1592.

(19) Späth, A.; König, B. *Beilstein J. Org. Chem.* **2010**, *6*.

(20) Zuo, W.; Jia, C.; Zhang, H.; Zhao, Y.; Yang, X.-J.; Wu, B. *Chem. Sci.* **2019**, *10* (8), 2483–2488.

(21) Danylyuk, O.; Fedin, V. P.; Sashuk, V. *Chem. Commun.* **2013**, *49* (18), 1859.

(22) Shivanyuk, A.; Rissanen, K.; Kolehmainen, E. *Chem. Commun.* **2000**, No. 13, 1107–1108.

(23) Kurihara, K.; Yazaki, K.; Akita, M.; Yoshizawa, M. *Angew Chem Int Ed* **2017**, *56* (38), 11360–11364.

(24) Alam, Md. A.; Nethaji, M.; Ray, M. *Inorg. Chem.* **2005**, *44* (5), 1302–1308.

(25) Sahoo, S. C.; Ray, M. *Dalton Trans.* **2009**, No. 17, 3230.

(26) Sahoo, S. C.; Ray, M. *Dalton Trans.* **2007**, No. 44, 5148.

(27) Long, C.; Ray, M. *Dalton Trans.* **2024**, *53* (15), 6642–6652.

(28) Alam, Md. A.; Koner, R. R.; Das, A.; Nethaji, M.; Ray, M. *Crystal Growth & Design* **2007**, *7* (9), 1818–1824.

(29) Sahoo, S. C.; Dubey, M.; Alam, Md. A.; Ray, M. *Inorganica Chimica Acta* **2010**, *363* (12), 3055–3060.

(30) Shongwe, M. S.; Al-Hatmi, S. K. M.; Marques, H. M.; Smith, R.; Nukada, R.; Mikuriya, M. *J. Chem. Soc., Dalton Trans.* **2002**, No. 21, 4064–4069.

(31) Shakya, R.; Imbert, C.; Hratchian, H. P.; Lanznaster, M.; Heeg, M. J.; McGarvey, B. R.; Allard, M.; Schlegel, H. B.; Verani, C. N. *Dalton Trans.* **2006**, No. 21, 2517–2525.

(32) Dasgupta, S.; Atta, S.; Singh, N. D. P.; Deb, D.; Kassel, W. S.; Bhattacharjee, M. *Eur J Inorg Chem* **2014**, *2014* (30), 5125–5134.

(33) Meier, R.; Molinier, M.; Anson, C.; Powell, A. K.; Kallies, B.; Van Eldik, R. *Dalton Trans.* **2006**, No. 46, 5506.

(34) Meier, R.; Maigut, J.; Kallies, B.; Lehnert, N.; Paulat, F.; Heinemann, F. W.; Zahn, G.; Feth, M. P.; Krautscheid, H.; Van Eldik, R.. *Chem. Commun.* **2007**, No. 38, 3960.

Chapter 3

The alkali and alkaline earth metal cation induced structural modification of labile Fe(III) complex

3.1 Introduction

In the previous chapter, we observed that the anionic complex $[M(L^{O\text{-ValTryp}})_2]^-$ (M = Co^{III} and Fe^{III}) can adopt different shapes to recognize two different ammonium ions (Et_4N^+ and Et_3NH^+). The isostructural $(Et_4N)[Co(L^{O\text{-ValTryp}})_2]$ and its iron(III)-analog showed the structural transformation from its extended form to the folded conformation in the presence of Et_3NH^+ ion, and the transformation process is fast for the labile Fe(III) complex. In this chapter, we tried to discover what would happen if we employed the anionic host complex to bind secondary metal cations instead of the ammonium ions. For this, we used a coordinatively saturated labile Fe(III) complex as a host for the binding of alkali and alkaline earth metal ions of different charges and sizes, and thus, we synthesized different heterometallic complexes. Here, we have used alkali and alkaline earth metal ions (Na^+, K^+, Ca^{2+}, Ba^{2+}) because these nonredox active Lewis acidic metal cations play an important role in the biological systems,[1–4] e.g., in biology, the Ca^{2+} ion combined with Mn_4O_5 cluster promotes water oxidation in the oxygen evolution complex (OEC) in Photosystem II. In recent years, salen-type ligands-based and other heterometallic complexes containing redox-active and redox-inactive metals have been reported.[5–12] These complexes are used as supramolecular building blocks,[13–15] in nonlinear-optical materials,[16,17] as interesting magnetic compounds,[18] and employed as catalysts for various organic reactions like C-H oxidation,[19,20] oxygen reduction reactions[21], etc. Also, the transition metal complexes containing crown ether-like functionalities that encapsulate alkali or alkaline earth metal ions and their various applications have been reported.[22–35] Our group recently reported that coordinatively saturated anionic bis iron(III) complexes of L-threonine derivative could bind different secondary metal cations (Li^+, Na^+, K^+, and Ba^{2+}) and can show multidirectional coordination polymer formation. The hydrophilic alcoholic side arms of L-threonine increased the water solubility of

the complexes through multiple hydrogen bonding. In this work, we used L-tryptophan having an aromatic indole side arm instead of the alcoholic arm in L-threonine and synthesized coordinatively saturated anionic bis iron(III) complexes of L-tryptophan derivative to bind alkali and alkaline earth metal ions.

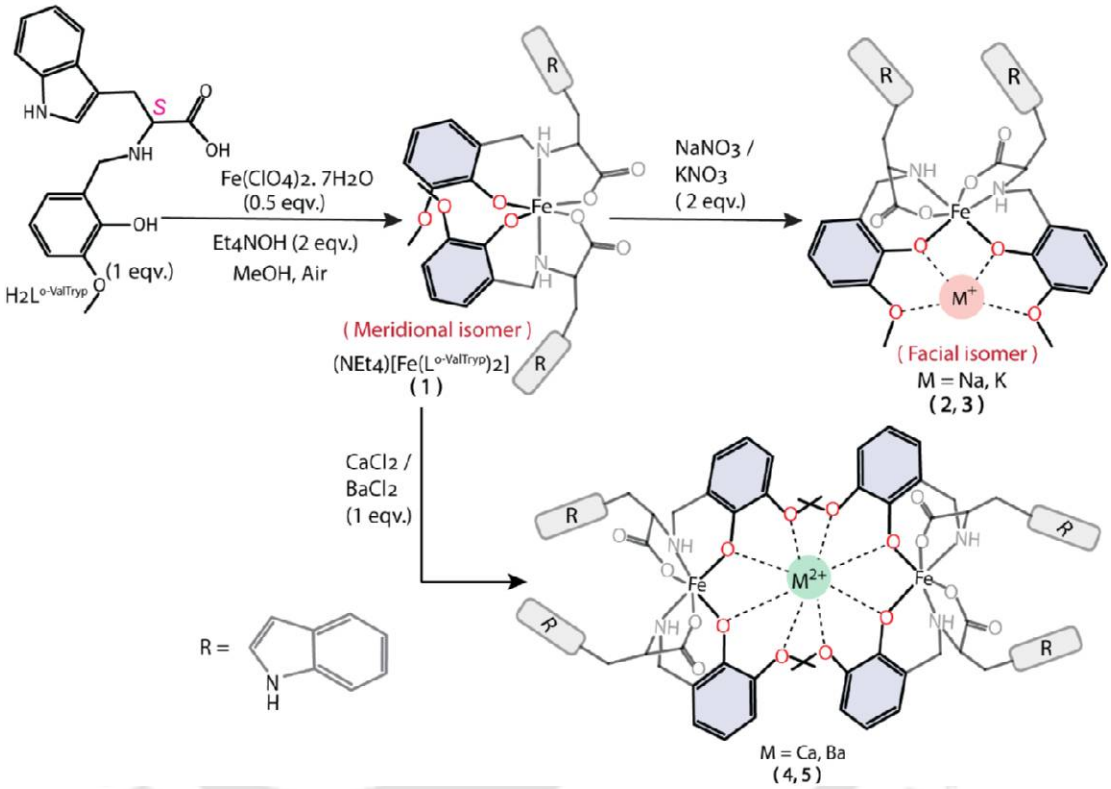

Scheme 3.1. Synthesis of the Fe(III)-complexes

3.2 Experimental Section

3.2.1 Materials and Methods

Solvents and reagents were obtained from commercial sources and used without further purifications unless otherwise asserted. Anhydrous grade *N*, *N*-dimethylformamide, $NaNO_3$, and KNO_3 were purchased from was purchased from Aldrich Chemical Co.

The IR spectra were recorded on a Nicolet FTIR spectrophotometer with KBr discs in the 4000-400 cm-1 range. UV-visible spectra of the samples were measured with a PerkinElmer Lambda

365+ UV/vis spectrometer. NMR spectra were recorded on Bruker 500 MHz. ESI-mass spectra were recorded with a high-resolution mass spectrometer (Agilent 6546 LC/Q-TOF). Circular Dichroism measurements were performed using JASCO-J-1500 CD spectrometer, and CD spectra were analyzed using JASCO spectra manager version 2.0. All the CD spectra were recorded under an inert N_2 atmosphere using HPLC grade DMF as a solvent and a high-precision cell made of quartz SUPRASIL cuvette with a path length of 1 mm. Powder X-ray diffraction patterns were recorded using MAKE Bruker, a D2 Phaser instrument with Cu-Kα radiation (λ = 1.5418 Å) equipped with an integrated PC and DIFFRAC.SUITE software. Diffraction patterns were collected over the 2θ range between 5-50˚ at a step scan rate of 0.03˚. Solid-state magnetic susceptibility of the complexes at room temperature was recorded using Sherwood Scientific Magnetic Balance MSB-1.

3.3 Syntheses

The ligand $H_2L^{O\text{-ValTryp}}$ and $(NEt_4)[Fe(L^{O\text{-ValTryp}})_2]$ synthesized in Chapter **2** are used as starting material in this chapter.

3.3.1 $(NEt_4)[Fe(L^{O\text{-ValTryp}})_2]$ (1). The detailed synthetic procedure of $(NEt_4)[Fe(L^{O\text{-ValTryp}})_2]$ was discussed in Chapter **2**.

Anal. Calcd for $(NEt_4)[Fe(L^{O\text{-ValTryp}})_2]$: C, 64.03; H, 6.54; N, 8.12. Found: C, 63.803; H, 7.183; N, 8.159. IR (KBr, cm^{-1}): $\upsilon(COO^-)_{asym}$ 1639; $\upsilon(COO^-)_{sym}$ 1453; υ(C-O) 1283; υ(C-H)o/p-ring H 757; υ(M-O) 579; υ(M-N) 426. μ_{eff} (solid, 292K); 5.7 μB/Fe. m/z (ESI-MS) $\{M+2H\}^+$, $\{[Fe(L^{O\text{-Val Tryp}})_2]^-+2H\}^+$; calcd: 734.20, found: 734.20.

3.3.2 $Na[Fe(L^{O\text{-ValTryp}})_2(MeOH)_2]$ (2). Solid $NaNO_3$ (0.090g, 1.06 mmol) was added to the stirring methanolic solution (15 mL) of $(NEt_4)[Fe(L^{O\text{-ValTryp}})_2]$**(1)** (0.300 g, 0.348 mmol), taken into a round bottom flask, and stirred for 1hr at room temperature. After that, the purple-coloured solid

appeared, filtered off, and washed with ethyl acetate. The solid was dissolved in 20 mL methanol; 2 ml of DMF was added to the solution and kept in a 50 mL beaker for slow evaporation of the solvent. Block-shaped dark-red coloured crystals were obtained after 8 days. Crystals were washed with ethyl acetate and diethyl ether and dried under a vacuum. Yield: 68%

Anal. Calcd for $Na[Fe(L^{O\text{-}ValTryp})_2]\cdot 1.5CH_3OH$: C, 60.15; H, 5.63; N, 8.03. Found: C, 59.95; H, 6.02; N, 7.56. IR (KBr, cm^{-1}): $\upsilon(COO^-)_{asym}$ 1651; $\upsilon(COO^-)_{sym}$ 1475; υ(C-O) 1245. μ_{eff} (solid, 292K); 5.94 μB/Fe.

A suitable X-ray single crystal of the complex was obtained by further recrystallization from the solution of the complex in the CH_3OH-H_2O solvent mixture.

3.3.3 $K[Fe(L^{O\text{-}ValTryp})_2(H_2O)]$ (3). This complex was synthesized using the same method described above for **2**, here the methanolic solution of $(NEt_4)[Fe(L^{O\text{-}ValTryp})_2]$ (0.300 g, 0.348 mmol) was treated with KNO_3 (0.106 g, 1.05 mmol) to obtain the desired product. Yield: 72%

Anal. Calcd for $K[Fe(L^{o\text{-}ValTryp})_2].1.5CH_3OH$: C, 57.88; H, 5.16; N, 6.83. Found: C, 57.97; H, 4.99; N, 7.02. IR (KBr, cm^{-1}): $\upsilon(COO^-)_{asym}$ 1655; $\upsilon(COO^-)_{sym}$ 1470; υ(C-O) 1240. μ_{eff} (solid, 292K); 5.9 μB/Fe.

A suitable X-ray single crystal of the complex was obtained by further recrystallization from the solution of the complex in the CH_3CN-H_2O solvent mixture.

3.3.4 $Ca[Fe(L^{O\text{-}ValTryp})_2]_2$ (4). Solid $CaCl_2$ (0.058g, 0.53 mmol) was added to the stirring methanolic solution (15 mL) of $(NEt_4)[Fe(L^{O\text{-}ValTryp})_2]$**(1)** (0.300 g, 0.360 mmol), taken into a round bottom flask, and stirred for 30 min. at room temperature. After that, the red-coloured solid appeared, filtered off, and washed with ethyl acetate. The solid was dissolved in a 15 mL MeOH-DMF (2:1) solvent mixture and kept in a 25 mL beaker for slow evaporation. Block-shaped red-

coloured crystals were obtained after 15 days. Crystals were washed with ethyl acetate and diethyl ether and dried under a vacuum. Yield: 67%

Anal. Calcd for Ca[Fe($L^{O\text{-ValTryp}}$)$_2$]$_2$·3DMF: C, 59.20; H, 5.43; N, 8.94. Found: C, 59.085; H, 4.93; N, 9.01. IR (KBr, cm^{-1}): $\upsilon(COO^-)_{asym}$ 1634; $\upsilon(COO^-)_{sym}$ 1476; υ(C-O) 1239. μ_{eff} (solid, 292K); 5.8 μB/Fe.

A suitable X-ray single crystal of the complex was obtained by further recrystallization from the solution of the complex in the CH_3OH-DMF solvent mixture.

3.3.5 Ba[Fe($L^{O\text{-ValTryp}}$)$_2$]$_2$ (5). Solid $BaCl_2 \cdot 2H_2O$ (0.125g, 0.512 mmol) was added to the stirring methanolic solution (15 mL) of (NEt_4)[Fe($L^{O\text{-ValTryp}}$)$_2$]**(1)** (0.300 g, 0.348 mmol), taken into a round bottom flask, and stirred for 30 min. at room temperature. After that, the purple-coloured solid appeared, filtered off, and washed with ethyl acetate. The solid was dissolved in a 25 mL MeOH-DMF (5:1) solvent mixture and kept in a 50 mL beaker for slow evaporation. Block-shaped reddish-purple coloured crystals were obtained after 12 days and used for X-ray single-crystal structure determination of the complex. Then, the crystals were washed with ethyl acetate and diethyl ether and dried under a vacuum. Yield: 64%

Anal. Calcd for Ba[Fe($L^{O\text{-ValTryp}}$)$_2$]$_2$·CH_3OH·DMF: C, 55.92; H, 5.04; N, 7.24. Found: C, 55.88; H, 5.22; N, 6.80. IR (KBr, cm^{-1}): $\upsilon(COO^-)_{asym}$ 1636; $\upsilon(COO^-)_{sym}$ 1471; υ(C-O) 1241. μ_{eff} (solid, 292K); 5.88 μB/Fe.

3.4 X-ray Crystallography

The crystal of the complexes obtained during synthesis was used for X-ray analysis. The crystals were mounted on glass fibre. All geometric and intensity data for the crystals were collected at room temperature using a Bruker SMART APEX CCD diffractometer equipped with a fine focus 1.75 kW sealed tube Mo-Kα (λ= 0.71073 Å) X-ray source, with increasing ω (width of 0.3º per frame) at a scan speed of either 3 or 4 s/frame. The SMART software was used for data acquisition, and the SAINT software for data extraction. Absorption corrections were done using a multi-scan. After the initial solution and refinement with SHELXL, the final refinement was performed on the WinGX environment using the SHELXL-97 programs. All non-hydrogen atoms were refined anisotropically. The hydrogen atoms were located from the Fourier maps and refined isotopically wherever possible. Thus, some C-H bonds will not be ideal and may vary. In complex **2**, the hydrogen atoms attached to the solvent water molecules cannot be located or fixed, so the molecular weight may not match. ORTEP obtained selected crystallographic data summarized in Table **3.1,** and the selected bond distances and bond angles of the respective complexes are listed in the tables below. Perspective views of the complexes were shown using ORTEP.

Table 3.1 Crystallographic data and refinement parameters of Fe(III) Complexes.

Complexes	**COM-2**	**COM-3**	**COM-4**	**COM-5**
Empirical Formula	$C_{41}H_{47}FeN_4NaO_{11}$	$C_{38}H_{36}FeKN_4O_9$	$C_{91}H_{106}CaFe_2N_{13}O_{25}$	$C_{82}H_{85}BaFe_2N_9O_{21}$
Formula Weight	850.66	787.66	1933.66	1781.62
Wavelength(Å)	0.71073	0.71073	0.71073	0.71073
Crystal system	triclinic	orthorhombic	monoclinic	orthorhombic
Space group	*P*1	$P2_1\ 2_1\ 2_1$	$P2_1$	$P2_1\ 2_1\ 2_1$
a, Å	9.434(3)	9.383(2)	13.397(3)	16.360(5)
b, Å	10.248(3)	10.395(3)	14.023(4)	16.523(5)
c, Å	11.733(4)	39.792(9)	25.188(6)	30.908(11)
α, deg	71.100(9)	90	90	90
β, deg	76.526(8)	90	100.065(7)	90
γ, deg	86.091(9)	90	90	90
Volume, $Å^3$	1043.7(6)	3881.3(16)	4659(2)	8355(5)
Z/ρ	1/1.353	4/1.348	2/ 1.378	4/1.416
μ	0.435	0.553	0.449	0.885
Coll reflns	7238	6843	15857	14721
Indep refln	5613	5231	10168	10584
FLACK para.	0.061(7)	0.061(7)	0.060(10)	0.052(6)
GOF	1.093	1.081	1.136	1.191
R1[a]	0.0558	0.0495	0.1056	0.0828
wR2[a]	0.1013	0.0914	0.1814	0.1367
R1[b]	0.0822	0.0800	0.1661	0.1278
wR2[b]	0.1149	0.1025	0.2126	0.1590

[a] $I > 2\sigma$. [b] All data

3.5 Result and Discussion

3.5.1 Syntheses and Selected Properties

The ligand, $H_2L^{O\text{-ValTryp}}$, was synthesized using the same procedure mentioned in the previous chapter (Chapter 2). Complex **1** was synthesized through the direct metal-ligand complexation reaction in the presence of tetraethylammonium hydroxide solution (20 wt% in water) as a base. Complex 1, having tetraethylammonium ion as a counter ion, was used as the starting material for synthesizing the other secondary metal ion-containing Fe(III) complexes. When the methanolic solution of 1 was treated with an alkali ($NaNO_3$, KNO_3) or alkaline earth metal salts ($CaCl_2$, $BaCl_2$), it gave a heterobimetallic complex. Several spectroscopic techniques, like elemental analyses and mass spectrometry, IR-spectroscopy, UV-visible spectroscopy, and CD-spectroscopy, characterized the Fe(III) complexes. The elemental analyses agreed well with the proposed composition of the complexes. The ESI (+) mass analysis of the complexes showed a prominent peak at m/z = 734.20 for $[Fe^{III}(L^{2-})_2 + 2H]^+$ in MeOH. IR spectra of the complexes showed a broad band near 3400 cm^{-1} corresponding to N-H (indole) and O-H (water) stretching vibration. The Fe(III) complexes also showed another strong and sharp band 1615-1635 cm^{-1} due to the Fe(III)-coordinated carboxylate stretching. The solid-state room temperature magnetic moments of **1**-**5** are close to 5.92 BM, typical for high-spin Fe(III) centers.

3.5.2 Crystal structures

Detailed solid-state structural analysis of **1** has been discussed in the previous chapter. The Fe(III) ion in **1** is meridionally coordinated by two deprotonated ligands where metal-coordinated carboxylates and phenolates are cis to each other, whereas the two anime nitrogen atoms coordinated to the metal ion are trans to each other. (Figure 3.1)

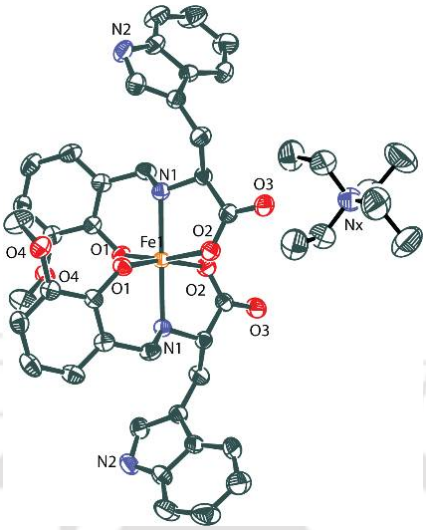

Figure 3.1 ORTEP figure of the of **1** with 40% ellipsoid probability.

Complex **2** crystallized in the triclinic space group *P1* (Table 3.1). The asymmetric unit of the complex consists of one anionic $[Fe(L^{O\text{-ValTryp}})_2]^-$ complex unit, one Na^+ counter ion, and three methanol molecules. The selected bond lengths and bond angles are given in Table 2. The shape of the complex is entirely different from the complex **1** described above. In **2**, two deprotonated tridentate ligands are facially coordinated to the Fe^{III} centre, where the metal-coordinated carboxylates are trans to each other. The chiral carbons (C8A & C8B) in complex **2** have *"S"* configuration, and two coordinated amine N atoms (N1A & N1B) have *"R"* conformation. This phenomenon of opposite conformation preference at chiral carbon (C8A & C8B) and metal amine nitrogen (N1A & N1B) has been observed in all previous complexes with this type of ligands. The axial $O_{carboxylate}$-Fe-$O_{carboxylate}$ angle value is 159.57(18)˚ (Fig. 3.2a), significantly deviating from the ideal value of 180˚ and also, the cisoid bond angles around the Fe(III) centre, $O_{phenolate}$-Fe-$O_{phenolate}$ = 89.39(2)˚) and (N_{amine}-Fe-N_{amine} = 96.9(2)˚, have deviated from the ideal value 90˚. The deviation of the bond angles from ideal 180˚ and 90˚ indicates the Fe^{III}-centre in **2** is in a highly distorted octahedral environment. In the facial arrangement, the Fe(III)-

coordinated two phenolates, and the two methoxy groups of the ligands formed a semi-circular O_4 coordination site. which binds the Na^+ ion and two methanol molecules, which are also coordinated with the sodium ion. Thus, in **2**, the Na^+ ion is located in a six-coordinate oxo-donor environment, and the Fe-Na distance is 3.352Å.

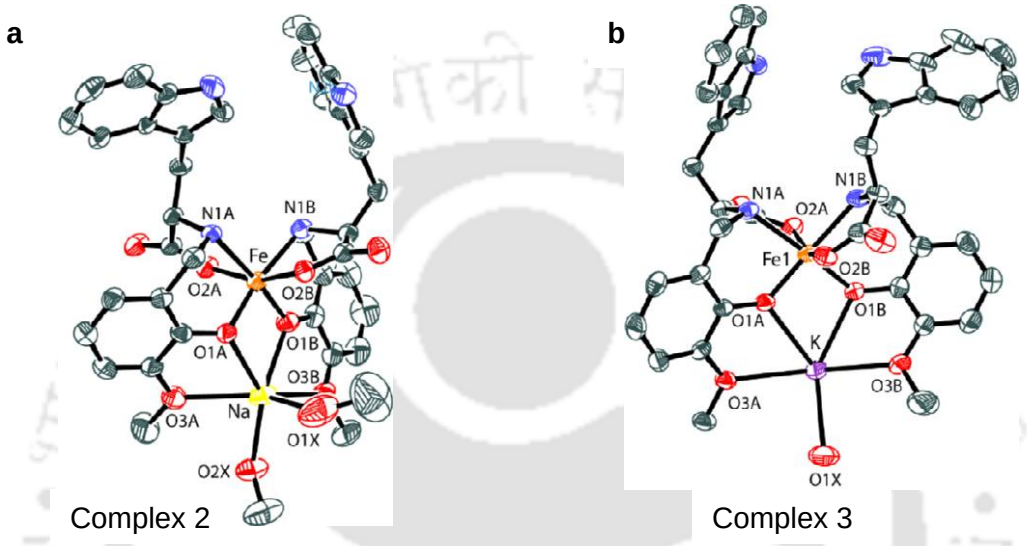

Figure 3.2 Molecular structures of complexes 2 and 3 with thermal ellipsoids set to a 40% probability level.

On the other side of the anion, the indole nitrogen atoms (N2A & N2B) are hydrogen bonded to both oxygen atoms of one carboxylate (O2A, O4A) of the neighboring anionic complex molecule through intermolecular indole…carboxylate H-bonding interactions and stitch the adjacent Fe(III)-complex anions in a linear chain along a-axis.

Complex **3** crystallized in the orthorhombic space group $P2_1\ 2_1\ 2_1$, and the asymmetric unit of the complex contains one $[Fe(L^{O\text{-ValTryp}})_2]^-$ complex anion bonded to one K^+ ion and one water molecule. The structural arrangement of this complex is similar to **2**, i.e., here, two deprotonated tridentate ligands are facially coordinated to the Fe^{III} centre, forming a semi-circular O_4 pocket where the K^+ ion has bound (Fig. 3.2b). The Fe-$O_{phenolate}$, Fe-$O_{carboxylate}$, and Fe-N_{amine} bond length values of **3** are very close to the complex **2** (Table 3.2), but due to the higher ionic radii of

potassium ion (138 pm), the K-$O_{phenolate}$ and K-$O_{methoxy}$ bond lengths have higher values than in **2**.

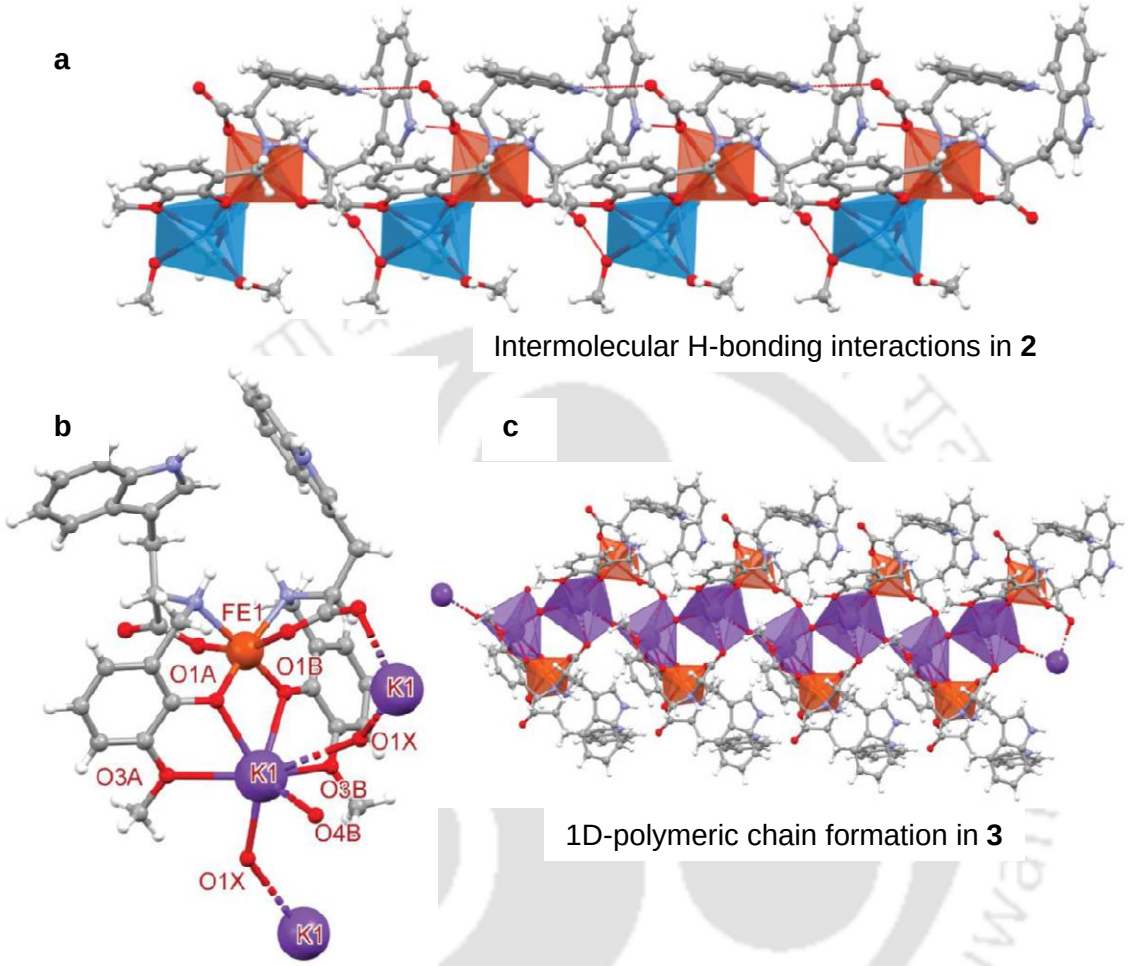

Figure 3.3 (a) Linear arrangement of complex molecules in **2**, (b) showing the coordination around the potassium ion in **3**, (c) 1D-polymeric chain formation along the a-axis in **3**.

In **3**, the K^+ ion also coordinated with the carboxylate oxygen (O4B) of the adjacent complex molecule and connected to the other K^+ ions of the neighboring complex through H_2O bridging, though the hydrogen atoms of the water molecule (O1X) could not be located in the Fourier difference map. Thus, in **3**, the K^+ ion is situated in a seven-oxo-donor environment, and in the lattice, the potassium ions are connected through water bridging, forming a one-dimensional polymeric chain along the a-axis (Fig. 3.3c).

Table 3.2. Selected bond distances (Å) and angles (˚)[a]

	1	**2**	**3**	**4**		**5**	
	(meridional)	***(facial)***	***(facial)***	***(facial)***		***(facial)***	
				Fe1	*Fe2*	*Fe1*	*Fe2*
Fe-O_p	1.943(3)	1.918(5), 1.920(5)	1.916(3), 1.925(4)	1.995(8), 1.980(10)	1.969(8), 1.986(8)	1.934(9), 1.930(8)	1.944(8), 1.940(10)
Fe-O_c	2.020(4)	2.004(4), 2.008(5)	1.990(4), 2.016(4)	1.964(9), 1.978(9)	2.003(10), 2.006(10)	2.010(9), 2.000(9)	2.008(9), 1.997(9)
Fe-N_a	2.160(4)	2.206(6), 2.180(6)	2.204(5), 2.207(4)	2.176(11), 2.184(10)	2.191(11), 2.191(11)	2.226(10), 2.177(10)	2.181(10), 2.222(10)
O_c-Fe-O_c	85.99(14)	159.57(18)	159.65(16)	151.4(4)	155.5(4)	154.5(4)	161.4(4)
O_p-Fe-O_p	100.55(15)	89.3(2)	92.81(14)	80.2(4)	80.9(4)	89.2(4)	89.7(4)
N_a-Fe-N_a	179.32(14)	96.9(2)	95.39(16)	106.3(4)	103.8(4)	96.2(4)	94.8(4)
M-O_p		2.412(6), 2.394(6)	2.643(4), 2.762(4)	2.420(9), 2.451(9)	2.462(10), 2.432(9)	2.755(8), 2.880(9)	2.889(9), 2.767(8)
M-O_m		2.585(7), 2.530(8)	2.732(5), 2.796(4)	2.458(10), 2.476(11)	2.462(10), 2.455(11)	2.847(10), 2.820(10)	2.848(10), 2.873(10)
M-$O_{methanol}$		2.382(11), 2.344(7)		2.803(6), 2.719(6)[c]		2.831(12), 2.867(12)	
M-O_{water}		-	2.632(5)				
M-O_c			2.777(5)				
Fe…M	-	3.352[d]	3.639[d]	3.592[d]	3.587[d]	3.826[d]	3.833[d]

[a] Subscripts *p* and *c* on the oxygen atom and [a] on the N atom denote phenolate, carboxylate, and amine, respectively. C Bridging oxygen atom. [d] calculated using mercury software.

Complex **4** crystallized in the monoclinic space group $P2_1$. In the asymmetric unit of the complex, two *fac*-$[Fe(L^{O\text{-ValTryp}})_2]^-$ complex anions coordinated to one Ca^{2+} ion. Each of the Fe^{III} centres (Fe1 and Fe2) has an N_2O_4 primary coordination sphere that adopts distorted octahedral geometry, evident from the deviation of the axial and equatorial bond angles from their ideal values of 180˚ and 90˚, respectively (Table 3.2). In **4**, due to the binding of Ca^{2+} to the anionic Fe^{III} complex, the Fe-$O_{phenolate}$ bond distances increased, whereas the Fe-$O_{carboxylate}$ and Fe-N_{amine} bond lengths became shorter than the values observed for complexes **2** and **3**. Complex **4** also showed a significant deviation in Fe-ligand coordination bond angle values compared to the other two complexes (**2** and **3**) (Table 3.2).

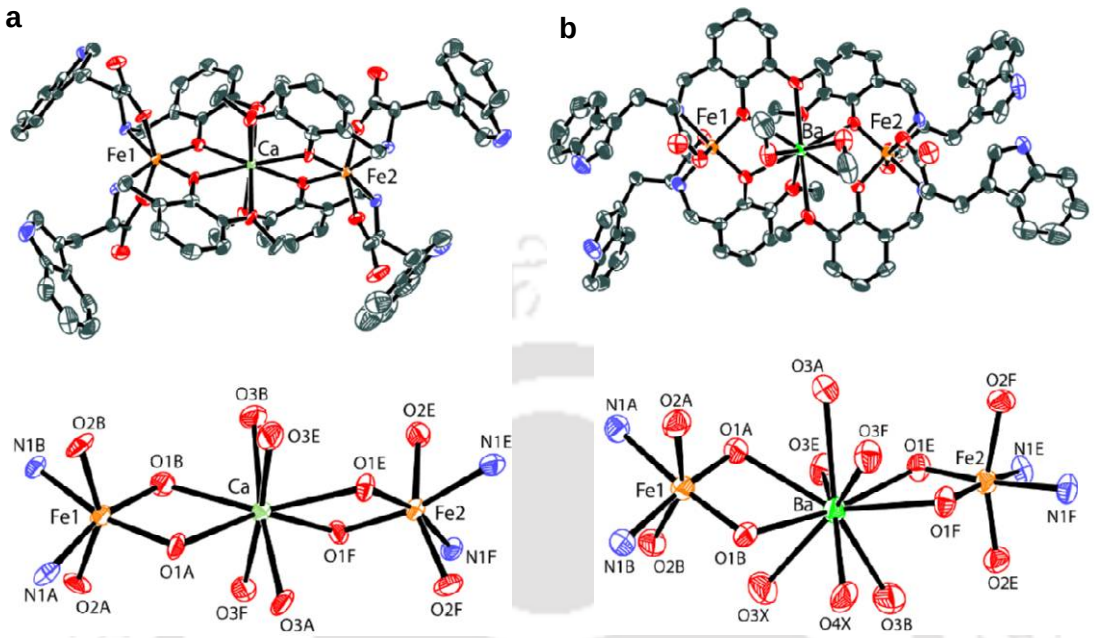

Figure 3.4 Molecular structure of complexes **4**(a) and **5**(b) with thermal ellipsoids set to a 40% probability level along with the coordination around the metal ions present in the complexes.

As the Ca^{2+} ion is coordinated to two anionic Fe^{III} complex units, each having a semi-circular O_4 pocket, it remains inside the circular O_8 oxo-donor environment (Fig. 3.4a). Ca^{2+} ion has a higher charge (+2)/ionic radius (100 pm) ratio than K^+ ion; it is strongly bound to the circular O8 pocket, showing shorter Ca-$O_{phenolate}$[2.420(9), 2.451(9), 2.462(10), and 2.432(9)] and Ca-$O_{methoxy}$[2.458(10), 2.476(11), 2.462(10), and 2.455(11)] bonds than **3**.

Complex **5** crystallized in the orthorhombic space group $P2_1\ 2_1\ 2_1$. Here, the Ba^{2+} ion is also coordinated to two *fac*-$[Fe(L^{O\text{-}ValTryp})_2]^-$ complex anions, but the orientation of these two anionic Fe^{III} complex units differs from **4** (Fig. 3.4b). The geometry of each bis-Fe^{III} complex anion is distorted octahedral like the Fe(III) complexes discussed above, which is evident from the bond length and angle values (Table 3.2). In **5**, the Ba^{2+} ion is inside the circular O_8 pocket and coordinated to all eight oxo donor sites. Also, the Ba^{2+} ion is coordinated with two methanol

molecules. As the Ca^{2+} ion in **4** has a smaller size, it well fitted inside the circular O_8 pocket having no vacant site for solvent coordination, but due to the larger size of the Ba^{2+} ion in **5**, it can expand its coordination number and coordinated to extra two solvent molecules (methanol) while it was bounded inside the O8 circular pocket (Fig. 3.5).

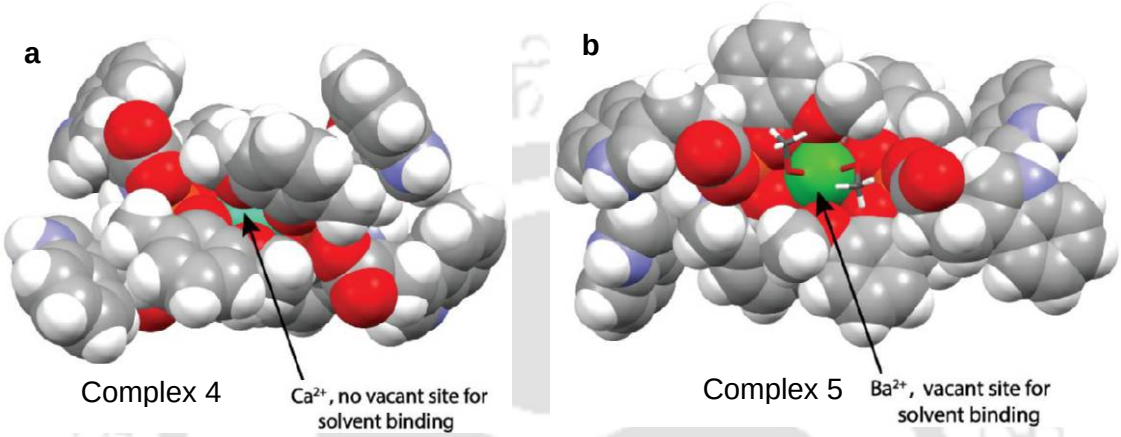

Figure 3.5 The space-fill views of complexes **4** and **5**.

The Ba-$O_{phenolate}$ and Ba-$O_{methoxy}$ bonds in **5** are longer than the other complexes (**2**, **3**, and **4**). (Table 3.2). The ionic radius of the Ba^{2+} (135 pm) is larger than the Na^{+} (95 pm) and Ca^{2+} (100 pm), and though similar to the K^{+} ion (138 pm), the Fe-Ba distance (3.833 Å) in **5** is longer than the Fe-M (M = Na, K, and Ca) distances observed in other hetero metallic complexes (**2**, **3**, and **4**) discussed above. This longer Fe-Ba distance observed in **5** is due to the stronger charge repulsion between the Fe^{3+} and Ba^{2+}, and it has also been observed in the case of other reported Fe^{3+}-Ba^{2+} heterobimetallic complex systems.[36]

All the four hetero-metallic complexes (**2**,**3**,**4** and **5**) discussed above have synthesized from **1** through the salt metathesis reaction. In the presence of alkali and alkaline earth metal ions, the *meridional*-$[Fe(L^{O\text{-ValTryp}})_2]^{-}$ complex anion in **1** showed a drastic structural change and transformed into *facial*-$[Fe(L^{O\text{-ValTryp}})_2]^{-}$ having a semi-circular O_4 polar pocket for secondary metal ion coordination, i.e., the *fac*-$[Fe(L^{O\text{-ValTryp}})_2]^{-}$ acts as a metallo-ligand to coordinate the

other secondary metal cations. For complexes **2** and **3**, one *fac*-$[Fe(L^{O\text{-ValTryp}})_2]^-$ unit bound to one unipositive secondary metal ion (Na^+ in **2** and K^+ in **3**). Due to the larger size of the K^+ favored 1D coordination polymer formation in **3**, which is absent in **2**. In the case of **4** and **5**, two *fac*-$[Fe(L^{O\text{-ValTryp}})_2]^-$ units coordinated to one alkaline earth metal ion (Ca^{2+} and Ba^{2+}) to neutralize its +2 charge. However, the solid-state orientations of these anionic Fe^{III}-complex units are different in **4** and **5**. Overall, all these five Fe(III)-complexes showed significant differences in their respective solid-state structural arrangements.

3.5.3 Powder X-ray diffraction analysis of the complexes

The phase purity of the complexes in bulk has been further checked by powder X-ray diffraction (PXRD) pattern (Fig. 3.6). The experimental diffraction pattern of each complex (2, 3, 4 & 5) matched their respective simulated PXRD pattern (obtained from single crystal X-ray diffraction using Mercury software) with good agreement. Complexes showed a significantly different PXRD pattern**,** which also agrees they have different structural arrangements in the solid state.

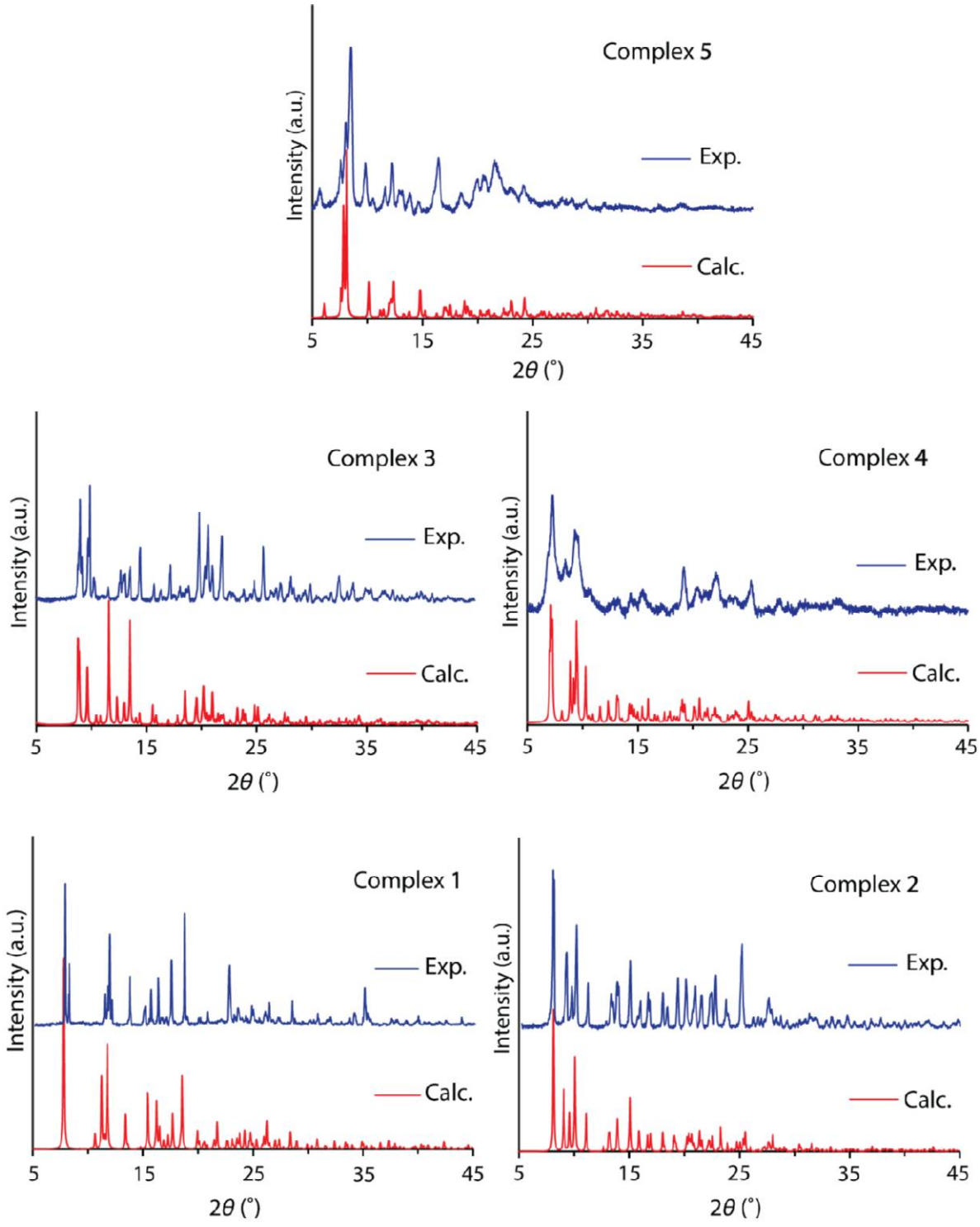

Figure 3.6 Powder X-ray diffraction patterns of the complexes (**1**-**5**).

3.5.4 UV-visible spectroscopy and CD spectroscopy

UV- Vis spectra of the Iron(III) complexes were recorded using their DMF solution. As the Fe(III) centre in all these five complexes (**1**-**5**) is octahedrally coordinated, the broadband that appeared between 475 nm and 468 nm can be assigned to a transition from the phenolate oxygen pπ orbital to the half-filled dπ* orbitals of the ferric ion, and such transitions are intense, and it can be attributed to the LMCT transitions. The shoulder appeared around 330 nm due to the charge transfer transition from the phenolate pπ orbital to the dσ* orbital of the Fe(III) ion.

The solid-state structural analyses of these iron(III)-complexes showed that except **1** (*meridional*), all other *fac*-Fe(III)-complexes bond the secondary metal cations inside the semi-circular O_4 (in **2** & **3**) or circular O_8 (in **4** & **5**) oxo-donor cavity where the Fe^{III} coordinated phenolate oxygens also coordinated to the secondary metal cations (Na^+, K^+, Ca^{2+}, Ba^{2+}). As the metal cations bond to the phenolate of the Fe(III) complex, the LMCT transition may shift according to the polarizing power of the secondary metal cations.

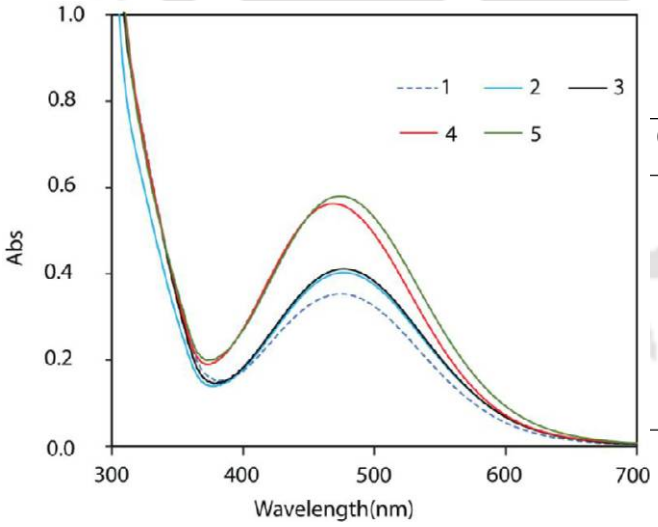

Table 3.3 UV-vis-data of the complexes (**1**-**5**)

Complexes	λ_{max}/nm (ε/$M^{-1}cm^{-1}$)
1	329 (sh), 475 (3052)
2	330 (sh), 476 (3462)
3	330 (sh), 476 (3169)
4	327 (sh), 468 (7062)
5	328 (sh), 475 (6917)

Figure 3.7 UV-visible spectra of the Fe(III)-complexes.

The LMCT band observed in **1** at 475 nm has slightly blue-shifted in **4**, ~7nm, whereas the other complexes showed a similar peak position to that of **1**. Ca^{2+} in **4** has higher polarizing power (high charge/ionic radius value), so it is more strongly connected to the phenolate oxygens than other secondary metal cations used and affects the phenolate of the Fe(III) charge transfer.

Thus, UV-visible spectroscopic analysis of the Fe(III)-complexes unveiled that the presence of alkali and alkaline earth metal ions (Na^+, K^+, Ca^{2+}, Ba^{2+}) at the secondary coordination sphere does not significantly modulate the electronic structure of the ion(III)-complex.

The CD spectra of the chiral bis-Fe(III)-complexes were recorded using their DMF solution. Complex **1** showed one negative CD signal at ~500 nm and one positive CD signal at ~300 nm. The CD spectra of heterometallic complexes (**2**, **3**, **4**, **5**) showed significant differences. **2** showed one positive CD signal at ~500 nm and one negative CD signal at ~300 nm, which is completely opposite from **1**.

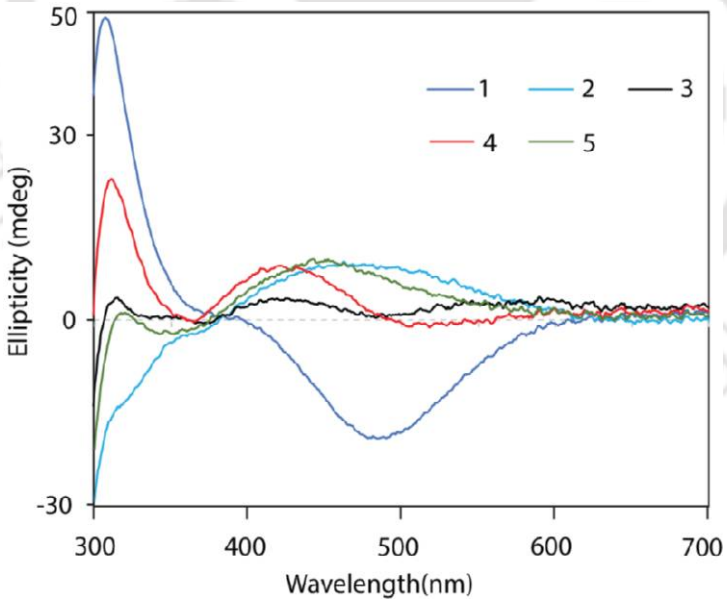

Figure 3.8 Circular dichroism spectra of the iron(III) complexes in DMF.

The positive CD signal that appeared at ~500 nm in **2** shifted to the lower wavelength region on moving from **2→5,** and they also showed a significant amplitude difference of the CD signal at

~300 nm. The solid-state structure of these Fe complexes revealed that the *meridional*-[Fe($L^{O\text{-}ValTryp}$)$_2$]$^-$ in **1** has transformed into the *facial* arrangement (in **2**, **3**, **4**, and **5**) in the presence of secondary metal cations. This *meridional* to *facial* structural rearrangement is also associated with the phase change of the CD signal from the negative (in **1**) to the positive (in **2**, **3**, **4**, and **5**) that appeared between 400 nm and 500 nm.

3.6 Conclusion

In conclusion, we have synthesized chiral bis-Fe(III) complex, (Et_4N)[Fe($L^{O\text{-}ValTryp}$)$_2$], using L-tryptophan derived tridentate ligand, which showed *meridional* to *facial* structural rearrangement in the presence of secondary metal ions (Na^+, K^+, Ca^{2+}, Ba^{2+}), through labile M-L coordination bonds breaking and reformation. The complex anion, [Fe($L^{O\text{-}ValTryp}$)$_2$]$^-$, rearranges its shape in the facial structure, forming a semi-circular O_4 cavity that acts as a tetradentate ligand and binds alkali and alkaline earth metal ions (Scheme 3.1). When Na^+ is coordinated inside this oxo-donor cavity, it exists as a discrete molecular complex, but K^+ ion coordination to the semi-circular O_4 cavity forms a 1D coordination polymer. The alkaline earth metal ions (Ca^{2+}, Ba^{2+}) coordinated to two units of fac-[Fe($L^{O\text{-}ValTryp}$)$_2$]$^-$ though their orientations are different in these two heterometallic complexes. The UV-vis spectra of these Fe complexes showed similar charge transfer transitions except Ca[Fe($L^{O\text{-}ValTryp}$)$_2$]$_2$, which showed about 7 nm blue shifting of LMCT. The CD spectra of all Fe(III) complexes revealed that they not only showed structural differences in the solid state but also behaved differently in the solution, i.e., the Fe(III)-complexes were able to maintain their structural differences in the solution state in spite of their labile nature. Thus, in the presence of alkali and alkaline earth metal ions, the [Fe($L^{O\text{-}ValTryp}$)$_2$]$^-$ rearranges itself to function as a tetradentate ligand, forming discrete multinuclear complexes, behaving like a

compartmental ligand. In other reported compartmental complexes, the strict planarity of the ligand backbone restricts the large-sized secondary metal cations from fitting into the second metal binding site, but our anionic Fe(III) complex system is flexible to accommodate a range of cations without size restriction.

References:

(1) Ferreira, K. N.; Iverson, T. M.; Maghlaoui, K.; Barber, J.; Iwata, S. *Science* **2004**, *303* (5665), 1831–1838.

(2) Yang, J.; Hatakeyama, M.; Ogata, K.; Nakamura, S.; Li, C. *J. Phys. Chem. B* **2014**, *118* (49), 14215–14222.

(3) Barber, J. *Inorg. Chem.* **2008**, *47* (6), 1700–1710.

(4) Cao, Y.; Jin, X.; Huang, H.; Derebe, M. G.; Levin, E. J.; Kabaleeswaran, V.; Pan, Y.; Punta, M.; Love, J.; Weng, J.; Quick, M.; Ye, S.; Kloss, B.; Bruni, R.; Martinez-Hackert, E.; Hendrickson, W. A.; Rost, B.; Javitch, J. A.; Rajashankar, K. R.; Jiang, Y.; Zhou, M. *Nature* **2011**, *471* (7338), 336–340.

(5) Akine, S.; Nabeshima, T. *Dalton Trans.* **2009**, No. 47, 10395.

(6) Finelli, A.; Hérault, N.; Crochet, A.; Fromm, K. M. *ACS Omega* **2019**, *4* (6), 10231–10242.

(7) Finelli, A.; Hérault, N.; Crochet, A.; Fromm, K. M. *Crystal Growth & Design* **2018**, *18* (2), 1215–1226.

(8) Datta, A.; Das, K.; Massera, C.; Clegg, J. K.; Sinha, C.; Huang, J.-H.; Garribba, E. *Dalton Trans.* **2014**, *43* (14), 5558–5563.

(9) Mahlooji, N.; Behzad, M.; Amiri Rudbari, H.; Bruno, G.; Ghanbari, B. *Inorganica Chimica Acta* **2016**, *445*, 124–128.

(10) Akine, S.; Utsuno, F.; Piao, S.; Orita, H.; Tsuzuki, S.; Nabeshima, T. *Inorg. Chem.* **2016**, *55* (2), 810–821.

(11) Akine, S.; Miyashita, M.; Nabeshima, T. *Inorg. Chem.* **2021**, *60* (17), 12961–12971.

(12) Goudarzi, A.; Saeidifar, M.; Aghapoor, K.; Mohsenzadeh, F.; Fenske, D.; Fuhr, O.; Ghassemzadeh, M. *Journal of Molecular Structure* **2023**, *1272*, 134224.

(13) Mousavi, M.; Béreau, V.; Costes, J.-P.; Duhayon, C.; Sutter, J.-P. *CrystEngComm* **2011**, *13* (19), 5908.

(14) Cunningham, D.; McArdle, P.; Mitchell, M.; Ní Chonchubhair, N.; O'Gara, M.; Franceschi, F.; Floriani, C. *Inorg. Chem.* **2000**, *39* (8), 1639–1649.

(15) Andruh, M. *Chem. Commun.* **2007**, No. 25, 2565.

(16) Lü, X.; Wong, W.; Wong, W. Self-Assembly of Luminescent Platinum-Salen Schiff-Base Complexes. *Eur J Inorg Chem* **2008**, *2008* (4), 523–528.

(17) Cheng, J.; Ma, X.; Zhang, Y.; Liu, J.; Zhou, X.; Xiang, H. *Inorg. Chem.* **2014**, *53* (6), 3210–3219.

(18) Takehara, C.; Then, P. L.; Kataoka, Y.; Nakano, M.; Yamamura, T.; Kajiwara, T. *Dalton Trans.* **2015**, *44* (41), 18276–18283.

(19) Chantarojsiri, T.; Ziller, J. W.; Yang, J. Y. *Chem. Sci.* **2018**, *9* (9), 2567–2574.

(20) Shao, H.; Muduli, S. K.; Tran, P. D.; Soo, H. S. *Chem. Commun.* **2016**, *52* (14), 2948–2951.

(21) Park, Y. J.; Cook, S. A.; Sickerman, N. S.; Sano, Y.; Ziller, J. W.; Borovik, A. S. *Chem. Sci.* **2013**, *4* (2), 717–726.

(22) Reath, A. H.; Ziller, J. W.; Tsay, C.; Ryan, A. J.; Yang, J. Y. *Inorg. Chem.* **2017**, *56* (6), 3713–3718.

(23) Van Veggel, F. C. J. M.; Verboom, W.; Reinhoudt, D. N. *Chem. Rev.* **1994**, *94* (2), 279–299.

(24) Bélanger, S.; Gilbertson, M.; Yoon, D. I.; Stern, C. L.; Dang, X.; Hupp, J. T. *J. Chem. Soc., Dalton Trans.* **1999**, No. 19, 3407–3411.

(25) Lowe, N. D.; Garner, C. D. *J. Chem. Soc., Dalton Trans.* **1993**, No. 14, 2197.

(26) Baylies, C. J.; Riis-Johannessen, T.; Harding, L. P.; Jeffery, John. C.; Moon, R.; Rice, C. R.; Whitehead, M. *Angew Chem Int Ed* **2005**, *44* (42), 6909–6912.

(27) Shrestha, S.; Gimbert-Suriñach, C.; Bhadbhade, M.; Colbran, S. B. *Eur J Inorg Chem* **2011**, *2011* (28), 4331–4337.

(28) Kita, M. R.; Miller, A. J. M. *J. Am. Chem. Soc.* **2014**, *136* (41), 14519–14529.

(29) Delgado, M.; Ziegler, J. M.; Seda, T.; Zakharov, L. N.; Gilbertson, J. D. *Inorg. Chem.* **2016**, *55* (2), 555–557.

(30) Kang, K.; Fuller, J.; Reath, A. H.; Ziller, J. W.; Alexandrova, A. N.; Yang, J. Y. *Chem. Sci.* **2019**, *10* (43), 10135–10142.

(31) Chantarojsiri, T.; Ziller, J. W.; Yang, J. Y. *Chem. Sci.* **2018**, *9* (9), 2567–2574.

(32) Golwankar, R. R.; Kumar, A.; Day, V. W.; Blakemore, J. D. *Chemistry A European J* **2022**, *28* (38), e202200344.

(33) Cai, Z.; Xiao, D.; Do, L. H. *J. Am. Chem. Soc.* **2015**, *137* (49), 15501–15510.

(34) Kim, Y.-H.; Hong, J.-I. *Chem. Commun.* **2002**, No. 5, 512–513.

(35) Li, C.-K.; Lu, X.-X.; Wong, K. M.-C.; Chan, C.-L.; Zhu, N.; Yam, V. W.-W. *Inorg. Chem.* **2004**, *43* (23), 7421–7430.

(36) Santra, A.; Gupta, G.; Biswas, B.; Das, A.; Ghosh, D.; Paria, S. *Inorg. Chem.* **2023**, *62* (25), 9818–9826.

Chapter 4

Structural elucidation of anionic Co(III) complexes with achiral and chiral primary ammonium ions

4.1 Introduction

In Chapter **2**, we observed that the Co(III)- complexes of L-Tryptophan-derived reduced Schiff base ligand imparted two different shapes for the recognition of tertiary and quaternary ammonium ions (Et_3NH^+ & Et_4N^+) using non-covalent bonding interactions. Mainly, The H-bonding interaction among the guest ammonium ion (Et_3NH^+) and Co(III) host complex causes more drastic structural modification than the other. In this chapter (Chapter 4), we have used the anionic Co(III)-complex for binding an achiral and two chiral (enantiomers) primary ammonium ions. The amino group is one of the most important functional groups in biomolecules, and in physiological conditions, the amino group usually remains as an ammonium ion. The biological protein receptors interact with these small ammonium ions to control various biological processes like signal transduction, substrate recognition, blood pressure regulation, etc.[1–7] Several synthetic receptors like crown ethers[8–17], calixarenes[18–24] (ref), resorcinarenes[25–32], cucurbiturils[33–38] and different types of metal complexes[39–44] based ammonium ion receptors have been developed, over the last few decades. In the case of biological and synthetic receptors, three types of interactions, hydrogen bonding, cation-π interactions, and ion pair-salt bridge interactions, are typically the most important non-covalent interactions required to recognize the different types of ammonium ions. Most metal complex-based receptors recognize the different ammonium ions using crown ether functionality attached to the ligand framework or with the complexation of the guest molecules to the suitable binding sites present in coordinatively unsaturated metal complexes. Previously, our group also reported the recognition of chiral ammonium ions using anionic binuclear Ni(II) complexes and showed how the non-covalent interactions play an important role in effective recognition.[45,46]

In Chapter **2**, we observed that the presence of a single H-bonding capable N-H group in triethyl ammonium cation triggered a structural transition of the anionic Co(III)-host complex, shifting it from an extended form to the folded conformation. This led us to investigate the structural organization of the $[Co(L^{O\text{-ValTryp}})_2]^-$ complex anion towards recognition of the primary ammonium ion ($R\text{-}NH_3^+$) having three N-H bonds capable of H-bonding. Additionally, since the Co(III) complex is chiral, we were interested in understanding how the chiral ammonium ions influence the recognition process. In this chapter, we used coordinatively saturated anionic Co(III) host complexes to bind both achiral and chiral primary ammonium ions, performed different solid-state and solution-state characterizations to explore how the presence of primary ammonium ions or their chirality affects guest recognition properties of the anionic Co(III)-host complex.

4.2 Experimental Section

4.2.1 Materials and Methods

Solvents were obtained from commercial sources and purified before use, following standard literature procedure. Benzylamine, (*S*)-(-)-α-Methylbenzylamine, (*R*)-(+)-α-Methylbenzylamine, were purchased from Aldrich Chemical and Co. $Co(ClO_4)_2{\cdot}6H_2O$ was purchased from Loba Chemicals Pvt. All the details of the instruments used for analysis have already been discussed in Chapter **2**.

4.3 Syntheses

The detailed synthetic procedure of the ligand $H_2L^{O\text{-ValTryp}}$ was discussed in Chapter 2. The same ligand is used as a starting material for synthesizing the complexes discussed here.

4.3.1 (Bezylammonium)[Co($L^{O\text{-ValTryp}}$)$_2$] (1)

The colour of the reaction mixture became pink. After 15 min., methanolic solution (10 mL) of benzylamine (0.315 g, 2.94 mmol) was slowly added to the reaction mixture, and the colour of the reaction mixture gradually changed from pink to reddish brown. The reaction mixture was stirred again for six hours. At room temperature. Then, the solvent was evaporated using a rotary evaporator to reduce the volume of the reaction mixture, and DMF was added to it in a proportion of 3:1 (methanol: DMF) and was kept in a 50 mL beaker. Block-shaped reddish-brown coloured crystals were obtained after two weeks of slow evaporation of the solvent mixture. The crystals were washed with ethyl acetate and diethyl ether and dried under a vacuum. Yield: 68%.

^{1}H NMR (d_6-DMSO, 500 MHz) δ 10.86 (s, 2H, $H^{NH\ indole}$), δ 7.82 (d, 2H, *J* = 8 Hz, H^{12}), δ 7.47-7.36 (m, 5H, *J* = 8 Hz, $H^{Ph,\ Guest}$), δ 7.30 (d, 2H, *J* = 8 Hz, H^{15}), δ 7.20 (s, 2H, H^{17}), δ 7.04 (t, 2H, *J* = 7.5 Hz, H^{14}), δ 6.98 (t, 2H, *J* = 7.5 Hz, H^{13}), δ 6.54 (d, 2H, *J* = 7.5 Hz, H^5), δ 6.17 (d, 2H, *J* = 8 Hz, H^3), δ 6.03 (t, 2H, *J* = 7.5 Hz, H^4), δ 5.50 (t, 2H, *J* =11 Hz, $H^{NH\ LIGAND}$), δ 4.12 - 4.09 (m, 2H, H^8), δ 4.17 (t, 2H, *J* = 12 Hz, H^7), δ 3.84 (d, *J* = 10.5, 2H, H^{7a}), δ 3.78 (dd, *J* = 4.5/5, 15 Hz 2H, H^9), δ 3.39 (dd, 2H, *J* = 4.5/5,15 Hz, H^{9a}), δ 2.46 (s, 6H, H^{-OCH3}), δ 4.03 (s, 2H, $H^{CH2,Guest}$), δ 8.06 (s, 3H, $H^{NH,Guest}$),; ^{1}H,^{1}H-COSY, was also performed. IR (KBr, cm^{-1}): υ(COO^-)$_{asym}$ 1637; υ(COO^-)$_{sym}$ 1475; υ(C-O) 1282; υ(C-H)o/p-ring H 745; υ(M-O) 535; υ(M-N) 435. m/z (ESI-MS) {M+H}$^+$, {(Bezylammonium)[Co($L^{O\text{-Val Tryp}}$)$_2$]+H}$^+$; calcd: 844.28, found: 844.28.

4.3.2 ((*S*)-(-)-α-methylbenzylammonium)[Co ($L^{O\text{-ValTryp}}$)$_2$)] (2)

This was synthesized following the same procedure described for **1** using (*S*)-(-)-α-methylbenzylamine instead of benzylamine as a base while synthesizing. Block-shaped crystals of the complex were obtained after 10-12 days from the slow evaporation of the complex solution

in a methanol-DMF (3:1) solvent mixture. The crystals were filtered, washed with acetonitrile and diethyl ether, and dried inside a vacuum desiccator. Yield: 65%.

^{1}H NMR (d_6-DMSO, 500 MHz) δ 10.86 (s, 2H, $H^{NH\ indole}$), δ 7.82 (d, 2H, *J* = 7.5 Hz, H^{12}), δ 7.49-7.35 (m, 5H, $H^{Ph,\ Guest}$), δ 7.30 (d, 2H, *J* = 8 Hz, H^{15}), δ 7.21 (s, 2H, H^{17}), δ 7.05 (t, 2H, *J* = 7.5 Hz, H^{14}), δ 6.98 (t, 2H, *J* = 7.5 Hz, H^{13}), δ 6.54 (d, 2H, *J* = 7.5 Hz, H^{5}), δ 6.17 (d, 2H, *J* = 8 Hz, H^{3}), δ 6.03 (t, 2H, *J* = 7.5 Hz, H^{4}), δ 5.49 (t, 2H, *J* =11 Hz, $H^{NH\ LIGAND}$), δ 4.12 - 4.09 (m, 2H, H^{8}), δ 4.18 (t, 2H, *J* = 12 Hz, H^{7}), δ 3.84 (d, *J* = 10.5, 2H, H^{7a}), δ 3.79 (dd, *J* = 4.5/5.5, 15 Hz 2H, H^{9}), δ 3.40 (dd, 2H, *J* = 4.5/5.5,15 Hz, H^{9a}), δ 2.47 (s, 6H, H^{-OCH3}), δ 1.49 (d, 3H, *J* = 6.5 Hz, $H^{CH3,Guest}$), δ 4.41 (m, 1H, $H^{x,Guest}$), δ 8.16 (s, 3H, $H^{NH,Guest}$); ^{1}H,^{1}H-COSY, was also performed. IR (KBr, cm^{-1}): $\upsilon_{as}(COO^{-})_{asym}$ 1600; $\upsilon_{s}(COO^{-})_{sym}$ 1480; υ(C-O) 1280; υ(C-H)o/p-ring H 750; υ(M-O) 540; υ(M-N) 440. m/z (ESI-MS) $\{M+H\}^{+}$, {((*S*)-(-)-α-Methylbenzylamine)[Co($L^{O\text{-Val Tryp}}$)$_2$]+H}$^{+}$; calcd: 858.29, found: 858.29.

4.3.3 ((*R*)-(+)-α-methylbenzylammonium)[Co ($L^{O\text{-ValTryp}}$)$_2$)] (3)

Complex **3** was synthesized following the same procedure described for **1.** We have used (*R*)-(+)-α-methylbenzylamine instead of benzylamine as a base. A few mL of DMF was added to the complex's methanolic solution. Block-shaped crystals of the complex were obtained after two weeks from the slow evaporation of the complex solution in a methanol-DMF solvent mixture. Crystals were filtered, washed with ethyl acetate and diethyl ether, and dried in a vacuum desiccator. Yield: 63%.

^{1}H NMR (d_6-DMSO, 500 MHz) δ 10.86 (s, 2H, $H^{NH\ indole}$), δ 7.82 (d, 2H, *J* = 8 Hz, H^{12}), δ 7.48-7.35 (m, 5H, $H^{Ph,\ Guest}$), δ 7.30 (d, 2H, *J* = 8 Hz, H^{15}), δ 7.21 (s, 2H, H^{17}), δ 7.04 (t, 2H, *J* = 7.5 Hz, H^{14}), δ 6.98 (t, 2H, *J* = 7.5 Hz, H^{13}), δ 6.54 (d, 2H, *J* = 7.5 Hz, H^{5}), δ 6.17 (d, 2H, *J* = 8 Hz, H^{3}), δ 6.03 (t, 2H, *J* = 7.5 Hz, H^{4}), δ 5.50 (t, 2H, *J* =11 Hz, $H^{NH\ LIGAND}$), δ 4.12 - 4.09 (m, 2H, H^{8}), δ 4.18 (t, 2H, *J* = 12 Hz, H^{7}), δ 3.84 (d, *J* = 10.5, 2H, H^{7a}), δ 3.79 (dd, *J* = 4.5/5.5, 15 Hz 2H, H^{9}), δ 3.40 (dd, 2H, *J* = 4.5/5.5,15 Hz, H^{9a}), δ 2.46 (s, 6H, H^{-OCH3}), δ 1.48 (d, 3H, *J* = 7 Hz, $H^{CH3,Guest}$), δ 4.40 (m, 1H, $H^{x,Guest}$), δ 8.12 (s, 3H, $H^{NH,Guest}$);

$^{1}H,^{1}H$-COSY, was also performed. IR (KBr, cm^{-1}): $\upsilon_{as}(COO^{-})_{asym}$ 1605; $\upsilon_{s}(COO^{-})_{sym}$ 1477; υ(C-O) 1280; υ(C-H)o/p-ring H 745; υ(M-O) 540; υ(M-N) 440. m/z (ESI-MS) $\{M+H\}^{+}$, {((*R*)-(-)-α-Methylbenzylammonium)[Co($L^{O\text{-}ValTryp}$)$_2$]+H$\}^{+}$; calcd: 858.29, found: 858.29.

4.4 X-ray Crystallography

The crystal of the complexes obtained during synthesis was used for X-ray analysis. The crystals were mounted on glass fibre. All geometric and intensity data for the crystals were collected at room temperature using a Bruker SMART APEX CCD diffractometer equipped with a fine focus 1.75 kW sealed tube Mo-Kα (λ= 0.71073 Å) X-ray source, with increasing ω (width of 0.3º per frame) at a scan speed of either 3 or 4 s/frame. The SMART software was used for data acquisition, and the SAINT software for data extraction. Absorption corrections were done using a multi-scan. After the initial solution and refinement with SHELXL, the final refinement was performed on the WinGX environment using the SHELXL-97 programs. All non-hydrogen atoms were refined anisotropically. The hydrogen atoms were located from the Fourier maps and refined isotropically wherever possible. Thus, some C-H bonds will not be ideal and may vary. In some complexes, the hydrogen atoms attached to the solvent molecules cannot be located or fixed, so the molecular weight may not match. ORTEP obtained selected crystallographic data summarized in Table **4.1,** and the selected bond distances and bond angles of the respective complexes are listed in the tables below. Perspective views of the complexes were shown using ORTEP.

Table 4.1 Crystallographic data and refinement parameters of Co(III) Complexes.

Complexes	**1**	**2**	**3**
Empirical Formula	$C_{93}H_{101}Co_2N_{11}O_{19}$	$C_{46}H_{50}CoN_5O_9$	$C_{47}H_{52}CoN_5O_9$
Formula Weight	1794.70	875.84	889.86
Wavelength(Å)	0.71073	0.71073	0.71073
Crystal system	monoclinic	orthorhombic	orthorhombic
Space group	$P2_1$	$P2_12_12_1$	$P2_12_12_1$
a, Å	9.0374(8)	9.0752(9)	9.1220(6)
b, Å	21.489(2)	21.449(2)	21.7742(10)
c, Å	22.705(2)	21.603(2)	22.1940(11)
α, deg	90	90	90
β, deg	90.686(3)	90	90
γ, deg	90	90	90
Volume, $Å^3$	4409.1(7)	4205.1(7)	4408.3(4)
Z/ρ	2/1.352	4/ 1.383	4/ 1.341
μ	0.453	0.472	0.451
Coll reflns	14657	7411	7151
Indep refln	8325	6666	4557
FLACK para.	0.051(8)	0.044(5)	0.00(3)
GOF	1.153	1.120	1.006
R1[a]	0.0867	0.0518	0.0782
wR2[a]	0.1600	0.1099	0.1858
R1[b]	0.1796	0.0617	0.1300
wR2[b]	0.2080	0.1169	0.2636

[a] $I > 2\sigma$. [b] All data

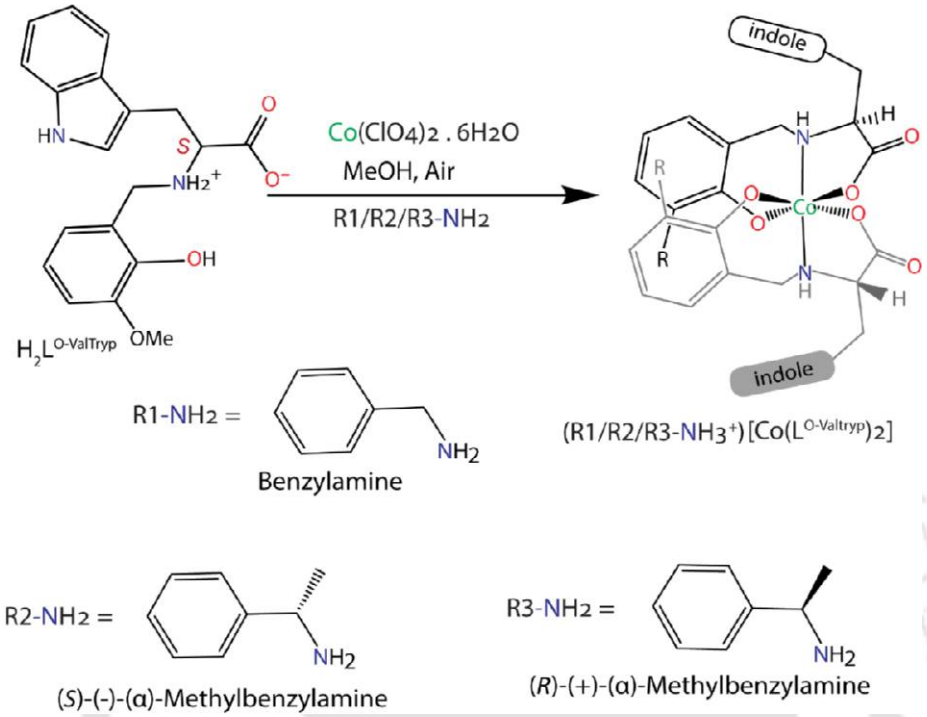

Scheme 4.1 Syntheses of the chiral Co(III) host-guest complexes.

4.5 Result and Discussion

4.5.1 Syntheses and Selected Properties

The reaction of the ligand $H_2L^{O\text{-ValTryp}}$ with 0.5 equivalent of $Co(ClO_4)_2 \cdot 6H_2O$ initially gave a pink-colored solution, which, upon treatment with two equivalents of amine as a base, gradually changed into reddish-brown. Thus, we have synthesized complexes **1** to **3**. For the synthesis of **1**, we used achiral benzylamine as a base, and in the complex, it remained as a benzyl ammonium ion. Whereas for the synthesis of the other two Co(III) complexes (**2**&**3**), we have used different isomers of α-methylbenzylamine as a chiral base, which formed two Co(III) salt complexes having ammonium ions of different chirality. All the Co(III) complexes were characterized by IR and UV-visible spectroscopy and mass spectrometry. In addition, the ^{1}H NMR spectra of

complex **1**-**3** showed sharp, well-resolved resonances, which indicate their diamagnetic nature. IR spectra of the complexes showed broad stretches at ~3415 cm^{-1} due to OH (water or H-bonded OH) stretch. The other sharp band observed in the range 1615 -1650 cm^{-1} is due to asymmetric stretching of coordinated carboxylate to the metal center.

4.5.2 Crystal structures

Complex **1** crystallized in chiral monoclinic space group $P2_1$. The asymmetric unit of complex-**1** contains two complex anions, two benzyl ammonium ions, two water molecules, and one DMF molecule. The hydrogen atoms on the one water molecule could not be found or attached.

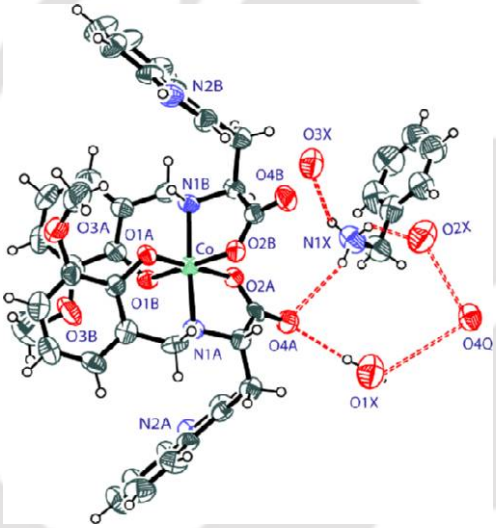

Figure 4.1 The ORTEP figures of complexes **1** with 40% ellipsoid probability show non-covalent interaction between anionic Co(III)-complex, benzyl ammonium ion, and the solvent molecules.

Table 4.2A Selected bond length (Å) and angles (°) of complex **1.**

	Co-Op	Co-Oc	Co-N	Op-Co-Op	Oc-Co-Oc	Op-Co-Oc	NH-Co-NH
1	1.884(8)	1.930(9)	1.946(10)	94.8(3)	89.1(4)	87.9(4)	176.2(5)
	1.891(9)	1.942(9)	1.927(11)				

In the anionic complex unit, the Co(III) center is octahedrally coordinated by two deprotonated tridentate ligands where two phenolate oxygen atoms and two carboxylate oxygen atoms occupy

the equatorial corners of the octahedron and the axial positions are occupied by two secondary nitrogen atoms. The geometry around the Co(III) ion is slightly distorted from the perfect octahedron, as evident from the deviation of angels from ideal 90˚ and 180˚ (Table 4.2A).

The bond lengths and angle values of the two anionic complex units present in the asymmetric unit of the complex are almost identical, so the values of the one unit are given here. The chiral carbons present in the complexes, C8A & C8B, have "*S*" conformation, originating from the use of L-tryptophan used for ligand synthesis, and Co(III)- coordinated amine N atoms, N1A & N1B, have "*R*" conformation. The opposite conformation preference at chiral carbon and amine N has been observed in all previous complexes with amino acid-derived reduced Schiff base ligands.[47–49]. Both benzyl cations present in asymmetric units of the complex are not in identical environments. The N1X cation, the three N-H, non-coordinated carboxylate(O4A), DMF, and one water (O1X) formed a multi-centered H-bonded network. The other cation, the three N-H (N2X), are H-bonded to two non-coordinated carboxylates from two different molecules (O4P and O4B) and the water (O1X) molecule.

In complex **1**, each anionic Co(III)-complex unit folded backward, exposing the polar carboxylate oxygens used in H-bonding with the $-NH_3^+$ group of the cationic guest molecules and with the solvent molecules and in the bc plane, forming a columnar structure along the a-axis axis. The indole NH groups in **1** participate in inter-molecular H-bonding with the ligand phenolate oxygen (N2AH2A…O1A and N2BH2B…O1B) of the neighboring complex units (Table 4.3).

Thus, stabilizing the column formation along the a-axis. The surface of the column is mostly aromatic. Non-H-bonded, non-covalent weak interactions hold columns together.

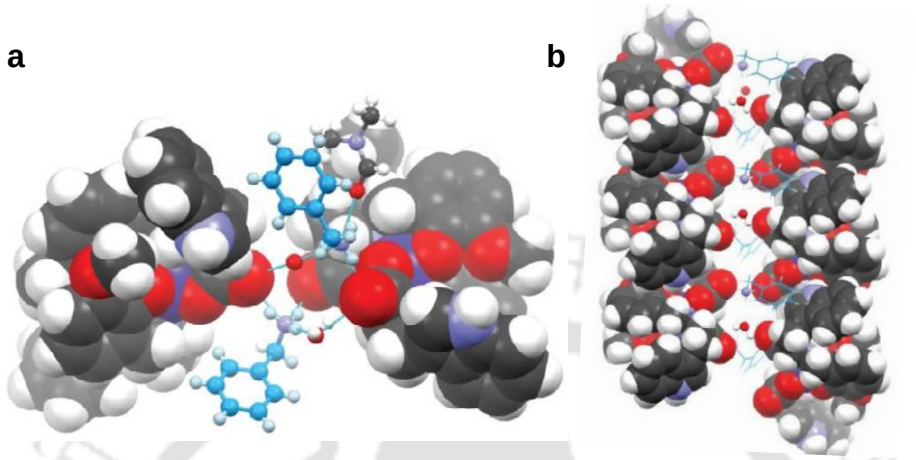

Figure 4.2 (a) The space-fill view of the asymmetric unit of complex **1**, (b) One-dimensional channel (space-filling model) encapsulated with guest cations (ball and stick)

Complexes **2** & **3** were synthesized using enantiopure amines and X-ray suitable single crystals of the complexes obtained from the slow evaporation of the methanolic solutions of the complexes at room temperature. Both **2** & **3** crystallized in identical space group $P2_12_12_1$ (Table 4.1) and have similar molecular structure and lattice organization types. The asymmetric unit of complex **2** contains one anionic bis-Co(III) complex, one (*S*)-(-)-α-methyl benzyl- ammonium ion, and one water molecule as solvent of crystallization, whereas the asymmetric unit of complex **3** contains one cation-anion pair, ((*R*)-(+)-α-methyl benzyl ammonium)[Co($L^{O\text{-ValTryp}}$)$_2$], and one methanol molecule. The geometry and the bond parameters of the anionic Co(III) complex unit are almost identical (Table 4.2B). In [Co($L^{O\text{-ValTryp}}$)$_2$]$^-$, the central Co(III) ion is meridionally coordinated by two tridentate deprotonated ligands where metal-coordinated carboxylates and phenolates are cis to each other, whereas the two amine nitrogen coordinated to the Co(III) center in trans manner.

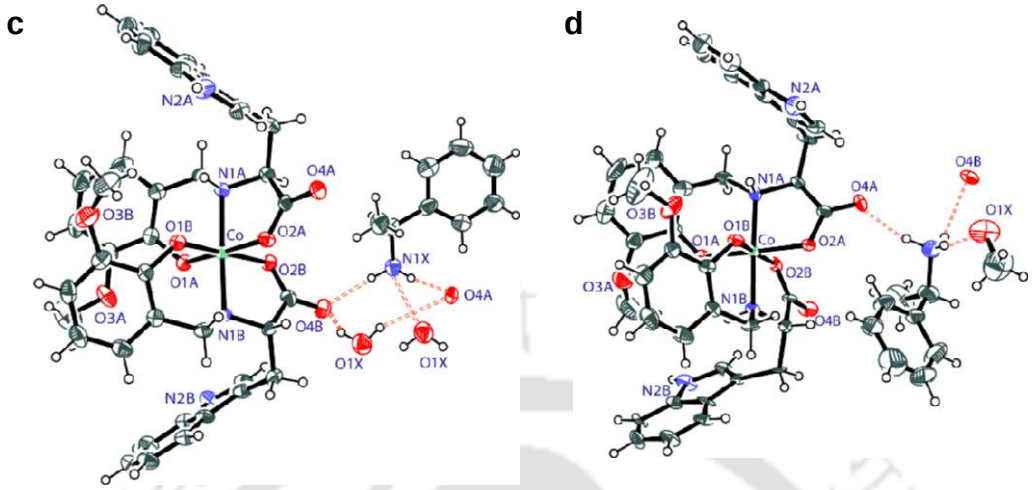

Figure 4.3 The ORTEP figures of complexes **2** (c) and **3** (d) with 40% ellipsoid probability showing non-covalent interactions present in the molecules.

Table 4.2B Selected bond length (Å) and angles (°) of complexes **2** & **3.**

	Co-Op	Co-Oc	Co-N	Op-Co-Op	Oc-Co-Oc	Op-Co-Oc	NH-Co-NH
2	1.872(3)	1.944(4)	1.943(4)	95.30(16)	87.32(15)	88.15(15)	177.82(19)
	1.889(4)	1.945(4)	1.936(4)				
3	1.891(8)	1.932(8)	1.931(9)	96.0(3)	87.3(3)	88.4(3)	178.0(4)
	1.881(8)	1.964(8)	1.938(7)				

In **2**, the three NH bonds of the -NH_3^+ group of (*S*)-(-)-α-methyl benzyl- ammonium ion formed intermolecular H-bonding with two non-coordinated carboxylate oxygens (O4A & O4B) of two adjacent complex molecules and one water molecule (O1X). In **3**, the -NH_3^+ group of (*R*)-(+)-α-methylbenzylammonium ion also formed a similar multicentered H-bonded network like complex **2**, but methanol molecules are present here instead of water.

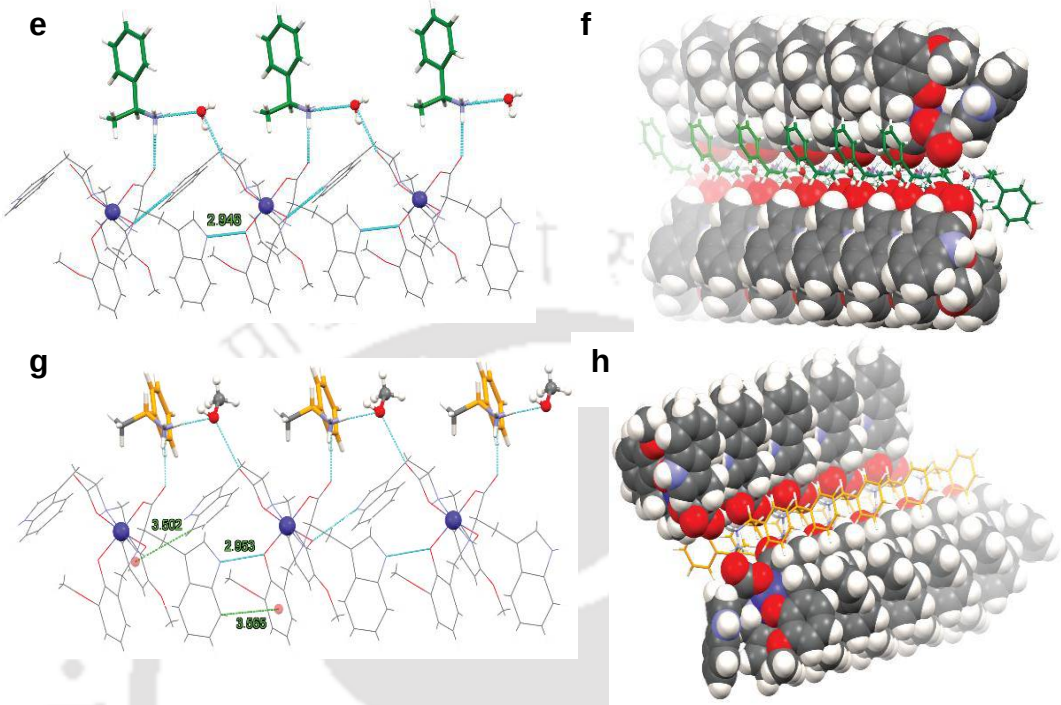

Figure 4.4 (e) Inter-molecular H-bonding interactions among the chiral ammonium ion and the adjacent complex units, in **2**, (f) column in **2** along the a-axis; (g) guest cations and solvent molecules holding two adjacent complex molecules through intermolecular H-bonding interactions, in **3**, (h) one-dimensional channel (space-filling model) encapsulated with guest cation (ball and stick) in **3**.

The indole NH groups are participating in inter-molecular H-bonding with the ligand phenolate oxygen (N2AH2A…O1A and N2BH2B…O1B) of the neighboring complex units (Fig. 4.4). Also, the CH-π interactions are present among the indole units of one complex unit to the phenolate rings of neighboring complex units. Thus, forming a 1D column along a-axis. Inside the column, the carboxylate oxygens of complex molecules, guest cations, and solvent molecules resided and connected through intermolecular H-bonding.

Table 4.3 Hydrogen bond and other non-covalent bond distances (Å) present in **1**.

Atoms	D-H (Å)	H…A (Å)	D…A(Å)	DHA(˚)
N2A-H2A…O1A	0.86	2.12	2.971(13)	168
N2B-H2B…O1B	0.86	2.13	2.980(15)	172
N2P-H2P…O1P	0.86	2.06	2.911(15)	172
N2Q-H2Q…O1Q	0.86	2.13	2.980(14)	172
N1X-H1XA…O2X	0.89	1.87	2.74(2)	164
N1X-H1XB…O2A	0.89	2.51	3.079(17)	123
N1X-H1XB…O4A	0.89	1.94	2.817(18)	167
N1X-H1XC…O3X	0.89	1.92	2.76(2)	157
N2X-H2XA…O4P	0.89	2.00	2.853(17)	161
OIX-H1XE…O4A	0.85	2.30	3.01(2)	140

Table 4.4 Hydrogen bond and other non-covalent bond distances (Å) present in **2**.

Atoms	D-H (Å)	H…A (Å)	D…A(Å)	DHA(˚)
O1X-H1XG…O4A	0.85	2.00	2.818(8)	162
O1X-H1XH…O4B	0.85	2.15	2.961(7)	159
N2A-H2A…O1A	0.86	2.05	2.906(6)	175
N2B-H2B…O1B	0.86	2.10	2.946(6)	170
N1X-H1XA…O1X	0.89	2.00	2.848(7)	160
N1X-H1XB…O4B	0.89	1.94	2.826(7)	175
N1X-H1XC…O4A	0.89	2.03	2.868(6)	157

Table 4.5 Hydrogen bond and other non-covalent bond distances (Å) present in **3**.

Atoms	D-H (Å)	H…A (Å)	D…A(Å)	DHA(˚)
N2A-H2A…O1A	0.86	2.10	2.953(14)	174
N2B-H2B…O1B	0.86	2.09	2.944(13)	173
N1X-H1XA…O4B	0.89	1.93	2.797(14)	166
N1X-H1XB…O1X	0.89	1.95	2.835(19)	172
O1X-H1XD…N1X	0.85	2.22	2.835(19)	129

4.5.3 The solid-state structural difference of complexes 1, 2 & 3

The single-crystal structure analyses of these three complexes showed that in the solid state, $[Co(L^{O\text{-ValTryp}})_2]^-$ units present in these complexes have identical structural arrangements. However, they recognized different primary ammonium ions. As these complexes have accommodated different achiral and achiral ammonium ions inside similar lattice arrangements, one might question how possible it is.

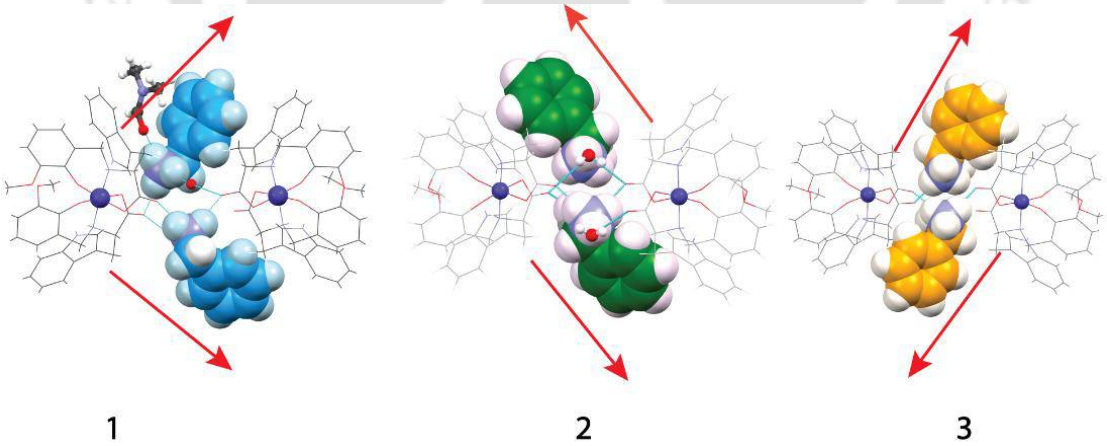

Figure 4.5 Different orientations of the three different ammonium ions in complexes **1**, **2**, and **3** to be accommodated inside a similar lattice arrangement in all these three complexes.

The detailed solid-state structural analyses of the complexes revealed that though the anionic host complex did not change its shape, the guest cations (both chiral and achiral primary

ammonium ions) themselves slightly reoriented in different directions to be accommodated in a similar type lattice arrangement. The orientations of the different ammonium ions are shown in Figure 4.5 with the red-colored arrow signs.

4.5.4 NMR spectroscopy

The low spin Co(III)-complexes being diamagnetic, the ^{1}H NMR spectra for all the complexes (**1**-**3**) were taken in d_6-DMSO. The NMR spectra of complexes **1**-**3** showed sharp, well-resolved resonances for anionic Co(III)-complex molecules and their respective chiral guest cations. ^{1}H-^{1}H COSY spectra of the complexes were also used wherever necessary to assign the proton signals. From the X-ray single crystal structure of the Co(III) complexes, we observed the identical structural arrangement for the main $[Co\ (L^{O\text{-}ValTryp})_2)]^-$ unit in the solid state. These observations are also reflected in the NMR solution study. From the ^{1}H NMR spectra of the complexes, we observed that in solution, the signals belonging to anionic Co(III) units showed identical chemical shift values, but peaks corresponding to their respective guest cations have

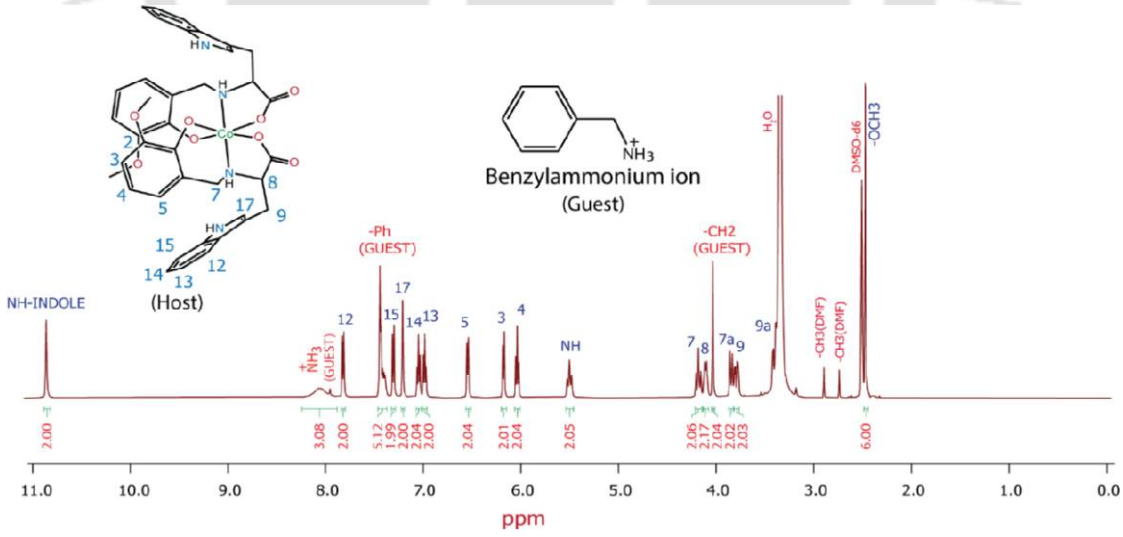

Figure 4.6 ^{1}H NMR (500 MHz, d_6-DMSO) of **1**.

differentiating identities. The chemical shift values of the respective protons, along with coupling constant values, are mentioned in the experimental section. The assignment of the peaks was achieved through ^{1}H-^{1}H COSY NMR correlations (given below).

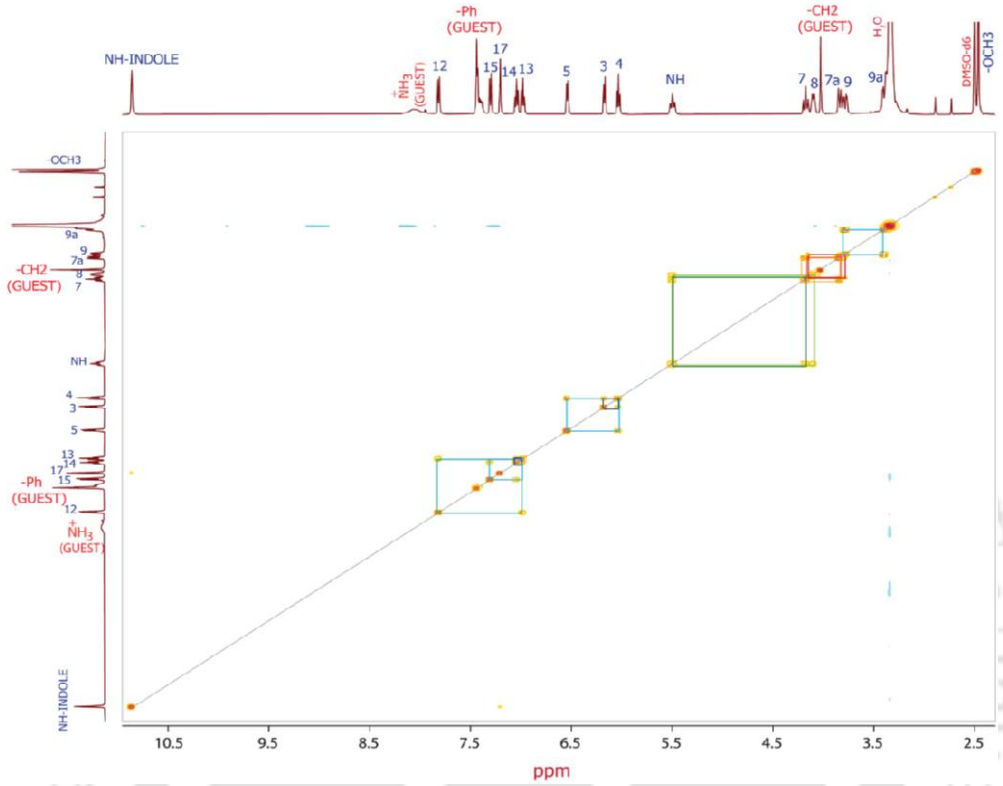

Figure 4.7 ^{1}H-^{1}H COSY NMR (500 MHz, d_6-DMSO) of **1**.

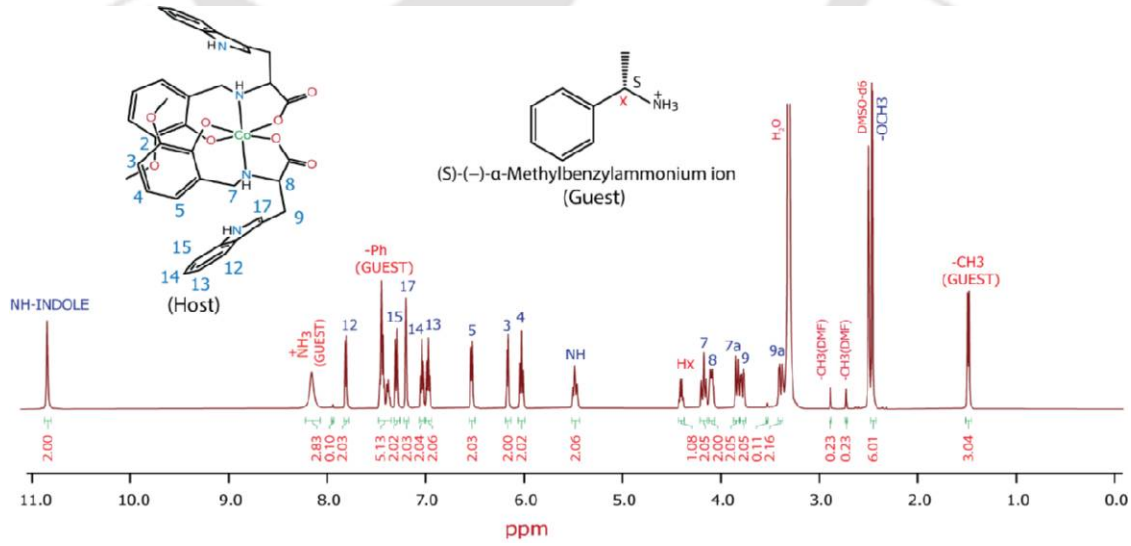

Figure 4.8 ^{1}H NMR (500 MHz, d_6-DMSO) of **2**.

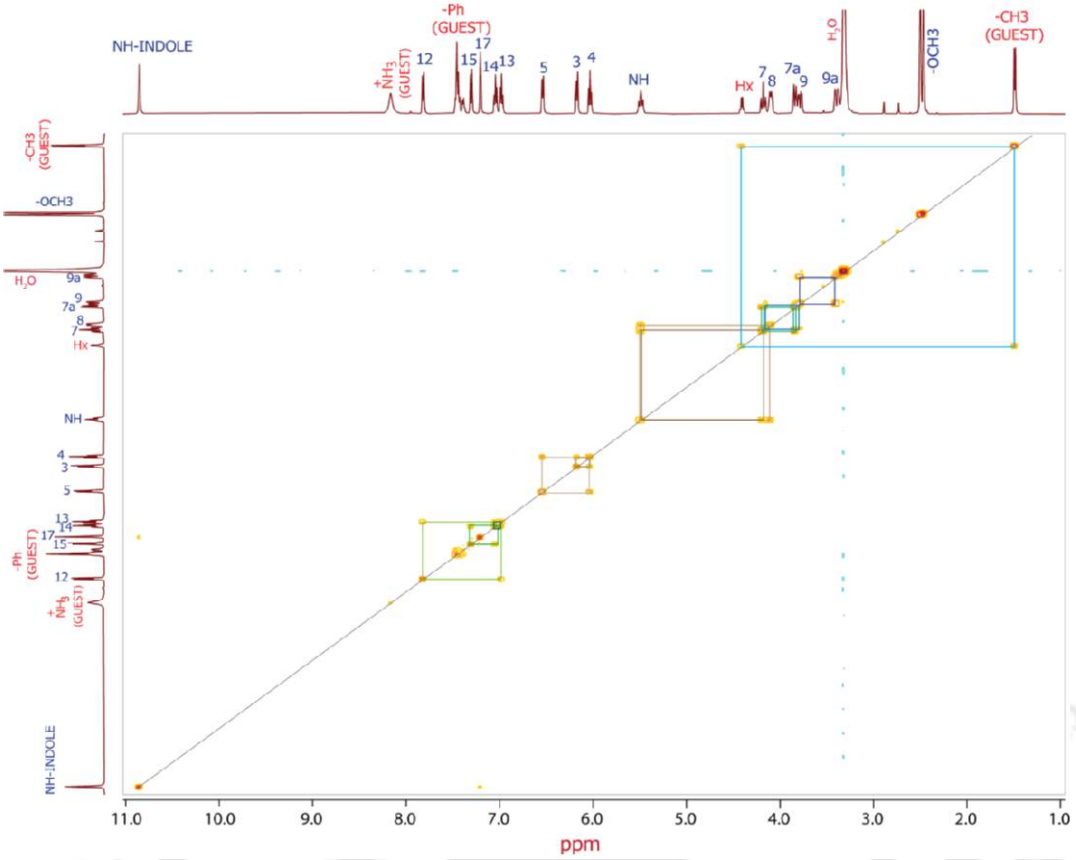

Figure 4.9 ^{1}H-^{1}H COSY NMR (500 MHz, d_6-DMSO) of complex-**2**.

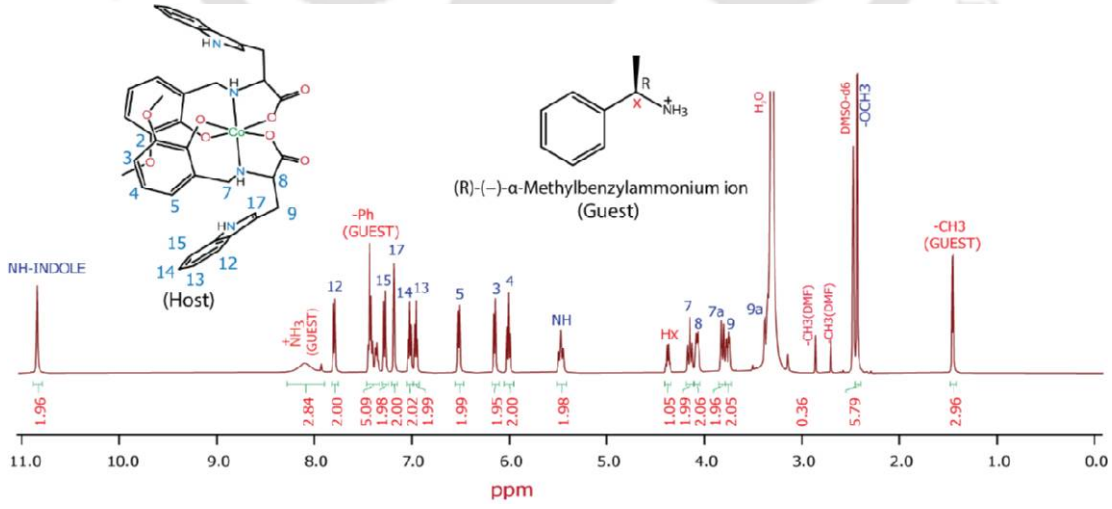

Figure 4.10 ^{1}H NMR (500 MHz, d_6-DMSO) of **3.**

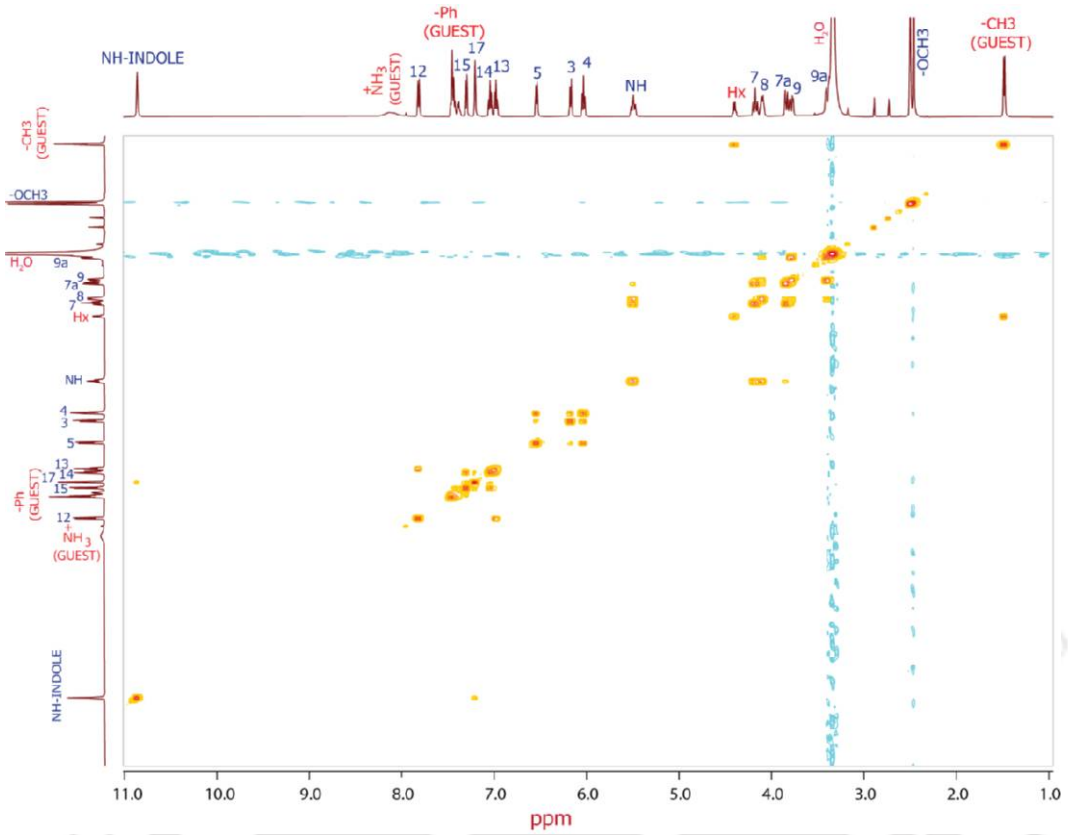

Figure 4.11 ^{1}H-^{1}H COSY NMR (500 MHz, d_6-DMSO) of **3**.

4.5.6 UV-visible spectroscopy and circular dichroism (CD) spectroscopy

The electronic spectrum of each complex was recorded using their DMF solution. All Co(III) – complexes (**1-3**) showed an intense band around 400 nm, one relatively weaker band between 510 nm and 530 nm, and one weak band around 700 nm, as shown in Fig.4.12. For Co(III) octahedral complexes, the higher energy intense band appeared around 400nm because of phenolate (O^-) $p_{\pi} \rightarrow$Co(III) d_{σ^*} charge transfer transition whereas the other two weaker, lower energy bands appeared because of the d $\rightarrow$d transitions, more precisely, the band appeared near 700 nm is corresponding to the $^{1}A_{1g} \rightarrow {}^{1}T_{1g}$ and the band appeared near 520 nm is corresponding to the $^{1}A_{1g} \rightarrow {}^{1}T_{2g}$. The DMF solution of the complexes exhibited significant positive CD signals

near 400 nm, i.e., in the LMCT transition region of the Co(III) complexes, and moderately intense positive CD signals near 300 nm. The complexes also showed two negative CD signals in the d-d electronic transition region, one intense negative signal near 700 nm and another moderately intense negative CD signal near 520 nm. (Fig. 4.12)

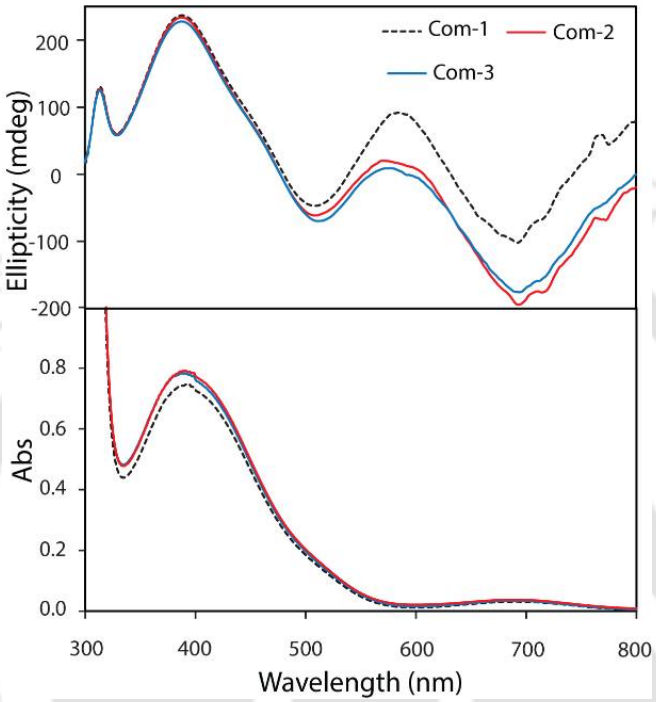

Figure 4.12 Combined UV-visible and CD spectra of Co(III)-complexes (**1-3**) in DMF at a concentration of 0.3 mM.

Table 4.6 Electronic spectroscopic data for complex **1-3** (In DMF)

Complexes	λ_{max}/nm (ε/$M^{-1}cm^{-1}$)
1	390 (2335), 520 (395) (sh), 690 (105)
2	390 (2340), 520 (400) (sh), 695 (106)
3	390 (2290), 520 (386) (sh), 695 (100)

The CD spectrum of complex **1**, which has an achiral benzyl ammonium ion, differs from the other two complexes (**2** and **3)**, which have chiral ammonium ions. The amplitude of the CD signals between 500 nm and 700 nm differ considerably. The intensity of the negative CD signals of **2** & **3** that appeared in that d-d transition region is higher than complex **1**. This difference

might have occurred due to the different kinds of solution state interactions among the anionic Co(III) complex and the chiral ammonium ions (in **2** & **3**) compared to the achiral ammonium ion (in **1**).

4.6 Conclusion

In this chapter, we have synthesized three Co(III) complexes with three different achiral and chiral primary ammonium ions. The solid-state structural analyses of the complexes revealed that the structure of the $[Co(L^{O\text{-}ValTryp})_2)]^-$ unit is different from $(Et_4N)[Co(L^{O\text{-}ValTryp})_2)]$ and $(Et_3NH)[Co(L^{O\text{-}ValTryp})_2)]$ (discussed in Chapter 2). Et_3NH^+ (tertiary) and $-NH_3^+$ (primary), both ammonium ions, have H-bond capable N-H functionality, but the structure of the $(Et_3NH)[Co(L^{O\text{-}ValTryp})_2)]$ is entirely different from the Co(III) complexes with different primary ammonium ions discussed in this chapter. Here, the anionic $[Co(L^{O\text{-}ValTryp})_2)]^-$ unit showed a new structural arrangement that is identical to the binding of achiral and chiral primary ammonium ions (Scheme 4.1). Again, we have used two different enantiopure isomers of α-methyl benzylamine (*S* & *R*) while synthesizing the complexes, but the anionic bis-Co(III) complex unit bound both chiral ammonium ions, i.e., the anionic Co(III) host complex could not exert any preferential binding toward the recognition of any one isomer of α-methyl benzylamine. In conclusion, we can say that the presence of three H-bond capable N-H bonds in the $-NH_3^+$ group in achiral and chiral primary ammonium ions triggered a new structural arrangement of the coordinatively saturated anionic Co(III) complex, and as the chiral guest cations (chiral ammonium ions) are interacting with the Co(III)-host anion only using the $-NH_3^+$ group, due to this minimum host-guest interactions no enantiomeric selectivity was observed.

References

(1) Braman, S. S. *allergy asthma proc* **1987**, *8* (2), 116–120.

(2) Ito, C. *Drug News Perspect* **2004**, *17* (6), 383.

(3) Yanai, K.; Tashiro, M. T *Pharmacology & Therapeutics* **2007**, *113* (1), 1–15.

(4) Idzko, M.; Sala, A. L.; Ferrari, D.; Panther, E.; Herouy, Y.; Dichmann, S.; Mockenhaupt, M.; Virgilio, F. D.; Girolomoni, G.; Norgauer, J. *Journal of Allergy and Clinical Immunology* **2002**, *109* (5), 839–846.

(5) Wolfbeis, O. S.; Li, H. *Biosensors and Bioelectronics* **1993**, *8* (3–4), 161–166.

(6) Cram, D. J.; Trueblood, K. N. *Host Guest Complex Chemistry I*; 1981; Vol. 98, pp 43–106.

(7) Sussman, J. L.; Harel, M.; Frolow, F.; Oefner, C.; Goldman, A.; Toker, L.; Silman, I. *Science* **1991**, *253* (5022), 872–879. https://doi.org/10.1126/science.1678899.

(8) Huszthy, P.; Tóth, T. Synthesis and Molecular Recognition Studies of Crown Ethers. *Per. Pol. Chem. Eng.* **2007**, *51* (2), 45.

(9) Kim, H.-S.; Park, H. J.; Oh, H. J.; Koh, Y. K.; Choi, J.-H.; Lee, D.-H.; Cha, G. S.; Nam, H. *Anal. Chem.* **2000**, *72* (19), 4683–4688.

(10) Solladié, N.; Walther, M. E.; Herschbach, H.; Leize, E.; Dorsselaer, A. V.; Duarte, T. M. F.; Nierengarten, J.-F. *Tetrahedron* **2006**, *62* (9), 1979–1987.

(11) Nagy, K.; Béni, S.; Szakács, Z.; Bényei, A. C.; Noszál, B.; Kele, P.; Kotschy, A. *Tetrahedron* **2008**, *64* (27), 6191–6195.

(12) Mandl, C. P.; König, B. Luminescent Crown Ether Amino Acids: *J. Org. Chem.* **2005**, *70* (2), 670–674.

(13) Dietrich, Bernard.; Kintzinger, J. Pierre.; Lehn, J. Marie.; Metz, Bernard.; Zahidi, Assou. Stability, *J. Phys. Chem.* **1987**, *91* (27), 6600–6606.

(14) Prodi, L.; Bolletta, F.; Montalti, M.; Zaccheroni, N.; Huszthy, P.; Samu, E.; Vermes, B. *New J. Chem.* **2000**, *24* (10), 781–785.

(15) Timko, J. M.; Moore, S. S.; Walba, D. M.; Hiberty, P. C.; Cram, D. J. *J. Am. Chem. Soc.* **1977**, *99* (13), 4207–4219.

(16) Pedersen, C. J. *J. Am. Chem. Soc.* **1967**, *89* (26), 7017–7036.

(17) Bühlmann, P.; Pretsch, E.; Bakker, E. *Chem. Rev.* **1998**, *98* (4), 1593–1688..

(18) Hong, J.; Song, J.; Ham, S. *Tetrahedron Letters* **2007**, *48* (8), 1327–1330.

(19) Ballistreri, F. P.; Notti, A.; Pappalardo, S.; Parisi, M. F.; Pisagatti, I. *Org. Lett.* **2003**, *5* (7), 1071–1074.

(20) Liu, S.-L.; Gong, S.-L.; Chen, Y.-Y. *Chin. J. Chem.* **2005**, *23* (12), 1651–1654.

(21) Le Gac, S.; Ménand, M.; Jabin, I. *Org. Lett.* **2008**, *10* (22), 5195–5198.

(22) Arena, G.; Casnati, A.; Contino, A.; Magrì, A.; Sansone, F.; Sciotto, D.; Ungaro, R. *Org. Biomol. Chem.* **2006**, *4* (2), 243–249.

(23) Atwood, J. L.; Szumna, A. *Journal of Supramolecular Chemistry* **2002**, *2* (4–5), 479–482.

(24) Zhang, L.; Macías, A.; Lu, T.; Gordon, J. I.; Gokel, G. W.; Kaifer, A. E. *Chem. Soc., Chem. Commun.* **1993**, *0* (12), 1017–1019.

(25) Trembleau, L.; Rebek, J. *Science* **2003**, *301* (5637), 1219–1220.

(26) Hooley, R. J.; Biros, S. M.; Rebek, J. *Angewandte Chemie* **2006**, *118* (21), 3597–3599.

(27) Szumna, A. *Org. Biomol. Chem.* **2007**, *5* (9), 1358.

(28) Ballester, P.; Sarmentero, M. *Org. Lett.* **2006**, *8* (16), 3477–3480.

(29) Tan, S.-D.; Chen, W.-H.; Satake, A.; Wang, B.; Xu, Z.-L.; Kobuke, Y. T *Org. Biomol. Chem.* **2004**, *2* (19), 2719.

(30) Hayashida, O.; Ito, J.; Matsumoto, S.; Hamachi, I. *Org. Biomol. Chem.* **2005**, *3* (4), 654.

(31) Melegari, M.; Suman, M.; Pirondini, L.; Moiani, D.; Massera, C.; Ugozzoli, F.; Kalenius, E.; Vainiotalo, P.; Mulatier, J.; Dutasta, J.; Dalcanale, E. *Chemistry A European J* **2008**, *14* (19), 5772–5779.

(32) Hooley, R. J.; Van Anda, H. J.; Rebek, J. *J. Am. Chem. Soc.* **2006**, *128* (12), 3894–3895.

(33) Kim, Y.; Kim, H.; Ko, Y. H.; Selvapalam, N.; Rekharsky, M. V.; Inoue, Y.; Kim, K. *Chemistry A European J* **2009**, *15* (25), 6143–6151.

(34) Huang, W.; Zavalij, P. Y.; Isaacs, L. *Angew Chem Int Ed* **2007**, *46* (39), 7425–7427.

(35) Lagona, J.; Wagner, B. D.; Isaacs, L. *J. Org. Chem.* **2006**, *71* (3), 1181–1190.

(36) Isobe, H.; Sato, S.; Nakamura, E. *Org. Lett.* **2002**, *4* (8), 1287–1289.

(37) Jon, S. Y.; Selvapalam, N.; Oh, D. H.; Kang, J.-K.; Kim, S.-Y.; Jeon, Y. J.; Lee, J. W.; Kim, K. *J. Am. Chem. Soc.* **2003**, *125* (34), 10186–10187.

(38) Lagona, J.; Mukhopadhyay, P.; Chakrabarti, S.; Isaacs, L. *Angew Chem Int Ed* **2005**, *44* (31), 4844–4870.

(39) Sun, Z.; Chen, Z.; Wang, Y.; Zhang, X.; Xu, J.; Bian, G.; Song, L. *Org. Lett.* **2020**, *22* (2), 589–593.

(40) Jang, S.; Kim, H. *Org. Lett.* **2020**, *22* (11), 4185–4189.

(41) Chin, J.; Lee, S. S.; Lee, K. J.; Park, S.; Kim, D. H. *Nature* **1999**, *401* (6750), 254–257.

(42) Li, X.; Tanasova, M.; Vasileiou, C.; Borhan, B. *J. Am. Chem. Soc.* **2008**, *130* (6), 1885–1893.

(43) Ma, C. T. L.; MacLachlan, M. J. *Angew Chem Int Ed* **2005**, *44* (27), 4178–4182.

(44) Jang, S.; Kim, H. *Asian J Org Chem* **2021**, *10* (4), 886–890.

(45) Das, C. R.; Dutta, T.; Ray, M. *Inorganica Chimica Acta* **2019**, *486*, 367–376.

(46) Das, C. R.; Sahoo, S. C.; Ray, M. C *Crystal Growth & Design* **2014**, *14* (8), 3958–3966.

(47) Sahoo, S. C.; Ray, M. *Chemistry A European J* **2010**, *16* (17), 5004–5007.

(48) Koner, R. R.; Haque Faizi, Md. S.; Ray, M. *Inorganica Chimica Acta* **2011**, *372* (1), 367–373.

(49) Sahoo, S. C.; Ray, M. *Dalton Trans.* **2009**, No. 17, 3230.

Chapter 5

Recognition of biogenic chiral amino alcohols using anionic Co(III)-host

5.1 Introduction

In the previous chapter (Chapter **3**), the chiral anionic host complex exserts a new shape while recognizing different achiral and chiral primary ammonium ions. That shape is quite different from the other structural arrangements of the same chiral host recognizing tertiary (Et_3NH^+) and quaternary ((Et_4N^+) ammonium ions, discussed in Chapter **2**. However, the anionic Co(III)-host complex did not show diastereomeric selectivity, possibly due to the minimum host-guest interaction (interaction through $-NH_3^+$ group of chiral guests). In this chapter, we employed ammonium ions of the chiral amino alcohols as guests, varying the position of the chiral center with respect to the $-NH_3^+$ ion and changing the smaller aliphatic to the larger aromatic sidearm. Expect that the presence of the alcoholic -OH group and the $-NH_3^+$ group might assist the better host-guest interactions, which will favor the selective recognition of one of the diastereomers from the racemic mixture of the respective chiral amino alcohols.

We have divided this chapter into two parts- part **A** and part **B**.

Part - A

Here, we have employed three different biogenic amino alcohols (Scheme 1) as a guest because of their structural similarity to adrenaline and nor-adrenaline, a hormone and neurotransmitter, respectively. In many bioactive molecules, natural and synthetic systems, these amino alcohol moieties are present, and they are also used as chiral building blocks and chiral catalysts[1,2] or ligands in various asymmetric syntheses[3]. Several organic macrocyclic receptors are employed in the literature for amine salt recognition; most of them have crown ether-like functionality where the ammonium group of the chiral guest is recognized through H-bonding and other non-covalent interactions.[4–11] In the past few years, chiral recognition using metal complexes or metallorganic receptors has gained attraction because of their easy syntheses and structural

characterizations.[12–20] The structural elucidation of these chiral metallo host-guest systems revealed a detailed understanding of the chiral host-guest interaction mechanism essential for chiral recognition. Previously, our group reported the recognition and resolution of two chiral amino alcohols using the rigid binuclear Ni(II) anionic chiral host and studied the interactions with chiral amino alcohols.[21] This time, we have used a flexible anionic Co(III) host complex to investigate how it binds different amino alcohol guest molecules through noncovalent interactions in the solid states. These non-covalent interactions are essential in the biological recognition process, where these weak interactions trigger the structural reorganization or conformational changes of the bio-receptors to respond to different stimuli.[22–27] Co(III)-complexes being kinetically inert, the solution state behavior of the complexes was monitored using ^{1}H NMR spectroscopy.

5A.1 Experimental Section

5A.1.1 Materials and Methods

Solvents were obtained from commercial sources and purified before use, following standard literature procedure. (*Racemic*)-2-amino-1-propanol, (*R*)-2-amino-1-propanol, (*racemic*)-norphenylephrine hydrochloride, (*S*)-2-phenylglycinol, were purchased from Aldrich Chemical and Co. $Co(ClO_4)_2 \cdot 6H_2O$ was purchased from Loba Chemicals Pvt. All the details of the instruments used for analysis have already been discussed in Chapter 2.

5A.2 Syntheses

The detailed synthetic procedure of the ligand $H_2L^{O\text{-ValTryp}}$ and $(NEt_4)[Co(L^{O\text{-ValTryp}})_2]$ were discussed in Chapter 2. These are used as a starting material for synthesizing other complexes discussed here.

5A.2.1 ((*R*)-2-ammonium-1-propanol)[Co($L^{O\text{-ValTryp}}$)$_2$] (1)

(NEt_4)[Co($L^{O\text{-ValTryp}}$)$_2$] (0.300 g, 0.346 mmol) was stirred in 15 mL acetonitrile. A few drops of methanol were added to the stirring solution to dissolve the complex properly. The hydrochloride salt of *racemic*-2-amino-1-propanol (0.77 g, 0.690 mmol) was dissolved in the minimum amount of MeOH and added to the stirring solution. After 15 min, precipitation appeared. Filtered it, washed with acetonitrile (2-3 times), dissolved in MeOH-DMF (3:1) solvent mixture, and kept for slow evaporation in a beaker at room temperature. Red block-shaped crystals were obtained after three weeks. The crystals were filtered, washed with acetonitrile, and dried under vacuum. Yield: 63%.

^{1}H NMR (d_6-DMSO, 500 MHz) δ 10.88 (s, 2H, $H^{NH\ indole}$), δ 7.82 (d, 2H, *J* = 8 Hz, H^{12}), δ 7.30 (d, 2H, *J* = 8 Hz, H^{15}), δ 7.21 (s, 2H, H^{17}), δ 7.04 (t, 2H, *J* = 7.5 Hz, H^{14}), δ 6.98 (t, 2H, *J* = 8 Hz, H^{13}), δ 6.55 (dd, 2H, *J* = 7.5, 2 Hz, H^5), δ 6.17 (dd, 2H, *J* = 7.5, 2 Hz, H^3), δ 6.03 (t, 2H, *J* = 7.5 Hz, H^4), δ 5.48 (t, 2H, *J* =10.5 Hz, $H^{NH\ LIGAND}$), δ 4.12 - 4.09 (m, 2H, H^8), δ 4.17 (t, 2H, *J* = 12 Hz, H^7), δ 3.87-3.85 (m, 2H, H^{7a}), δ 3.79 (dd, *J* = 4.5/5, 15 Hz 2H, H^9), δ 3.40 (dd, 2H, *J* = 4.5/5,15 Hz, H^{9a}), δ 2.45 (s, 6H, H^{-OCH3}), δ 7.67 (s, 3H, $H^{NH,Guest}$), δ 5.27 (t, 1H, *J* = 5 Hz, $H^{OH,Guest}$), δ 3.2 – 3.12 (m, 1H, $H^{x,Guest}$), δ 3.42 – 3.34 (m, 1H, $H^{a,Guest}$), δ 3.54 – 3.49 (m, 1H, $H^{b,Guest}$),δ 1.13 (d, 3H, *J* = 6.5 Hz, $H^{CH3,Guest}$); ^{1}H-^{1}H-COSY and HSQC were also performed. IR (KBr, cm^{-1}): $\upsilon_{as}(COO^-)_{asym}$ 1653; $\upsilon_s(COO^-)_{sym}$ 1448; υ(C-O) 1278; υ(C-H)o/p-ring H 747; υ(M-O) 540; υ(M-N) 434. m/z (ESI-MS) $\{M+H\}^+$, {((*R*)-2-ammonium-1-propanol)[Co($L^{O\text{-Val Tryp}}$)$_2$]+H}$^+$; calcd: 812.27, found: 812.27.

Alternatively, solid $Co(ClO_4)_2 \cdot 6H_2O$ (0.269 g, 0.735 mmol) was added to the methanolic solution (20 mL) of the ligand, $H_2L^{O\text{-ValTryp}}$ (0.500 g, 1.47 mmol), and the reaction mixture was stirred for 15 min. The color of the reaction mixture became pink. After 15 min., methanolic solution (10 mL) of (*R*)-2-amino-1-propanol (0.221 g, 2.94 mmol) was slowly added to the reaction mixture, and the color of the reaction mixture changed from pink to reddish brown. The reaction mixture

was stirred again for four hours at room temperature. Then, the solvent was evaporated using the rotary evaporator to reduce the volume of the reaction mixture; DMF was added to it in a proportion of 3:1 (methanol: DMF) and was kept in a 50 mL beaker. Block-shaped, plate-like red-colored crystals were obtained after two weeks of slow evaporation of the solvent mixture. Crystals were filtered, washed with ethyl acetate and diethyl ether, and dried in a vacuum desiccator. Yield: 68%.

The FTIR and ^{1}H NMR spectra of this product are identical to the product from the first method.

5A.2.2 ((*S*)-2-Ammonium-2-phenylethanol) [Co ($L^{O\text{-}ValTryp}$)$_2$)] (2)

Solid $Co(ClO_4)_2 \cdot 6H_2O$ (0.269 g, 0.735 mmol) was added to the methanolic solution (20 mL) of $H_2L^{o\text{-}ValTryp}$ (0.500 g, 1.47 mmol) in stirring condition. The colour of the reaction mixture became pink. After 15 min., methanolic solution (10 mL) of (*S*)-2-amino-2-phenylethanol (0.403 g, 2.94 mmol) was slowly added to the stirring reaction mixture, and the colour of the reaction mixture immediately changed from pink to reddish brown. After one hour, a few reddish-brown coloured precipitations appeared, and it was filtered using a G-4 crucible. The filtrate part was again stirred for another 3 hr. Then, the filtrate volume was reduced using a rotary, and DMF was added to it in a proportion of 1:3 (methanol: DMF) and kept in a 50 mL beaker. After 10-12 days of slow solvent evaporation, the solvent mixture gave block-shaped reddish-coloured crystals. Crystals were filtered, washed with ethyl acetate and diethyl ether, and dried in a vacuum desiccator. Yield: 67%.

^{1}H NMR (d_6-DMSO, 500 MHz) δ 10.88 (s, 2H, $H^{NH\ indole}$), δ 7.82 (d, 2H, J = 8 Hz, H^{12}), δ 7.30 (d, 2H, J = 8 Hz, H^{15}), δ 7.20 (s, 2H, H^{17}), δ 7.04 (t, 2H, J = 8 Hz, H^{14}), δ 6.98 (t, 2H, J = 7 Hz, H^{13}), δ 6.55 (dd, 2H, J = 7.5, 2 Hz, H^{5}), δ 6.17 (dd, 2H, J = 8, 2 Hz, H^{5}), δ 6.03 (t, 2H, J = 7.5 Hz, H^{4}), δ 5.47 (t, 2H, J =11 Hz, $H^{NH\ LIGAND}$), δ 4.12 - 4.08 (m, 2H, H^{8}), δ 4.17 (t, 2H, J = 12 Hz, H^{7}), δ 3.87-3.85 (m, 2H, H^{7a}), δ 3.79

(dd, J = 4.5/5, 15 Hz 2H, H^{9}), δ 3.39 (dd, 2H, J = 4.5/5,15 Hz, H^{9a}), δ 2.45 (s, 6H, H^{-OCH3}), δ 8.27 (s, 3H, $H^{NH,Guest}$), δ 7.47 – 7.37 (m, 5H, $H^{Ar-H,Guest}$), δ 5.55 (t, 1H, J = 5 Hz, $H^{OH,Guest}$), δ 4.29 – 4.26 (m, 1H, $H^{x,\ Guest}$), δ 3.73 – 3 (m, 1H, $H^{b,\ Guest}$), δ 3.66 – 3.69 (m, 1H, $H^{a,\ Guest}$);

^{1}H-^{1}H-COSY and HSQC were also performed. Anal. Calcd for ((*S*)-2-Ammonium-2-phenylethanol) [Co ($L^{O\text{-Val Tryp}}$)$_2$)]·DMF: C, 62.15; H, 5.85; N, 8.87. Found: C, 62.03; H, 5.732; N, 8.72. IR (KBr, cm^{-1}): υ(COO^-)$_{asym}$ 1657; υ(COO^-)$_{sym}$ 1456; υ(C-O) 1278; υ(C-H)o/p-ring H 738; υ(M-O) 540; υ(M-N) 431. m/z (ESI-MS) {M+H}$^+$, {((*S*)-2-Ammonium-2-phenylethanol) [Co ($L^{O\text{-Val Tryp}}$)$_2$)] + H}$^+$; calcd: 874.29, found: 874.29.

A suitable X-ray single crystal of the complex was obtained by further recrystallization from its' methanolic solution.

5A.2.3 ((*R*)-*m*-octopamine H$^+$) [Co($L^{O\text{-ValTryp}}$)$_2$] (3)

(NEt_4)[Co($L^{o\text{-ValTryp}}$)$_2$] (0.200 g, 0.232 mmol) was stirred to a 50 mL RB containing 10 mL of acetonitrile. A few drops of methanol were added to dissolve the complex properly. Methanolic solution (2 mL) of *racemic*-*m*-octopamine (norphenylephrine) hydrochloride (0.088 g, 0.464 mmol) was added to the stirring solution. After 10 minutes of stirring, precipitation appeared, and the solid was filtered and washed 2-3 times with acetonitrile. Then, the solid was re-dissolved in 10 mL methanol, and 3 mL of acetonitrile was added. The reddish-brown coloured solution was kept at room temperature for slow evaporation in a 25 mL beaker. Reddish-brown coloured crystals obtained after 6-7 days. The crystals were collected, washed with acetonitrile and diethyl ether, and dried in a vacuum desiccator. Yield: 61%.

^{1}H NMR (d_6-DMSO, 500 MHz) δ 10.88 (s, 2H, $H^{NH\ indole}$), δ 9.45 (s, 1H, H^{OH1}), δ 7.82 (d, 2H, J = 8 Hz, H^{12}), δ 7.80 (s, 3H, $H^{NH_3^+,\ guest}$), δ 7.30 (d, 2H, J = 8 Hz, H^{15}), δ 7.20 (s, 2H, H^{17}), δ 7.16 (t, 1H, J = 8 Hz, $H^{5'}$), δ 7.04 (t, 2H, J = 7 Hz, H^{14}), δ 6.98 (t, 2H, J = 7.5 Hz, H^{13}), δ 6.83-6.76 (m, 2H, $H^{2',\ 6'}$), δ 6.70 (d, 1H, J = 8 Hz, $H^{4'}$), δ 6.55 (d, 2H, J = 9.5 Hz, H^{5}), δ 6.17 (d, 2H, J = 9.5 Hz, H^{3}), δ 6.03 (t, 2H, J = 7.5 Hz,

H^{4}), δ 5.99 (s, 1H, H^{OH2}), δ 5.47 (t, 2H, *J* =12 Hz, $H^{NH\ LIGAND}$), δ 4.73-4.65 (m, 1H, H^{X}), δ 4.17 (t, 2H, *J* = 12 Hz H^{7}), δ 4.13-4.05 (m, 2H, H^{8}), δ 3.89-3.82 (d, 2H, *J* = 12 Hz H^{7a}), δ 3.78 (dd, 2H, *J* = 5, 15 Hz H^{9}), δ 3.39 (dd, 2H, *J* = 5, 15 Hz H^{9a}), δ 3.03-2.96 (m, 1H, H^{b}), δ 2.84 2.76 (m, 1H, H^{a}), δ 2.44 (s, 6H, H^{OCH3}); ^{1}H-^{1}H-COSY and HSQC were also performed.

Anal. Calcd for ((*R*)-*m*-octopamineH^{+}) $[Co(L^{O\text{-}ValTryp})_2]\cdot CH_3OH$: C, 61.23; H, 5.69; N, 7.6. Found: C, 61.224; H, 6.16; N, 7.763. IR (KBr, cm^{-1}): $\upsilon(COO^{-})_{asym}$ 1657; $\upsilon(COO^{-})_{sym}$ 1456; υ(C-O) 1278; υ(C-H)o/p-ring H 738; υ(M-O) 540; υ(M-N) 431. m/z (ESI-MS) $\{M+H\}^{+}$, {((*R*)- *m*-octopamineH^{+}) $[Co(L^{O\text{-}ValTryp})_2]$ + H$\}^{+}$; calcd: 890.28, found: 890.28.

5A.3 X-ray Crystallography

The crystals of the complexes obtained during synthesis were used for X-ray analysis. The crystals were mounted on glass fibre. All geometric and intensity data for the crystals were collected at room temperature using a Bruker SMART APEX CCD diffractometer equipped with a fine focus 1.75 kW sealed tube Mo-Kα (λ= 0.71073 Å) X-ray source, with increasing ω (width of 0.3º per frame) at a scan speed of either 3 or 4 s/frame. The SMART software was used for data acquisition and the SAINT software for data extraction. Absorption corrections were done using a multi-scan. After the initial solution and refinement with SHELXL, the final refinement was performed on the WinGX environment using the SHELXL-97 programs. All non-hydrogen atoms were refined anisotropically. The hydrogen atoms were located from the Fourier maps and refined isotropically wherever possible. Thus, some C-H bonds will not be ideal and may vary. In some complexes, the hydrogen atoms attached to the solvent molecules cannot be located or fixed, so the molecular weight may not match. ORTEP obtained selected crystallographic data summarized in Table **5A.1**. Perspective views of the complexes were shown using ORTEP.

Table 5A.1 Crystallographic data and refinement parameters of Co(III) Complexes.

Complexes	**1**	**2**	**3**
Empirical Formula	$C_{45}H_{47}CoN_6O_{11}$	$C_{47}H_{52}CoN_5O_{10}$	$C_{47}H_{52}CoN_5O_{11}$
Formula Weight	906.81	905.86	921.86
Wavelength(Å)	0.71073	0.71073	0.71073
Crystal system	orthorhombic	orthorhombic	orthorhombic
Space group	$P2_1\ 2_1\ 2_1$	$P2_1\ 2_1\ 2_1$	$P2_1\ 2_1\ 2_1$
a, Å	9.0342(14)	9.1209(6)	8.8832(5)
b, Å	21.978(3)	21.6944(15)	19.5391(11)
c, Å	22.310(3)	22.1858(15)	25.7137(15)
α, deg	90	90	90
β, deg	90	90	90
γ, deg	90	90	90
Volume, $Å^3$	4429.7(12)	4390.0(5)	4463.1(4)
Z/ρ	4/1.360	4/ 1.371	4/ 1.372
μ	0.454	0.456	0.452
Coll reflns	7803	8608	7870
Indep refln	6721	7651	6289
FLACK para.	0.069(4)	0.061(5)	0.030(5)
GOF	1.144	1.156	1.131
R1[a]	0.0457	0.0747	0.0459
wR2[a]	0.1174	0.1611	0.1002
R1[b]	0.0619	0.0862	0.0731
wR2[b]	0.1360	0.1665	0.1191

[a] $I > 2\sigma$. [b] All data

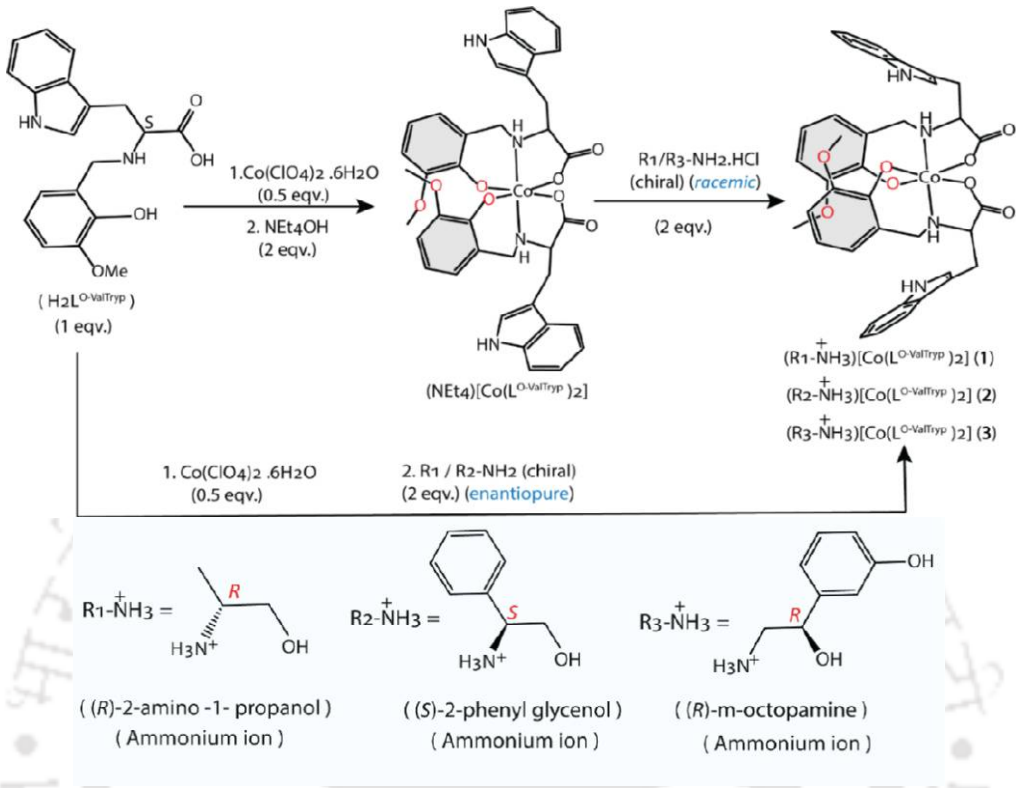

Scheme 5A.1 Syntheses of the Co(III) complexes with ammonium ion of chiral amino alcohols.

5A.4 Result and Discussion

5A.4.1 Syntheses and Selected Properties

We have synthesized complexes **1** & **3** through the salt metathesis reaction where one equivalent of $(NEt_4)[Co(L^{O\text{-}ValTryp})_2]$ was treated with two equivalents of racemic hydrochloride salts of two different amino alcohols to get the desired products. Also, complex **1** could be synthesized directly from the ligand metal complexation reaction where (*R*)-2-amino-1-propanol was used as a base. The reaction of the ligand $H_2L^{O\text{-}ValTryp}$ with 0.5 equivalent of $Co(ClO_4)_2{\cdot}6H_2O$ initially gave a pink-colored solution which, upon treatment with two equivalents of chiral amino alcohol, as a base, gradually changed into reddish-brown. Thus, we have synthesized complexes **1** and **2**. All the Co(III) complexes were characterized by IR and UV-visible spectroscopy and mass spectrometry. In addition, the ^1H NMR spectra of complex **1**-**3** unveil sharp, well-resolved

resonances, which indicate their diamagnetic nature. IR spectra of the complexes showed broad stretches at~3415 cm^{-1} due to OH (water or H-bonded OH) stretch. The other sharp band observed in the range 1615 -1650 cm^{-1} is due to asymmetric stretching of coordinated carboxylate to the metal center, the same as the other reported complexes of similar ligands.[28,29] The elemental analysis results of the complexes (**1**- **3**) are given in the experimental section. The number of solvents in the bulk and crystal structure differs. The formula obtained from the elemental analysis was used for experiments on the bulk.

5A.4.2 Crystal structures

Complex **1** obtained from two different synthetic procedures crystallized in an identical chiral space group i.e., chiral orthorhombic space group $P2_1\,2_1\,2_1$. Here, we have discussed the crystal structure of **1** obtained from 1st method (mentioned in the experimental section). The crystal refinement parameters have been provided in Table 5A.1. The asymmetric unit of complex-**1** contains one complex anion, one ammonium ion of (*R*)-2-amino-1-propanol, one methanol molecule, and one disordered DMF molecule. The atoms of the disordered DMF molecules were refined anisotropically to avoid A and B-level alerts in checkcif.

In **1**, the Co(III) center is octahedrally coordinated by two deprotonated tridentate ligands where two phenolate oxygen atoms (O1A & O1B) and two carboxylate oxygen atoms (O2A & O2B) occupy the equatorial corners of the octahedron and the axial positions are occupied by two secondary nitrogen atoms N1A & N1B. The geometry around the Co(III) ion is slightly distorted from the perfect octahedron, as evident from the deviation of angels from ideal 90˚ and 180˚ (Table 5A.2). The chiral carbons present in the complexes (C8A & C8B) have ***S*** conformation, originating from the use of L-tryptophan used for ligand synthesis and Co(III)- coordinated amine N atoms, N1A & N1B, have ***R*** conformation. The opposite conformation preference at chiral

carbon and amine N has been observed in all previous complexes with amino acid-derived reduced Schiff base ligands.[30–34] In **1**, the $[Co(L^{O\text{-}ValTryp})_2]^-$ unit folded backward, exposing the polar carboxylate oxygens, which are used in H-bonding with the cationic guest molecules and with the solvent molecules.

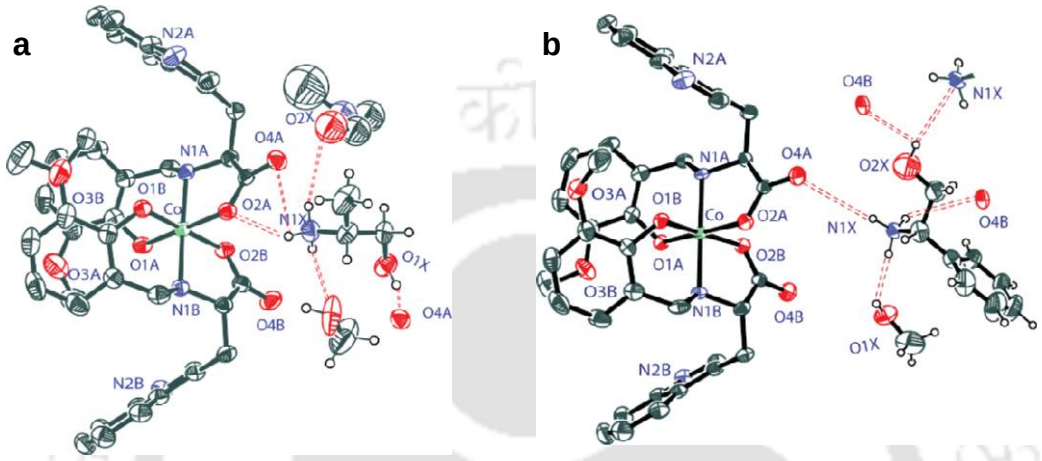

Figure 5A.1 The ORTEP figures of complexes **1** (a) and **2** (b) with 40% ellipsoid probability show non-covalent interaction between host, guest amino alcohol (in ammonium form), and the solvent molecules.

In **1**, the $-NH_3^+$ of the chiral guest formed H-bonded to the one carboxylate oxygen (N1X…O4A), one DMF oxygen (N1X…O2X), and one methanol oxygen atom, the -OH group of the guest is H-bonded to the carboxylate oxygens (O2A & O4A) of the neighboring complex molecule (Table 5A.3). The indole NH groups in **1** participate in inter-molecular H-bonding with the phenolate oxygen (N2AH2A…O1A and N2BH2B…O1B) of the neighboring complex units, thus forming a 1D chain along the a-axis. Also, the CH-π interactions present among the indole units of one complex unit to the phenolate rings of neighboring complex units strengthened the chain formation. (Fig. 5A.2a)

The chiral guest cations and solvent molecules bridged between two adjacent chains through intermolecular H-bonding, thus forming a 1D column along the a-axis. The outer surface of the

column is mostly aromatic, and inside the column, the carboxylate oxygens of complex molecules reside, which participate in the chiral guest recognition.

Table 5A.2 Selected bond distances (Å and angles (˚) of complexes **1** - **3**.

Complexes	Bond distances (Å)			Bond angles (˚)		
	Co-O_p	Co-O_c	Co-N_a	O_c-Co-O_c	O_p-Co-O_p	N_a-Co-N_a
1	1.886(4)	1.930(4)	1.942(4)	88.30(15)	95.30(16)	177.68(17)
(meridional)	1.881(4)	1.931(4)	1.935(4)			
2	1.883(5)	1.935(5)	1.926(5)	87.51(19)	96.20(18)	179.1(2)
(meridional)	1.884(5)	1.940(5)	1.933(6)			
3	1.880(4)	1.928(4)	1.935(4)	88.45(16)	95.38(16)	176.75(18)
(meridional)	1.886(4)	1.931(4)	1.927(4)			

Complex **2** was crystallized in a chiral orthorhombic space group $P2_12_1\ 2_1$. The crystal refinement parameters have been provided in Table 5A.1, and selected bond lengths and angles in Table 5A.2. The asymmetric unit of **2** contains one anionic $[Co(L^{O\text{-}ValTryp})_2]^-$ unit, one ammonium form of (*S*)-2-phenylglycinol, and one methanol molecule. The molecular structure of $[Co(L^{O\text{-}ValTryp})_2]^-$ and the geometry around the Co(III) center present in complex anion are identical to **1**. (Fig. 5A.1b) Complex **2** contains a large number of fairly strong H-bonds as well as other non-covalent interactions (Table 5A.4). Two out of three NH of the $-NH_3^+$ of the chiral guest are connected to the two non-coordinated carboxylate oxygens (O4A & O4B) and the third NH is connected to the oxygen atom of methanol (O1X) through intermolecular H-bonding interactions. The alcoholic -OH of the guest is H-bonded to the carboxylate oxygen of another neighboring complex unit (O2XH2X…O4B). The intermolecular H-bonding interactions between indole NH groups of the complex and the phenolate oxygen atoms of the adjacent complex units (N2AH2A…O1A and N2BH2B…O1B) formed a similar type of 1D chain like **1**. Here in **2**, the polar groups of the guest (-OH and $-NH_3^+$) molecules not only H-bonded to the

carboxylate groups of the adjacent complex molecules but also inter-connected within themselves, thus participating in the self-recognition process.

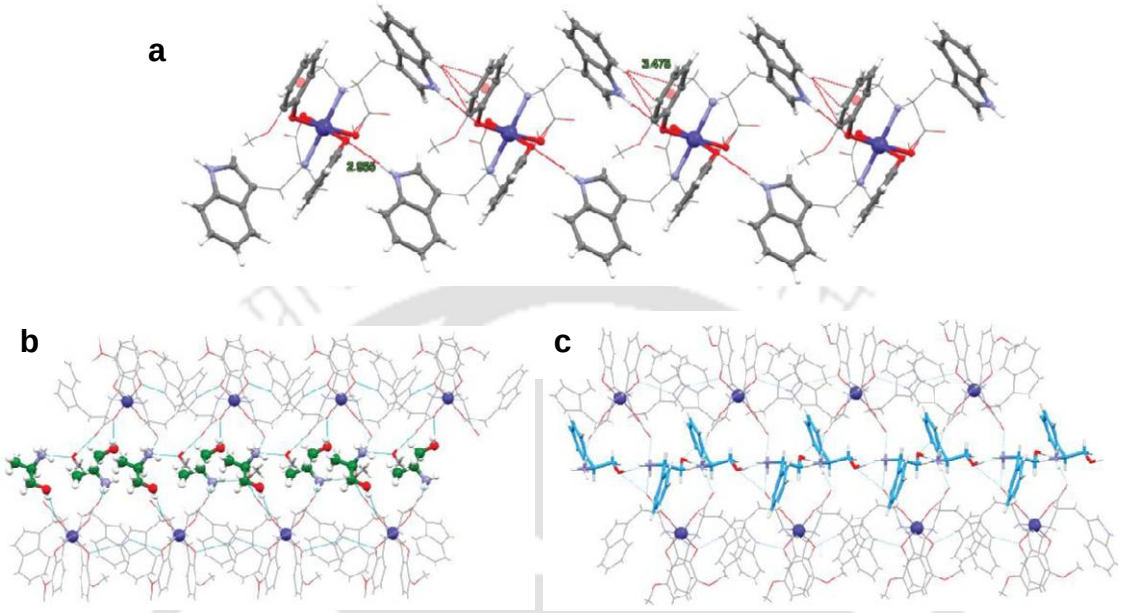

Figure 5A.2 Inter-molecular H-bonding interactions and CH-π interactions among the adjacent complex units (a); one-dimensional channel (space-filling model) encapsulated with guest cation (ball and stick) in **1** (b) and **2** (c).

Complex **3** was crystallized in chiral orthorhombic space group $P2_1\ 2_1\ 2_1$. The asymmetric unit of the complex contains one anionic $[Co(L^{O\text{-ValTryp}})_2]^-$ unit, one ammonium ion of (*R*)-m-octopamine, and one methanol molecule. While synthesizing the complex, we used hydrochloride salt of *racemic*- norphenylephrine, but the crystal structure showed that only the *R* isomer was recognized. (Fig. 5A.3a) The crystal refinement parameters are mentioned in Table 5A.1. The geometry around the anionic host's Co(III) center is similar to all the previous complexes described above. The selected bond lengths and bond angles of the complex are mentioned in Table 5A.2. In complex **3**, each indole NH group of the host connected to the adjacent host molecule through intermolecular H-bonding, thus forming a 1D chain along the a-axis. The cationic guest molecules and the methanol molecules act as bridges between two

adjacent chains along the a-axis through multiple intermolecular H-bonding interactions and other non-covalent interactions. (Fig. 5A.3b) The phenolic OH group of the guest cation formed intermolecular H-bonding to the carboxylate oxygen O4A (O6H6…O4A = 2.925) (Table 5A. 5). The phenolic -OH of the guest cation also acts as an H-bond acceptor and is connected to the alcoholic -OH of the adjacent guest cation, thus participating in the self-recognition process like complex **2**.

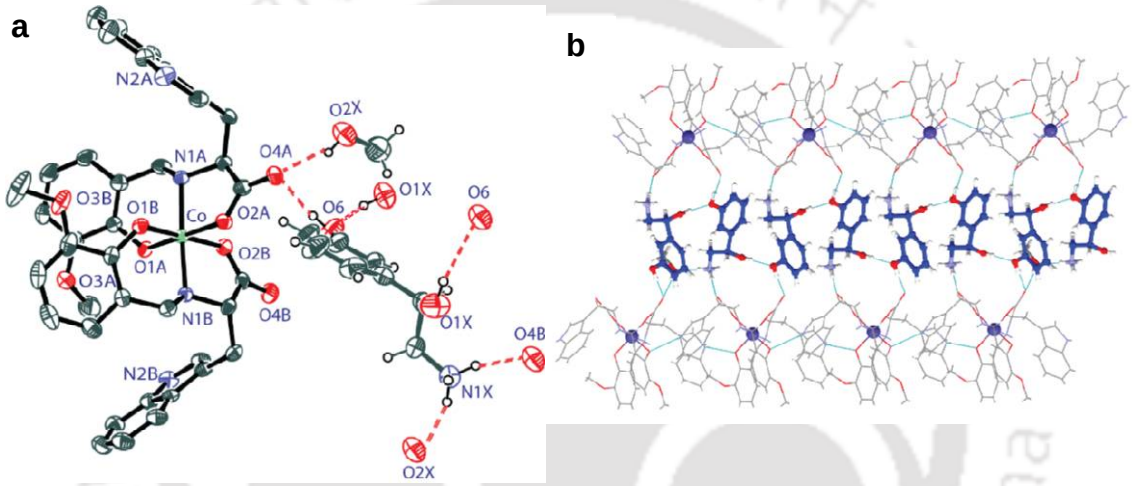

Figure 5A.3 (a) ORTEP diagram of complex **3** with 40% ellipsoid probability, showing non-covalent interactions in the complex; (b) Molecular structure of host-guest complex showing intermolecular H-bonding interactions between two adjacent molecules.

The -NH_3^+ group of the cationic guest is H-bonded to one of the non-coordinated carboxylate oxygen atom O4B (NH...O4B = 2.668 Å) of the neighboring host and one methanolic oxygen O2X (NH...O2X = 2.685 Å). These intermolecular H-bonds between the non-coordinated carboxylates (O4A, O4B) of complex anion, phenol (O6), amine (N1X), and alcohol (O1X) of guest cation, and the methanolic oxygen (O2X) formed a zigzag chain along the *a*-axis. Complex **3** also showed a 1D column formation along the a-axis, like the previous complexes discussed above.

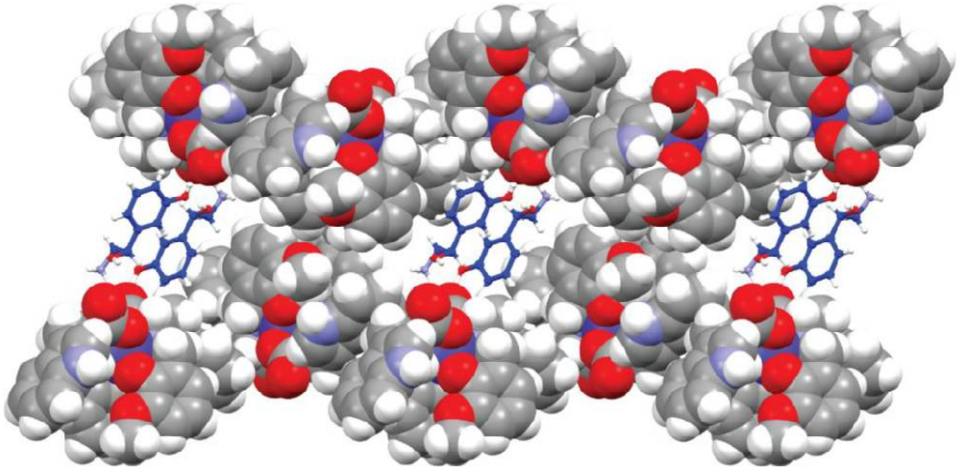

Figure 5A.4 One-dimensional channel (space-filling model) along the a-axis encapsulated with guest cation (ball and stick).

Overall, in all three complexes (**1**-**3**), the $[Co(L^{O\text{-}ValTryp})_2]^-$complex anion imparted a common structural motif. The single crystal structure analyses of **1** and **3** also revealed that the Co(III) complex anion recognized one of the enantiomers from their respective racemic analog. It is not surprising because previously, our group reported the chiral recognition of amino alcohol from its racemic mixture using the metal complex of a similar type of amino acid-derived ligand. The chiral guest cations, using their -OH and $-NH_3^+$ functional groups, act as a bridge between two adjacent anionic Co(III)-complex units. The position of the chiral center in the guest cations affects the width of the bridging. When the chiral carbon is at the α-position with respect to the $-NH_3^+$ group (in the ammonium ion of (*R*)-2-amino-1-propanol and (*S*)-2-phenylglycinol), then narrow bridging occurs in the complex (in **1** and **2**) but when the chiral carbon is at the β-position (in (*R*)-*m*-octopamine), then the guest cation formed wider bridging between two adjacent anionic complex units (in **3**).

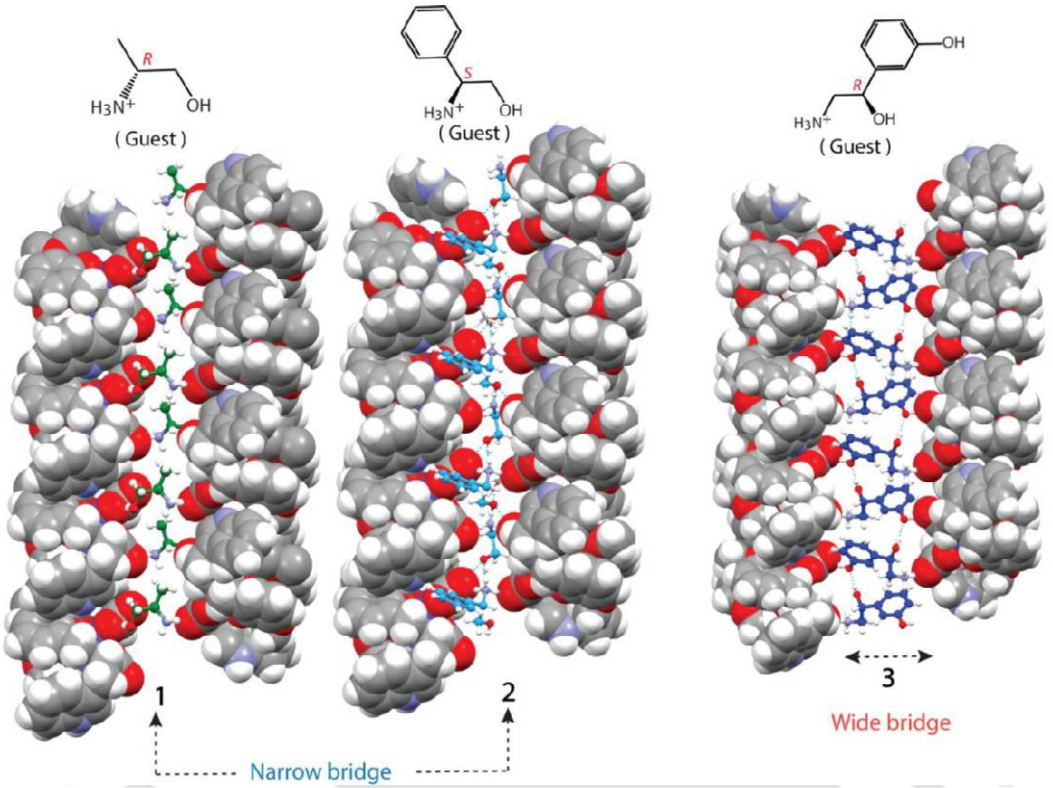

Figure 5A.5 Narrow channel (in **1** and **2**) and wider channel (in **3**) with different amino alcohol (in ammonium form) bridging**.**

Table 5A.3 Hydrogen bond and other non-covalent bond distances (Å) present in **1**.

Atoms	D-H (Å)	H…A (Å)	D…A(Å)	DHA(˚)
N1X-H1XA…O4B	0.89	1.88	2.737(6)	162
O1X-H1X…O2A	0.82	2.13	2.939(6)	167
O1X-H1X…O4A	0.82	2.50	3.139(6)	136
N1X-H1XB…O1X	0.89	2.51	2.887(6)	106
N1X-H1XB…O3X	0.89	1.92	2.753(8)	154
N2A-H2A…O1A	0.86	2.15	3.003(6)	171
N2B-H2B…O1B	0.86	2.10	2.955(6)	176
N1X-H1XC…O2X	0.89	1.95	2.822(10)	166
O3X-H3X…O4A	0.82	1.97	2.740(8)	156

Table 5A.4 Hydrogen bond and other non-covalent bond distances (Å) present in **2.**

Atoms	**D-H (Å)**	**H…A (Å)**	**D…A(Å)**	**DHA(˚)**
N1X-H1XA…O4B	0.89	1.97	2.844(9)	167
O1X-H1X…N1X	0.82	2.25	2.824(12)	128
N1X-H1XB…O4A	0.89	2.00	2.870(9)	168
N2A-H2A…O1A	0.86	2.06	2.920(8)	172
N2B-H2B…O1B	0.86	2.11	2.966(8)	171
N1X-H1XC…O1X	0.89	1.95	2.824(12)	169
O2X-H2X…N1X	0.82	2.34	3.034(14)	143
O2X-H2X…O1X	0.89	1.95	2.824(12)	169
C19B-H19C…O1B	0.96	2.28	2.891(15)	121

Table 5A.5 Hydrogen bond and other non-covalent bond distances (Å) present in **3.**

Atoms	D-H (Å)	H…A (Å)	D…A(Å)	DHA(˚)
N1X-H1XA…O4B	0.89	1.78	2.668(7)	174
O1X-H1X…O6	0.82	1.94	2.753(9)	176
N1X-H1XB…O2X	0.89	1.80	2.685(8)	175
N2A-H2A…O1A	0.86	2.15	3.005(7)	171
O2X-H2X…O4A	0.82	1.88	2.691(7)	173
N2B-H2B…O1B	0.86	2.07	2.925(6)	173
O6-H6…O4A	0.82	1.85	2.925(6)	160
C5X-H5X…O1X	0.93	2.50	2.827(9)	101
C8A-H8A…O2B	0.98	2.55	2.973(7)	106
C9A-H9AA…O4A	0.97	2.57	2.905(7)	100
C19A-H19C…O1A	0.96	2.45	2.883(11)	107

5A.4.3 NMR spectroscopy

The low spin Co(III)-complexes being diamagnetic, the ^{1}H NMR spectra for all the complexes (**1-3**) were taken in d_6-DMSO. The NMR spectra of the complexes showed sharp, well-resolved resonances for anionic complex molecules along with their respective chiral guest cations. ^{1}H-^{1}H COSY spectra and HSQC spectra of the complexes were also used wherever necessary for the assignment of the proton signals. From the X-ray single crystal structure of the Co(III) complexes, we observed the identical structural arrangement for the main [Co ($L^{O\text{-ValTryp}}$)$_2$)]$^-$ unit in the solid state. These observations are also reflected in the NMR solution study. From the ^{1}H NMR spectra of the complexes, we observed that in solution, the signals belonging to anionic Co(III) units showed identical chemical shift values, but peaks corresponding to their respective guest cations have differentiating identities. The chemical shift values of the respective protons, along with coupling constant values, are mentioned in the experimental section.

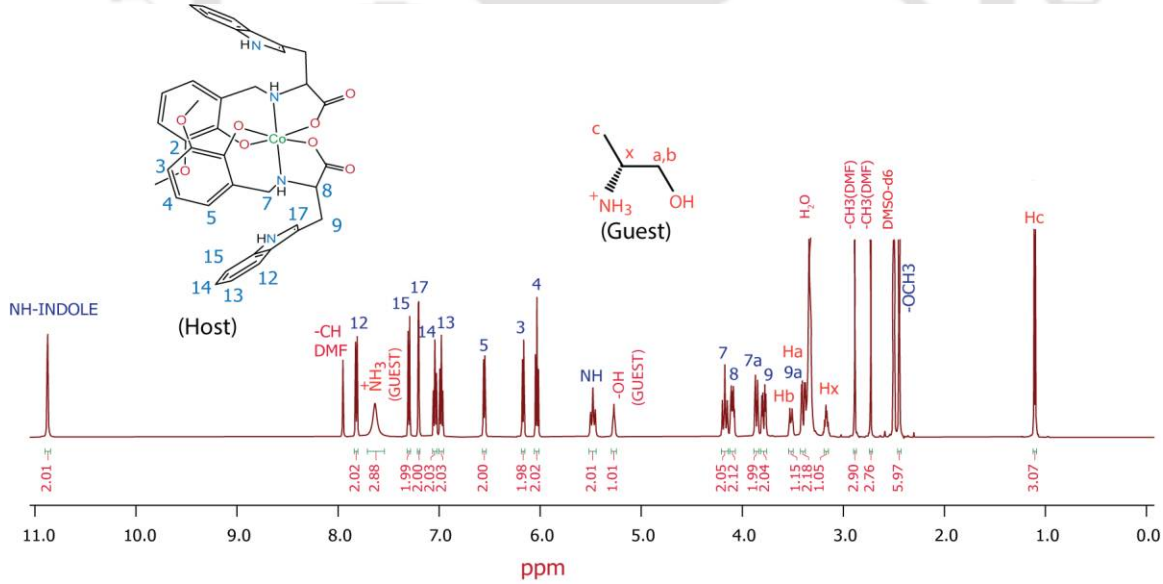

Figure 5A.6 ^{1}H NMR (500 MHz, d_6-DMSO) of **1.**

The assignment of the peaks was achieved through ^{1}H-^{1}H COSY NMR correlations (given below). The peaks for NH and OH protons are assigned using the ^{1}H-^{13}C HSQC NMR spectrum

of the complex. In the HSQC spectrum of **1**, the ^{1}H NMR signals of the NH protons and the OH protons are not coupled to any of the ^{13}C signals, as shown in Fig. 5A.8.

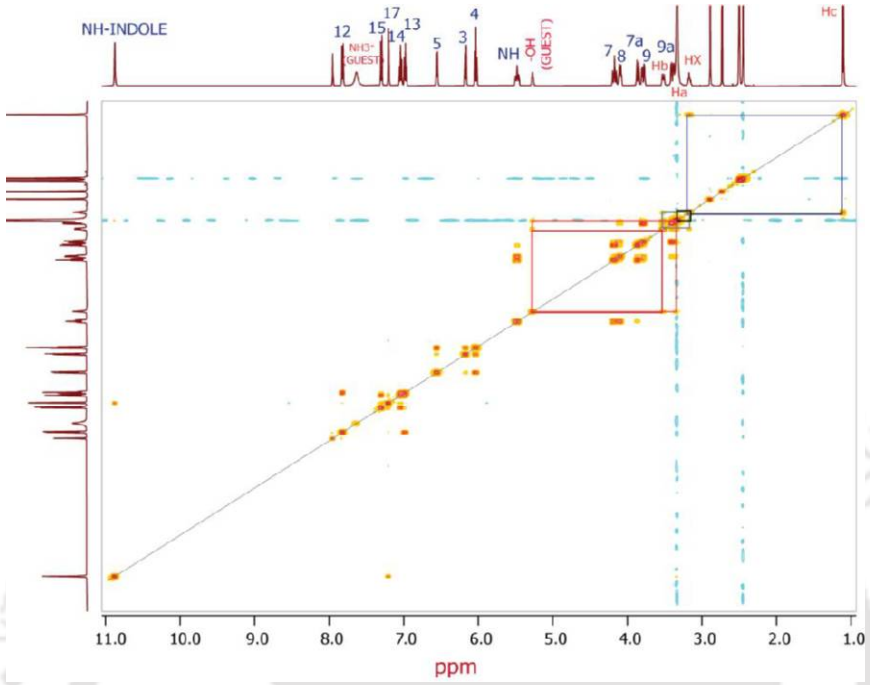

Figure 5A.7 ^{1}H-^{1}H COSY NMR (500 MHz, d_6-DMSO) of **1**.

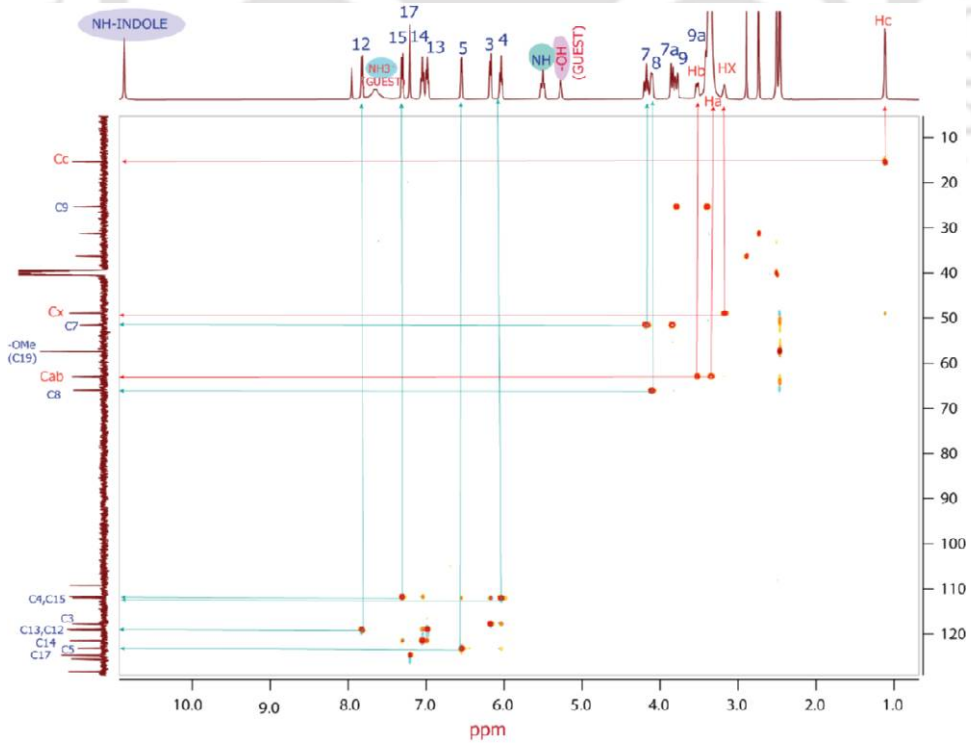

Figure 5A.8 HSQC NMR (500 MHz, d_6-DMSO) of complex-**1**.

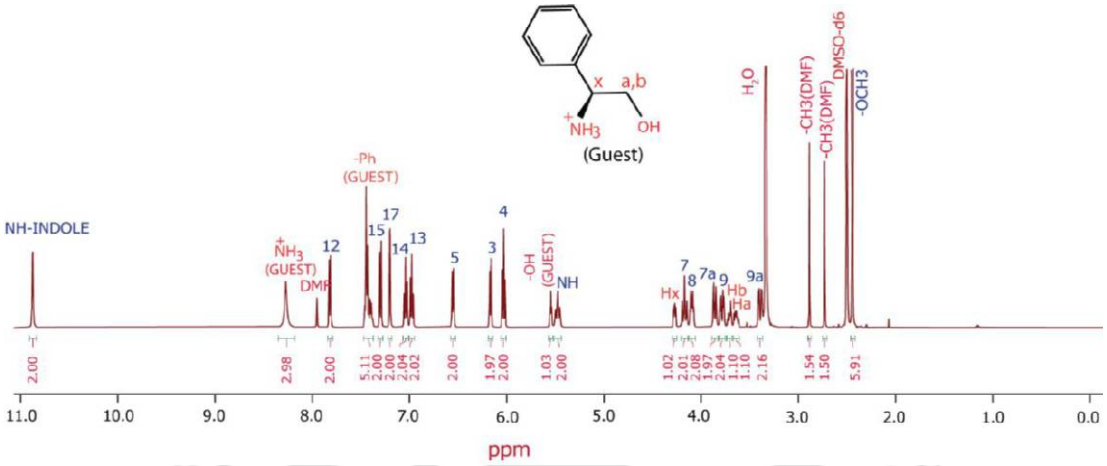

Figure 5A.9 ^{1}H NMR (500 MHz, d_6-DMSO) of **2**. The assignment of the peaks was achieved through ^{1}H-^{1}H COSY NMR correlations.

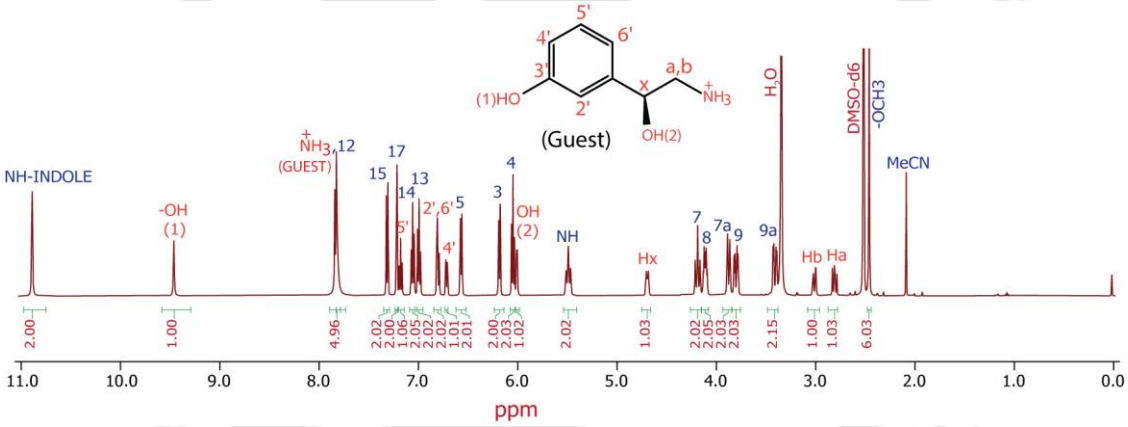

Figure 5A.10 ^{1}H NMR (500 MHz, d_6-DMSO) of **3**. The assignment of the peaks was achieved through ^{1}H-^{1}H COSY NMR correlations.

5A.4.4 UV-visible spectroscopy and Circular dichroism (CD) spectroscopy

The electronic spectrum of each complex was recorded using their DMF solution. All Co(III) – complexes show an intense band around 400 nm, one relatively weaker band between 510 nm to 530 nm, and one weak band around 700 nm, as shown in Fig.5A.11a. As the geometry around the central Co(III) ion is octahedral, we can say the higher energy intense band appeared around 400nm is because of phenolate (O^{-}) $p_{\pi} \rightarrow Co^{III}$ d_{σ^*} charge transfer transition whereas the other two

weaker, lower energy bands appeared because of the d →d transitions, more precisely, the band appeared near 700 nm is corresponding to the $^1A_{1g} \rightarrow {}^1T_{1g}$ and the band appeared near 520 nm is corresponding to the $^1A_{1g} \rightarrow {}^1T_{2g}$.

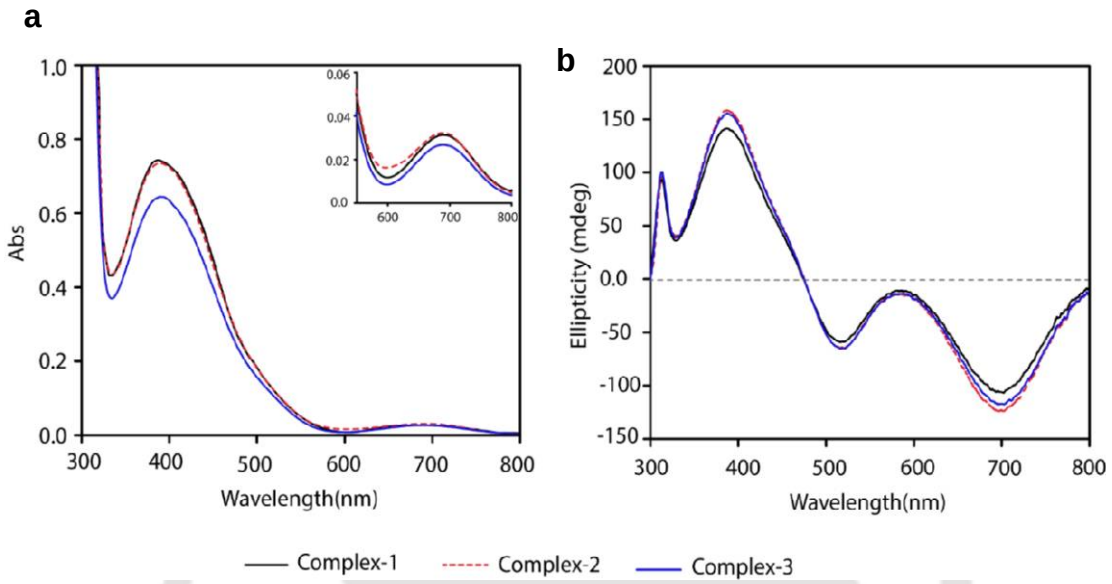

Figure 5A.11 (a) Electronic spectra of Co(III)-complexes (**1**-**3**) in DMF at a concentration of 0.3 mM; (b) CD spectra of Co(III) complexes (**1**-**3**) using their DMF solution.

Table 5A.6 Electronic spectroscopic data for complex **1**-**3** (In DMF)

Complexes	λ_{max}/nm (ε/$M^{-1}cm^{-1}$)
1	391 (2008), 519 (335) (sh), 690 (87)
2	390 (2142), 518 (354) (sh), 691 (93)
3	390 (1909), 517 (315) (sh), 691 (82)

The DMF solution of the complexes exhibited significant positive CD signals near 400 nm, i.e., in the LMCT transition region of the Co(III) complexes, and moderately intense positive CD signals near 300 nm. The complexes also showed two negative CD signals in the d-d electronic transition region, one intense negative signal near 700 nm and another moderately intense negative CD signal near 520 nm. (Fig. 5A.11b)

5A.4.5 Recognition of chiral amino alcohols and structural change

We have synthesized complexes **1** and **3** by reacting **$(NEt_4)[Co(L^{O\text{-}ValTryp})_2]$** with the racemic hydrochloride salt (2 equivalent.) of respective chiral amino alcohols. When a methanolic solution of racemic hydrochloride salt (2-amino-1-propanol.HCl for **1** and *m*-octopamine.HCl for **3**) to the acetonitrile solution of **$(NEt_4)[Co(L^{O\text{-}ValTryp})_2]$**, initially we got a reddish brown colored solid, which upon crystallization gave X-Ray suitable single crystals of **1** & **3**. From the single crystal structure of the complexes, we observed that in the solid state, the structures of the newly synthesized complexes have changed (Fig. 5A.12), and they have recognized "*R*" isomers of the respective chiral amino alcohols from their racemic analog.

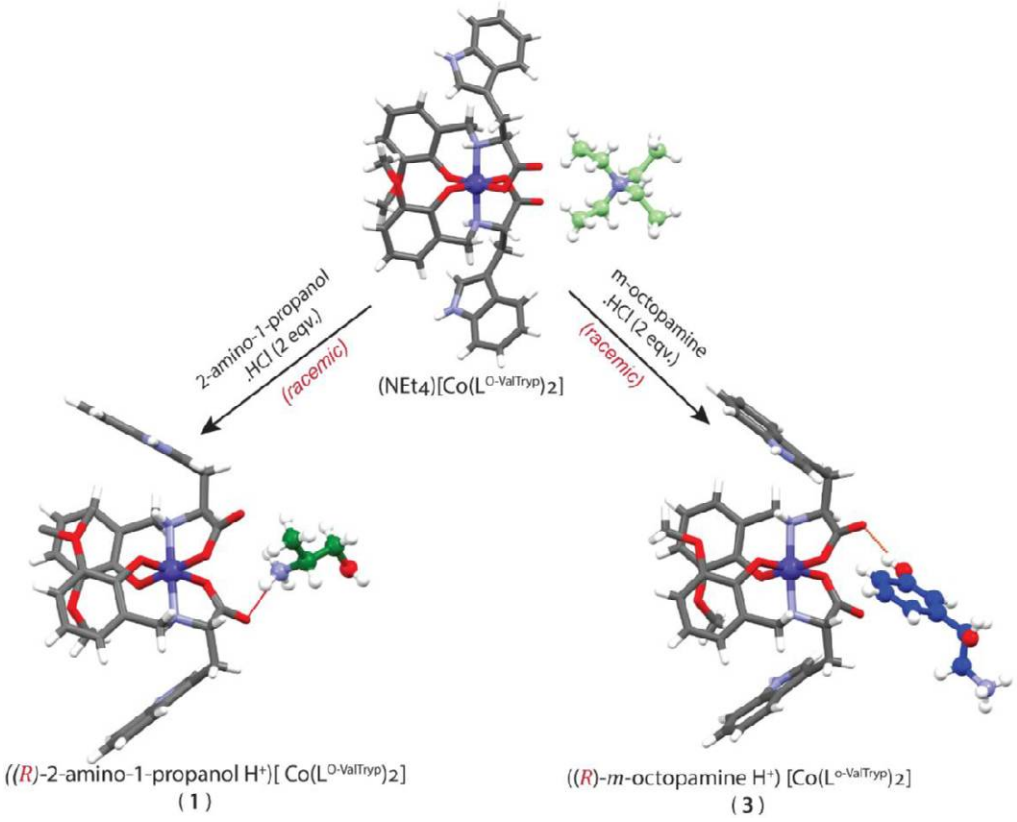

Figure 5A.12 The structural change of $[Co(L^{O\text{-}ValTryp})_2]^-$ while recognizing the "*R*" isomer of two different chiral amino alcohol guests from their *racemic* hydrochloride salts.

In the solid state, **1** & **3** showed the structural change in comparison to the starting complex, but comparing the NMR spectra of complexes did not exhibit any differences in chemical shift values

of the ^{1}H NMR signals for the anionic $[Co(L^{O\text{-ValTryp}})_2]^-$ unit apart from their positive counter ion part. (Figure 5A.13)

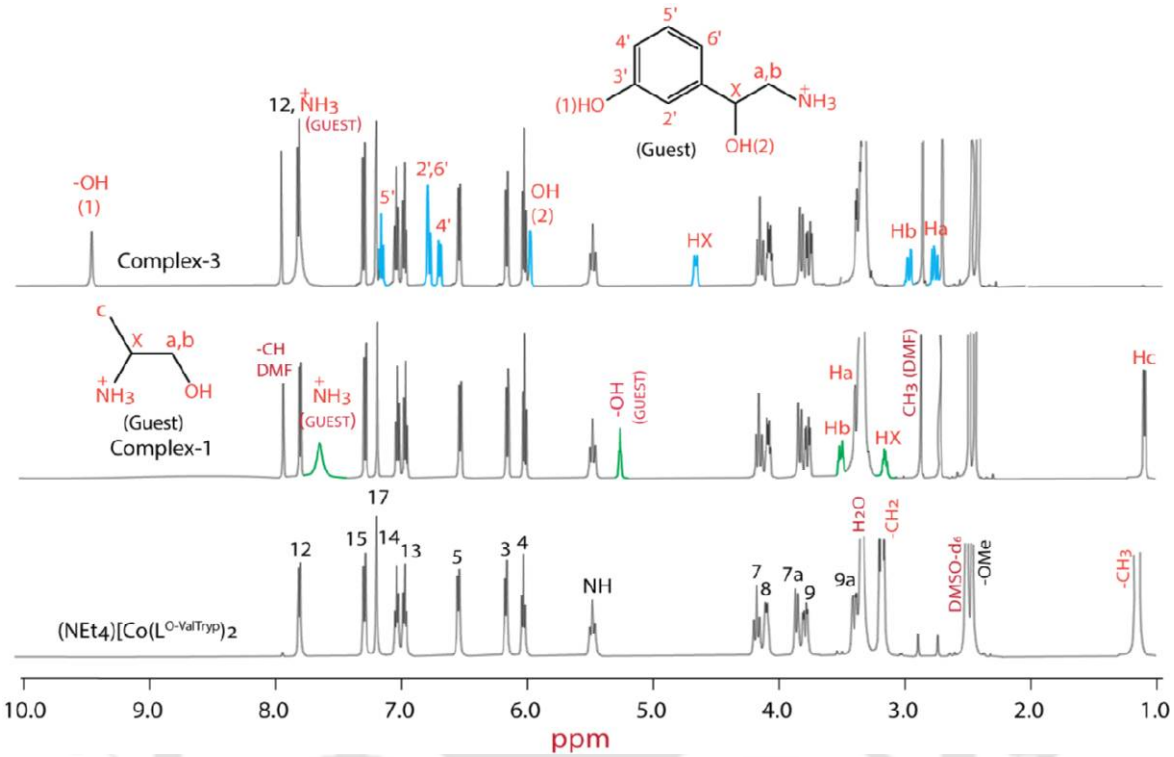

Figure 5A.13 Combined ^{1}H NMR spectra (500 MHz, in d_6-DMSO) of $(NEt_4)[Co(L^{O\text{-ValTryp}})_2]$, **1** and **3**.

When the NMR solutions **1** and **3** were warmed in a hot water bath at 60˚C for 44 hours and then re-recorded their NMR spectra, it showed the appearance of new signals.

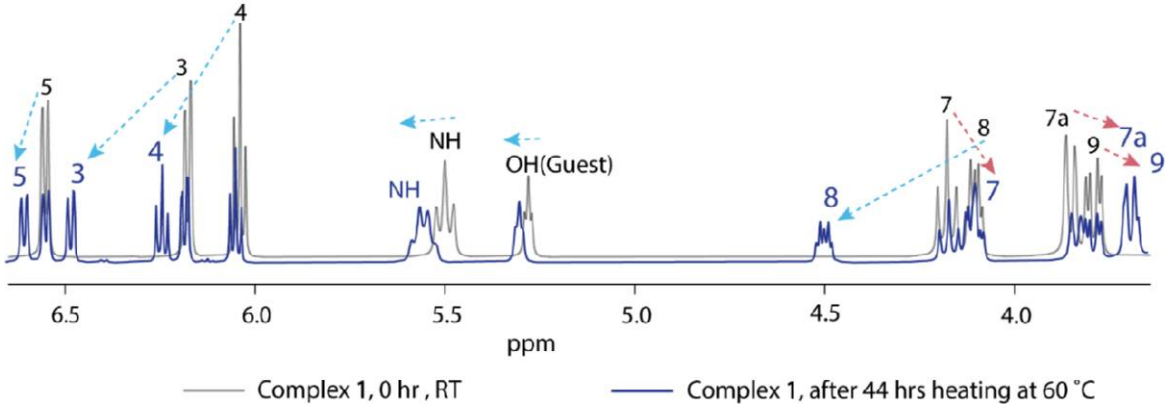

Figure 5A.14 Stacked partial ^{1}H NMR of **1** before and after warming.

Comparing these newly recorded NMR spectra with the initial one, it was observed that the intensity peaks for the ^{1}H NMR signals present in the initially recorded NMR spectra decreased

and shifted to a new position, indicating the structural change of the complexes in solution. The differences between NMR spectra of **1** collected at two different conditions are shown in Fig. 5A.14, where ^{1}H NMR signals appeared for H3, H4, H5, H8, and NH have shifted to the de-shielded region, whereas H7, H7a, H9 proton signals have shifted to the more shielded region.

Table 5A.7 Chemical shift differences between two NMR spectra of **1** collected before and after heating.

Types of proton	Complex 1, 0hr, RT	Complex 1, 44hr, 60˚C	Chemical shift change, Δδ (ppm)
-NH (indole)	10.88	10.94	+0.06
H12	7.30	7.34	+0.04
H13	7.04	7.08	+0.04
H14	6.98	7.03	+0.05
H5	6.55	6.62	+0.07
H4	6.03	6.24	+0.21
H3	6.17	6.48	+0.31
NH	5.41	5.55	+0.14
H7	4.18	4.11	-0.07
H7a	3.85	3.70	-0.15
H8	4.10	4.50	+0.40
H9	3.79	3.69	-0.10
-OCH3	2.46	3.54	+1.46

Complex-**3** exhibited similar types of ^{1}H NMR signal shifting when it was recorded after 44 hrs. warming at 60˚C on a hot water bath.

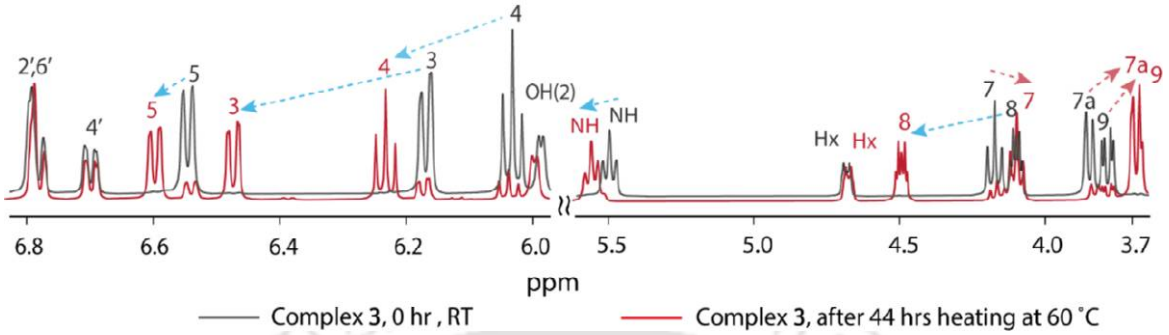

Figure 5A.15 Stacked partial 1H NMR spectra of **3** recorded before and after heating.

After 44 hrs of heating at 60˚C, complex **1** showed only ~ 47% structural conversion, determined by intensity change of the ^{1}H NMR signals, but complex 2 showed ~ 80% structural conversion under identical conditions.

5A.5 Conclusion

The above characterizations revealed that the anionic Co(III) host complexes could selectively recognize one isomer of chiral cationic guest molecules from their racemic analog. The chiral guest amino alcohols (in ammonium form) act as a bridge between the adjacent complex molecule, and the dredging depends on the no. of H-bond donor sites and the size of these chiral cations. The chiral host-guest complexes can reorganize their shapes in solution with external heat energy, which is evident from NMR spectroscopic characterization.

Part - B

In **Part A**, we observed that the anionic Co^{III} host complex could selectively recognize one enantiomer of the ammonium ion of different types of amino alcohols from their respective racemic mixtures where our synthesized metal complex host incorporated convergent binding sites for efficient interactions with the functional groups in the guest amino alcohols. Because amino alcohols have structural similarities to adrenaline and nor-adrenaline, here, we employed the anionic Co^{III} host complex to recognize the ammonium ion of adrenaline. Adrenaline is an essential molecule that facilitates signal transduction across cell membranes.[35,36] Adrenaline plays important roles in many physiological processes, such as promoting the elevation of blood sugar, glycogenolysis, heartbeat, and lipolysis, and has a significant impact on osteoarthritis pain reduction and the development of cartilaginous arthrosis.[37–40] The highly polar adrenaline molecule is efficiently bound to the natural G-protein coupled receptors through various non-covalent interactions. A recognition-induced structural change occurs in the transmembrane helices of the receptor.[41,42] An enormous amount of research has been done in the last few decades to develop artificial adrenergic receptor molecules for pharmacological purposes and to better understand the structure and function of the adrenergic receptor family.[43–47] The catechol -OH groups in protonated adrenaline have lower pK_a values and are prone to oxidize in their semi-quinone form in aerobic conditions. So, recognition of adrenaline using metal complex hosts is challenging. Here, in Part B, we synthesized a Co(III) complex with adrenaline ammonium ion as a counter ion. As the Co(III)-complex is diamagnetic, we used ^1H NMR spectroscopy to understand the interactions in the solution.

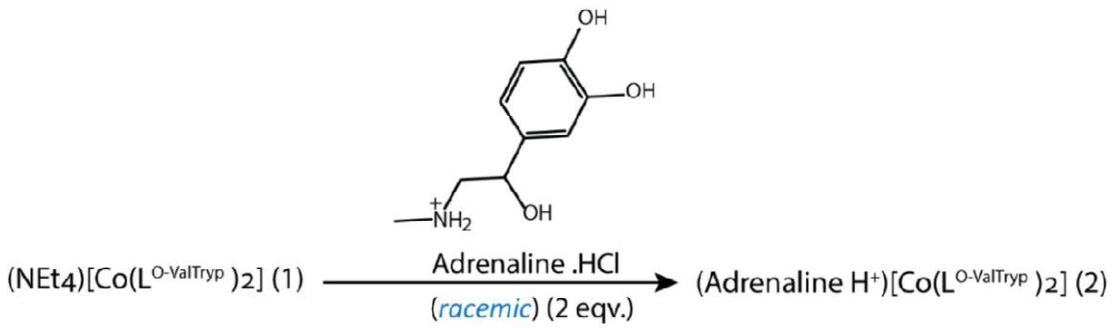

Scheme 1. Syntheses of (Adrenaline H^+) $[Co(L^{o\text{-}ValTryp})_2]$ (**2**)

5B.1 Experimental Section

5B.1.1 Materials and Methods

Solvents were obtained from commercial sources and used without further purifications unless otherwise stated. Racemic epinephrine (adrenaline) hydrochloride was purchased from Aldrich Chemical.

The IR spectra were recorded on a Nicolet FT-IR spectrophotometer with KBr discs in the 4000-400 cm-1 range. UV-visible spectra of the samples were measured with a PerkinElmer Lambda 365^+ UV/vis spectrometer. NMR spectra were recorded on Bruker 500 MHz. ESI-mass spectra were recorded with a high-resolution mass spectrometer (Agilent 6546 LC/Q-TOF). Circular Dichroism measurements were performed using a JASCO-J-1500 CD spectrometer, and CD spectra were analyzed using JASCO spectra manager version 2.0. All the CD spectra were recorded under an inert N_2 atmosphere using HPLC grade DMF as a solvent and a High Precision Cell made of Quartz SUPRASIL cuvette having a path length of 1 mm.

5B.2 Syntheses

5B.2.1 $(NEt_4)[Co(L^{O\text{-}ValTryp})_2]$ (1) was synthesized using the procedure reported in Chapter **2**.

^{1}H NMR (d_6-DMSO, 500 MHz) δ 10.93 (s, 2H, $H^{NH\ indole}$), δ 8.95 (s, 1H, $H^{NH\ TEA}$), δ 7.83 (d, 2H, J = 7.5 Hz, H^{12}), δ 7.34 (d, 2H, J = 8 Hz, H^{15}), δ 7.21 (s, 2H, H^{17}), δ 7.08 (t, 2H, J = 7.5 Hz, H^{14}), δ 7.03 (t, 2H, J

= 7.5 Hz, H^{13}), δ 6.62 (d, 2H, *J* = 7.5 Hz, H^{5}), δ 6.48 (d, 2H, *J* = 7 Hz, H^{3}), δ 6.24 (t, 2H, *J* = 8 Hz, H^{4}), δ 5.55 (t, 2H, *J* =11.5 Hz, $H^{NH\ LIGAND}$), δ 4.50 (dd, 2H, *J* = 4.5, 5.5 Hz, H^{8}), δ 4.11 (t, 2H, *J* = 11.5 Hz, H^{7}), δ 3.75-3.65 (m, 4H, $H^{7a,9}$), δ 3.54 (s, 6H, H^{-OCH3}), δ 3.39 (dd, 2H, *J* = 4.5/5.5,16 Hz, H^{9a}), δ 2.93 (q, 6H, *J* = 7 Hz, H^{CH2}), δ 1.06 (t, 9H, *J* = 7 Hz, H^{CH3}); ^{1}H-^{1}H-COSY was also performed. Anal. Calcd for $(Et_3NH)[Co(L^{O\text{-}ValTryp})_2]$: C, 63.07; H, 6.25; N, 8.36. Found: C, 62.708; H, 6.143; N, 8.034. IR (KBr, cm^{-1}): $\upsilon(COO^-)_{asym}$ 1615,1596; $\upsilon(COO^-)_{sym}$ 1458; υ(C-O) 1281; υ(C-H)o/p-ring H 744; υ(M-O) 532; υ(M-N) 431. m/z (ESI-MS) $\{M+H\}^+$, $\{[(Et_3NH)[Co(L^{O\text{-}ValTryp})_2]+H\}^+$; calcd: 838.32, found: 838.32.

5B.2.2 (Adrenaline H^+) $[Co(L^{O\text{-}ValTryp})_2]$ (2)

$(NEt_4)[Co(L^{O\text{-}ValTryp})_2]$ (0.200 g, 0.232 mmol) was stirred to a 50 mL RB containing 10 mL of acetonitrile. 1 mL methanol was added to dissolve the complex properly. Methanolic solution (1 mL) of racemic-adrenaline hydrochloride (0.116 g, 0.464 mmol) was added to the stirring solution. After 10 minutes of stirring, precipitation appeared, and the solid was filtered and washed 2-3 times with acetonitrile. The solid was collected, washed with acetonitrile and diethyl ether, and dried in a vacuum desiccator. Yield: 72%.

^{1}H NMR (DMSO-*d6*, 500 MHz) δ 10.88 (s, 2H, $H^{NH\ indole}$), δ 8.95 (s, 2H, $H^{NH1,NH2}$), δ 8.39 (s, 2H, $H^{OH1,\ OH2}$), δ 7.82 (d, 2H, *J* = 8 Hz, H^{12}), δ 7.30 (d, 2H, *J* = 8 Hz, H^{15}), δ 7.20 (s, 2H, H^{17}), δ δ 7.04 (t, 2H, *J* = 8 Hz, H^{14}), δ 6.97 (t, 2H, *J* = 7.5 Hz, H^{13}), δ 6.77 (s, 1H, $H^{2'}$), 6.72 (t, 1H, *J* = 8 Hz, $H^{5'}$), δ 6.61 (d, 1H, *J* = 8 Hz, $H^{6'}$), δ 6.55 (d, 2H, *J* = 7.5 Hz, H^{5}), δ 6.17 (d, 2H, *J* = 7.5 Hz, H^{3}), δ 6.03 (t, 2H, *J* = 7.5 Hz, H^{4}), δ 5.95 (d, 1H, *J* = 4 Hz, H^{OH3}), δ 5.49 (t, 2H, *J* =12 Hz, $H^{NH\ LIGAND}$), δ 4.69-4.62 (m, 1H, H^{X}), δ 4.17 (t, 2H, *J* = 12 Hz H^{7}), δ 4.13-4.04 (m, 2H, H^{8}), δ 3.89-3.82 (m, 2H, *J* = 12 Hz H^{7a}), δ 3.78 (dd, 2H, *J* = 4.5, 15 Hz H^{9}), δ 3.39 (m, 2H, *J* = 5, 15 Hz H^{9a}), δ 3.04-2.98 (m, 1H, H^{b}), δ 2.96-2.88 (m, 1H, H^{a}), δ 2.57 (s, 3H, H^{CH3}), δ 2.45 (s, 6H, H^{OCH3}); ^{1}H-^{1}H-COSY and HSQC were also performed. Anal. Calcd for

(Adrenaline H^+)[Co($L^{O\text{-ValTryp}}$)$_2$].H_2O.$(CH_3CN)_{0.5}$: C, 60.15; H, 5.63; N, 8.03. Found: C, 59.95; H, 6.02; N, 7.56. IR (KBr, cm^{-1}): $\upsilon_{as}(COO^-)_{asym}$ 1634; $\upsilon_s(COO^-)_{sym}$ 1457; υ(C-O) 1280; υ(C-H)o/p-ring H 745; υ(M-O) 538; υ(M-N) 430. m/z (ESI-MS) $\{M+H\}^+$, {(Adrenaline H^+)[Co($L^{O\text{-Val Tryp}}$)$_2$]+H}$^+$; calcd: 920.29, found: 920.29.

5B.3 Result and Discussion

5B.3.1 Syntheses and selected properties

All the detailed characterization data of (NEt_4)[Co($L^{O\text{-ValTryp}}$)$_2$] (**1**), used for the synthesis of complex-2, have been provided in Chapter II. For the synthesis of **2,** we employed a metathesis reaction where complex-**1** was treated with two equivalents of the *racemic* hydrochloride salt of adrenaline, and we got complex-**2** as a yellow-colored solid and was characterized by IR, NMR, UV-visible, and CD spectroscopy and mass analysis. Along with the other bands, the IR spectra of the complex showed a broad band at 3397 cm^{-1} due to the hydrogen-bonded O-H stretching and one sharp band at 1634 cm^{-1} due to the stretching of the metal ion-coordinated carboxylates. The ^{1}H NMR spectra of **2** showed distinct and well-resolved resonances, suggesting that it is diamagnetic i.e., low-spin Co(III) complex.

5B.3.2 ESI-Mass spectrometry

The ESI-Mass (+ve) spectra of **2** was recorded in MeOH. The ESI mass analysis of **2** showed a peak at m/z = 737.20, corresponding to the {[Co($L^{O\text{-ValTryp}}$)$_2$]$^-$ + 2H}$^+$, indicating the presence of the anionic complex unit. It also showed a prominent peak at m/z = 920.29, which corresponds to {(Adrenaline H^+)[Co($L^{O\text{-ValTryp}}$)$_2$] + H}$^+$. The experimental and simulated peak pattern at m/z = 920.29 for complex-2 showed excellent agreement between position and isotopic distribution. (shown in Figure 5B.1).

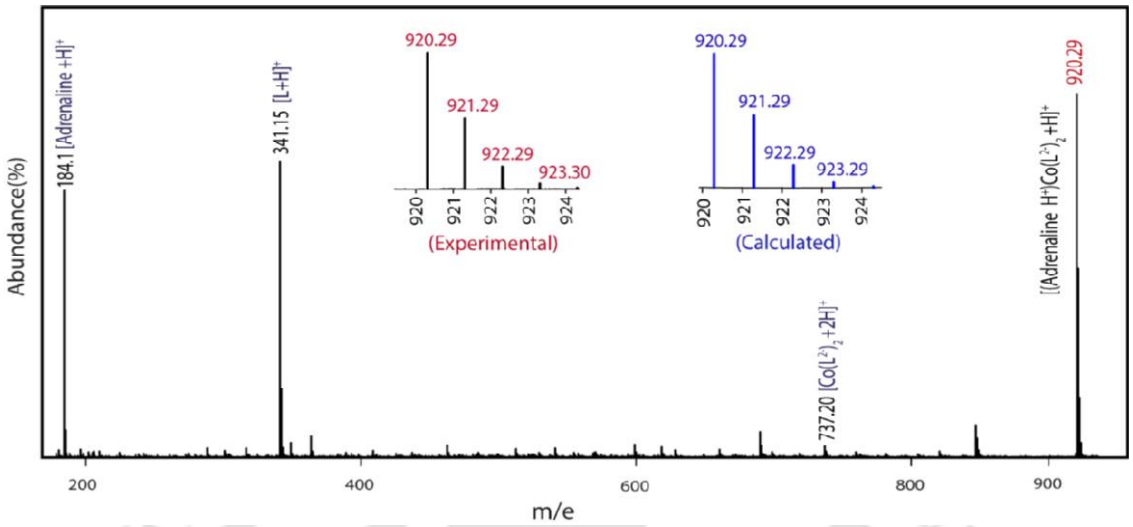

Figure 5B.1 (+)-ESI-Mass spectra of **2** in MeOH.

The above ESI (+ve) mass analysis suggests the existence of host-guest binding in the solution.

5B.3.3 NMR spectroscopy

The low spin Co(III)-complex being diamagnetic, the ^{1}H NMR spectra for complexes **2** were taken in d^{6}-DMSO. It has shown sharp, well-resolved resonances for anionic Co(III)-complex and chiral guest cation.

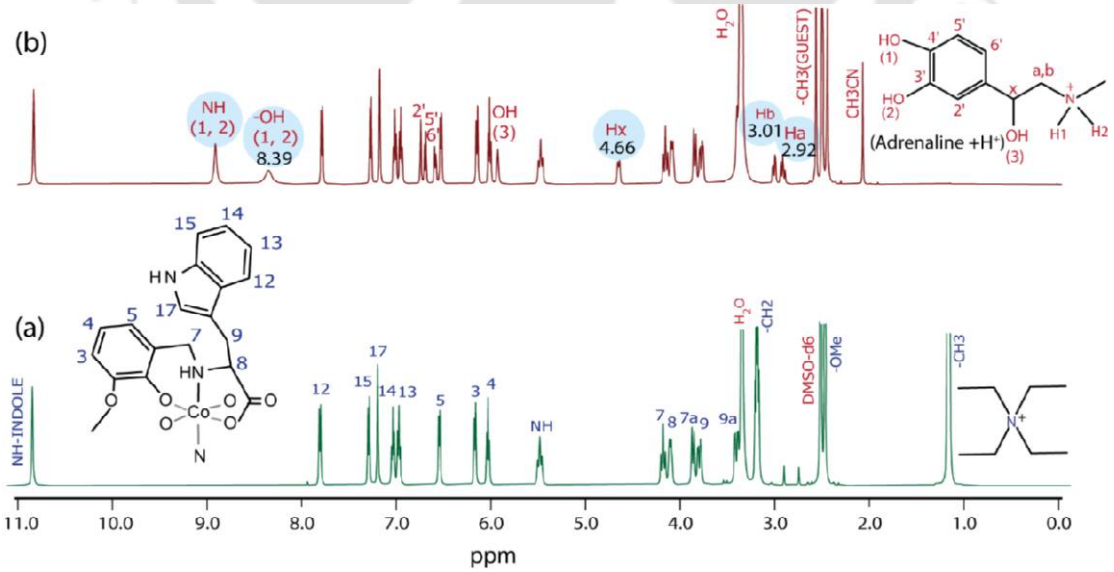

Figure 5B.2 ^{1}H NMR spectra of (a) starting complex, i.e., (NEt$_4$)[Co(L$^{O\text{-ValTryp}}$)$_2$], (b) complex-**2** in d$_6$-DMSO.

^{1}H-^{1}H COSY and HSQC spectra of the complexes were also used wherever necessary to assign the proton signals. We have used $(NEt_4)[Co(L^{O\text{-}ValTryp})_2]$ (**1**) as the starting complex and replaced the Et_4N^+ ion with an adrenaline ammonium ion to synthesize **2**. The 1H NMR spectra of **2** showed that the anionic host complex, $[Co(L^{O\text{-}ValTryp})_2]^-$, binds adrenaline ammonium ion (guest), and their intensity ratio showed 1:1 host-guest complexation. Comparing the ^{1}H NMR spectra of **1** & **2**, it was observed that the ^{1}H NMR signals of the $[Co(L^{O\text{-}ValTryp})_2]^-$ unit had identical chemical shift values, which suggest similar structural arrangements of **1** & **2** in the solution. (Figure 5B.2).

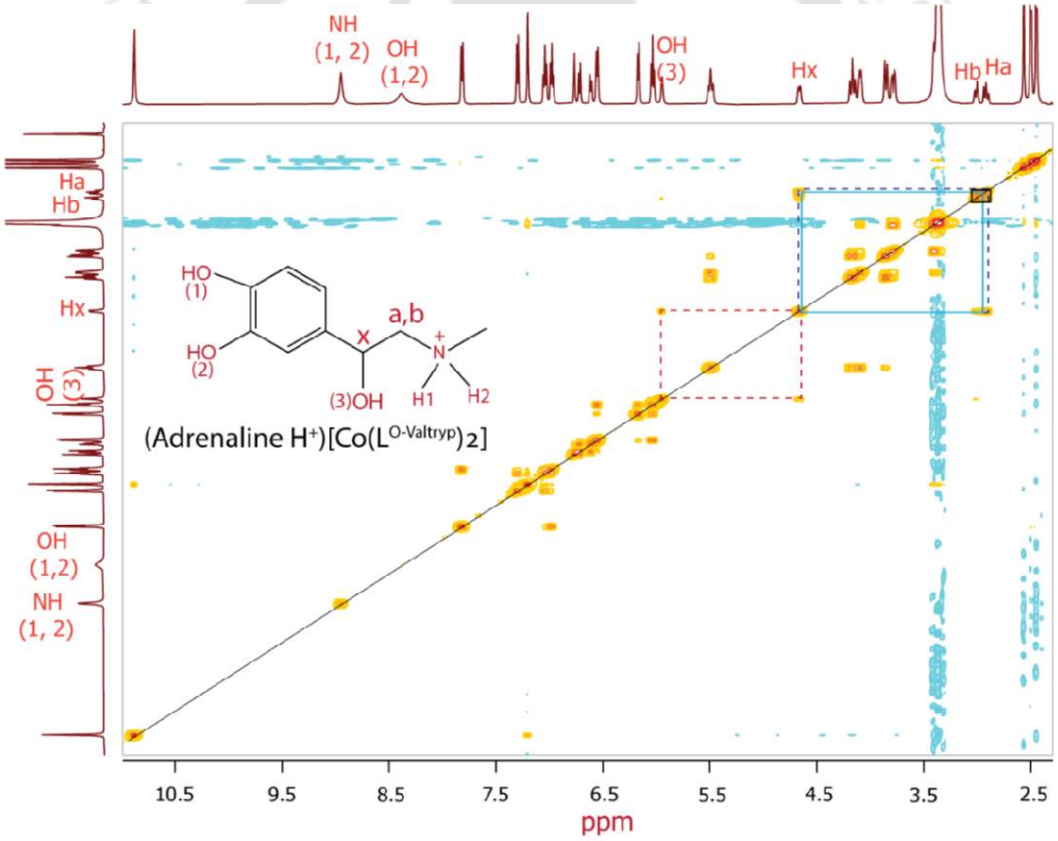

Figure 5B.3 ^{1}H-^{1}H COSY spectrum of **2** in d_6-DMSO.

5B.3.4 Structural change of complex 2 in solution

In the solution state, the structural change of **2** was monitored by ^{1}H NMR spectroscopy. Initially, the ^{1}H NMR spectrum of the complex was recorded in d_6-DMSO, and the appropriate positions of all kinds of protons were analyzed. Some new, very low-intensity signals appeared when the NMR spectrum of the same mother solution was recorded after three days. Then, the NMR spectrum of the same solution was collected every 3-4 days up to two months, and it was observed that the intensity of the newly appeared signals gradually increased and the intensity of the initially existing signals decreased. Assignments of the newly appeared signals showed that most proton signals in the initial ^{1}H NMR spectrum of **2** have shifted to a new position. Some of the protons showed upfield shifting, and others showed downfield shifting.

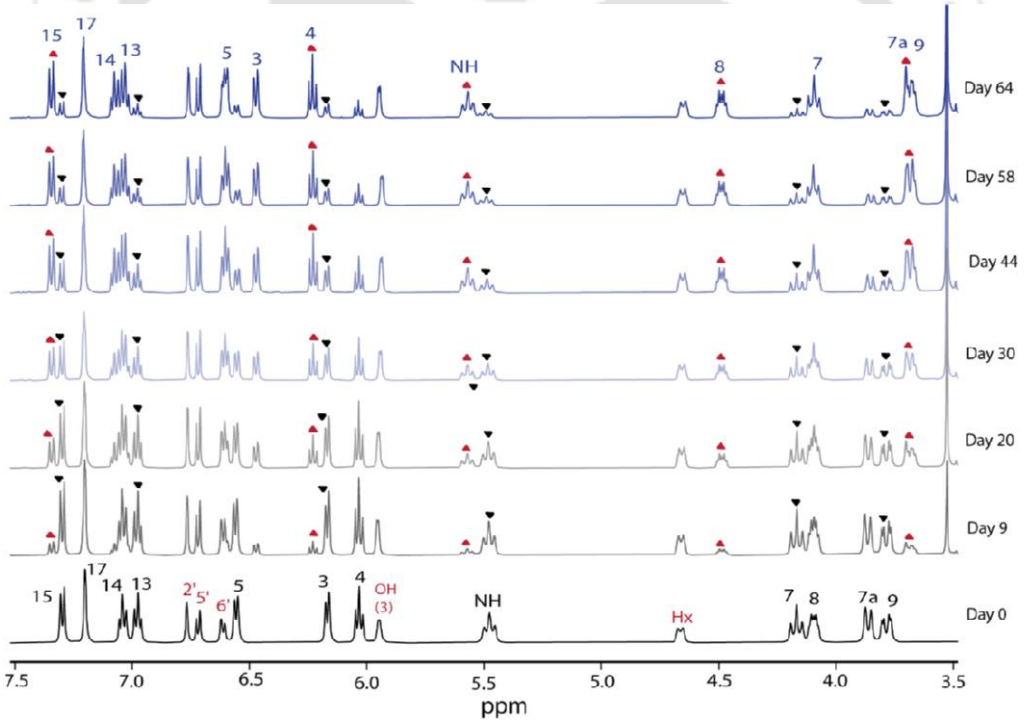

Figure 5B.4 Combined partial ^{1}H NMR spectra of **2** changes at room temperature (RT).

The solution state structural changing process of **2** is very slow at room temperature. It took about two months for ~80% of the conversion. However, the structural conversion process became faster at elevated temperatures. At 333K,>85% structural conversion occurred within 44 hrs.

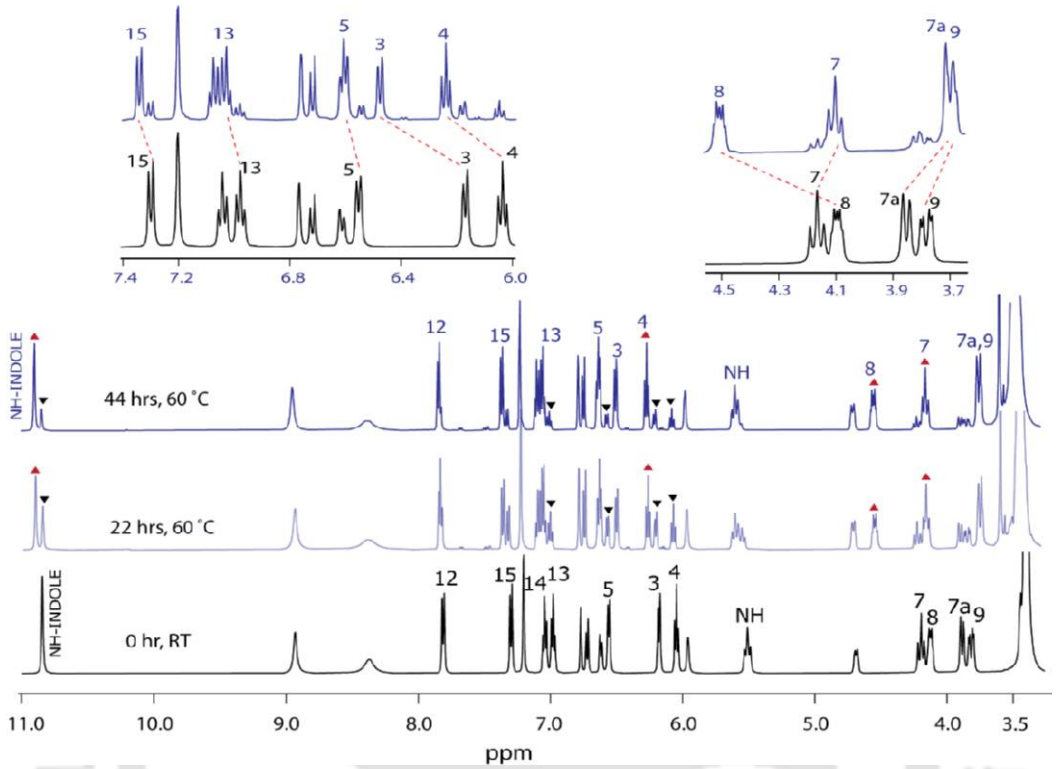

Figure 5B.4 Combined partial ^{1}H NMR spectroscopic changes of **2** at 60˚C.

5B.3.5 Effect of structural change on UV-visible and CD spectra of Complex 2

The electronic spectrum of complex **2** was recorded using its 0.3 mM DMF solution. It shows an intense band at 392 nm, one relatively weaker band at 520, and one weak band around 692 nm, as shown in Figure 5B.6. As the geometry around the central Co(III) ion is octahedral, we can say the higher energy intense band that appeared at 392 nm is because of phenolate (O^{-}) $p_{\pi}\rightarrow Co^{III}$ d_{σ^*} charge transfer transition whereas the other two weaker, lower energy bands appeared because of the d-d transitions, more precisely, the band that appeared at 692 nm is corresponding to the $^{1}A_{1g}\rightarrow{}^{1}T_{1g}$ and the band appeared at 520 nm is corresponding to the $^{1}A_{1g}\rightarrow{}^{1}T_{2g}$. When the UV-visible spectrum of 0.3 mM DMF solution of the complex was collected after heating at 333K for 44 hr, it showed differences from its initial spectrum. After heating, the absorption band intensities have increased both in LMCT and d-d electronic transition regions,

which is associated with the shifting of the band positions. One of the d-d bands shifted from 520 nm to 527 nm, and the other d-d band that initially appeared at 692 nm has shifted to 680 nm. Also, hypsochromic shifting of the LMCT band occurred after heating i.e., it has shifted from 392 nm to 377 nm.

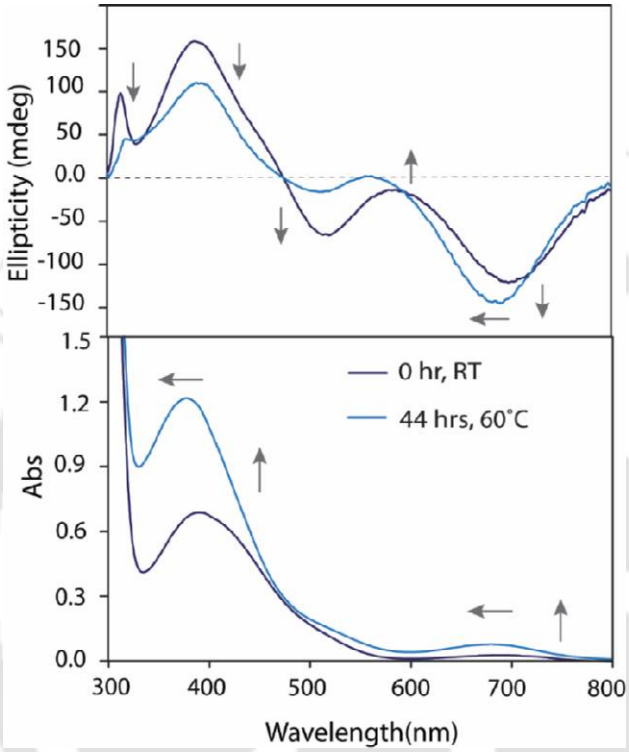

Figure 5B.6 Combined UV-visible and CD spectra of **2** collected before and after heating showing spectral change associated with the structural change of the complexes in solution.

Table 5B.1 Electronic spectroscopic data for complex **2** (In DMF)

Complex 2	**λ_{max}/nm (ε/$M^{-1}cm^{-1}$)**	
(0 hr, RT)	**LMCT**	**d-d**
	392 (2104)	520 (343) (sh), 692 (83)
(44 hrs, 60˚C)	377 (3731)	527 (404) (sh), 680 (236)

5B.4 Conclusion

In conclusion, we have synthesized an anionic Co(III) chiral host complex using L-tryptophan and ortho-vanillin-derived reduced Schiff base ligand that can bind protonated adrenaline. The low solubility of the host-guest complex allowed us to isolate the complex in the solid state. However, we cannot determine which isomer of the adrenaline molecule has bound as we could not get the single crystal structure of **2**. The solution state characterizations of the complex, like ESI-mass spectrometry and ^{1}H NMR spectroscopy, are evidence of a 1:1 complex formation between the anionic complex unit and the adrenaline ammonium ion. The ^{1}H NMR spectroscopic change of **2** has revealed that the complex showed structural change in the solution. Co(III)-complex being kinetically inert, the solution state structure changing process is very slow, but it becomes faster when extra heat energy is supplied.

References

(1) Qin, D.; Lai, W.; Hu, D.; Chen, Z.; Wu, A.; Ruan, Y.; Zhou, Z.; Chen, H. *Chemistry A European J* **2012**, *18* (34), 10515–10518.

(2) Li, H.; Wang, B.; Deng, L. *J. Am. Chem. Soc.* **2006**, *128* (3), 732–733.

(3) Pu, L.; Yu, H.-B. *Chem. Rev.* **2001**, *101* (3), 757–824.

(4) Darbost, U.; Zeng, X.; Giorgi, M.; Jabin, I. *J. Org. Chem.* **2005**, *70* (25), 10552–10560.

(5) Erdemir, S. *Journal of Molecular Structure* **2012**, *1007*, 235–241. h

(6) Han, X.; Li., P.; Han, Y.; Chen, C. *Angew Chem Int Ed* **2022**, *61* (21), e202202527.

(7) Mao, X.; Zhao, H.; Luo, L.; Tian, D.; Li, H. *J. Mater. Chem. C* **2015**, *3* (6), 1325–1329.

(8) Perraud, O.; Lefevre, S.; Robert, V.; Martinez, A.; Dutasta, J.-P. *Org. Biomol. Chem.* **2012**, *10* (5), 1056–1059.

(9) Schneider, H. *Angew Chem Int Ed* **2009**, *48* (22), 3924–3977.

(10) Yang, K.; Li, S.-Z.; Wang, Y.-H.; Zhang, W.-Z.; Xu, Z.-H.; Zhou, X.-Y.; Zhu, R.-X.; Luo, J.; Wan, Q. *RSC Adv.* **2014**, *4* (13), 6517.

(11) Yang, K.; Li, S.-Z.; Wang, Y.-H.; Zhang, W.-Z.; Xu, Z.-H.; Zhou, X.-Y.; Zhu, R.-X.; Luo, J.; Wan, Q. *RSC Adv.* **2014**, *4* (13), 6517.

(12) Dong, J.; Tan, C.; Zhang, K.; Liu, Y.; Low, P. J.; Jiang, J.; Cui, Y. *J. Am. Chem. Soc.* **2017**, *139* (4), 1554–1564.

(13) Fox, O. D.; Leung, J. F.-Y.; Hunter, J. M.; Dalley, N. K.; Harrison, R. G. *Inorg. Chem.* **2000**, *39* (4), 783–790.

(14) Gao, L.-L.; Gao, E.-Q. *Coordination Chemistry Reviews* **2021**, *434*, 213784.

(15) Jang, S.; Kim, H. *Org. Lett.* **2020**, *22* (11), 4185–4189.

(16) Jang, S.; Kim, H. *Asian J Org Chem* **2021**, *10* (4), 886–890.

(17) Kim, H.-J.; Kim, W.; Lough, A. J.; Kim, B. M.; Chin, J. *J. Am. Chem. Soc.* **2005**, *127* (48), 16776–16777.

(18) Saha, B.; Ikbal, S. A.; Rath, S. P. *Inorg. Chem.* **2020**, *59* (11), 7795–7809.

(19) Sun, Z.; Chen, Z.; Wang, Y.; Zhang, X.; Xu, J.; Bian, G.; Song, L. *Org. Lett.* **2020**, *22* (2), 589–593.

(20) Tsukube, H.; Hosokubo, M.; Wada, M.; Shinoda, S.; Tamiaki, H. *Inorg. Chem.* **2001**, *40* (4), 740–745.

(21) Sahoo, S. C.; Ray, M. *Chemistry A European J* **2010**, *16* (17), 5004–5007.

(22) Koide, A.; Abbatiello, S.; Rothgery, L.; Koide, S. *Proc. Natl. Acad. Sci. U.S.A.* **2002**, *99* (3), 1253–1258.

(23) Orellana, L. *Front. Mol. Biosci.* **2019**, *6*, 117.

(24) Ma, J. C.; Dougherty, D. A. *Chem. Rev.* **1997**, *97* (5), 1303–1324.

(25) Salonen, L. M.; Ellermann, M.; Diederich, F. *Angew Chem Int Ed* **2011**, *50* (21), 4808–4842.

(26) Song, G.; Ren, J. *Chem. Commun.* **2010**, *46* (39), 7283.

(27) Hoffmann, C.; Zürn, A.; Bünemann, M.; Lohse, M. J. *British J Pharmacology* **2008**, *153* (S1).

(28) Shongwe, M. S.; Al-Hatmi, S. K. M.; Marques, H. M.; Smith, R.; Nukada, R.; Mikuriya, M. *J. Chem. Soc., Dalton Trans.* **2002**, No. 21, 4064–4069.

(29) Shakya, R.; Imbert, C.; Hratchian, H. P.; Lanznaster, M.; Heeg, M. J.; McGarvey, B. R.; Allard, M.; Schlegel, H. B.; Verani, C. N. *Dalton Trans.* **2006**, No. 21, 2517–2525.

(30) Das, C. R.; Dutta, T.; Ray, M. *Inorganica Chimica Acta* **2019**, *486*, 367–376.

(31) Das, C. R.; Sahoo, S. C.; Ray, M. *Crystal Growth & Design* **2014**, *14* (8), 3958–3966.

(32) Dubey, M.; Koner, R. R.; Ray, M. *Inorg. Chem.* **2009**, *48* (19), 9294–9302.

(33) Rajesh, C. M.; Ray, M. *Dalton Trans.* **2014**, *43* (34), 12952–12960.

(34) Sahoo, S. C.; Ray, M. *Dalton Trans.* **2009**, No. 17, 3230.

(35) Rüdiger, M.; Haupts, U.; Moore, K. J.; Pope, A. J. *SLAS Discovery* **2001**, *6* (1), 29–37.

(36) Korać, J.; Todorović, N.; Zakrzewska, J.; Žižić, M.; Spasojević, I. *Struct Chem* **2018**, *29* (5), 1533–1541.

(37) Bergquist, J.; Ściubisz, A.; Kaczor, A.; Silberring, J. *Journal of Neuroscience Methods* **2002**, *113* (1), 1–13.

(38) Phillips, K.; Clauw, D. J. *Best Practice & Research Clinical Rheumatology* **2011**, *25* (2), 141–154.

(39) Cai, W.; Lai, T.; Du, H.; Ye, J. *Sensors and Actuators B: Chemical* **2014**, *193*, 492–500.

(40) Tavana, T.; Khalilzadeh, M. A.; Karimi-Maleh, H.; Ensafi, A. A.; Beitollahi, H.; Zareyee, D. *Journal of Molecular Liquids* **2012**, *168*, 69–74.

(41) Wu, Y.; Zeng, L.; Zhao, S. Ligands of Adrenergic Receptors: A Structural Point of View. *Biomolecules* **2021**, *11* (7), 936. https://doi.org/10.3390/biom11070936.

(42) Ring, A. M.; Manglik, A.; Kruse, A. C.; Enos, M. D.; Weis, W. I.; Garcia, K. C.; Kobilka, B. K. *Nature* **2013**, *502* (7472), 575–579.

(43) Schrader, T. *J. Org. Chem.* **1998**, *63* (2), 264–272.

(44) Danylyuk, O.; Fedin, V. P.; Sashuk, V. *Chem. Commun.* **2013**, *49* (18), 1859.

(45) Herm, M.; Molt, O.; Schrader, T. *Chem. Eur. J.* **2002**, *8* (6), 1485–1499.

(46) Herm, M.; Schrader, T. *Chem. Eur. J.* **2000**, *6* (1), 47–53.

(47) Kawai, H.; Katoono, R.; Fujiwara, K.; Tsuji, T.; Suzuki, T. *Chemistry A European J* **2005**, *11* (3), 815–824.

Chapter 6

Effect of kinetic lability on the recognition of chiral amino alcohols using anionic Fe^{III}-host complex

6.1 Introduction

In Chapter **2**, we observed that the anionic complex $[M(L^{O\text{-ValTryp}})_2]^-$ (M = Co^{III} and Fe^{III}) can adopt two different shapes to recognize Et_4N^+ and Et_3NH^+ ions where the $(Et_4N)[Co(L^{O\text{-ValTryp}})_2]$ and $(Et_3NH)[Co(L^{O\text{-ValTryp}})_2]$ are isostructural to their labile Fe(III) analogs. Again, in Chapter **5**, we have shown that the presence of the $-Et_3N^+$ group and alcoholic -OH group in the ammonium ion of chiral amino alcohol enhanced the electrostatic attraction between the cationic ammonium guest and the anionic Co(III)-host complex, hence the $[Co(L^{O\text{-ValTryp}})_2]^-$ complex anion exert a new shape to selectively recognize one isomer of different chiral amino alcohols from their racemic mixture. In this chapter, we wanted to see the effect of kinetic lability of the metallo-host complexes toward recognizing these amino alcohol ammonium ions having multiple H-bond donor sites potential for H-bonding with the anionic host complex. For that, we have synthesized and characterized a set of coordinatively saturated bis-Fe(III) complexes with different chiral amino alcohol ammonium ions. Also, we have discussed how the non-covalent interactions between chiral guest ammonium ion and the labile Fe(III)- anionic host triggered the drastic structural change of $[Fe(L^{O\text{-ValTryp}})_2]^-$ complex anion. Metal complexes that can undergo dynamic structural change in response to external stimuli like light[1,2], heat, pH change[3], redox reaction[3], and binding with chiral achiral guest molecules are reported.[4–14] In most cases, these responsive molecules either contain a binding site for guest molecules[15–17] or a photo/redox-responsive site[18] to exert their responsive functions. On the other hand, in our case, we have entirely focused on the non-covalent bonding interaction-induced structural rearrangement of coordinatively saturated bis-Fe(III) complexes as non-covalent interactions are essential in the biological recognition process, where these weak interactions trigger the structural reorganization or conformational changes of the bio-receptors to respond to different stimuli.[19]

6.2 Experimental Section

6.2.1 Materials and Methods

Solvents were obtained from commercial sources and purified before use, following standard literature procedure. (*Racemic*)-2-amino-1-propanol, (*R*)-2-amino-1-propanol, (*racemic*)-*m*-octopamine/nor phenylephrine hydrochloride, (*S*)-2-phenylglycinol, and Co. $Fe(ClO_4)_2.7H_2O$ were purchased from Aldrich Chemical. All the details of the instruments used for analysis have already been discussed in Chapter 2.

6.3 Syntheses

The detailed synthetic procedure of the ligand $H_2L^{O\text{-ValTryp}}$ and $(NEt_4)[Fe(L^{O\text{-ValTryp}})_2]$ were discussed in Chapter 2. These are used as a starting material for synthesizing other complexes discussed here.

6.3.1 ((*R*)-2-Ammonium-1-propanol) $[Fe(L^{O\text{-ValTryp}})_2]$ (1)

$(NEt_4)[Fe(L^{O\text{-ValTryp}})_2]$(0.300g, 0.348 mmol) was stirred in 15 mL acetonitrile, giving a red-coloured solution. The methanolic solution of the hydrochloride salt of *racemic*-2-amino-1-propanol (0.077g, 0.695 mmol) was added to the stirring solution, and the reaction mixture became bluish-purple coloured. After 30 minutes of stirring, the solution was undisturbed for one day. The next day, a bluish-purple-coloured solid precipitated, and it was filtered and washed with acetonitrile (2-3 times). Then, the solid was dissolved in a MeOH-DMF (3:1) solvent mixture and kept for slow evaporation in a beaker at room temperature. Dark-red, block-shaped crystals were obtained after two weeks. The crystals were filtered, washed with acetonitrile and diethyl ether, and dried in a vacuum. Yield: 70%.

Anal. Calcd for ((*R*)-2-amino-1-propanol H^+)$[Fe(L^{O\text{-ValTryp}})_2]$·DMF: C, 59.93; H, 6.07; N, 9.53. Found: C, 60.129; H, 6.229; N, 9.159. IR (KBr, cm^{-1}): $\upsilon(COO^-)_{asym}$ 1634; $\upsilon(COO^-)_{sym}$ 1469; υ(C-

O) 1287; υ(C-H)o/p-ring H 745; υ(M-O) 557; υ(M-N) 424. μ_{eff} (solid, 292K); 5.9 μB/Fe. m/z (ESI-MS) $\{M+H\}^+$, {((*R*)-2-amino-1-propanol H^+)[Fe($L^{O\text{-Val Tryp}}$)$_2$]+H}$^+$; calcd: 809.28, found: 809.27.

Crystals suitable for X-ray data collection were grown by slow evaporation of a methanol-water solution of the complex in open air over several days.

Alternatively, solid $Fe(ClO_4)_2 \cdot 7H_2O$ (0.270 g, 0.736 mmol) was added to the methanolic solution (15 mL) of the ligand, $H_2L^{O\text{-ValTryp}}$ (0.500 g, 1.47 mmol), and the reaction mixture was stirred for 15 min. The color of the reaction mixture became blue. After 15 min., methanolic solution (5 mL) of (*R*)-2-amino-1-propanol (0.221 g, 2.94 mmol) was slowly added to the reaction mixture, and the color of the reaction mixture changed from blue to reddish purple. After 1hr stirring, precipitation started appearing, and the reaction mixture was left for another 1hr stirring. After that, the precipitate was filtered using a G2 crucible, washed with ethyl acetate and diethyl ether, and dried in a vacuum. The bluish-purple-colored solid was taken into a 50 mL beaker, dissolved in 10 mL of DMF, and excess acetonitrile (DMF: MeCN =1:3) was added and kept for slow evaporation at room temperature. Block-shaped, dark-red-colored crystals were obtained after two weeks. The crystals were collected, washed with acetonitrile and diethyl ether, and dried inside the vacuum desiccator. Yield: 72%.

The FTIR spectrum of this product is identical to the product obtained from the first method.

6.3.2 ((*S*)-2-phenylglycinol H^+)[Fe($L^{O\text{-ValTryp}}$)$_2$] (2)

Solid $Fe(ClO_4)_2 \cdot 7H_2O$ (0.270 g, 0.736 mmol) was added to the methanolic solution (15 mL) of the ligand, $H_2L^{O\text{-ValTryp}}$ (0.500 g, 1.47 mmol), and the reaction mixture was stirred for 15 min. The color of the reaction mixture became blue. After 15 min., methanolic solution (5 mL) of (*S*)-2-phenylglycinol / (*S*)-2-amino-2-phenylethanol (0.403 g, 2.94 mmol) was slowly added to the

reaction mixture, and the color of the reaction mixture changed from blue to reddish purple. After 1hr stirring, precipitation started appearing, and the reaction mixture was stirred for another 1hr. After that, the precipitate was filtered using a G2 crucible, washed with acetonitrile, and redissolved in a DMF-MeCN solvent mixture. Dark red-colored, block-shaped crystals were obtained after 10-12 days of slow evaporation of the complex solution in a DMF-MeCN (1:3) solvent mixture. The crystals were filtered, washed with acetonitrile and diethyl ether, and dried in a vacuum. Yield: 73%.

Anal. Calcd for ((*S*)-2- phenylglycinol H^+)[Fe($L^{O\text{-ValTryp}}$)$_2$]·2DMF: C, 61.41; H, 6.15; N, 9.64. Found: C, 61.567; H, 6.339; N, 9.23. IR (KBr, cm^{-1}): υ(COO^-)$_{asym}$ 1622; υ(COO^-)$_{sym}$ 1470; υ(C-O) 1289; υ(C-H)o/p-ring H 744; υ(M-O) 558; υ(M-N) 424. μ_{eff} (solid, 292K); 5.8 μB/Fe. m/z (ESI-MS) $\{M+H\}^+$, {((*S*)-2-phenylglycinol H^+)[Fe($L^{O\text{-ValTryp}}$)$_2$]+H}$^+$; calcd: 871.29, found: 871.29.

6.3.3 ((*R*)-*m*-octopamine H^+)[Fe($L^{O\text{-ValTryp}}$)$_2$] (3)

Racemic-*m*-octopamine hydrochloride salt (0.09 g, 0.29 mmol) was added to the methanolic solution (10 mL) of (NEt_4)[Fe($L^{O\text{-ValTryp}}$)$_2$] (0.200 g, 0.142 mmol), and the reaction mixture was kept for stirring. After 30 min of stirring, 5mL acetonitrile was added to the reaction mixture, and the reddish-brown coloured solution was kept for slow evaporation in a beaker at room temperature. Block-shaped red-coloured crystals were obtained after one week. The crystals were collected, washed with acetonitrile and diethyl ether, and dried in a vacuum. Yield:68%. Anal. Calcd for ((*R*)-*m*-octopamine H^+)[Fe($L^{O\text{-ValTryp}}$)$_2$]. CH_3OH: C, 61.44; H, 5.71; N, 7.62. Found: C, 61.14; H, 5.845; N, 7.932. IR (KBr, cm^{-1}): υ(COO^-)$_{asym}$ 1646; υ(COO^-)$_{sym}$ 1459; υ(C-O) 1275; υ(C-H)o/p-ring H 750; υ(M-O) 538; υ(M-N) 413. μ_{eff} (solid, 292K); 5.8 μB/Fe. m/z (ESI-MS) $\{M+H\}^+$, {((*R*)-m-octopamine H^+)[Fe($L^{O\text{-Val Tryp}}$)$_2$]+H}$^+$; calcd: 887.29, found: 887.28.

6.4 X-ray Crystallography

The crystal of the complexes obtained during synthesis was used for X-ray analysis. The crystals were mounted on glass fibre. All geometric and intensity data for the crystals were collected at room temperature using a Bruker SMART APEX CCD diffractometer equipped with a fine focus 1.75 kW sealed tube Mo-Kα (λ= 0.71073 Å) X-ray source, with increasing ω (width of 0.3º per frame) at a scan speed of either 3 or 4 s/frame. The SMART software was used for data acquisition and the SAINT software for data extraction. Absorption corrections were done using a multi-scan. After the initial solution and refinement with SHELXL, the final refinement was performed on the WinGX environment using the SHELXL-97 programs. All non-hydrogen atoms were refined anisotropically. The hydrogen atoms were located from the Fourier maps and refined isotropically wherever possible. Thus, some C-H bonds will not be ideal and may vary. In some complexes, the hydrogen atoms attached to the solvent molecules cannot be located or fixed, so the molecular weight may not match. ORTEP obtained selected crystallographic data summarized in Table 6.1**,** and the selected bond distances and bond angles of the respective complexes are listed in Table 6.2. Perspective views of the complexes were shown using ORTEP.

Table 6.1 Crystallographic data and refinement parameters of Fe(III) Complexes.

Complexes	**1**	**2**	**3**
Empirical Formula	$C_{42}H_{52}FeN_5O_{11}$	$C_{52}H_{57}FeN_7O_{12}$	$C_{49}H_{57}FeN_6O_{12}$
Formula Weight	858.73	1027.89	977.85
Wavelength(Å)	0.71073	0.71073	0.71073
Crystal system	triclinic	orthorhombic	orthorhombic
Space group	*P1*	$P2_1\ 2_1\ 2_1$	$P2_1\ 2_1\ 2_1$
a, Å	9.609(3)	10.6455(18)	9.324(2)
b, Å	10.764(4)	18.615(3)	22.266(5)
c, Å	12.087(4)	26.209(4)	22.575(5)
α, deg	116.093(9)	90	90
β, deg	102.689(10)	90	90
γ, deg	97.196(10)	90	90
Volume, $Å^3$	1059.6(7)	5193.8(15)	4686.5(19)
Z/ρ	1/ 1.346	4/ 1.315	4/1.386
μ	0.421	0.358	0.392
Coll reflns	7407	9136	8256
Indep refln	6154	6942	6169
FLACK para.	0.068(7)	0.036(8)	0.032(11)
GOF	1.087	1.139	1.069
R1[a]	0.0538	0.0687	0.0582
wR2[a]	0.1164	0.1461	0.1316
R1[b]	0.0712	0.1020	0.0872
wR2[b]	0.1278	0.1689	0.1316

[a] $I > 2\sigma$. [b] All data

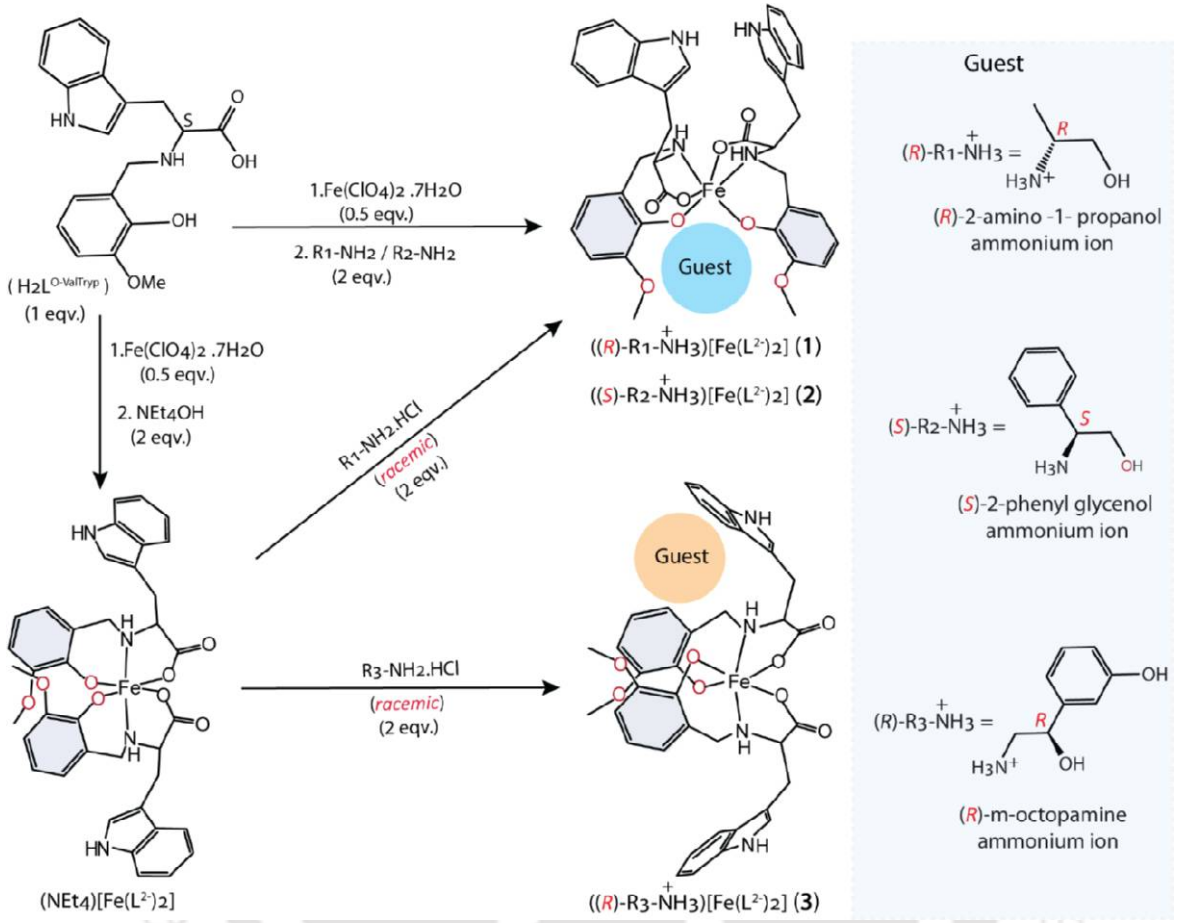

Scheme 6.1 Syntheses of the Fe(III) complexes with ammonium ion of chiral amino alcohols.

6.5 Result and Discussion

6.5.1 Syntheses and selected properties

$H_2L^{O\text{-}ValTryp}$, a reduced Schiff base of *o*-vanillin and L-tryptophan, was synthesized, maintaining the similar procedure mentioned in the reported analogous amino-acid-based ligands.[20–22] The ligand was characterized using ESI-mass spectrometry, FTIR, and NMR spectroscopy. $(NEt_4)[Fe(L^{O\text{-}ValTryp})_2]$ was synthesized directly from the reaction of the ligand ($H_2L^{O\text{-}ValTryp}$), $Fe(ClO_4)_2{\cdot}7H_2O$ and tetraethylammonium hydroxide (20 wt% in water). Complexes **1** & **3** were synthesized by metathesis of $(NEt_4)[Fe(L^{O\text{-}ValTryp})_2]$ with the hydrochloride salt of racemic-2-amino-1-propanol and racemic-*m*-octopamine, respectively. Alternatively, **1** could be

synthesized directly by reacting ligand, iron(III) salt, and (*R*)-2-amino-1-propanol (as a base). For the synthesis of **2** through the direct reaction of the ligand, iron(III) salt, we have used (*S*)-2-amino-2-phenylethanol as a base. The ESI-mass (+ve) spectra of all Fe(III) complexes showed well-defined peaks for the Fe(III) complex anion with their respective chiral cation (amino alcohol ammonium ions), indicating that binding of cationic chiral guest with the anionic iron(III) host exists in the solution. IR spectra of the complexes showed broad stretches at ~3415 cm^{-1} due to OH (water or H-bonded OH) stretch, and other sharp bands observed in the range 1615 - 1650 cm^{-1} are due to asymmetric stretching of coordinated carboxylate to Fe(III) center.

The solid-state structure of each of the Fe(III) complexes was determined by X-ray single-crystal structure analysis. Before the elemental analysis and bulk measurements, the crystals of the complexes were dried inside a vacuum desiccator for several days. So, the elemental analysis results of the Fe-complexes (provided in in the experimental section) showed that the number of solvents in the bulk and in the crystal structure are different. The elemental analysis of **1** showed the presence of a DMF molecule, but the single crystal structure of the complex contains different solvents (MeOH and H_2O). The bulk quantity crystals of **1** were obtained from the slow evaporation of the complex's solution in a MeOH-DMF (3:1) solvent mixture, but it contains disordered DMF molecules in the unit cell, which showed the A-level alerts in check-cif. To avoid this, **1** was recrystallized by slow evaporation of a methanol-water solution of the complex. The formula of the iron(III) complexes obtained from their elemental analyses was used for other experiments on the bulk. The solid-state room temperature magnetic moments of **1**-**3** are close to 5.92 BM, an ideal value for the high-spin Fe(III) complexes.[23]

6.5.2 Crystal structures

Complex **1** obtained from two different synthetic procedures crystallized in an identical chiral space group i.e., chiral triclinic space group *P1*. Here, we have discussed the crystal structure of 1 obtained from 1st method (mentioned in the experimental section). The crystal refinement parameters have been provided in Table 6.1. The asymmetric unit consists of an ammonium form of (*R*)-2-amino-1-propanol bound to anionic $[Fe(L^{O\text{-ValTryp}})_2]^-$ unit with one methanol and one water molecule. For the synthesis of **1**, we have used hydrochloride salt of *racemic*-2-amino-1-propanol, and the crystal structure showed that it had recognized only one isomer, i.e., ammonium ion of (*R*)-2-amino-1-propanol.

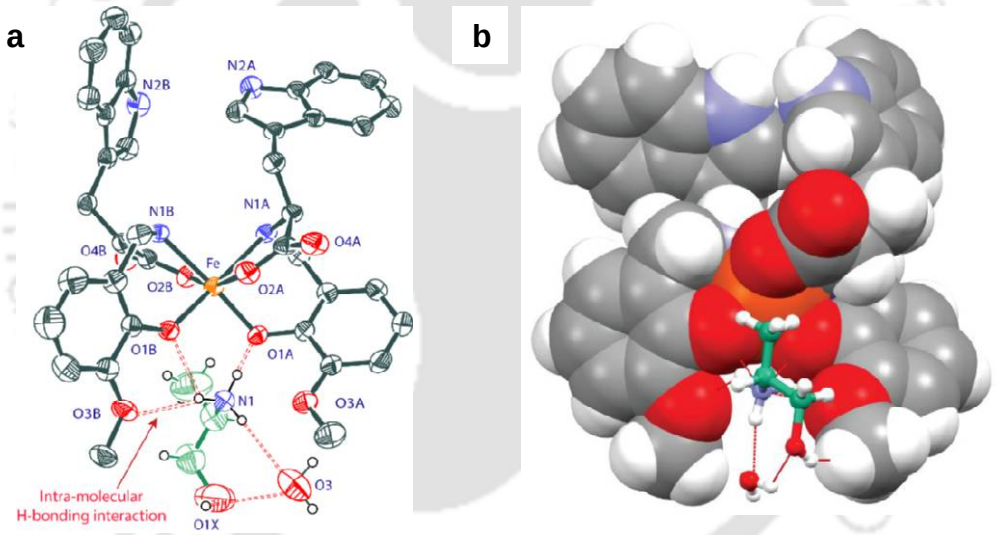

Figure 6.1 The ORTEP figures of **1** (a) with 40% ellipsoid probability show non-covalent interaction between host, guest amino alcohol (in ammonium form), and the solvent molecules, (b) spacefill view of **1**.

In **1**, two tridentate ligands are facially coordinated to the metal center. (Figure 6.1) The Fe-$O_{phenolate}$, the Fe-$O_{carboxylate}$, and Fe-N_{amine} bond lengths (Table 6.2) of the complex are similar to the reported octahedral high-spin Fe(III)-complexes.[24,25] The chirality of the carbons, C8A & C8B, present in the complex is "*S*" conformation originated from the use of L-tryptophan and Fe(III)-coordinated amine N atoms, N1A & N1B, have "*R*" conformation. This phenomenon of

opposite conformation preference at the chiral carbon and amine N has been observed in all the characterized complexes of this type of ligand.[26–28]

The shape of the complex is entirely different from its Co(III) analog (Complex1 in Chapter **5**). Unlike Co(III) analog, Fe(III)-coordinated carboxylates are trans to each other. The Fe^{III} complex anion rearranged the shape so that phenolate and methoxy groups formed a semi-circular O_4 polar pocket where the $-NH_3^+$ group of the chiral cation bound through intra-molecular hydrogen bonding interactions. (Fig. 6.1a) Three N-H of the $-NH_3^+$ group of chiral amino alcohol are within the H-bonded distance of two phenolate oxygen atoms (O1A & O1B) and two methoxy oxygen atoms (O3A & O3B). The H_2O molecule in the lattice acts as an H-bond acceptor to the alcoholic -OH group and one of the N-H of the $-NH_3^+$ group of the chiral cation.

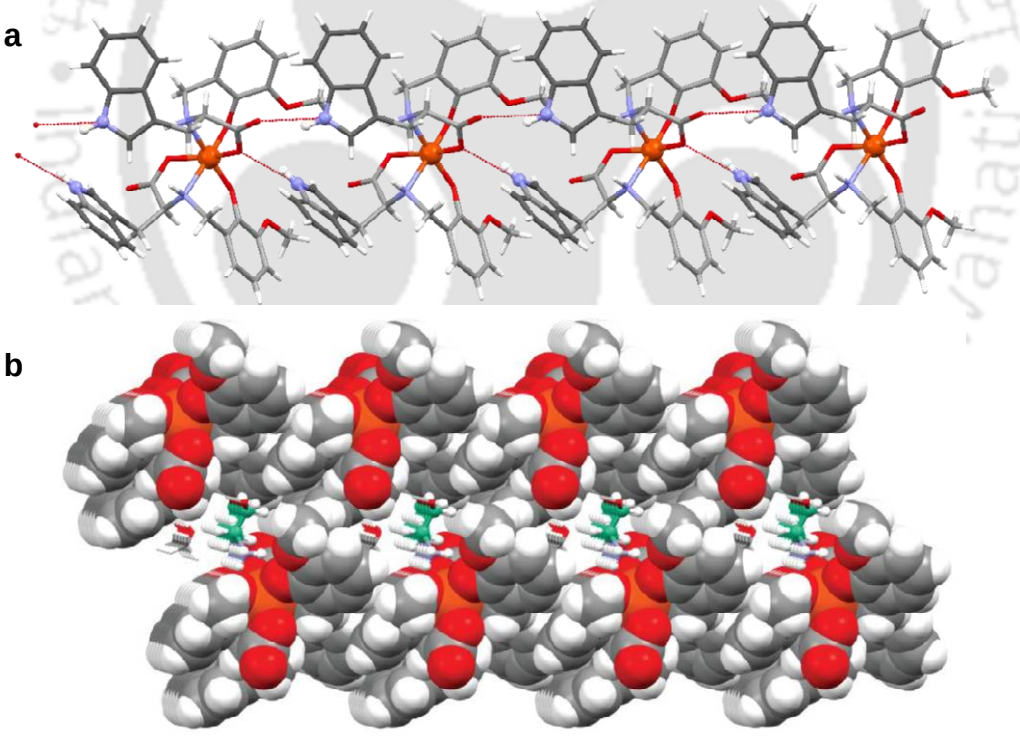

Figure 6.2 (a) 1D chain along the a-axis in **1**, (b) column in **1** filled with guest cations and solvent molecules along the a-axis.

On the other side of the anion, the indole nitrogen atoms (N2A & N2B) are hydrogen bonded to both oxygen atoms of one carboxylate (O4A, O2A) of the adjacent anionic complex molecule

through intermolecular indole…carboxylate H-bonding interactions and hold the anions in a linear chain along a-axis. (Fig. 6.2) The H_2O and MeOH molecules in the lattice act as bridges between two consecutive layers and form a one-dimensional channel along the a-axis, leaving the polar pocket aligned on the same side.

Table 6.2 Selected bond distances (Å and angles (˚) of complexes **1** - **3**.

Complexes	Bond lengths (Å)			Bond angles (˚)		
	Fe-O_p	Fe-O_c	Fe-N_a	O_c-Fe-O_c	O_p-Fe-O_p	N_a-Fe-N_a
1	1.936(5)	2.022(4)	2.218(5)	159.63(17)	94.08(19)	92.91(18)
(facial)	1.912(4)	2.009(4)	2.194(5)			
2	1.922(5)	2.005(5)	2.172(6)	165.4(2)	97.0(2)	91.8(2)
(facial)	1.916(4)	2.028(5)	2.188(6)			
3	1.926(4)	2.034(4)	2.174(4)	89.07(16)	95.95(18)	163.79(17)
(meridional)	1.951(4)	2.029(4)	2.152(5)			

Complex **2** crystallized in a chiral orthorhombic space group $P2_12_12_1$. The crystal refinement parameters have been provided in Table 6.1. and the selected bond length and angle values are given in Table 6.2. The asymmetric unit of the complex consists of one (S)-(+)-2-phenylglycinol ammonium ion, one anionic $[Fe(L^{O\text{-ValTryp}})_2]^-$ complex unit, two DMF molecules, and one water molecule. One of the DMF molecules is disordered, so it is refined isotropically. The two deprotonated tridentate ligands facially coordinated to the Fe(III) center. The molecular structure of $[Fe(L^{O\text{-ValTryp}})_2]^-$ and the geometry around the Fe(III) center present in **2** are identical to **1**.

In **2**, the Fe(III) coordinated phenolate oxygens (O1A & O1B) and the methoxy groups (O3A & O3B) formed a semi-circular O_4 polar pocket like **1**, the (*S*)-(+)-2-phenylglycinol ammonium ion (the cationic chiral guest) bound to this pocket (Fig. 6.3). The chiral guest cation bonded to anionic host, $[Fe(L^{O\text{-ValTryp}})_2]^-$, maintained the three-point contact rule- first, the three N-H bonds in $-NH_3^+$ group of guest cation connected to the phenolate oxygens (O1A & O1B) and methoxy

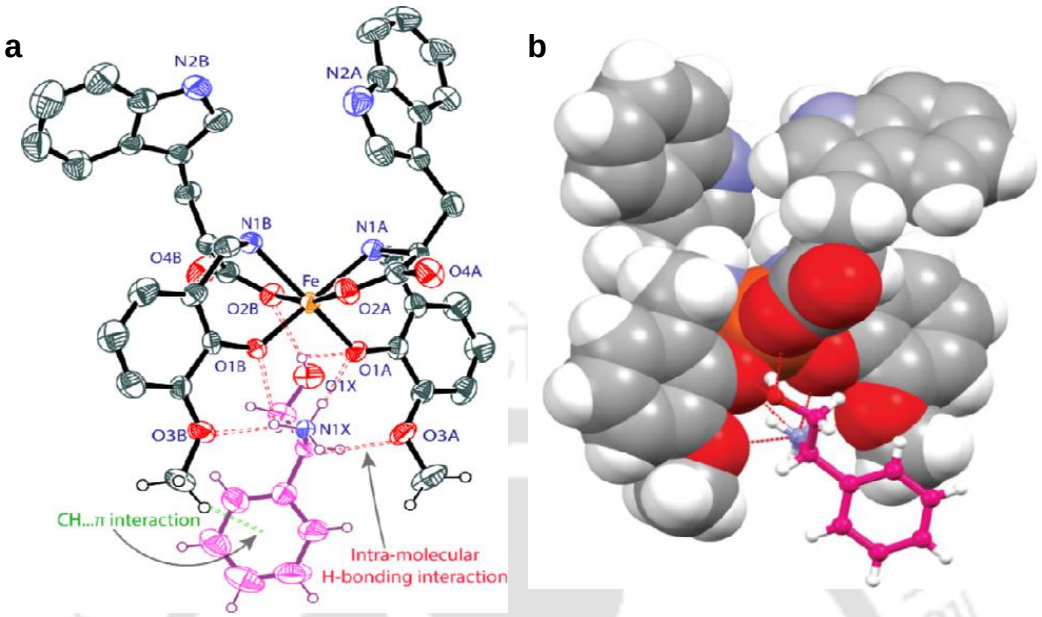

Figure 6.3 The ORTEP figures of **2** (a) with 40% ellipsoid probability show non-covalent interaction between host, guest amino alcohol (in ammonium form), and the solvent molecules, (b) space-fill view of **2**.

oxygens (O3A & O3B) of anionic Fe(III)-host through intra-molecular H-bonding interactions; second, the alcoholic -OH of the guest cation connected to one of the metal-coordinated carboxylate oxygens through a strong intramolecular H-bond (O1XH1X…O2B); and third, the phenyle ring of the chiral cation showed CH-π interaction with the methyl proton (C19B-H) of the host-anion.

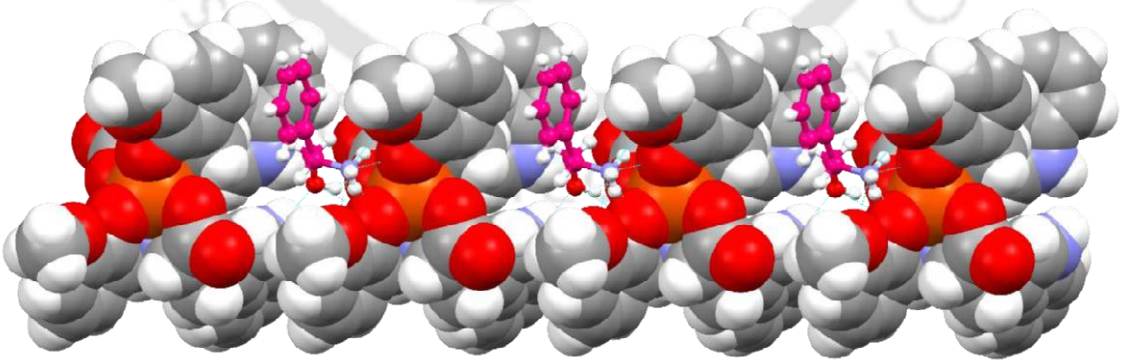

Figure 6.4 1D chain (space-filling model) in **2** along the a-axis recognizing the guest molecules (in ball and stick model).

The two indole nitrogen (N2A and N2B) present in the host complex take part in two different types of intermolecular H-bonding- the first one, where the H_2O molecule present in the lattice acts as both H-bond donor-acceptor and intermolecular hydrogen bonding occurred between N2B-H2B(indole NH)…H_2O(lattice water)…O4B, O2B(carboxylate of adjacent host) and the second type of intermolecular H-bonding where alcoholic OH(O1XH1X) group of guest cation acts as a bridge between another indole NH(N2AH2A) and O1A(phenolate), O2B(carboxylate) of two adjacent host molecules. These two types of intermolecular H-bonding hold the anionic complex molecules in a linear arrangement, forming a 1D linear chain along the a-axis (Fig. 6.4). The intermolecular H-bonding interaction between one of the NH (N1X-H1XB) of $-NH_3^+$ in the chiral cation and carboxylate oxygen (O4A) of the neighboring host molecule connected two adjacent 1D chains along the a-axis.

Complex **3** crystallized in the orthorhombic space group $P2_12_12_1$. The crystal refinement parameters have been provided in Table 6.1. Selected bond lengths and angles in 3 are given in Table 6.2. The asymmetric unit of the complex consists of one (*R*)-*m*-octopamine ammonium ion, one anionic $[Fe(L^{O\text{-ValTryp}})_2]^-$ complex unit, one methanol molecule, one acetonitrile molecule, and one water molecule. The shape of the complex is entirely different from the other two Fe(III) complexes (**1** & **2**) described above. In **3**, the Fe(III) is hexacoordinated by two meridional tridentate ligands where the carboxylate and phenolate groups from the ligands are cis to each other. The geometry around the Fe(III) ion is distorted from the perfect octahedron, as evident from the deviation of angles from its ideal values of 90˚ and 180˚ (Table 6.2). The average Fe(III)- donor atom distances i.e., Fe^{III}-O(phenolate), Fe^{III}-O(carboxylate), and Fe^{III}-N(amine) bond lengths (mentioned in Table 6.2) around the Fe(III) ion are similar to the other reported octahedral high-spin Fe(III)- complexes.

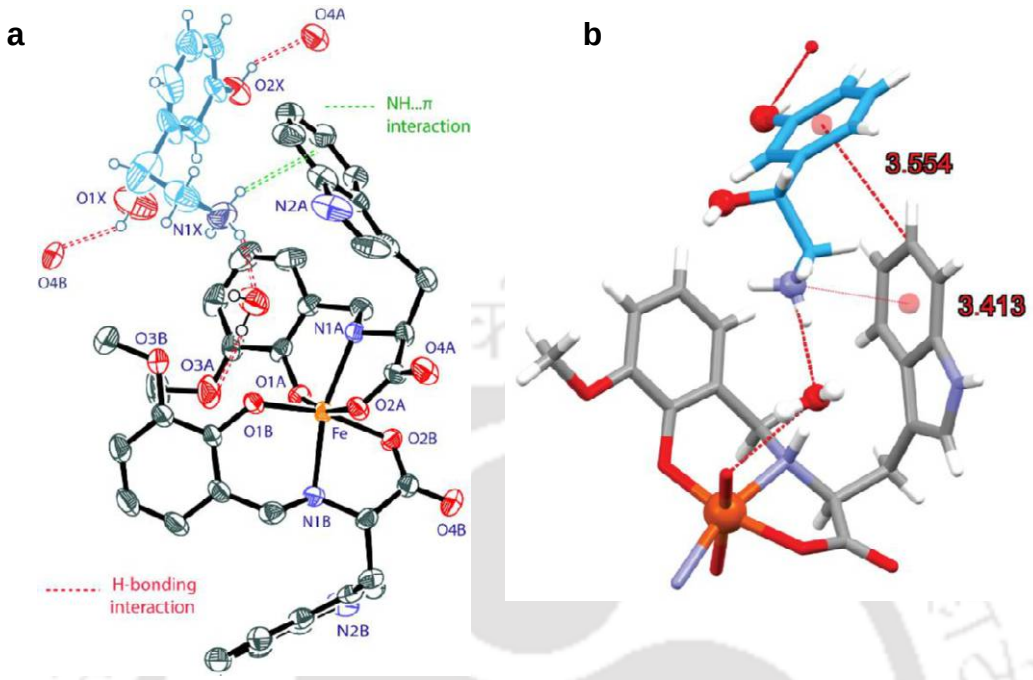

Figure 6.5 The ORTEP figures of **3** (a) with 40% ellipsoid probability, (b) non-covalent interaction between host, guest amino alcohol (in ammonium form), and the water molecule in **3**

The chiral carbons (C8A & C8B) in the complex have *S* conformation, and two coordinated amine N atoms (N1A & N1B) have *R* conformation. The chiral carbon (C7X) present in counter cation has *R* conformation, though, during the complexation reaction, we used hydrochloride salt of *racemic*-*m*-octopamine.

In complex **3**, one of the indole units and one phenolate unit folded to form a chiral cleft inside the molecule. Inside this cleft, one water molecule and an ammonium group of the chiral guests are bound through intermolecular hydrogen bonding. The ammonium group of the chiral guest cation also stabilized inside the cavity through NH-π interaction between the $-NH_3+$ group and the indole unit. (Fig. 6.5) The phenolic -OH group of the (*R*)-*m*-octopamine ammonium ion is H-bonded to the carboxylate oxygen O4A of the adjacent complex molecule, and the aliphatic -OH group of guest cation is also connected to the carboxylate oxygen O4B of another adjacent complex anion through intermolecular H-bonding.

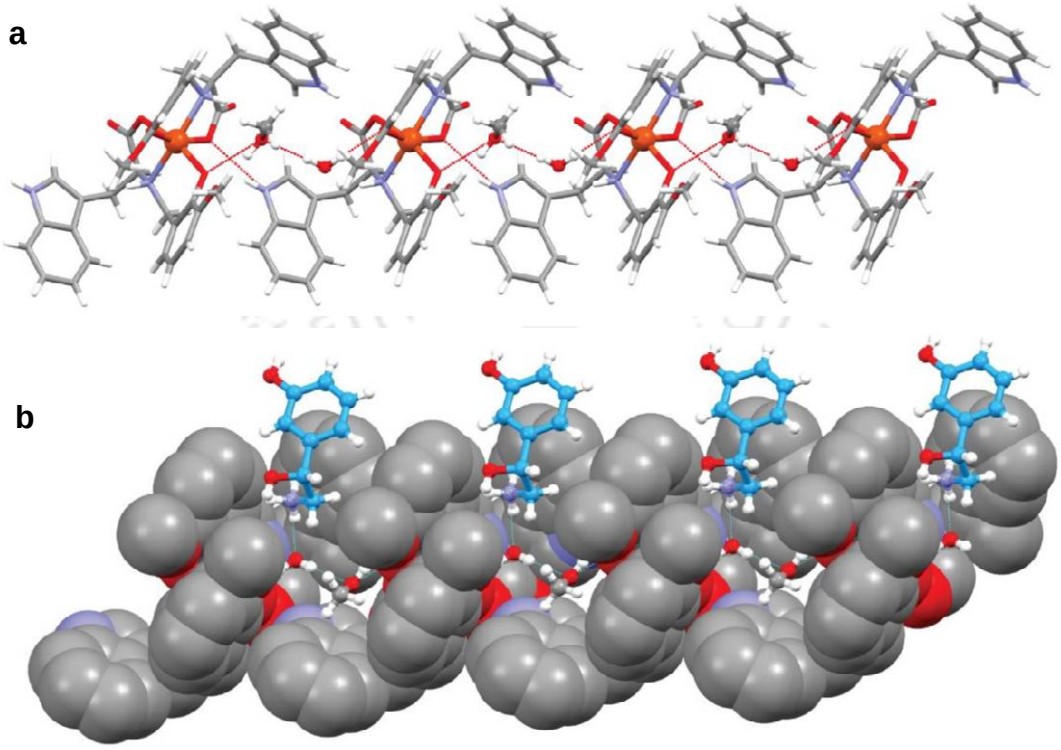

Figure 6.6 (a)Intermolecular H-bonding between solvent molecules and the adjacent Fe(III) complex anions forming a 1D chain along the a-axis in **3**, (b) space fill view of the chain with guest cation (in a ball and stick model, blue colored).

The water molecule inside the cleft also H-bonded to the Fe^{III} coordinated -NH group (N1AH1A). The other -NH group(N1BH1B) H-bonder to the methanolic oxygen O3X. Two indole -NH's (N2H2A & N2H2B) are H-bonded to the oxygen atoms of phenolate groups (O1A & O1B), and Fe^{III}-coordinated carboxylate oxygen atoms (O2A & O2B) of the adjacent complex anion which holds the anions in a linear chain along the a-axis. H_2O and MeOH molecules present in the lattice act as a bridge between two neighboring complex molecules through intermolecular H-bonding interactions; these hydrogen bonding interactions also strengthen the 1D chain formation along the a-axis (Fig. 6.6).

Table 6.3 Hydrogen bond and other non-covalent bond distances (Å) in **1**.

Atoms	D-H (Å)	H…A (Å)	D…A(Å)	DHA(˚)
N1-H1C…O1B	0.89	2.28	2.954(7)	133
N1-H1C…O3B	0.89	2.11	2.925(8)	152
N1-H1D…O1A	0.89	1.94	2.772(7)	155
N1-H1D…O3A	0.89	2.53	3.119(7)	125
N1-H1E…O3	0.89	1.93	2.806(9)	166
N2A-H2A…O4A	0.86	2.15	2.918(7)	149
N2B-H2B…O2A	0.86	2.05	2.869(7)	159
O2-H2C…O4A	0.82	2.05	2.804(11)	152
O3-H3F…O1	0.85	2.15	2.738(14)	126

Table 6.4 Hydrogen bond and other non-covalent bond distances (Å) in **2**.

Atoms	D-H (Å)	H…A (Å)	D…A(Å)	DHA(˚)
N1X-H1XA…O1A	0.89	2.00	2.848(8)	158
N1X-H1XA…O3A	0.89	2.24	2.854(8)	126
O1X-H1X…O1A	0.82	2.39	3.034(9)	136
O1X-H1X…O2B	0.82	2.19	2.922(8)	149
N2A-H2A…O1X	0.86	2.30	3.063(11)	148
N1X-H1XC…O1B	0.89	2.25	2.918(7)	132
N1X-H1XC…O3B	0.89	2.13	2.926(8)	148
O3X-H3XA…O4B	0.85	2.15	2.881(11)	144

Table 6.5 Hydrogen bond and other non-covalent bond distances (Å) in **3**.

Atoms	D-H (Å)	H…A (Å)	D…A(Å)	DHA(˚)
N1A-H1A…O4X	0.98	2.32	3.203(8)	150
N1B-H1B…O3X	0.98	2.34	3.234(8)	151
O1X-H1X…O4B	0.82	2.37	2.861(11)	119
O4X-H4XB…O1B	0.85	1.99	2.738(7)	146
O4X-H4XB…O3B	0.85	2.55	3.248(8)	141
O2X-H2X…O4A	0.82	1.92	2.707(8)	162
N1X-H1XA…O1X	0.89	2.32	2.713(14)	107
C4X-H4X…O1X	0.93	2.46	3.072(14)	124

6.5.3 UV-visible spectroscopy

UV- Vis spectra of the Iron(III) complexes were recorded using their DMF solution. The spectra displayed two absorption bands in between the 300 nm to 700 nm wavelength range. The UV-visible spectra of all of these Fe(III)-complexes (**1**-**3**) showed identical transitions; each showed a shoulder near 330 nm and a band near 475 nm. As the Fe(III) centre is octahedrally coordinated, the broadband that appeared near 475 nm can be assigned to a transition from the phenolate oxygen p_π orbital to the half-filled d_π* orbitals of the ferric ion. Such transitions are intense and can be attributed to the LMCT transitions.[29],[30] The shoulder appeared near 330 nm due to the charge transfer transition from the phenolate pπ orbital to the dσ* orbital of the ferric ion.

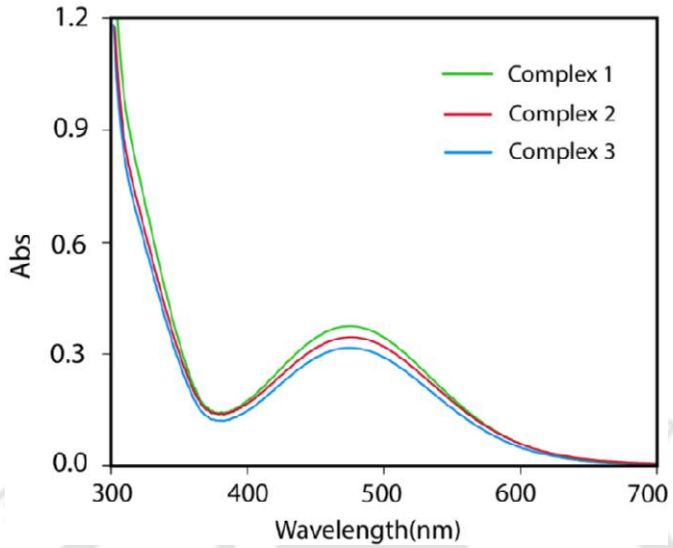

Figure 6.7 UV-visible spectra of the Fe(III) complexes.

Table 6.6 Electronic spectroscopic data of Fe(III) complexes (In DMF)

Complexes	λ_{max}/nm (ε/$M^{-1}cm^{-1}$)
1	336 (4766) (sh), 475 (3347)
2	334 (4096) (sh), 475 (2757)
3	333 (4690) (sh), 476 (3071)

6.5.4 Recognition of chiral amino alcohols and structural change

We have synthesized complexes **1** and **3** by salt metathesis of **$(NEt_4)[Fe(L^{O\text{-}ValTryp})_2]$** with the racemic hydrochloride salt (2 equivalents) of respective chiral amino alcohols. When $(NEt_4)[Fe(L^{O\text{-}ValTryp})_2]$ was treated with *racemic*-2-amino-1-propanol.HCl, it formed **1** where the $[Fe(L^{O\text{-}ValTryp})_2]^-$ complex anion changed its shape from ***meridional*** to ***facial*** structural arrangement and recognized only "*R* "isomer of 2-amino-1-propanol ammonium ion. The reaction of $(NEt_4)[Fe(L^{O\text{-}ValTryp})_2]$ with racemic hydrochloride salt of *m*-octopamine gave **2** where the Fe(III) complex anion also changed its shape to selectively recognize the "*R* "isomer of *m*-octopamine ammonium ion. So, the solid-state structural analysis of the iron(III) complexes

revealed that the $[Fe(L^{O\text{-ValTryp}})_2]^-$ complex anion could adopt two different shapes to recognize two different chiral guest cations.

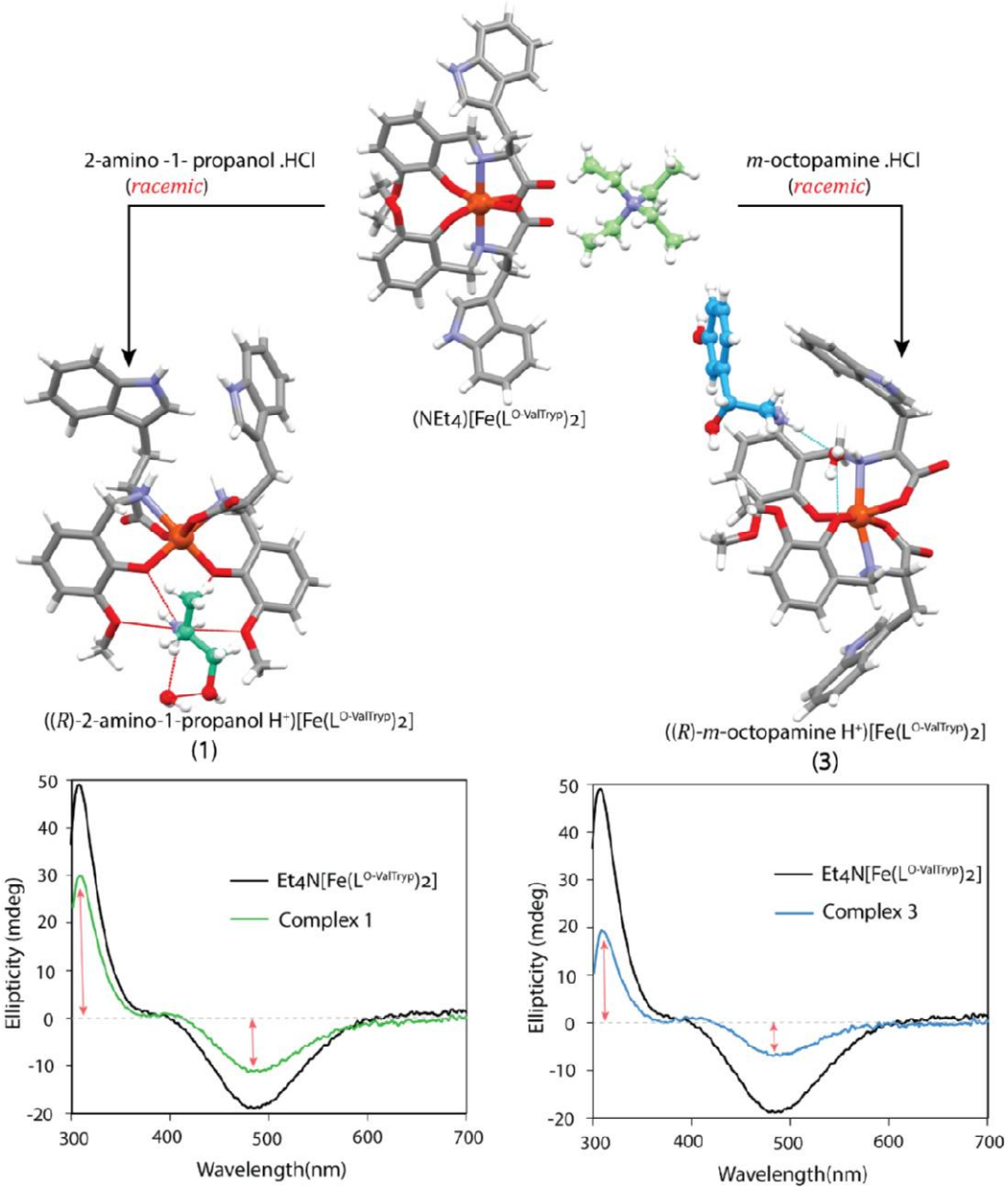

Figure 6.8 The solid-state structural difference and CD spectral change of **1** and **3** compared to the starting complex **$(NEt_4)[Fe(L^{O\text{-ValTryp}})_2]$**.

Complexes **1** and **3** being chiral, the interactions between the chiral host (anionic Fe^{III} complex) and chiral guests (ammonium ion of chiral amino alcohols) have been investigated by circular dichroism (CD) spectroscopy. The DMF solution of $(NEt_4)[Fe(L^{O\text{-ValTryp}})_2]$ showed one positive

CD signal near 300 nm and one negative CD signal near 480 nm i.e., in the LMCT transition region. When the tetraethyl ammonium ion in $(NEt_4)[Fe(L^{O\text{-ValTryp}})_2]$ is replaced with the cationic guests having one chiral centre in **1** and **3** then only the amplitude of the CD signals was decreased, however, the phase of the CD spectrum remain unaltered as the anionic iron(III) host itself contains four chiral centers. The intensity of the CD signals of **1** (one positive CD signal near 300 nm and one negative CD signal near 480 nm) is higher than **3**, which might be due to the different types of interactions between the chiral guest cations and the anionic host complex in the solution state.

6.6 Structural differences between Fe(III)-complexes and their kinetically inert Co(III) analogs while recognizing different chiral guests from their racemic mixtures.

To recognize (*R*)-2-amino-1-propanol ammonium ion and (*R*)-*m*-octopamine ammonium ion the kinetically inert anionic Co(III) host complex, $[Co(L^{O\text{-ValTryp}})_2]^-$, adopt a common structural motif where the anionic host complex folded backward, exposing the polar carboxylate oxygens which are used in H-bonding with the cationic guest molecules, discussed in Chapter 5. But kinetically labile Fe(III) analogs of these chiral host-guest complexes showed very different structures. To recognize (*R*)-2-amino-1-propanol ammonium ion from its racemic mixture, $[Fe(L^{O\text{-ValTryp}})_2]^-$ complex anion showed drastic structural transformation where the Fe^{III}-coordinated phenolates and the methoxy groups formed a polar pocket and inside it the $-NH_3^+$ group of guest cation bound through intramolecular H-bonding. Whereas the anionic iron(III) host complex showed a different guest recognition mode for the recognition of (R)-m-octopamine ammonium ion, which could not match either its Co(III) analog or the other Fe(III) complex. Here, one of the indole units and one phenolate unit folded to form an achiral cleft inside the molecule. Inside this cleft, one water molecule and an ammonium group of the chiral guests bound through intermolecular

hydrogen bonding with the host complex. The ammonium group of the guest molecule also stabilized inside the cavity through NH-π interaction between the $-NH_3^+$ group and the indole unit.

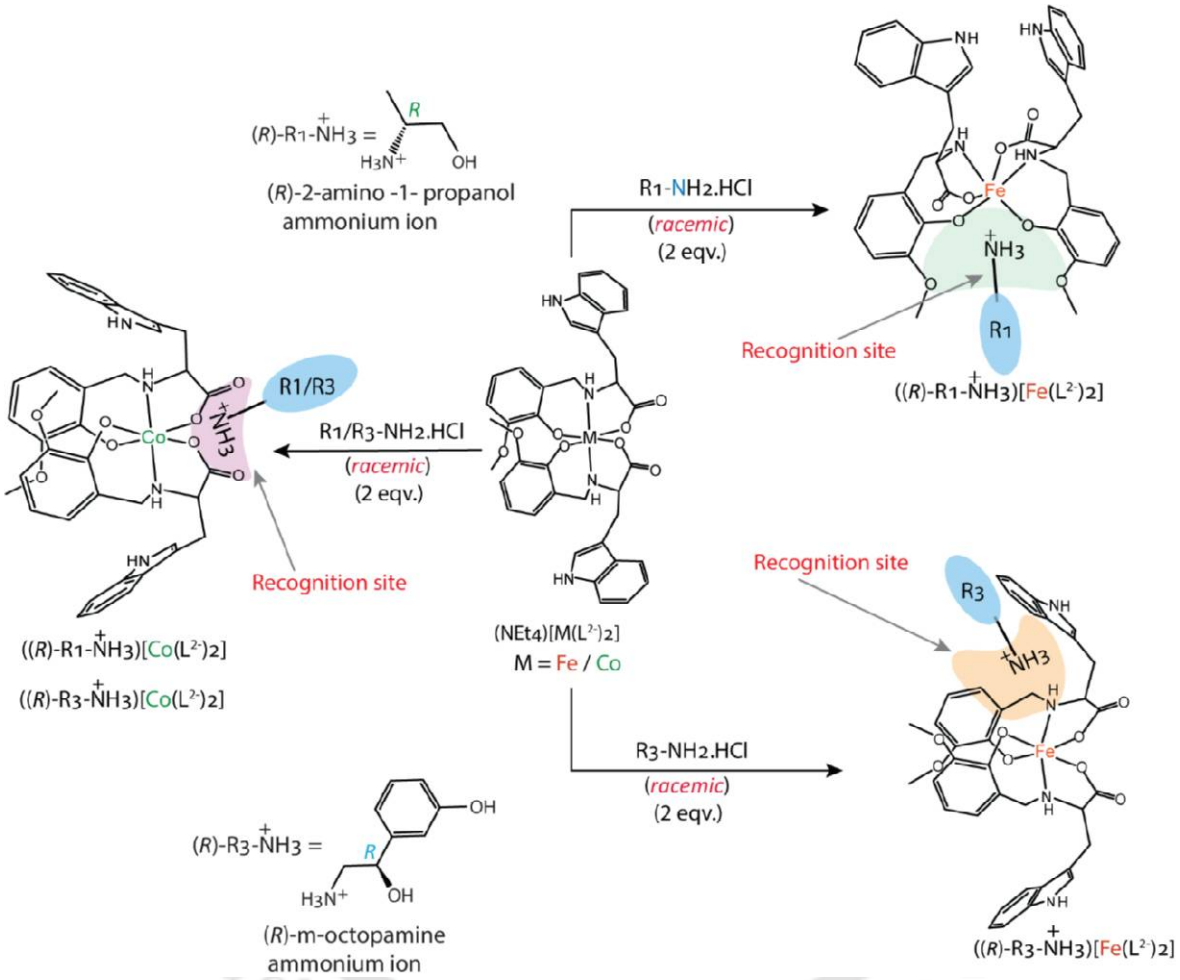

Figure 6.9 Structural difference of Co(III) and Fe(III) anionic host complexes to recognize the chiral guest cations.

6.7 Conclusion

So, we have synthesized metal complex-based chiral host-guest systems where the iron(III) anionic complexes of an L-tryptophan-derived flexible tridentate ligand bind different chiral amino alcohols ammonium ions and showed different solid state structural arrangements. For the selective recognition of one of the isomers of racemic amino alcohols, we employed

coordinatively saturated iron(III) complex, $(NEt_4)[Fe(L^{O\text{-ValTryp}})_2]$, which recognized (*R*)- isomer of either 2-amino-1-propanol ammonium ion or meta-octopamine ammonium ion from their respective racemic mixture. To recognize these two chiral guest cations, the $[Fe(L^{O\text{-ValTryp}})_2]^-$ complex anion adopts two distinct structural arrangements, and the shapes of these chiral host-guest sats are very different from their inert Co(III) analogs. Due to the labile nature of the metal-ligand coordination bonds in $[Fe(L^{O\text{-ValTryp}})_2]^-$, it can dynamically change its shape to two distinct geometrical arrangements to recognize two different chiral guest cations, but their Co(III) analogs did not show significant structural changes unless heated at 60˚C for several hours due to the presence of inert metal-ligand coordination bonds, discussed in the previous chapter. In conclusion, we can say that the peripheral non-covalent interactions between the anionic host and the chiral guest cations are sufficient to modify the structure of a kinetically labile Fe(III) complex but insufficient to do the same on an inert Co(III) complex without extra energy.

References

(1) Bisoyi, H. K.; Li, Q. *Angew Chem Int Ed* **2016**, *55* (9), 2994–3010.

(2) Boillot, M.-L.; Roux, C.; Audière, J.-P.; Dausse, A.; Zarembowitch, J. *Inorg. Chem.* **1996**, *35* (13), 3975–3980.

(3) Zahn, S.; Das, D.; Canary, J. W. *Inorg. Chem.* **2006**, *45* (15), 6056–6063.

(4) Crassous, J. T *Chem. Commun.* **2012**, *48* (78), 9684.

(5) Miyake, H.; Tsukube, H. *Supramolecular Chemistry* **2005**, *17* (1–2), 53–59.

(6) Maeda, K.; Yashima, E. *Top Curr Chem (Z)* **2017**, *375* (4), 72.

(7) Zahn, S.; Canary, J. W. *Science* **2000**, *288* (5470), 1404–1407.

(8) Miyake, H.; Yoshida, K.; Sugimoto, H.; Tsukube, H. *J. Am. Chem. Soc.* **2004**, *126* (21), 6524–6525.

(9) Akine, S. *Inorganics* **2018**, *6* (3), 80.

(10) Miyake, H.; Tsukube, H. *Chem. Soc. Rev.* **2012**, *41* (21), 6977.

(11) Pijper, D.; Feringa, B. L. *Soft Matter* **2008**, *4* (7), 1349.

(12) Saha, B.; Petrovic, A. G.; Dhamija, A.; Berova, N.; Rath, S. P. *Inorg. Chem.* **2019**, *58* (17), 11420–11438.

(13) Saha, B.; Ikbal, S. A.; Petrovic, A. G.; Berova, N.; Rath, S. P. *Inorg. Chem.* **2017**, *56* (7), 3849–3860.

(14) Miyake, H.; Hikita, M.; Itazaki, M.; Nakazawa, H.; Sugimoto, H.; Tsukube, H. *Chemistry A European J* **2008**, *14* (18), 5393–5396.

(15) Sakata, Y.; Chiba, S.; Miyashita, M.; Nabeshima, T.; Akine, S. *Chemistry A European J* **2019**, *25* (12), 2962–2966.

(16) Miyake, H.; Kamon, H.; Miyahara, I.; Sugimoto, H.; Tsukube, H. *J. Am. Chem. Soc.* **2008**, *130* (3), 792–793.

(17) Sairenji, S.; Akine, S.; Nabeshima, T. *Chemistry Letters* **2014**, *43* (7), 1107–1109.

(18) Agarkar, H.; Dave, D.; Das, D. *Spectrochimica Acta Part A: Molecular and Biomolecular Spectroscopy* **2020**, *242*, 118735.

(19) Ring, A. M.; Manglik, A.; Kruse, A. C.; Enos, M. D.; Weis, W. I.; Garcia, K. C.; Kobilka, B. K. *Nature* **2013**, *502* (7472), 575–579.

(20) Sahoo, S. C.; Ray, M. *Chemistry A European J* **2010**, *16* (17), 5004–5007.

(21) Dubey, M.; Koner, R. R.; Ray, M. *Inorg. Chem.* **2009**, *48* (19), 9294–9302.

(22) Sahoo, S. C.; Ray, M. *Dalton Trans.* **2009**, No. 17, 3230.

(23) Figgis, B. N.; Lewis, J, *Progress in Inorganic Chemistry*; Cotton, F. A., Ed.; Wiley, 1964; Vol. 6, pp 37–239.

(24) Shongwe, M. S.; Kaschula, C. H.; Adsetts, M. S.; Ainscough, E. W.; Brodie, A. M.; Morris, M. J. *Inorg. Chem.* **2005**, *44* (9), 3070–3079.

(25) Dasgupta, S.; Atta, S.; Singh, N. D. P.; Deb, D.; Kassel, W. S.; Bhattacharjee, M. *Eur J Inorg Chem* **2014**, *2014* (30), 5125–5134.

(26) Long, C.; Ray, M. *Dalton Trans.* **2024**, *53* (15), 6642–6652.

(27) Das, C. R.; Sahoo, S. C.; Ray, M. *Crystal Growth & Design* **2014**, *14* (8), 3958–3966.

(28) Rajesh, C. M.; Ray, M. *Dalton Trans.* **2014**, *43* (34), 12952–12960.

(29) Ainscough, E. W.; Brodie, A. M.; Plowman, J. E.; Brown, K. L.; Addison, A. W.; Gainsford, A. R. *Inorg. Chem.* **1980**, *19* (12), 3655–3663.

(30) McDevitt, M. R.; Addison, A. W.; Sinn, E.; Thompson, L. K. *Inorg. Chem.* **1990**, *29* (18), 3425–3

Findings of the Thesis

The work presented in this thesis stems from earlier observations on the recognition of chiral amine and amino alcohol ammonium cations (guest) using an anionic binuclear Ni(II) complex (host). The chiral guest ammonium ions formed the host-gest adduct with the anionic host through multiple non-covalent interactions. The rigid anionic host showed nearly identical structural motifs toward the recognition of chiral guest ammoniums, and the retention of the interactions in host-guest complexes could not be determined due to their paramagnetic nature. We intend to solve this problem by making Co(III) complex with our sets of ligands, due to the diamagnetic character, it will allow us to ascertain the solution interactions with the aid of NMR spectroscopy.

For this, we have used a coordinatively saturated octahedral Co(III) complex anion (host) with a modified chiral ligand backbone having multiple H-bond capable sites and used it with a series of achiral and chiral ammonium cations (guest). The resulting host-guest complexes were structurally characterized, and their solution-state characteristics were also determined (described in Chapters 2-5). The structural analyses of the host-guest complexes revealed that the anionic could adopt different shapes irrespective of the number of H-bond donor groups present in guest molecules. Also, we have synthesized labile Fe(III) analogs that allowed us to check the effect of lability of the host complex while recognizing the achiral (in Chapter 2) as well as chiral (in Chapter 6) guests.

First, we have shown that the coordinatively saturated anionic Co(III)-host could distinguish two chemically similar alkyl ammonium ions where the only difference is the presence of one H-bond capable NH and three ethyl arms in Et_3NH^+ than four ethyl arms in Et_4N^+. The anionic host

complex showed two completely different structural arrangements to recognize these two alkyl ammonium ions (Et_4N^+ and Et_3NH^+). The single NH in Et_3NH^+ triggered a drastic structural transformation of the anionic Co(III)-host complex from its non-folded to folded conformation, which involved breaking and reforming the kinetically inert metal-ligand coordination bonds in a way that hasn't been observed in any other synthetic systems. The structural transformation occurs slowly at room temperature but speeds up in isostructural labile Fe(III) analogs. This indicates that the rate of the single H-bond-triggered transformation of the anionic host can be controlled by adjusting the lability of the central metal ion.

Second, we have shown that the alkali and alkaline earth metal cations (Na^+, K^+, Ca^{2+}, Ba^{2+}) triggered the meridional to facial structural transformation of the Fe(III) complex anion. Each hetero-metallic complex has unique solid-state structural characteristics that are retained in solution despite their labile nature.

Third, we have demonstrated that the presence of $-NH_3^+$ and -OH groups in guest cations (amino alcohol ammonium ions) leads to multiple intra- and inter-molecular hydrogen bonds, which results in a new structural arrangement of the anionic Co(III)-host, distinct from those observed with Et_4N^+ and Et_3NH^+ ions. Additionally, these interactions enable the anionic Co(III)-host to selectively recognize one enantiomer of various amino alcohols from their racemic mixtures.

Fourth, we employed the anionic Co(III)-host to bind adrenaline (in its ammonium form) because it can recognize structurally similar amino alcohols (ammonium ions). Despite adrenaline's instability under aerobic conditions, we successfully isolated a stable host-guest complex. This demonstrates that a simple first-row transition metal complex anion can bind a biologically active neurotransmitter like adrenaline. With increasing temperature, the chiral host-guest complexes

showed structural transformation in solution. However, we could not determine which isomer was bound due to limitations in structural characterization.

Fifth, we have shown the effect of metal center labilty on the structural transformation of the anionic host while recognizing the chiral guest cations (amino alcohol amino alcohols). The anionic Fe(III) host displayed a markedly different structural arrangement than its inert Co(III) analog when recognizing the same guest cation. In the Fe(III) host, multiple hydrogen bonds and other weak non-covalent interactions between the host and chiral guest cations drive significant structural changes in the host complex, owing to the labile nature of the metal-ligand coordination bonds.

List of publications

1. "A single H-bond triggers the formation of a cleft around Et_3NH^+ through bond rearrangement and rotations of arms in both Co(III) and Fe(III) complexes"

Somnath Paik and Manabendra Ray *Dalton Trans.* **2024**, doi:10.1039/D4DT02515F

2. " Visual detection of Hg^{2+} without interference by alkali and alkaline earth metal ions using an iron(III) complex in a heterobimetallic environment" **Somnath Paik** and Manabendra Ray. (***Submitted***)

3. " Guest-induced chiral recognition in inert vs. labile complex within an L-tryptophan based complex host " **Somnath Paik** and Manabendra Ray. (Manuscript under preparation)

Conferences

1. "**Frontiers in Chemical Sciences**" (FICS-2022), Poster Presentation, 2nd - 4th December 2022, Department of Chemistry, at IIT Guwahati, Assam, India.

2. "**Modern Trends in Inorganic Chemistry**" (MTIC XIX), Poster presentation, 15th -17th December 2022, Department of Chemistry, Institute of Science, Banaras Hindu University, Varanasi, India.

3. "**6th Symposium on Advanced Biological Inorganic Chemistry**" (SABIC-2024), Poster presentation, 7th-11th January, Tata Institute of Fundamental Research (TIFR) and Indian Association for the Cultivation of Science (IACS), Kolkata, India.